Grain Boundary Relaxation in 18-carat Gold Alloys

PAR

Ann-Kathrin AUDREN

EPFL

ÉCOLE POLYTECHNIQUE
FÉDÉRALE DE LAUSANNE

Suisse
2014

To my parents Beate and Theo
and my brother Tobias
and my husband Benjamin

Acknowledgements

It was almost four years ago that I started the PhD work at EPFL. At that time I remember myself having only a vague idea what the work of an experimental physicist looked like. In retrospect, I am very grateful and happy that I decided for this particular thesis subject, since it allowed me to merge high quality experimental data, simulations and a theoretical description of a complex process. The outcome of this project depended on many other people, without them it would not have been possible. Therefore, I am glad about the support and help from many people throughout these four years.

First of all, I would like to express my thanks to both the thesis directors Prof. Robert Schaller and Dr. Daniele Mari. They were a complementary team in guiding my thesis work and I never had the feeling to be sitting between two chairs.

Robert Schaller not only proposed the project but also guided me through it, even after his official retirement one year ago. He convinced me that mechanical spectroscopy is a beautiful and extremely powerful technique to study complicated materials. I admire him for his extensive knowledge of the physics of material and for his intuition, in which direction the research should be focused. I am very grateful for the fruitful discussions that opened new doors for further research and from which I learned plenty of things. Thank you very much for the good collaboration.

I am equally grateful to my other supervisor, Daniele Mari. I have profited on many occasions from his open door in order to engage him in spontaneous discussions. Thanks to his detailed knowledge and experimental know-how, he helped me a lot in my every-day research activity. He has a good ability to distinguish between the necessity of deadlines in order to get a project done and the necessary freedom to be able to develop new ideas. I appreciated this a lot during my time here.

I would like to extend my gratitude to Iva Tkalčec, my officemate and friend, from whom I learned all the lab work skills connected to screws, cables, pumps and measurements of all sorts. Alessandro Sellerio helped me greatly to set up the simulation part and to explain to me advanced issues in statistics or thermodynamics. Thanks to Raffaele Cosimati for the good moments together, at EPFL, Lyon or Hefei. A big part of the experimental work would not have been possible without the technical assistance of Gérald Beney (polishing, chemical

Abstract

Grain boundaries (GBs) play an important role for the mechanical properties of metals. In addition to dislocation motion inside the grains, some metal alloys, especially fine grained materials, deform along the GBs at high temperatures. GBs can also be the cause of a brittle behaviour of some metallic alloys, where crack propagation along the GBs is observed. This thesis aims to understand the role of GBs on the thermo-mechanical behaviour of metallic materials and especially to define the microscopic mechanism, which leads to a deformation at the GBs.

In this thesis, polycrystals, single crystals and bi-crystals of a yellow gold alloy are studied in detail, primarily by mechanical spectroscopy. The analysis and interpretation of the experimental data identifies different anelastic relaxations (internal energy dissipation processes), that produce peaks in the mechanical loss spectrum at different temperatures.

The mechanical loss spectrum of polycrystals shows a relaxation peak at about 780 K (P2), which is absent in single crystals made from the same alloy. Stepwise deformation of a single crystal causes an increase of the high temperature mechanical loss background and the appearance of a high temperature peak (P3). Above a critical deformation, the high temperature peak disappears and the peak P2, which is normally observed in polycrystals, appears. The increase of the exponential background is interpreted as due to the introduction of new dislocations whereas the high temperature peak P3 is attributed to a dislocation relaxation mechanism in the sub-grain boundaries.

The peak of polycrystalline samples located at intermediate temperatures (P2) depends on the grain size : with grain growth, the peak position shifts to higher temperatures. It is shown that the relaxation time τ is proportional to the grain size d. Such a grains size dependence is in agreement with the Zener model based on geometrical considerations of an assembly of elastic grains, which can slide against each other.

The investigations on bi-crystals containing a single GB with a specific misorientation between crystal lattices and a specific boundary plane orientation show that the relaxation peak P2 is closely related to a mechanism taking place at the boundary. The peak height is proportional to the GB density in a bi-crystal, whereas a single crystalline part cut from a bi-crystal does not show a relaxation peak.

Abstract

Molecular dynamics simulations are performed in order to illustrate the potential microscopic mechanisms responsible for the stress relaxation peak P2 in polycrystals. A Σ5 grain boundary is submitted to a shear deformation parallel to the boundary plane. The grain boundary shows a migration perpendicular to the boundary plane coupled to shear for temperatures below 700 K. Above 1000 K, only grain boundary sliding is observed.

Two models are developed that provide expressions for the relaxation strength Δ and the relaxation time τ that are compared to experimental measurements performed on polycrystals. The observed grain size dependence of Δ and τ favours the sliding model over the migration model.

Measurements as a function of stress allow a refinement of the sliding model. The stress amplitude dependence of the GB peak P2 indicates a depinning mechanism, which is interpreted as due to GB dislocations between zones where sliding of different amount occurred. Obstacles to the sliding movement like steps or extended coincidence sites in the GB plane act as pinning points. The pinning points can be overcome at high temperatures close to the melting point, which results in the onset of local microscopic creep.

Key words : grain boundaries, dislocations, 18-carat gold alloys, mechanical spectroscopy, anelasticity, grain boundary sliding, coupled migration, molecular dynamics, recrystallization, dislocations, bi-crystals

Résumé

Les joints de grains jouent un rôle important pour les propriétés mécaniques des métaux. En plus du mouvement des dislocations à l'intérieur des grains certains alliages métalliques se déforment le long des joints de grains à haute température. Ces interfaces peuvent aussi être la cause d'une fragilisation de certains alliages, où la propagation des fissures est observée le long de ces joints. Cette thèse cherche à comprendre le rôle des joints de grains sur le comportement thermo-mécanique de matériaux métalliques et en particulier à définir le mécanisme microscopique responsable de la déformation aux joints de grains.

Dans cette thèse, des polycristaux, des monocristaux et des bi-cristaux fabriqués à partir d'un alliage d'or jaune sont étudiés en détail principalement par spectroscopie mécanique. L'analyse et l'interprétation des données experimentales révèlent différentes relaxations anélastiques (des processus de dissipation d'énergie) qui produisent des pics de pertes mécaniques à différentes températures.

Le spectre des pertes mécaniques des polycristaux montre un pic de relaxation à environ 780 K (P2), qui est absent dans les monocristaux produits à partir du même alliage. Une déformation pas à pas d'un monocristal donne lieu à une augmentation du fond des pertes mécaniques à haute température et à l'apparition d'un pic à haute température (P3). Au-delà d'une déformation critique, le pic P3 disparaît et le pic P2, généralement observé dans les polycrystaux, apparaît. L'augmentation du fond exponentiel est interprété comme êtant dû à l'introduction de nouvelles dislocations et le pic P3 est attribué à une relaxation de dislocations dans les sous-joints de grains.

Le pic P2 observé à des températures intermédiaires dépend de la taille des grains : la croissance de grains provoque un déplacement du pic vers les hautes températures. Nous montrons que le temps de relaxation τ est proportionnel à la taille des grains d. Une telle dépendance de d est en accord avec le modèle de Zener. Ce modèle est basé sur des considérations géométriques d'un assemblage de grains élastiques, pouvant glisser les uns contre les autres.

Afin d'évaluer le rôle des joints de grains sur le pic P2, nous étudions le cas simplifié d'un bi-cristal. Les échantillons produites contiennent un seul joint de grains avec une désorientation spécifique entre les réseaux cristallins et une orientation spécifique du plan de joint. Cette étude montre que le pic P2 est causé par un mécanisme microscopique situé dans le joint de

Résumé

grains. La hauteur du pic est proportionnelle à la densité de joints de grains dans un bi-cristal. Un échantillon monocristallin obtenu par la découpe d'un bi-cristal ne montre en effet pas de pic de relaxation.

Des simulations de dynamique moléculaire sont faites pour illustrer un mécanisme microscopique potentiellement responsable de la présence du pic P2 dans les polycrystaux. Un joint de grains de type Σ5 est soumis à une contrainte de cisaillement parallèle au plan de joint. En dessous de 700 K, le joint de grains migre perpendiculairement au plan ; le mouvement est couplé aux déformations en cisaillement. Au-delà de 1000 K, un glissement au joint de grains est observé.

Deux modèles sont dévelopés pour calculer l'intensité de relaxation Δ et le temps de relaxation τ. Ces expressions sont comparées avec des mesures expérimentales de polycristaux. La dépendancede Δ et τ en fonction de la taille des grains favorise le modèle de glissement aux joints de grains par rapport au modèle de migration.

Les mesures en fonction de la contrainte permettent de raffiner le modèle de glissement. La dépendance en contrainte du pic de joints de grains P2 indique un mécanisme de désancrage. Une partie du pic est attribuée aux dislocations situées aux joints de grains entre des zones qui glissent plus ou moins loin. Les points d'ancrage qui s'opposent au glissement sont des marches du joint ou des sites de coïncidence étendus. Ces points d'ancrage peuvent être franchis à haute température proche de la fusion, ce qui se traduit en micro-fluage localisé.

Mots-clés : joints de grains, dislocations, or jaune de 18-carat, spectroscopie mécanique, anélasticité, glissement aux joints de grains, migration couplée, dynamique moléculaire, recristallisation, dislocations, bi-cristaux

Zusammenfassung

Korngrenzen spielen eine wichtige Rolle für die mechanischen Eigenschaften von Metallen. Zusätzlich zu der Bewegung von Versetzungen im Inneren der Körner zeigen manche metallische Legierungen Verformungen an den Korngrenzen bei hohen Temperaturen. Dieses Phänomen tritt insbesondere in feinkörnigen Materialien auf. Korngrenzen können auch die Ursache von Versprödung in gewissen metallischen Legierungen sein, in denen die Ausbreitung von Rissen entlang der Korngrenzen beobachtet wird. Die Zielsetzung der vorliegende Arbeit ist das Verständnis der Funktion von Korngrenzen auf die thermo-mechanischen Eigenschaften von Metallen. Im Wesentlichen soll der mikroskopische Mechanismus definiert werden, welcher zu einer Verformung an Korngrenzen führt.

In dieser Dissertation werden Polykristalle, Einkristalle und Bikristalle einer Gelbgold-Legierung detailliert untersucht, in erster Linie mit mechanischer Spektroskopie. Durch die Analyse und Interpretation der experimentellen Daten werden verschiedene anelastische Relaxationstypen (interne Dissipationsprozesse) identifiziert, welche zu Peaks bei verschiedenen Temperaturen im mechanischen Verlustspektrum führen.

Das mechanische Verlustspektrum von Polykristallen weist einen Relaxationspeak (P2) bei etwa 780 K auf, welcher in Einkristallen der selben Legierung nicht vorhanden ist. Die schrittweise Verformung eines Einkristalls führt zu einem Anstieg des Hochtemperatur-Hintergrundes im mechanischen Verlustspektrum und zum Auftreten eines Hochtemperatur-Peaks (P3). Oberhalb einer kritischen Verformung verschwindet der Peak P3 und wird abgelöst von Peak P2, welcher gewöhnlich in Polykristallen beobachtet wird. Der Anstieg des exponentiellen Hintergrundes ist auf das Einbringen neuer Versetzungen zurückzuführen, wohingegen der Hochtemperatur-Peak einem Relaxationsmechanismus von Versetzungen in Unterkorngrenzen zugeschrieben wird.

Der Peak P2 in Polykristallen, welcher sich bei mittelhohen Temperaturen befindet, ist von der Korngröße abhängig: Kornwachstum führt zu einer Verschiebung des Peaks zu höheren Temperaturen. Es wird gezeigt, dass die Relaxationszeit τ proportional zur mittleren Korngröße d ist. Solch eine Abhängigkeit ist in Übereinstimmung mit dem Zener-Model, welches auf geometrischen Annahmen eines Gefüges elastischer Körner beruht, die gegen einander gleiten können.

Zusammenfassung

Die Studie eines Bikristalls, welcher genau eine Korngrenze mit spezifischer Fehlorientierung der Kristallgitter und spezifischer Flächennormalen enthält, zeigt, dass der Relaxations-Peak P2 eng mit einem Mechanismus an der Korngrenze verbunden ist. Die Peak-Höhe ist proportional zur Korngrenzendichte in einem Bikristall. In einem Einkristall, welcher von der Seite eines Bikristalls geschnitten wird, wird kein Peak beobachtet.

Molekulardynamik-Simulationen veranschaulichen den potentiellen mikroskopischen Mechanismus, der für den Relaxations-Peak P2 in Polykristallen verantwortlich ist. Eine Korngrenze vom Typ Σ5 wird einer Scherspannung parallel zur Grenzfläche ausgesetzt. Unter 700 K zeigt die Korngrenze eine Migrationsbewegung in orthogonale Richtung, welche mit der Scherverformung gekoppelt ist. Bei Temperaturen über 1000 K wird Korngrenzengleiten beobachtet.

Zwei Modelle werden entwickelt, die explizite Ausdrücke für die Relaxationsstärke Δ und die Relaxationszeit τ liefern. Ein Vergleich mit den experimentellen Messungen an Polykristallen zeigt, dass die beobachtete Abhängigkeit von der Korngröße d dem Korngrenzengleit-Modell den Vorzug gibt und dass das Migrations-Modell ausgeschlossen werden kann.

Spannungsabhängige Messungen erlauben eine Verfeinerung des Korngrenzengleit-Modells. Die Abhängigkeit des Korngrenzen-Peaks P2 von der Spannungsamplitude weist auf einen Ablöseprozess (depinning) von Korngrenzen-Versetzungen hin. Diese Versetzungen sind Liniendefekte zwischen Zonen unterschiedlich weiten Gleitens. Hindernisse, die sich dem Gleitprozess entgegensetzen, sind entweder Stufen in der Korngrenze oder ausgedehnte Koinzidenzstellen. Diese Befestigungspunkte können bei hohen Temperaturen nahe des Schmelzpunktes überwunden werden, was zu einem Einsetzen von lokaler mikroskopischer Kriechdehnung führt.

Stichwörter: Korngrenzen, Versetzungen, 18-Karat Gold-Legierungen, Mechanische Spektroskopie, Anelestizität, Korngrenzengleiten, gekoppelte Migration, Molekulardynamik, Rekristallisation, Versetzungen, Bikristalle

Contents

Contents

Introduction

The mechanical properties of solids depend essentially on their microstructure: point defects, dislocations, grain boundaries (GBs). It is well known that plastic deformation of metals is achieved by dislocation motion. However, in polycrystalline specimens, a deformation between adjacent grains is often observed at high temperatures. Moreover, some metallic alloys exhibit a brittle behaviour associated with crack propagation along the GBs. It is then evident that GBs also play a very important role on the thermo-mechanical behaviour of metallic materials.

It is well known that GB sliding is the predominant deformation mechanism in ceramics, since dislocation motion is in large part suppressed. In metals on the other hand, it is less sure that deformation can be achieved by GB sliding. In any case, a number of studies testify the existence of this phenomenon occurring in metals as well; especially in fine grained materials, where the GB density is high. GB sliding has been observed experimentally in ultrafine-grained Cu [Golo12], Al [Whee13], Au thin films [Sim14] and in AuPd [Skro13] as well as in Pd [Yang14] nanocrystalline materials. The deformation mechanism was observed indirectly, since the experimental techniques are mostly tensile tests and indentation tests. Direct observation of GB sliding has been made on single incommensurate boundaries in nanopillars [Lanc10] and in Zn bi-crystals [Shei95].

Mechanical spectroscopy is a non-destructive experimental technique that probes the mechanical response of a specimen (the deformation or strain) to a periodic external excitation (an applied stress). The technique is sensitive to point defect relaxations, to dislocation movement and in particular to the motion of GBs.

In a recent study on gold alloys by Hennig [Henn10], a relaxation peak at high temperature (~0.5 T_m = melting temperature) has been observed in the mechanical loss spectrum. This relaxation peak could be due to the motion of dislocations in the bulk material or in the vicinity of GBs, or it could be a GB peak due to sliding along the grain interfaces.

A first model for GB relaxations in metals was developed by Zener in 1941 [Zene41]. The model was verified experimentally in 1947 by Kê [Ke47a, Ke47b] in his interpretation of the spectrum of poly- and mono-crystalline aluminium. He observed a rather huge peak at 0.5 T_m in an aluminium polycrystal. Since this peak was absent in single crystals, he concluded that the cor-

responding relaxation resulted from the relative sliding of neighbouring grains along their common GB. However the truthfulness of Kê's interpretation has been disputed [Woir81, Beno04] and even rejected over the years. At small stress amplitudes that are used during mechanical spectroscopy experiments, it seemed questionable how, in a metal, a two-dimensional macroscopic defect such as a GB can slide at a temperature only slightly higher than the one for which, under the same experimental conditions, zero-dimensional point defects or one dimensional dislocations become mobile.

To this day the debate is still going on with research groups of the two different schools: GB peak [Bone83, Beno04] or dislocation peak [Rivi93]. It is however important to know whether grain boundaries do effectively slide and in such case to determine the sliding mechanism.

Scientific objectives

The present study aims at defining the mechanism responsible for high temperature relaxations in metals that can be attributed to GBs. As a consequence, we might be able to discriminate if such relaxations need the presence and collective movement of dislocations or not. The goal is to obtain sufficient data to develop a theoretical model of the dynamics of a GB under external stress and of the microscopic mechanism, which is responsible for the high temperature anelastic relaxation due to GBs.

Technological objectives

Hardness and damping capacity at different temperatures can determine the application of a metal alloy. On the other hand, a proper understanding of the microscopic mechanisms can lead to improvements of the mechanical properties of a material in the case of a specific application. The present work aims at giving guidelines to improve the mechanical properties of metal alloys. In a very ductile material, hardness can be improved by blocking not only the movement of dislocations inside the grains, but also prevent softening at the GBs. Contrarily, a brittle material suffering from decohesion and from the formation of cavities at GBs could be improved by enhancing the dynamical properties of GBs.

Investigation methods

A systematic study of the high temperature mechanical loss spectrum of metallic alloys as a function of the alloy composition, the grain size and the dislocation density will be performed measuring the activation energy, relaxation time and relaxation strength in isothermal and isochronal conditions.

Choosing alloys instead of pure metals allows the modification of the GB viscosity or even to impede any GB sliding by alloying elements. In the debate concerning the GB peak, other authors always worked with pure metals in which dislocation mobility is very high in the

investigated temperature range. As a consequence, dislocation peaks were observed in single crystals, which were not very different from the peaks observed in polycrystals.

In order to observe the impact of GBs on the mechanical loss spectrum, single crystals of the same alloy have been processed by the Bridgman technique. These single crystals can be compared to the polycrystalline samples. Dislocations can be introduced by plastic deformation leading to recrystallization and the appearance of new freshly formed GBs.

A first model of GB sliding was developed by Zener [Zene41], which is based on topological considerations and which predicts very precise peak characteristics as a function of the grain size. The model describes a polycrystal being formed of elastic grains that can slide with respect to each other. Measurements of polycrystals with different grain size will be confronted with the predictions of the Zener model.

A second approach to study GB sliding in well controlled conditions is the production and measurement of bi-crystals. Bi-crystals allow the study of the dependence of the mechanical loss on the GB type and orientation. The objective is to collect sufficient data to develop a theoretical model of the mechanical loss due to the stress relaxation of GBs. Since geometrical parameters of an individual GB can be changed separately in a bi-crystal, such type of samples can give further insight into the microscopic mechanism, which is responsible for the high temperature anelastic relaxation due to GBs.

In this context, the present research aims at a better understanding of the dynamics of GBs, and consequently at increasing our knowledge for modifying the GB viscosity. Controlling the GB viscosity is important for controlling the thermo-mechanical behaviour of metallic alloys.

The main part of the measurements are performed on yellow gold as a model material. The main technique used is the mechanical spectroscopy, since we aim at explaining GB relaxations. Other experimental techniques as well as Molecular Dynamics simulations are used to interpret the results from mechanical spectroscopy experiments. This approach allows the development of a theoretical model of GB anelastic relaxation in metals.

Thesis outline

The **first chapter** presents a brief review on the literature about the microstructure and the mechanical properties of grain boundaries as well as their influence on the mechanical loss spectrum in metals.

In the **second chapter**, the materials used in the measurements as well as the experimental techniques are described. The focus is set on anelasticity measurements and mechanical spectroscopy.

Chapter three presents the experimental results and analysis of the GB peak in yellow gold. The spectra of polycrystals, single crystals and bi-crystals are discussed in detail.

In the **fourth chapter**, molecular dynamics simulations are presented, which illustrate the microscopic stress relaxation mechanisms acting at the GB.

These relaxation mechanism are then used to develop a theoretical model of GB relaxation in **chapter five**, which can explain the origin of the GB peak observed in the experiments.

Chapter six is a general analysis and discussion of the results, bringing together experiments, simulations and theoretical models.

1 Scientific Background

Grain boundary sliding is a well known mechanism to achieve deformation in ceramic materials [Dara07, Lakk95, Test02]. It plays a fundamental role in the deformation at high temperatures and it is the responsible mechanism for ceramic superplasticity [Waka86, Jime98]. GB sliding occurring in metals has been observed in different materials [Golo12, Whee13, Sim14, Skro13, Yang14, Lanc10, Shei95], but it is a less well established mechanism. Also in geology, GB sliding receives much attention from the scientific community [Hans11, Take14]: GB sliding in olivine is supposed to be the most important deformation mechanism of the earth mantle [Poir85].

Several models have been developed for polycrystalline materials, but GB sliding in metals was only rarely observed on macroscopic scales. This thesis concentrates on the comprehension of the physical mechanisms responsible for GB sliding. Mechanical spectroscopy is an experimental technique sensitive to the dynamics of defects like dislocations and GBs and it has been applied successfully to the study of GB sliding in ceramics [Lakk95]. The analysis of relaxation peaks can give valuable information on the dynamics of the underlying stress relaxation mechanism.

1.1 The Zener Model

A first model of anelastic GB sliding was developed by Zener in 1941 [Zene41], which describes a polycrystal as an assemblage of elastic grains separated by glissile boundaries. The model was found to be in excellent agreement with Kê's measurements of the mechanical loss in aluminium six years later showing a relaxation peak [Ke47a, Ke47b] in polycrystals. Therefore, the main statements of the model shall be recalled here.

Let us consider the periodic assembly of hexagonal grains in Figure 1.1 under an external shear stress. If the entire polycrystal behaves like an isotropic elastic material, the displacement field is given by $\vec{u}(x, y, z) = (\gamma y, 0, 0)$, where $\gamma = \sigma / M_u$ is the shear angle and M_u the unrelaxed elastic modulus. Therefore, all volume elements are in a state of pure shear. If the assembly is

now allowed to slide along the GBs, the structure relaxes and the shear angle increases when the stress is maintained constant. The relaxed state is characterized by the condition that GBs shall no longer transmit any shear stress. The remaining rigidity is due to the stresses accumulated near triple junctions, where three GBs meet and further sliding is impossible.
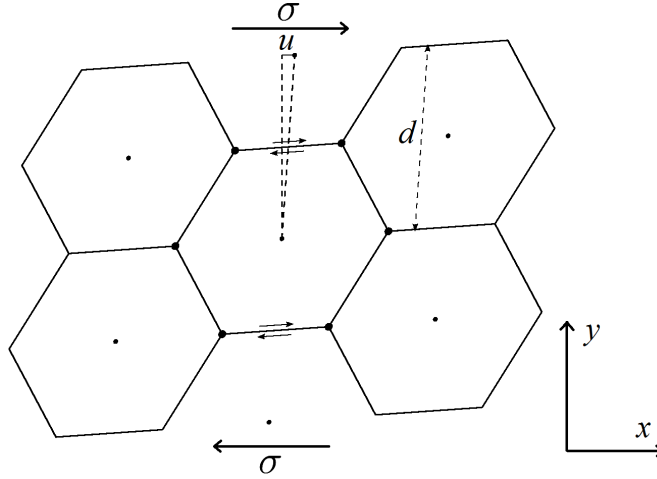
Figure 1.1 – Shearing of a honeycomb type polycrystal, which is made of uniform grains of size d shaped like hexagonal prisms.

Obviously, the scenario is hypothetical, otherwise bi-crystals would slide over macroscopic distances at the temperature at which GB sliding becomes active. In reality, GBs are not perfectly flat, but they contain ledges that represent additional obstacles apart from triple junctions. This problem was addressed by Raj and Ashby [Raj71] who calculated the sliding rate of a GB with a periodic wavy or stepped profile. Nonetheless, the Zener model with its flat profile should give a lower bound for the relaxed shear modulus.

In the relaxed state, the stress and strain fields are inhomogeneous and the displacement field even presents a discontinuity across the GBs. Due to symmetry reasons, the grain centres remain subjected to a pure shear stress, whereas for volume elements next to the boundaries, the shear stress is relaxed. The GB sliding is therefore accommodated by an elastic deformation of the grains. The average shear angle in the relaxed state can be calculated from the relative displacement of neighbouring grain centres [Foti95]. The resolution of the equilibrium equations of elastostatics can be formulated as a boundary value problem and the expression of the relaxed shear modulus is generally given by a numerical solution.

Considering the dimensions of the variables involved in the GB sliding process, some important conclusions can be drawn beforehand. First, the deformation field is an intensive thermodynamic variable since it is invariant under a spacial scaling transformation: $\epsilon(\alpha\vec{r}) = \epsilon(\vec{r})$. Therefore, the relaxed and the unrelaxed shear angle are independent of the grain size d in a periodic arrangement of Figure 1.1. This can also be seen more straightforward from Figure 1.1, which does not involve any absolute length scale. Changing the size of the grains does not change the shear angles. Since the relaxation strength Δ is given by the ratio of the shear angle

due to GB sliding and the unrelaxed shear angle, Δ is independent of d, too.

This argumentation distinguishes the sliding accommodated by elastic deformation of the grains from an accommodation by diffusion such as Coble [Cobl63] or Nabarro-Herring creep [Naba48, Herr50] in ceramics. Creep occurs at rather high temperatures with respect to the material's melting temperature, and diffusive mechanisms transport matter over long distances. The shape of the grains are changed and the symmetry arguments for the shear angles cannot be applied for the creep mechanisms.

Secondly, the displacement field $\vec{u}$ is an extensive field, i.e. $\vec{u}(\alpha) = \alpha \vec{u}$, which means that the relative sliding distance of a volume element near a grain boundary with respect to a volume element in the adjacent grain scales with the grain size d. Since the GB viscosity is an intrinsic property of the GB, it should be independent of the polycrystal's geometry and therefore the sliding rate should not depend on the overall sliding distance. The time scale, after which the equilibrium configuration is reached, i.e. the relaxation time τ, should be proportional to the grain size, $\tau \propto d$. A unitary grain size exponent ($m = 1$) distinguishes elastic accommodation from diffusional creep, where the exponent takes values of 2 or 3 for volume controlled or boundary-controlled diffusion respectively.

The boundary value problem for the displacement field in the polycrystal is generally difficult to solve. Zener assumed a spherical shape for the originally hexagonal grains, for which he could solve the problem of a polycrystal under tensile stress. Adapting the formulas to shearing, Kê calculated the ratio between relaxed and unrelaxed shear modulus [Ke47a]:

$$\frac{M_r}{M_u} = \frac{2}{5} \cdot \frac{7 + 5\nu}{7 - 4\nu} \tag{1.1}$$

The modulus ratio is a constant for one material, since it depends exclusively on the Poisson's ratio ν. From Equation (1.1), the relaxation strength can be calculated:

$$\Delta = \frac{M_u}{M_r} - 1 = \frac{3}{2} \cdot \frac{7 - 10\nu}{7 + 5\nu} \tag{1.2}$$

i.e. for $\nu = 0.3$, the relaxation strength is $\Delta = 0.7$ and for $\nu = 0.4$ one finds $\Delta = 0.5$.

1.2 Improved Grain Boundary Sliding Models

As mentioned above, Zener's approximations were rather crude, since the model is based on the boundary conditions of spherical grains, which do not fill the entire crystal volume and where the grains only touch in a few points. A more precise method was applied by Ghahremani [Ghah80] and later by Fotiu [Foti95], who used finite elements (FE) calculations to solve the problem of hexagonal prisms as shown in Figure 1.1. Their numerical solution can

be approximated by the formula

$$\frac{M_r}{M_u} = \frac{1+v}{1-v} \cdot \frac{0.86 - 0.83v}{1.14 + 0.83v} \tag{1.3}$$

The FE calculations always predict a lower relaxation strength than the Zener model (1.2), especially for small Poisson's ratio v. In comparison, the values of the relaxation strength of $v = 0.3$ and $v = 0.4$ are $\Delta = 0.22$ and $\Delta = 0.19$ respectively.

Raj and Ashby [Raj71] addressed the problem of GB sliding from a slightly different point of view. Instead of considering a polycrystal being built of individual grains, they calculated the sliding rate on one non-planar surface in a polycrystal, which is the sequence of many GBs between different crystallites. In Figure 1.1, this would correspond to a regular zig-zag line crossing the whole polycrystal. The model is applied to different boundary profiles like sinusoidal, stepped or irregular boundary planes. The advantage of this model is, that it can be directly applied to the shearing of bi-crystals, where the unique GB is generally non-planar [Ashb72, Sutt95, Hsie89]. Instead of representing different grain facets in a polycrystal, the irregularities of the surface account for ledges and steps on one GB.

Morris [Morr09] and Lee [Lee10, Lee11] calculated the mechanical loss spectrum of a polycrystal, adding the contribution of GBs according to the Raj-Ashby model. The model considers two different processes acting in the inter-facial region: viscous slip [Mosh74] and GB diffusion. The formulation of the boundary value problem is rather complicated and it does not provide simple formula for the mechanical loss as a function of the grain size d or the GB viscosity η. Numerical calculations show that the mechanical loss for a sawtooth interface is composed of a low-frequency background superimposed on a relaxation peak. The analysis of a sample composed of grains with different sizes and different GB viscosities showed, that a size distribution leads to a decrease of the relaxation peak without changing its shape. Different viscosities in one polycrystal on the other hand result in a broadened double peak [Lee10].

1.3 Experimental Results on Medium and High Temperature Relaxation Peaks

In addition to Kê's work on aluminium [Ke47b], GB peaks were observed in a number of materials, among them in gold [Okud94], in copper [Mort66, Pete64]. Often, the relaxation strength varied considerably between materials and the grain size exponent was sometimes found to take values between 1 and 2 [Nowi72b]. Moreover, instead of a symmetric single peak, many high purity metals (5N = 99.999%) have a double shaped peak. This, and the fact that GB sliding involves the mobility of a surface prompted some authors to question the existence of a GB peak. The high temperature relaxation peak in pure Al was attributed to the damping of dislocations instead [Rivi81, No89, Rivi09].

In 1981, Woirgard et al. [Woir81] reported about mechanical loss measurements in different

pure metals (Al, Cu, Ni). They observed similar relaxation peaks as well in single than in polycrystals. The amplitude dependence of the observed peaks in single crystals and their behaviour upon annealing led them to conclude that damping originates mainly from lattice dislocation motion and not, as previously assumed, from GB sliding.

In the literature, one can find many results, which argue for one or the other interpretation of high temperature relaxation peaks in metals. In 2004, W. Benoit published a review paper on the high temperature relaxations in metals [Beno04]. In this paper he shows that the solution is not simple. In some cases, the relaxation peaks would be due to dislocations, in other cases, such as Ni-Cr [Cao94], to GBs.

In 2005, Shi et al. [Shi05, Shi06] reported about a mechanical loss peak in pure aluminium bi-crystals with different misorientations. They show that the peak is strongly related to the GB separating the two crystals. As a matter of fact, this peak is absent in a single crystal taken as one part of the bi-crystal. They also found a distinct transition in the activation parameters between low- and high-angle GBs [Jian05]. The peak for low-angle GBs is interpreted by the motion of dislocations composing the GB and controlled by dislocation climb.

The interpretation of the high-angle GB peak [Kong09] is based on Ngai's coupling model [Ngai79]. The idea behind this approach is that the single step processes are not independent of each other but correlated. The consequences of the coupling is a retardation of the relaxation response, which presents itself in an asymmetric and broadened peak shape with respect to a Debye peak. Furthermore, the measurement of activation parameters yields only apparent values E^* and τ_0^*, which are related to the true values by

$$E = (1-n)E^* \qquad \text{and} \qquad \tau_0 = t_c^n \tau_0^{*(1-n)} \tag{1.4}$$

where n is the coupling parameter taking values between 0.2 and 0.5 for the bi-crystals and $t_c \approx 10^{-12}$ s is the crossover time from the Debye regime to the coupled regime. The parameter n acts as a broadening factor. When, in an earlier evaluation [Jian05], the same data was fit to a regular Debye peak, the broadening parameter β ranged between 1.0 and 0.25, which is much narrower than a polycrystals peak, but broader than a perfect Debye peak. The "decoupling" (1.4) reduces the measured activation energy to a more reasonable value according to the authors. However, the question of the atomistic relaxation process in high-angle GBs is not addressed.

Assuming that the observed relaxation peak in metals is due to GBs and that sliding occurs in a viscous manner, the main characteristics of the Zener model, i.e. $\tau \propto d$ should be observed in polycrystals. The GB viscosity would be thermally activated and would determine the activation energy of the peak. Peters et al. [Pete64] studied the GB peak in copper, which turned out to be very broad showing a broadening factor $\beta > 5$.

Granted that $\tau \propto d$ to be true, the authors noted that the distribution of grain sizes would only account for a small part of the overall broadening leading to $\beta < 1$. The remaining broadening

can only be explained by attributing it to a wide distribution of activation energies. It is quite understandable that the viscosity and therefore the activation energy of a specific boundary should depend on the microstructure of the GB. The diversity of the atomic structures of the various GB present in a polycrystal lead to a broadening of the GB peak, whereas the peak is much narrower in a bi-crystal.

Furthermore, in many metals the measured activation energy is relatively high with respect to the self-diffusion activation energy in the boundary and the relaxation time τ_0 is often several orders of magnitude smaller than that for point defect relaxation [Beno01b, Nowi72b]. The relaxation parameters are therefore apparent values indicating a weak temperature dependence of the activation energy.

In summary, metals generally show a GB relaxation peak in the medium to high temperature regime situated above approximately half the melting temperature T_m. There is little reason to doubt the existence of such a peak given the widespread experimental evidence in polycrystals and bi-crystals, where the peak was absent in a single crystal cut from the same grown produce as the bi-crystal. The process is thermally activated with an activation energy not far from the one for single atom diffusion. The sliding process is a viscous process with a threshold stress sufficiently small, such that it is not detected during mechanical spectroscopy measurements.

The results of mechanical spectroscopy show that the relaxation peak is linked to the presence of GBs, but there is no interpretation of the microscopic stress relaxation mechanism. The broadening of the peak in polycrystals and the apparent values of activation energy and limit relaxation time indicate that the microstructure of individual GBs must be taken into consideration in order to understand the origin of the GB peak. This is the objective of the presented work.

1.4   Impact of the Structure and the Mobility of Grain Boundaries

The question, which microscopic single-step mechanism causes GB relaxation has been addressed by many authors, but so far no definitive answer. Darinskii et al. [Dari03] connected GB sliding to the reorganisation of the atomic structure at the GB surfaces. This mechanism is mainly due to the formation and diffusion of vacancies and interstitial atoms in the GB. Experiments on fcc metals have shown that the activation energy of atomic diffusion along the core of a GB is about half of the energy for self-diffusion inside the grain [Beno01a]. Diffusion is enhanced by the higher amount of disorder at the boundary. However, this implies that the microscopic structure of GBs differs from the crystalline structure and that GBs resemble an amorphous phase. In ceramics, such an amorphous phase has been observed [Dara07], but in metals, the GB structure appears crystalline, at least at room temperature [Pond03].

1.4.1 Microstructure and Coincidence

It becomes clear that the question of the microscopic relaxation mechanism is always a question of the local atomic structure at the GB. A general GB has 5 macroscopic degrees of freedom [Prie13, Rand93]: 3 angles to define the relative orientation of one crystal lattice with respect to the other and 2 parameters to define the orientation of the GB plane. If the lattice misorientation is below 15° [Sutt87, Winn05] the GB can be seen as a regular array of one or more dislocation families [Read50]. Therefore, a possible relaxation mechanism in low angle GBs is the movement of individual dislocation segments under an external stress [Rivi09].

In GBs with misorientation angles above than 15°, the dislocation model is no longer applicable, since the dislocation cores are too close to each other and overlap. A convenient way to classify special GBs is the coincidence-site lattice (CSL) model [Boll70, Pond79], where a certain fraction of lattice points belong to both lattices. This means, in the GB plane, certain atoms are in a good position with respect to both lattices and therefore, the GB is more stable than a random GB. The resulting GB structure for high coincidence (which means low Σ-values) is periodic and highly crystalline.

With respect to random high angle GBs, only the low-Σ (up to $\Sigma 11$) CSL boundaries show a significant dip in the energy landscape of GBs [Bula14]. The energy of a GB is defined by the excess energy per unit area with respect to a perfect crystal without boundary. Another classification of GBs consists in identifying the tilt and twist components of a specific GB. In a pure twist boundary, one crystal lattice can be transformed into the second crystal lattice by a rotation around an axis perpendicular to the GB plane, whereas a pure tilt boundary has its rotation axis in the boundary plane.

One deformation mechanism acting on the tilt component of GBs is the so-called coupled shear migration [Molt97, Winn03, Cahn04, Ivan08, Molo13], where a shear deformation parallel to the boundary plane is accompanied by a normal boundary migration. In symmetrical low angle tilt GBs, this deformation mechanism can be understood as a collective glide of edge dislocations [Read50]. The shear stress acting parallel on the boundary causes a glide force on each GB dislocation which results in a migration of the GB plane. In GBs with higher misorientations, the dislocation model is no longer applicable, but theoretical analysis by Cahn et al. [Cahn04, Cahn06] and Caillard et al. [Cail09] predicted that coupled GB migration should also occur in the case of high angle GBs.

On microscopic level, a GB can contain irregularities like steps of various sizes. A step of height h having at the same time a dislocation character with a Burgers vector b has been defined as a "disconnection" [Hirt96, Hirt06]. If this kind of line defect is mobile and can glide along the GB [Pond03], the step is propagated along the GB and after the passage of a disconnection, the GB has migrated by a distance h. Since the disconnection has a dislocation character at the same time, the crystal is sheared at the same time that the GB migrate. Thus, disconnection motion can be seen as a single step process of coupled GB migration. Khater et al. [Khat12] showed, that in hexagonal closed packed metals, symmetric tilt boundaries respond more

easily to an applied strain and show a coupled shear migration, when the boundary contains pre-existing glissile disconnections.

1.4.2 Effect of the Temperature

At high temperatures just below the equilibrium melting point T_m, a thin, liquid-like film at the interface between two grains can form, which is referred to as premelting [Hoyt09, Fens10, Powe13]. The GB structure becomes disordered and also the position of GB layer undergoes large fluctuations. Structures like GB dislocations or disconnections loose their meaning. Even at lower temperature, the GB can be "wetted" by a solid layer of several nanometers thickness [Stra14]. In Al-Zn alloys, pure Zn as well as Zn-enriched layers have been observed at GB connecting two Al grains. These Zn enriched layers can explain the very ductile properties of ultra-fine grained Al-Zn alloys, where GB sliding is probably the dominant deformation mechanism.

For one and the same GB, the structure changes when increasing the temperature. One example is the roughening/de-faceting transformation [Hsie89], where the microscopic GB structure becomes smooth upon heating. It is likely that the mechanical response of such a GB will also change drastically upon heating. On flat GBs, the temperature dependence of coupled GB migration has been subject to several experimental and simulation-based studies [Wata84, Cahn06, Scha12]. The authors observed a low temperature regime, in which the GB undergoes a coupled GB migration with a fixed amount of shearing with respect to the migration distance. In an intermediate temperature span, the migration is interrupted by sliding events, whereas at high temperatures, GB sliding is the deformation mechanism acting at the GB.

1.4.3 Effect of Alloying Elements

Alloying elements cannot only facilitate deformation mechanisms acting at the GBs, but GB can also be pinned by segregated atoms or precipitates. Second phase particles tend to precipitate at GBs, since these offer preferential nucleation sites due to their intrinsic disorder and faster diffusion. The precipitates extend far into the adjacent grains since GB are objects of a few atoms thickness. The grain surface is roughened and GB sliding can be blocked by the presence of precipitates [Monz93].

Not only extended second phase particles but also segregated atoms can hinder the mobility of GBs. Molecular dynamics (MD) simulations on Al [Else09] have shown that the critical shear stress to induce coupled GB migration is increased by the presence of oxygen atoms on the GB plane. The presence of triple junctions and the interaction with dislocations can reduce the mobility of GBs in a nano-crystalline materials, as has been demonstrated by Velasco et al. [Vela11]. The triple junctions act as strong pinning points, which can only be overcome when entering the plastic regime by nucleating dislocations.

In summary, GBs being the interfaces between grains of different lattice orientations can show a variety of microscopic structures dependent on parameters like the misorientation, the material/composition and the temperature. Different deformation mechanisms have been observed as a response to a stress: GB sliding, where the position of the boundary plane remains fix, and coupled shear deformation, where a shear parallel to the boundary is accompanied by a migration. Other mechanisms, which have not been discussed in the previous text are GB migration without shear, which can be important for recrystallization and grain growth phenomena as well as grain rotation.

In order to understand the influence of GBs on the mechanical properties of metals and metal alloys, it is essential to identify the deformation mechanism acting on microscopic level. Mechanical spectroscopy allows us to study the overall influence of GBs on the mechanical properties by measuring polycrystalline samples, but also the effect of a single boundary in a bi-crystal. A specific GB type with a certain structure and misorientation angle can be analysed. Since the measurements are typically performed as a function of temperature, changes of the GB mobility with temperature are readily detected. With the knowledge, how GB become mobile and how the deformation is achieved, material properties can then be modified on purpose by changing the GB structure, for example by changing the material's composition.

2 Materials and Experimental Techniques

2.1 Yellow Gold

Gold alloys have a long tradition in jewellery and watch-making industry. Because of the softness of pure gold (24-carat), it is usually alloyed with other elements. The alloying elements influence the mechanical properties as well as the colour of the metal. During the manufacturing process, a sufficiently ductile material is required in order to cut and form fine parts. On the other hand, the finished product should be as resistant as possible to deformations and scratches.

The carat number indicates the purity of the gold alloy: 18-carat corresponds to 18/24=75% weight of pure Au in the alloy. The atomic fraction of Au atoms can change with different alloying elements.

As mentioned above, alloying elements influence the colour of the metal. In 18-carat gold-silver-copper alloys the colour varies from a pale yellow on the silver rich side to a reddish colour on the copper rich side. The bleaching effect of Ag is not strong enough to make a white gold alloy only by adding silver to gold. A strong bleaching element is nickel, but it is only rarely used in parts of jewellery that come into contact with the skin, because of common nickel allergies. Today most white gold alloys contain palladium (Pd) as the major alloying element. Palladium is a good bleaching element and usually 12.5 wt% Pd is sufficient to obtain a white gold alloy.

The hardening mechanism in yellow gold differs from that in white gold. In yellow gold containing at least 9 wt% Cu, a phase separation between a silver-rich and a copper-rich phase occurs. Within the copper-rich phase, the ordered phase AuCuI containing equal percentage of Au and Cu atoms causes the alloy to harden.

In Pd containing white gold alloys the hardening mechanism is different. The addition of other elements like Cu, In, Ga and Fe can cause precipitates to form in the material, which results in a precipitation hardening mechanism.

2.1.1 Composition

The present study is mainly based on measurements of 18-carat yellow gold, which contains 75 wt% Au, 4 wt% Cu and 21 wt% Ag. Due to the high silver content, the alloy structure contains many Au atoms with respect to other 18-carat gold alloys. It contains approximately 59.5% Au atoms, 9.9% Cu atoms and 30.5% Ag atoms. The colour is light yellow as the silver content is three times as high as the copper content.

The material undergoes no phase transition in the whole temperature range below the melting temperature of $T = 1245$ K. The crystalline structure is a face centred cubic system (fcc), where the atoms are sitting on the corners of a cube and in the middle of each of the 6 faces. Gold, copper and silver atoms take random positions, which results in a slightly deformed structure on atomic level as the different elements have different radii. The lattice parameter measured for example with an X-ray powder diffraction experiment is a mean distance between atoms on the corner of a unit cell. The yellow gold alloy has a lattice parameter of $a = 3.93$ Å.

2.1.2 Mechanical Properties

Gold alloys are very ductile materials. They can be cut or laminated easily at room temperature without breaking or fissuring. This is an advantage for shaping fine pieces. It is a soft material and it is therefore very easily scratched. Since plastic deformation in metals is mainly due to dislocation movement through the crystal, alloying elements slightly increase the hardness with respect to pure gold because of solution hardening. Therefore, the gliding of dislocations becomes more difficult if more than one element is present in the material and the hardness is increased with respect to a pure metal.

Commercial gold alloys can be obtained easily, especially in the case of 18-carat yellow gold alloys. Their composition is well monitored and the samples have a uniform microstructure. It has been shown by John Hennig [Henn10] that the mechanical loss spectrum of the yellow gold alloy containing 30.5% Ag atoms is particularly simple. The spectrum contains 2 stable and reproducible relaxation peaks superimposed on a high temperature background.

2.1.3 Microstructure and Metallography

The starting material is typically an extruded cylindrical wire with 2 mm in diameter. The sample has a very high dislocation density, which can be reduced by an annealing treatment of 30 min at 650 °C or 923 K. The resulting sample shows a recrystallized grain structure with a mean grain size of 30 μm. The dislocation density is reduced and the grain structure can be visualized by metallography. For this, the sample is mechanically polished down to 4μm particle size. In some cases, especially for the fine grained samples, it was necessary to perform additional polishing steps down to 1μm particle size using diamond solution.

A mirror polished sample was then chemically etched to visualize separate grains and grain
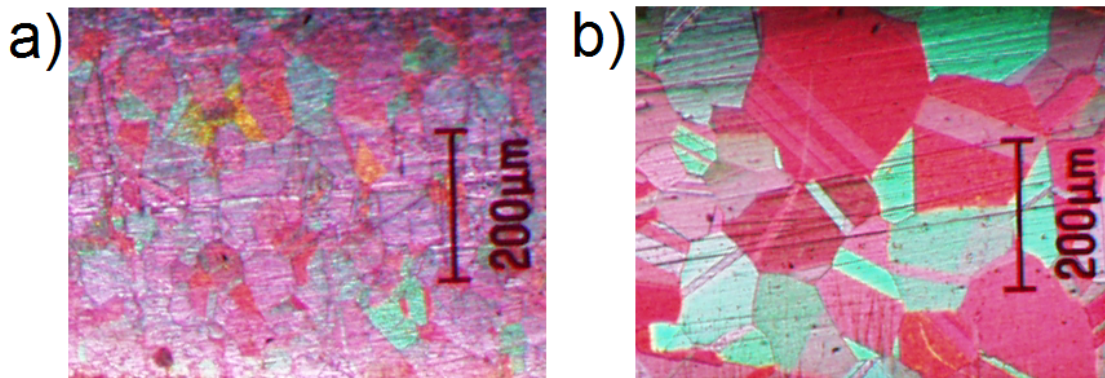
Figure 2.1 – a) Grain structure of a fully recrystallized polycrystal after the first heat treatment at 923 K. The sample is polished and chemically attacked. The mean grain size is approximately 30 μm. The mostly violet colour comes from crossed polarization filters. b) Polycrystal after additional annealing to provoke grain growth. Many grains show twinning which results in zones of repeated colouring of the form ABAB.

boundaries. An etching solution of equal parts of 5%-KCN solution and 5% $(NH_4)S_2O_8$-solution for a couple of minutes was used. This etchant highlights grain boundaries as lines by removing atoms from the disordered zones at the boundaries and it provokes a grain colouring by attacking different lattice orientation differently. The best colour contrast under an optical microscope is obtained with crossed polarization filters (Figure 2.1).

2.1.4 Growth of Single Crystals and Bi-crystals

In order to understand the role of grain boundaries, single and bi-crystals were produced by means of the vertical Bridgman technique. As illustrated in Figure 2.2, the polycrystalline source material was introduced into a graphite crucible inside a quartz tube under vacuum. The crucible is heated by an induction furnace above the melting temperature of the alloy. The entire graphite crucible is lowered very slowly (less than 1 mm /min) so that the melt starts to crystallize from the bottom in the pointed tip. One grain orientation in the tip serves as a seed for the single crystal. With this geometry, a particular orientation of the single crystal cannot be influenced. It turned out that the resulting lattice orientation was arbitrary and no preferred growth direction was observed.

The bi-crystals were grown in the same induction furnace with a different crucible geometry. The idea is to have two spatially separated single crystals in the bottom part of the graphite mould that join in the upper part. Figure 2.3a) shows the graphite crucible with a bi-crystalline sample. During the growth of the bi-crystal, the grain boundary needs to be guided by the crucible form.

A grain boundary possesses a surface energy and therefore, from an energetic point of view, the overall sample energy can be lowered by removing the grain boundary from the crystal. In
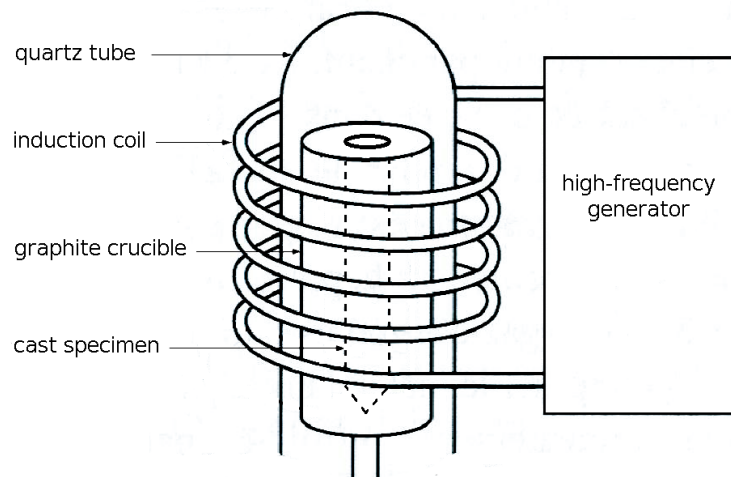
Figure 2.2 – Growth of a single crystal from melted material inside a graphite crucible in an induction furnace.

a vertical cylindrical geometry it is close to impossible to grow a bi-crystal with a vertical grain boundary plane, even if at some point there are two seeds in the bottom. At each moment the grain boundary surface can be decreased with respect to a vertical boundary by growing to one side. In an 8-shaped cross section as shown in Figure 2.3, the grain boundary is guided during the growth process. In such a configuration, the motion of the grain boundary to the specimen surface needs an increase in the GB area and thus an increase in energy. As a consequence, the GB is trapped in the specimen.

Once a proper bi-crystalline specimen was grown, it could be cut in slices of 1 mm thickness. With means of metallography, the grain boundary could be located with high precision for further cutting. Thus, one could produce samples with grain boundary planes oriented differently with respect to the sample axis. Typical sample dimensions were 1 mm x 5 mm x 20 mm.

2.1.5   Preparation of Bi-crystals by Diffusion Bonding

A complementary technique to prepare bi-crystals is called diffusion bonding. The idea is to start from a well known and easily producible single crystal, which has already the shape needed to perform the mechanical spectroscopy measurements. The sample is cut at a well defined position and with a well defined orientation with respect to the sample geometry. The new surfaces after cutting, which will form the GB plane later on, are prepared by mechanical polishing down to 1 μm particle size to obtain mirror quality. The surfaces need to be extremely flat, since a curved surface would result in a small contact area and the sample would not stick together well. To enhance the surface quality, the sample is chemically polished with the same attack solution as used for metallography based on KCN and $(NH_4)S_2O_8$.

Both crystal halves are placed into a supporting crucible, which allows to apply a pressure
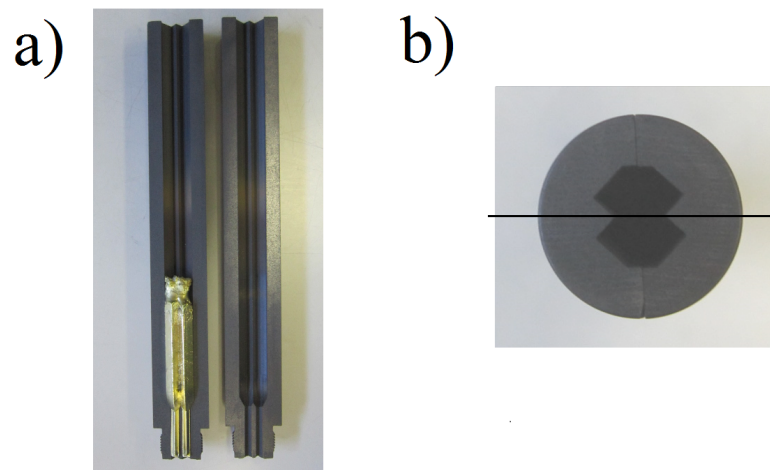
Figure 2.3 – a) Graphite crucible to grow bi-crystalline samples. b) Cross section of the crucible to guide the horizontal grain boundary (black line) during solidification.
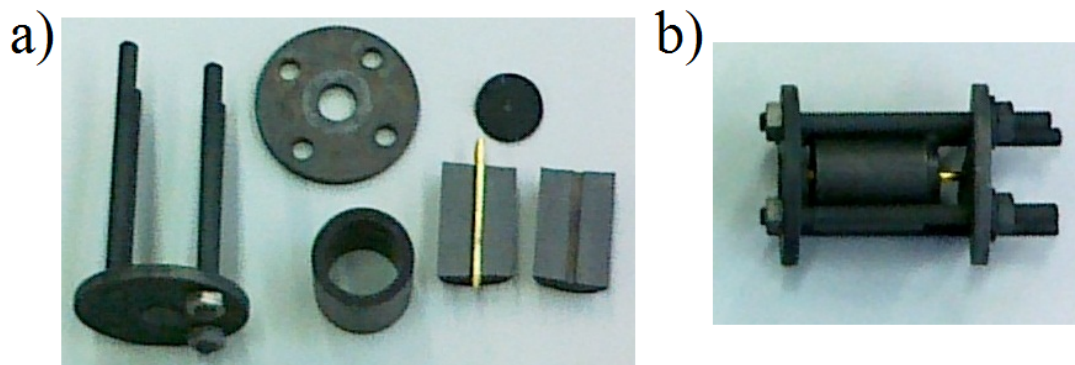
Figure 2.4 – a) Crucible parts for the diffusion bonding to prepare bi-crystalline samples. The sample (yellow) is surrounded by graphite parts to permit an easy removal after the annealing. b) Assembled parts. The screws are tightened to apply a pressure along the sample axis.

onto the GB plane while heating the material. The parts together with the sample are shown in Figure 2.4 a). The half cylinders with the vertical groove on the left side of Figure 2.4 a) and the ring are made of graphite to allow an easy removal of the sample after the annealing step. The two sample parts are hold in place due to the graphite crucible (Figure 2.4 b) and the disk screwed onto the support applies a pressure to the crystal parts. The whole assembly is heated up to 1183 K for 7 h under vacuum, which is 94 K below the melting temperature of the alloy.

Due to the high temperature, diffusion is very high and the prepared surfaces are joined together. The advantage of this method is, that the boundary plane is flat and can be chosen on purpose as well as the misorientation angle. On the other hand, it turned out that the samples prepared by diffusion bonding often broke apart at the boundary plane. The analysis of the broken parts by optical microscopy revealed that the boundary was only joined partially. Nevertheless, some samples allowed a study by mechanical spectroscopy.

19
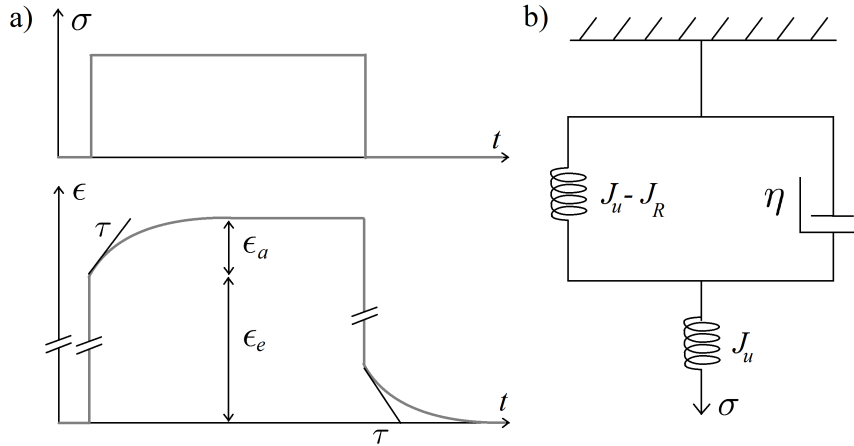
Figure 2.5 – a) Deformation of an anelastic solid: A stress applied at time $t = 0$ causes an instantaneous elastic deformation and a time dependent anelastic deformation. The sample returns to its initial shape upon unloading. b) Rheological model for the standard anelastic solid.

2.2 Mechanical Spectroscopy

Mechanical spectroscopy is a non-destructive experimental technique that probes the motion of lattice defects such as point defects, dislocations and grain boundaries. In this work, a low-frequency forced torsion pendulum has been used to measure the mechanical loss at a given temperature and a given frequency. A periodic stress of small amplitude is applied to the sample and its response is analysed. The mechanical loss corresponds to the energy loss during one oscillation cycle with respect to the maximal deformation energy stored in the material. Because of the low level of stress and strain, mechanical spectroscopy deals with the elastic and anelastic behaviours of materials.

2.2.1 Anelasticity

Ordinarily, the deformation of a solid is divided into to classes: elastic deformation and plastic deformation. Elastic deformation occurs instantaneously after applying a stress and the material returns to its initial shape after unloading. The stress-strain relationship at any instant t can be described by a Hooke's law:

$$\sigma(t) = M\epsilon(t) \tag{2.1}$$

where M is the elastic modulus. Dependent on the deformation mechanism (traction/compression or shear), M denotes Young's modulus or the shear modulus. The inverse of M is called the elastic compliance $J = M^{-1}$. If the deformation exceeds the elastic limit, the sample will not recover its initial shape any more and the solid is deformed plastically.

For lower stresses than the yield stress, a third category of deformation can be defined by

loosening the criterion of instantaneous deformation and according a time dependence and by maintaining the criterion of full shape recovery. Such a deformation is known as anelastic or viscoelastic and it is represented ideally in Figure 2.5. At a time $t = 0$, a stress of low intensity is applied and the solid first deforms elastically (ϵ_{el}). The anelastic strain ϵ_{an} increases with time from zero to an equilibrium value ϵ_{an}^{∞}. The relaxation process is characterized by a time scale τ, which is visualized in Figure 2.5a). One can write

$$\epsilon = \epsilon_{el} + \epsilon_{an}^{\infty}(1 - e^{-t/\tau}) \tag{2.2}$$

When the equilibrium is reached, the total strain is

$$\epsilon = \epsilon_{el} + \epsilon_{an}^{\infty} = J_u \sigma + \epsilon_{an}^{\infty} = J_r \sigma \tag{2.3}$$

where J_u and J_r are the unrelaxed and relaxed compliance respectively. One can define the relaxation strength

$$\Delta = \frac{\epsilon_{an}^{\infty}}{\epsilon_{el}} = \frac{J_r - J_u}{J_u} \tag{2.4}$$

In practice, ϵ_{an} is very small with respect to its elastic counterpart and it is more convenient to perform a dynamic measurement. Therefore, when a periodic excitation of the form $\sigma = \sigma_0 e^{i\omega t}$ is applied to the sample the strain also takes a periodic form, but the response function can be phase shifted: $\epsilon = \epsilon_0 e^{i(\omega t - \phi)}$.

A model for a large number of mechanical relaxations is the standard anelastic solid drawn in Figure 2.5. The spring in series having a compliance J_u, accounts for the instant elastic deformation. The dash-pot stands for a viscous friction mechanism where a piston moves in a liquid of viscosity η. The stress σ_η acting on the dash-pot is proportional to the strain rate: $\sigma_\eta = \eta \dot{\epsilon}_\eta$. The spring parallel to the dash-pot accounts for the additional compliance due to the anelasticity of the solid. Without it, the solid would show a creep behaviour and would not saturate at a finite strain ϵ_{an}^{∞} for an applied stress σ. The equation of motion for the linear anelastic solid can be derived by using Equation (2.3):

$$J_r \sigma + \tau J_u \dot{\sigma} = \epsilon + \tau \dot{\epsilon} \tag{2.5}$$

where $\tau = \eta(J_r - J_u) = \eta \delta J$ is the relaxation time at constant stress. This equation can be solved for a periodic excitation of the form $\sigma = \sigma_0 e^{i\omega t}$ and a phase shifted response function $\epsilon = \epsilon_0 e^{i(\omega t - \phi)}$. The relation between stress and strain takes the form:

$$\epsilon = \left[J_u + \frac{J_r - J_u}{1 + \omega^2 \tau^2} - i \frac{(J_r - J_u)\omega\tau}{1 + \omega^2 \tau^2} \right] \cdot \sigma \tag{2.6}$$

On the other hand, a complex compliance $J^*(\omega)$ can be defined as:

$$\epsilon = J^*(\omega)\sigma = (J_1(\omega) - iJ_2(\omega)) \cdot \sigma \tag{2.7}$$
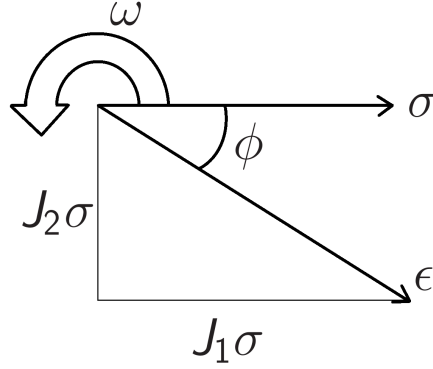
Figure 2.6 – Representation of the phase angle ϕ between stress σ and strain ϵ.

The real part of the complex compliance becomes:

$$J_1(\omega) = J_u + \frac{\delta J}{1 + \omega^2 \tau^2} \tag{2.8}$$

and the imaginary part is given by

$$J_2(\omega) = \frac{\delta J \cdot \omega \tau}{1 + \omega^2 \tau^2} \tag{2.9}$$

In metals, the anelastic strain is generally much smaller than the elastic strain and therefore $\delta J << J_u$. According to the rotating vector diagram (Figure 2.6) one can calculate the tangent of the phase angle ϕ between stress σ and strain ϵ:

$$\tan\phi = \frac{J_2}{J_1} \cong \frac{J_2}{J_u} = \frac{\delta J}{J_u}\frac{\omega\tau}{1 + \omega^2\tau^2} \tag{2.10}$$

Since $\frac{\delta J\sigma}{J_u\sigma} = \frac{\epsilon_{an}(t\rightarrow\infty)}{\epsilon_{el}}$, we can express the mechanical loss in a more compact form using the relaxation strength Δ from Equation (2.4):

$$\tan\phi = \Delta\frac{\omega\tau}{1 + \omega^2\tau^2} = \frac{\Delta}{2}\cdot\frac{1}{\cosh(\ln\omega\tau)} \tag{2.11}$$

The variation of the dynamic compliance $\delta J/J_u$ due to anelasticity is given by:

$$\frac{\delta J}{J} \cong \frac{\delta J}{J_u} = \frac{\Delta}{1 + \omega^2\tau^2} \tag{2.12}$$

The two equations (2.11) and (2.12) are called Debye equations [Nowi72a]. The same set of equations can also be found in the theory of dielectric relaxation phenomena. In order to formulate an expression for the dynamic modulus, it is possible to use the fact that the complex modulus $M^*(\omega) = M_1 + iM_2$ is the inverse quantity of the complex compliance J^*. The real
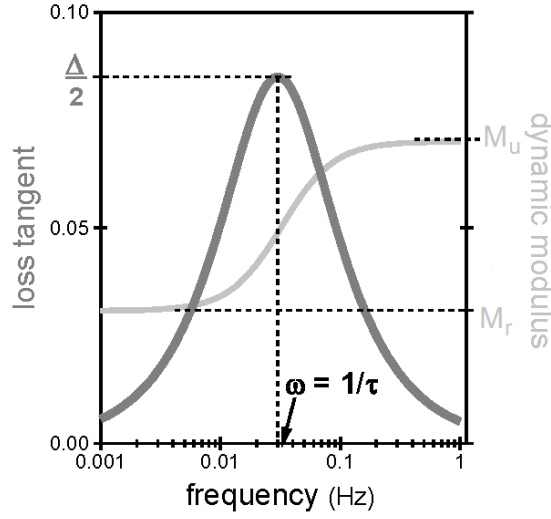
Figure 2.7 – Debye peak and dynamic modulus as a function of frequency.

part of the dynamic modulus is

$$M_1(\omega) = M_u - \frac{\delta M}{1 + \omega^2 \tau_\epsilon^2} \tag{2.13}$$

where $M_u = 1/J_u$ is the unrelaxed modulus, $\delta M = \delta J/(J_u J_r) = M_r - M_u$ is the modulus defect and $\tau_\epsilon = \tau M_r / M_u$ is the relaxation time at constant strain.

The mechanical loss ($\tan\phi$) as a function of the logarithmic frequency $\log\omega$ shows a peak, which is named "Debye Peak" after the Dutch physicist Peter Debye who first derived it for dielectric relaxation phenomena [Nowi72c]. Mechanical loss spectra are usually plotted versus a logarithmic scale since it represents the Debye peak in a symmetric shape. For a deca-logarithmic scale, this is shown in Figure 2.7. The peak is centred at $\omega\tau = 1$ and the height at its maximum is $\Delta/2$. With increasing frequency, the modulus changes from the relaxed modulus M_r to the unrelaxed modulus M_u with a step height of Δ. The peak height can therefore be related to the modulus change via

$$2\tan\phi_{max} = \frac{\delta M}{M_r}. \tag{2.14}$$

A Debye peak is characterized by 2 parameters: the relaxation time τ defines the peak position and Δ fixes the peak height. For a given Δ, the width is a fixed value. Many anelastic relaxations are diffusion controlled since they take place at atomic level. Therefore, most of the relaxation phenomena are thermally activated and the relaxation time generally follows an Arrhenius relationship:

$$\tau = \tau_0 \exp\left(\frac{H_{act}}{k_B T}\right). \tag{2.15}$$

23

H_{act} is the activation enthalpy and τ_0 is the limit relaxation time characterizing the underlying microscopic mechanism. k_B is the Boltzmann constant and the absolute temperature T is measured in K. Equation 2.15 describes a thermally activated process needed to overcome an energy barrier of height H_{act}. At infinite temperature the barrier height becomes insignificant and the attempt frequency becomes $\nu_0 = 1/\tau_0$.

For thermally activated processes, it is possible to fix the excitation frequency ω and to vary the temperature T. The peak maximum is reached as before under the condition $\omega\tau = 1$ and the peak temperature at its maximum is

$$T_p = -\frac{H_{act}}{k_B \ln(\omega\tau_0)} \qquad (2.16)$$

This measurement mode is called isochronal condition where a temperature spectrum is recorded at a fixed excitation frequency. If the temperature is fixed and the frequency is changed, the isothermal conditions give access to frequency spectra. Temperature scans generally give access to a wider range of relaxation phenomena, because the temperature has to be varied on a linear range (for example 100 K for a typical mechanical loss peak) and not exponentially as in the case of the frequency for isothermal conditions (2 to 3 decades for a full peak).

In order to extract the activation enthalpy H_{act} and the limit relaxation time τ_0 for a given relaxation process, an Arrhenius plot can be constructed by reporting ω on a logarithmic scale as a function of the inverse temperature. Arrhenius plots can be constructed from both frequency and temperature spectra. In the first case, frequency spectra have to be recorded at several temperatures and one point of the Arrhenius plot is obtained from the fixed measurement temperature and the frequency of the peak maximum. In the second case, temperature spectra at several frequencies are used and each time the peak temperature has to be extracted. The slope of the Arrhenius plot yields the activation energy and the intercept of the regression line with the vertical axis gives the limit relaxation time.

If, due to experimental conditions, only a flank of a relaxation peak is visible or if the relaxation process gives rise to an exponential background without a maximum, the activation energy can still be extracted by constructing a master curve. The construction of such curve is obtained by superimposing the points measured at different frequencies using an offset on the frequency axis. Since the Arrhenius plot requires a value of the logarithmic frequency, the offset needs to be extracted in terms of $\ln\omega$ or $\ln f$. One curve is chosen arbitrarily without offset and the Arrhenius plot is constructed with the relative offset values and the corresponding measurement temperatures. As before, the slope of the linear regression yields the activation energy H_{act}.

Due to the rather complex microstructure of most materials, more than one relaxation mechanism becomes activated during the anelastic evolution of the material. This results in a mechanical loss spectrum with several peaks that have to be identified and separately anal-

ysed. This is why the term "spectrum" is used. If the peaks are partially superimposed, a deconvolution must be performed initially to extract individual relaxation strengths and relaxation times.

For many relaxation processes, the relaxation time is not a well defined quantity, but it rather varies continuously in a certain range. The result is a broadening of the corresponding relaxation peak in the mechanical loss spectrum with respect to the Debye peak in Equation (2.11). It is usually difficult to know the distribution function of the relaxation time, but in many cases one can assume that they scatter around some mean value τ_m according to a log-normal distribution [Fuos41]:

$$\Psi(z) = \frac{1}{\sqrt{\pi}\beta} \exp\left(-\frac{z^2}{\beta^2}\right) \qquad \text{with} \quad z = \ln\left(\frac{\tau}{\tau_m}\right) \tag{2.17}$$

This is a Gaussian distribution of $\ln\tau$ around $\ln\tau_m$. In a thermally activated process according to the Arrhenius law (2.15), this corresponds to a Gaussian distribution of the activation energy around some mean value.

The broadening is characterized by the distribution parameter β that can vary in the interval $[0,\infty[$. $\beta = 0$ corresponds to the perfect Debye peak and high values of β (>2) generate broadened relaxation peaks. Assuming that the relaxation strength Δ is identical for all values of τ, one can calculate the analytic expression of the broadened Debye peak as a convolution of equation (2.11) with (2.17):

$$\tan\phi = \frac{\Delta}{2\sqrt{\pi}\beta} \int\limits_{-\infty}^{\infty} \frac{\exp\left(-\frac{z^2}{\beta^2}\right)}{\cosh((\ln\omega\tau) + z)} \, dz. \tag{2.18}$$

A thermally activated and broadened Debye peak can be fully described by 4 parameters: the relaxation strength Δ, the activation energy H_{act}, the limit relaxation time τ_0 and the broadening factor β.

Thermally activated relaxation peaks can have different physical origins: they can be due to point defects, as it is the case for Zener peaks [Zene47] or Snoek peaks [Snoe41]. The stress relaxation mechanism is due to the reorientation of elastic dipoles, which are created by substitutional or interstitial atoms respectively. In order to change the orientation of the dipole, at least one atom has to change its position. This is achieved by diffusion. The activation parameters of point defects are therefore closely linked to the activation energy of the diffusion and the attempt frequency for atomic movement (Debye frequency).

For most materials, the Debye frequency is of the order of 10^{13} Hz. It is element specific and can be calculated from the Debye temperature [Kitt05b] via $\nu_D = \Theta_d \cdot k_B/\hbar$. For gold, the Debye frequency is $\nu_D = 2.36 \cdot 10^{13}$ Hz and for Cu it is $\nu_D(Cu) = 1.24 \cdot 10^{13}$ Hz. The limit relaxation time can be calculated for models like the Zener model or the Snoek model and it turns out that τ_0 is often very close to the inverse Debye frequency ν_D. Therefore, one would expect τ_0

between $4.2 \cdot 10^{-14}$ s and $8.1 \cdot 10^{-14}$ s for a point defect relaxation that includes the movement of Cu and Au atoms.

If a relaxation peak is due to the movement of dislocations, more than one atom has to be moved to perform the smallest possible step of the microscopic relaxation process. This can be the creation of a kink pair, for example [Seeg56]. Since more than one atom have to move together, the probability for this to happen is lower with respect to a single atom movement and the attack frequency to overcome an energy barrier is lowered. In general, one expects $\tau_0 = 10^{-12}$ Hz for dislocation relaxations.

In the case of grain boundary relaxation, it is difficult to say, what value would be expected a priori for the activation energy and the limit relaxation time, since the microscopic mechanism is not well established. It is evident that several atoms are included in the smallest relaxation step. As in the case of dislocations, τ_0 should be larger than 10^{-13} s.

2.2.2 Forced Torsion Pendulum

A forced torsion pendulum is an experimental set-up to measure the mechanical loss spectrum and the dynamic modulus of a specimen. The measurement can be carried out at different temperatures and at different excitation frequencies. A schematic drawing is shown in Figure 2.8 a). A harmonically varying torque T is applied to the sample via a magnetic excitation system. Two magnetic coils driven by a harmonic current I attract or repel a pair of permanent magnets, which are attached to the rod. The sample is twisted such that the top end rotates whereas the bottom part remains fixed.

The torsion angle is measured by a laser spot that is reflected on an mirror attached to the rod. The position of the laser spot is detected by a photocell. In order to compensate for slight plastic deformation of the sample during the experiment, the photocell is mounted on a centring stage. A furnace surrounds the sample and the control of the heating coils allows one to vary the temperature between 290 K and 1200 K.

A balance system with a counterweight attached to it compensates the weight of the rod and the permanent magnets such that no compression or tension acts on the sample. The upper end of the rod is attached to the balance by a three-wire suspension (upper part of Figure 2.8) b), which permits the rod to turn freely around its vertical axis. During the measurement, the installation is set under vacuum with the exception of the laser and the photocell. A pallet pump creates a primary vacuum, a secondary vacuum of 10^{-5} mbar is maintained with a oil-diffusion pump.

The output signal from the photocell is analysed by a Solartron 1250 frequency analyser. By comparing the output signal with the excitation, the relation between input and output amplitudes gives access to the dynamic modulus of the specimen. The phase lag of the output signal with respect to the excitation signal provides directly a measurement of the mechanical loss (2.11).
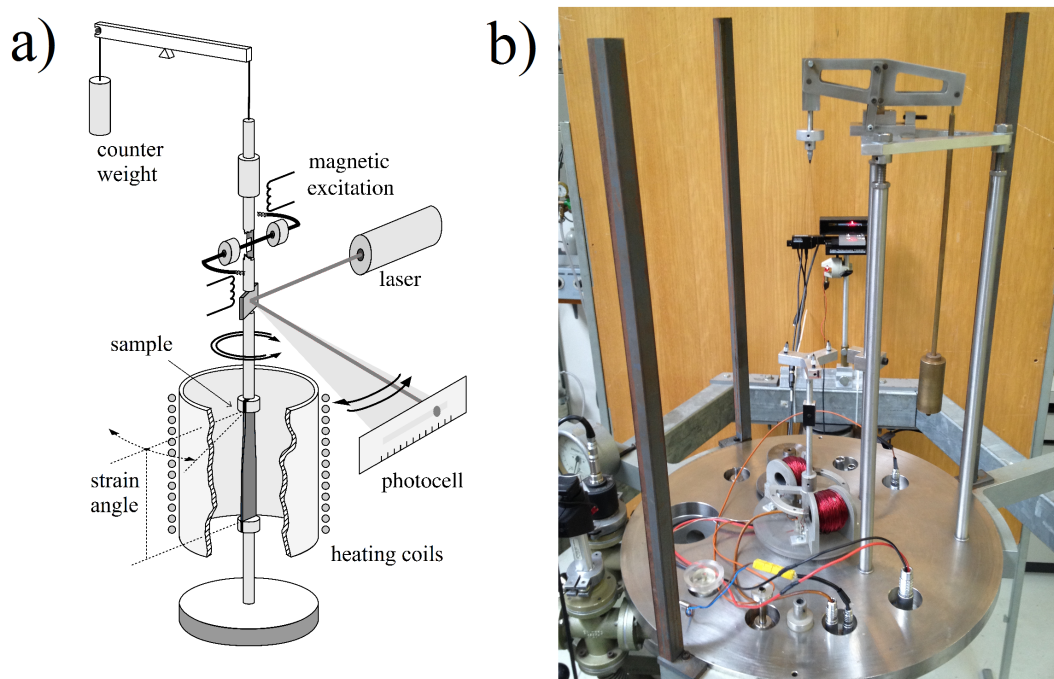
Figure 2.8 – a) Sketch of an inverted forced torsion pendulum. b) Photo of the upper part of the mechanical spectroscopy experimental installation. The balance with the counter weight is visible in the upper part. The mirror (black) in the middle reflects the laser spot to a photocell in the background. The electromagnets (red) excite the rod in torsion. The sample is situated below the metallic disc and cannot be seen on the photo.
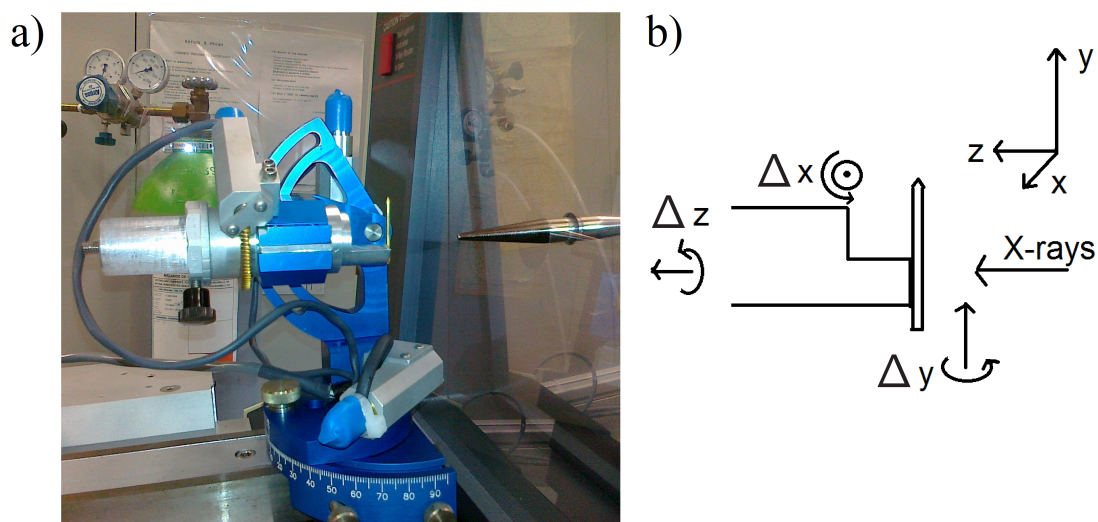
Figure 2.9 – a) Laue camera in back-reflection with a sample in the centre. The incoming beam from the right side is reflected onto the screen surrounding the beam nozzle (right). b) Schematic drawing of the rotational axes of the goniometer head. The screen corresponds to the xy-plane

A calibration with a sample of known shear modulus permits to measure the absolute value of the shear modulus of any unknown sample. More details on the calibration procedure can be found in the thesis of John Hennig [Henn10]. If not stated differently, the torsion pendulum is used in constant strain mode. This means that the input voltage is adapted for each measurement point in order to have a maximum vibration amplitude of 10^{-5} at the sample surface.

2.3   X-ray Diffraction with a Laue Camera

X-ray diffraction was performed on single crystalline or bi-crystalline specimens either to ensure the unique lattice orientation or to measure the misorientation of large grains. X-rays have a small penetration depth for gold based samples. With a common laboratory source, the X-rays probe a surface layer of several μm. When an electromagnetic wave strikes a periodic array of atoms, the wave is scattered and reflections of high intensity only appears in special directions where constructive interference occurs. An incoming wave of wave-vector $\vec{k} = 2\pi\vec{n}/\lambda$ produces a reflection spot in the direction of the outgoing wave of wave-vector $\vec{k'} = 2\pi\vec{n'}/\lambda$ if the difference of the wave-vectors

$$\vec{K} = \vec{k'} - \vec{k} \tag{2.19}$$

is a vector of the reciprocal lattice [Ashc81c]. The reciprocal lattice is defined as the ensemble of all wave-vectors $\vec{K}$ that fulfil the condition $\exp(i\vec{K} \cdot \vec{R}) = 1$ for all lattice vectors $\vec{R}$ of the direct lattice. The reciprocal lattice of an fcc lattice is a body-centred cubic (bcc) lattice.

In order to make sure that at least some directions produce constructive interference, the Laue method consists in using polychromatic instead of monochromatic X-rays [Ashc81a]. Figure 2.9 a) shows the measurement chamber of a Laue camera. The incoming X-ray beam from the right hits the sample and is back-reflected on the CCD screen surrounding the beam guide on the right. The sample can be moved in space and turned with the help of a goniometer stage.

The CCD camera allows a real time observation of the diffraction pattern produced by the crystal zone hit by the X-ray beam. If the probed part of the sample is single crystalline, the diffraction pattern will be a stereoscopic projection of the reciprocal lattice. An example of a diffraction pattern seen along the [111] crystallographic direction is shown in Figure 2.10.

The crystal orientation is always probed locally since the beam spot usually has a diameter of 0.5 mm. Therefore, an abrupt change in the diffraction pattern when moving the X-ray spot indicates the presence of a GB. If the diffraction spots are broadened or if the pattern turns continuously, the crystal lattice is not unique over large distances and it is a sign for a high dislocation density. A multitude of small diffraction spots is an evidence for a polycrystalline microstructure.
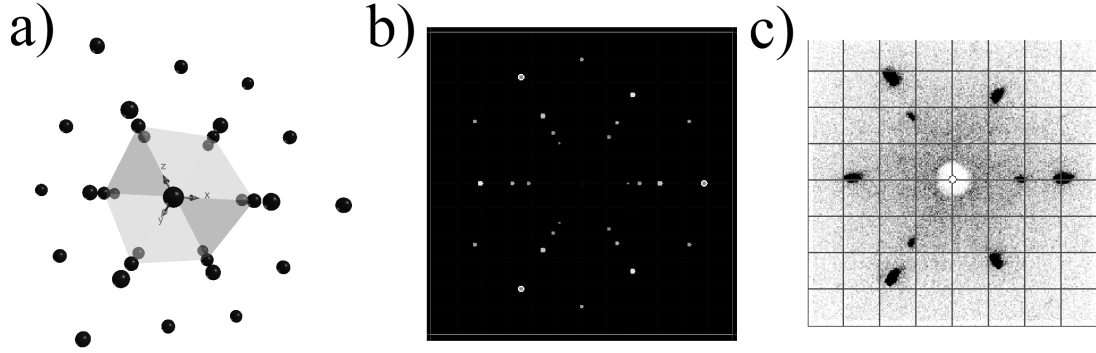
Figure 2.10 – a) bcc lattice seen along the [111] crystallographic direction. The cubic unit cell is shown in grey. b) Simulated Laue diffraction pattern for the [111] direction. The spot size reflects the intensity of the reflected beam. c) Diffraction pattern of a gold alloy single crystal aligned along the [111] direction.

In the framework of the present thesis, the Laue camera was used to characterize samples, to show the single or poly-crystalline nature of samples used for mechanical spectroscopy experiments and to characterize grain boundaries for example in bi-crystals. One important parameter for describing bi-crystals is the misorientation angle θ of adjacent grain orientations. It is defined as $\theta = \sqrt{\psi_1^2 + \phi^2 + \psi_2^2}$, where ψ_1, ϕ and ψ_2 are the Euler angles needed to rotate the crystal lattice of grain 1 into the crystal lattice of grain 2.

Since the cubic system has a high symmetry, the Euler angles are not uniquely defined. The misorientation angle is then understood to be the smallest angle within the above definition. Practically, the misorientaiton angle permits to distinguish between low angle grain boundaries (LAGB) and high angle grain boundaries (HAGB). LAGBs are commonly defined to have a misorientation angle below 10°.

In order to measure the misorientation between two adjacent crystallites, the diffraction pattern of both grains needs to be indexed. A general method to establish sample orientation and to calculate setting angles is described in [Busi67]. The indexing is done automatically by a software, which calculates first angles between reciprocal lattice direction. With the knowledge of the distance between screen and sample, one can attribute an angle to each pair of diffraction spots. These angles are then compared with theoretical angles for an fcc crystal and the software attributes lattice directions to each diffraction spot.

Figure 2.11 shows the diffraction patterns of two grains separated by an LAGB. Due to the indexing of most diffraction spots, the patterns can be compared to each other and the black arrows in Figure 2.11 a) indicate the position of the corresponding spots of b). In order to bring pattern a) in superposition with pattern b), the crystal lattice of a) should be turned around the x-axis and slightly around the y-axis. The program calculated misorientation angles $\Delta x = 5.65°$, $\Delta y = 3.18°$ and $\Delta z = 0.44°$. The total misorientation of this GB is then $\sqrt{\Delta x^2 + \Delta y^2 + \Delta z^2} = 6.5°$.

29
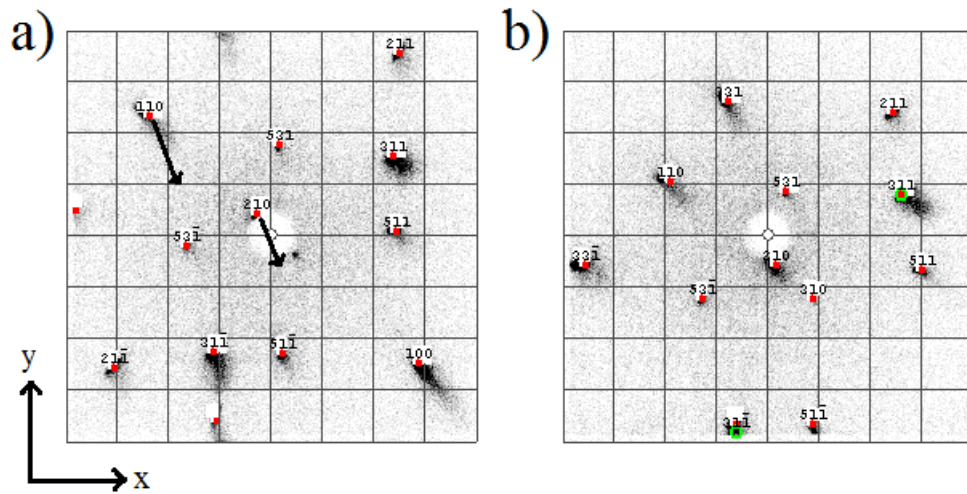
Figure 2.11 – Indexed Laue patterns of a sample containing a low angle grain boundary. The pattern shown in a) has to be rotated around the y-axis and around the z-axis to obtain the pattern b). The black arrows indicate the new position of the diffraction spots [110] and [210] in b).
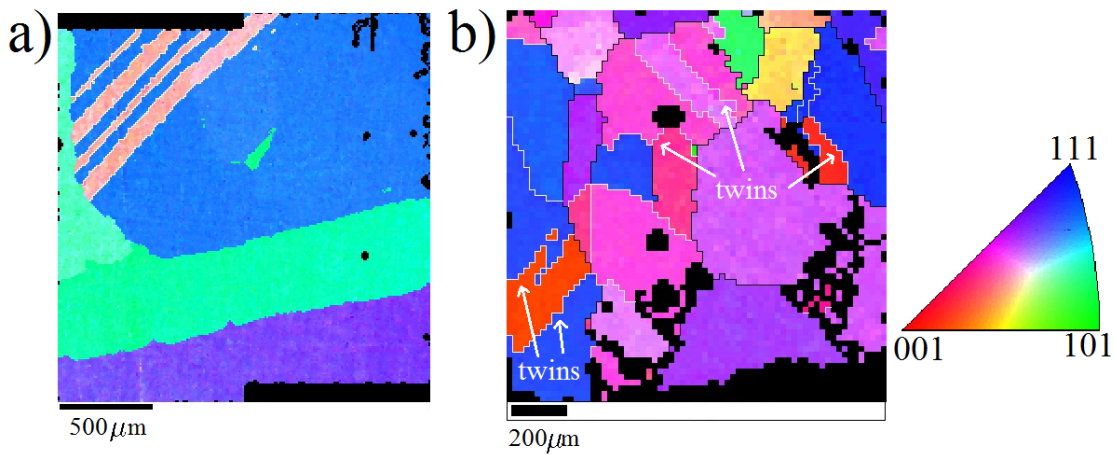
Figure 2.12 – EBSD maps of a) a copper sample with very large grains and b) a gold alloy polycrystal. The grain colouring is the inverse pole figure colouring with respect to the sample axis (corresponds to the horizontal axis of the maps). Twin boundaries are shown in white.

The misorientation measurement for a general boundary was usually done at several positions along the GB by analysing pairs of diffraction patterns at different positions. The scattering along a boundary is typically of the order of 1-3°.

2.4 Electron Back Scattering Diffraction

Another experimental technique that can visualize the local crystal orientation is Electron Back Scattering Diffraction (EBSD). Instead of X-rays, an electron beam interacts with the sample surface. Inside a scanning electron microscope, an additional screen (CCD camera) registers a diffraction pattern composed of the so-called Kikuchi-bands. The bands are best visible if the sample surface is titled by 70° with respect to the electron beam.

The microscope works in scanning mode, which means that the sample surface is probed pixel by pixel. At each position the diffraction pattern is analysed automatically and the crystal orientation is determined. The EBSD method produces maps, from which the grain structure at the surface can be extracted.

In order to visualize the grain structure, pixels in the maps are coloured according to the local lattice orientation. One choice is to colour the pixels with the inverse pole figure (IPF) scheme. For this, one axis of the sample is chosen as reference, for example a growth direction or a deformation axis. The lattice orientation in this direction determines the pixel colour. Figure 2.12 shows two examples of IPF maps. The colour legend shows one eighth of a pole figure circle, which is sufficient to represent all lattice orientations of a cubic crystal system. If the [111] direction is close to the reference axis, the grain will be coloured in blue, a [100] direction would be red.

The advantage of this colouring is that the contrast is quite high and that it is a "continuous" way of colouring. This means that small differences in the lattice orientation results in similar colours and high angle grain boundaries are marked by a large difference of colour.

Figure 2.12 a) shows an EBSD map of a copper polycrystal that has been grown by the Bridgman technique. The growth direction is the horizontal axis in the EBSD map, which has also been chosen as a reference axis for the inverse pole figure. It can be seen that the sample contains mainly blue and green grains, which corresponds to growth directions along the [111] and the [110] axis respectively. In the upper left corner, there are four pink twins. A misorientation angle of 60° between the light pink and the blue grains is marked with thin white line to underline twinning.

Figure 2.12 b) shows a gold alloy polycrystal, which was obtained by cold deformation of a single crystal. General HAGBs are marked by a black line between individual pixels to distinguish from the special twin boundaries, which can also be interpreted as a stacking fault of dense planes in an fcc crystal. The twin boundaries have a very low surface energy and their microscopic structure is crystalline. It is likely that their physical properties differ drastically from other HAGBs and should be treated differently.

3 Experimental Results

In this chapter, the mechanical loss spectra of the 18-carat yellow gold alloy containing 30% Ag atoms and 10% Cu atoms are analysed. An overview is presented on the various relaxation mechanisms that can be observed in the intermediate temperature range (around half the melting temperature). A particular attention is given to grain boundary relaxation. The results are analysed with the help of other experimental techniques like metallography, optical microscopy, X-ray diffraction and electron microscopy.

The first part focuses on recrystallization phenomena and the transition between a deformed single crystal and a fully recrystallized polycrystal. The second part analyses the presence of Low Angle Grain Boundaries (LAGB) and their influence on the loss spectrum. The grain boundary peak of a polycrystal is then analysed in different materials and under different experimental conditions such as changing the strain amplitude or the frequency. In the third part, we investigate isolated grain boundaries in bi-crystals, where different parameters like the boundary plane orientation or the grain boundary density can be controlled.

3.1 Mechanical Loss Spectra of Yellow Gold Polycrystals and Single Crystals

3.1.1 Typical Spectrum of a Polycrystal

A typical mechanical loss spectrum of a yellow gold polycrystal is shown in Figure 3.1 as a function of temperature. The measurement frequency is $f = 0.5$ Hz. Both heating and cooling curves are plotted, which are very well superimposed at all temperatures. Below 500 K, the mechanical loss is flat. Around 600 K, a first peak P1 appears and it is followed by a second peak P2 at about 750 K.

The right axis shows the dynamic shear modulus, which is recorded at the same time as the mechanical loss. At low temperatures, the modulus decreases slightly in a linear fashion, which is a general behaviour due to the decrease of the elastic modulus. At the peak temperatures, an

additional drop of the dynamic modulus occurs. The amplitude of the drop is directly related to the peak height via the relation $\delta M/M = 2\tan\phi_{max}$ (2.14) in the case of a Debye peak.

The relative variation of the modulus is measured with a very high precision and the measurements on one sample are well reproducible. On the other hand, the absolute value of the modulus has a large systematic error of the order of 10%, because the dimensions of the sample cannot be controlled better than 2-3% and the modulus depends on the square of the thickness.

In order to fit the peaks in the mechanical loss spectrum, the high temperature background must be taken into consideration. It has been shown by Schoeck [Scho64] that an exponential background can be described by three parameters K, n and H_{act}:

$$\tan\phi = \frac{K}{(2\pi f)^n}\exp\left(-\frac{nH_{act}}{k_B T}\right) \tag{3.1}$$

where f is the frequency, n is the broadening factor of the background and K is the amplitude, which are valid over limited ranges of temperature. If this formula is used to fit a temperature spectrum, f is constant in a forced pendulum and (3.1) reduces to a common exponential function.

In most cases it is not possible to determine if the observed increase in the mechanical loss at high temperatures is actually an exponential background or if it is the low temperature side of a relaxation peak. In fact, a Debye peak reduces to an exponential function in the approximation of small values of $k_B T$ with respect to the activation energy or for the high frequency limit [Scha01].

The mechanical loss spectrum of the yellow gold polycrystal can be fitted using a sum of two broadened Debye peaks (Equations (2.11) and (2.18)) and a high temperature exponential background (3.1). The results of the fit and its decomposition into peaks plus background are shown in Figure 3.2. It can be said that the quality of the fit is very good. Only slight deviations occur at the very high temperature part. The fits allow one to extract the peak temperature at its maximum with high precision, but they do not contain enough information to extract the activation energy, the limit relaxation time and the broadening factor β from a single temperature scan, since the mentioned parameters are correlated and cannot be fitted at the same time. H_{act} and τ_0 can be obtained with an Arrhenius plot. The method is described later in more detail.

The peak P1 has been studied previously and attributed to a Zener relaxation [Zene47]. The relaxation mechanism is related with the reorientation of elastic dipoles formed by pairs of copper atoms. Under the application of an external stress, atoms locally rearrange, thereby minimizing the strain energy. For low concentrations of one alloying element, for example Cu, the Zener mechanism can be related to the relaxation of stress due to the reorientation of substitutional atom pairs as shown in Figure 3.3 a).
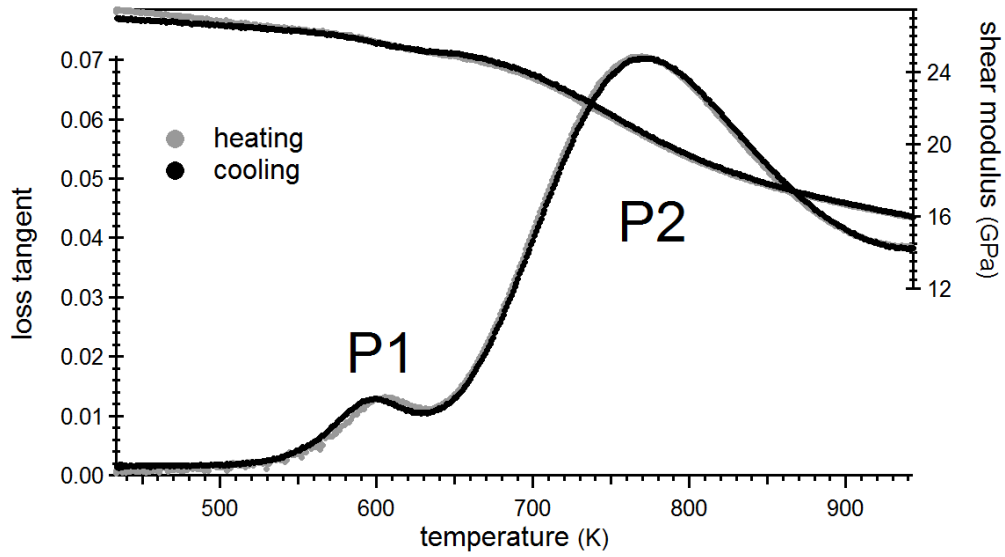
Figure 3.1 – Typical mechanical loss spectrum of a yellow gold polycrystal as a function of temperature together with the corresponding dynamic shear modulus. The heating and cooling are well superposed.
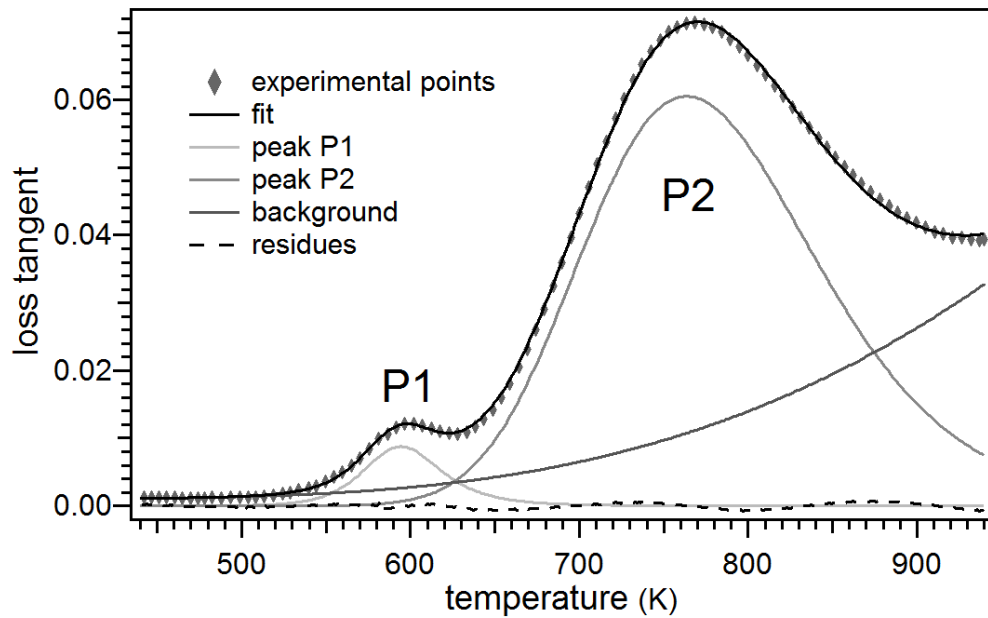

Figure 3.2 – Decomposition of the polycrystal spectrum into 2 broadened Debye peaks and an exponential background. The fitting curve to the data points and the residues are also shown.

In more concentrated alloys as in the presented case with 10% Cu atoms, the substitutional pairs are not isolated any more and the atomic structure resembles to that in Figure 3.3 b). Due to different interaction between identical atom pairs and dissimilar atom pairs, the lattice structure is locally distorted. The Zener peak has been studied in detail by Hennig et al. [Henn09a, Henn09b, Henn10] in the AuAgCu system. It has been shown that the peak height depends quadratically on the copper concentration. The Ag atoms play the same role as Au as solvent. Removing the Ag atoms does not change the system from a fundamental point of view. The relaxation peak P1 in the present yellow gold alloy is due to the same mechanism as the one found in the binary AuCu system.
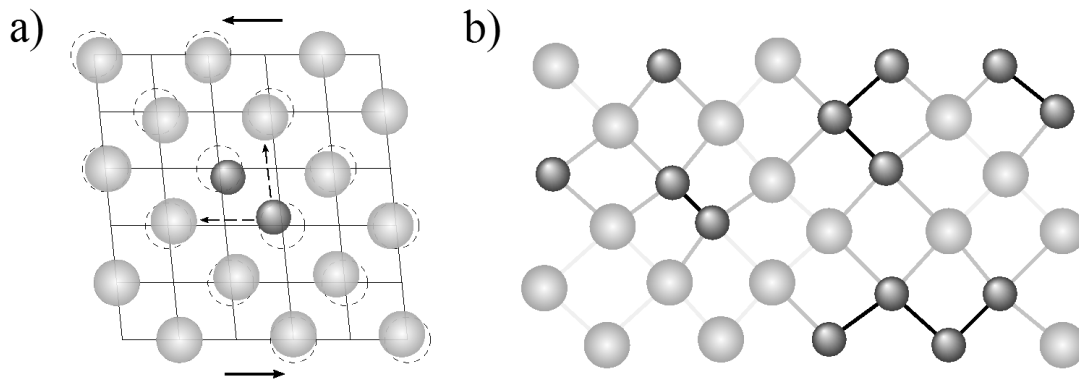
a)   b)

Figure 3.3 – Elastic dipole formed by a pair of substitutional atoms in a diluted alloy. The dipole reorients under an external stress to minimize the elastic strain energy. b) Schematic image of the atoms in a concentrated alloy. The lattice is locally distorted. Taken from [Henn10].

The peak P2 dominates the loss spectrum between 700 K and 900 K. It is a broadened Debye peak that appears somewhat tilted due to the presence of the high temperature background. In Figure 3.2 the maximum of the peak P2 after background subtraction lies at slightly lower temperature than the maximum of the original measurement points. The height of the polycrystal's peak varies between 0.55 and 0.7 between one polycrystalline sample and another.

The fact that P2 is broadened is a first indication of its microscopic origin. It is very improbable that P2 is due to a point defect relaxation, since for single atom movements, the energy barrier that has to be overcome and the attempt frequency take well defined values. For a point defect relaxation, it can be expected that the peak shape is very close to a perfect Debye peak without broadening. A widely spread peak indicates a spread of energies and relaxation times.

Dislocation movement is one possibility that has to be considered as origin for the P2 peak. In high purity metals, many different dislocation peaks are observed at temperatures below 300 K. These peaks are caused by gliding dislocations that interact with the crystal lattice or they are due to interactions of dislocations with point defects. A moving dislocation can be described by the advancing of small line segments. A part of the dislocation line leaves its position and moves to an energetically more favourable position.

Another possible source for a relaxation causing the peak P2 are grain boundaries. Due to the spectroscopic character of internal friction, i.e. to show characteristic peaks associated with a damping mechanism, it will be quite useful to analyse the spectrum of a single crystal.

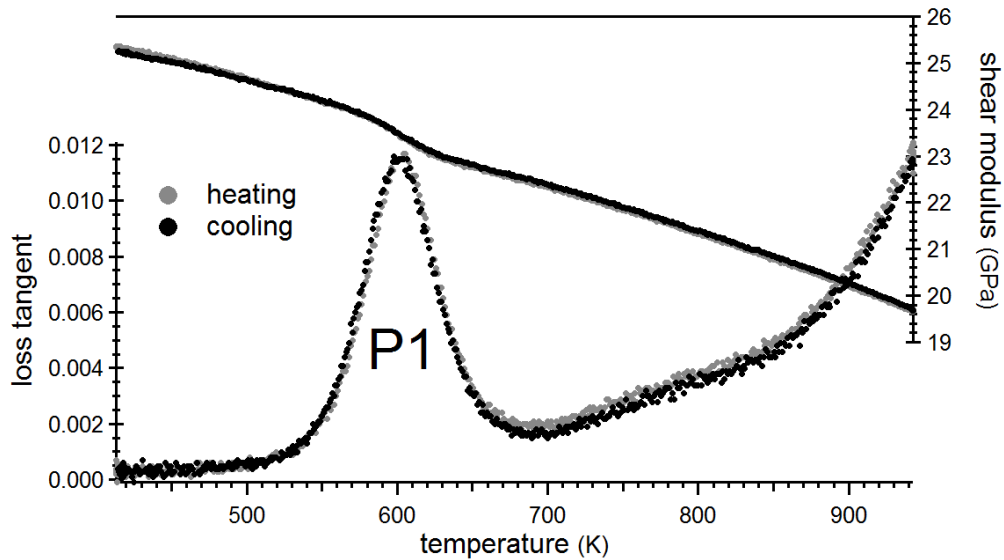### 3.1.2   Mechanical Loss of Single Crystals

Figure 3.4 – Mechanical loss and dynamic modulus of a yellow gold single crystal.

In a first step, a single crystalline specimen obtained from the same material as the polycrystal is measured by mechanical spectroscopy. Such a sample contains only one crystalline orientation without grain boundaries. On the other hand, dislocations are present in both single crystal and polycrystal. However, the dislocation density is probably higher in the polycrystal. In Figure 3.4, the spectrum of a single crystal in heating and cooling is presented. The peak P1 is centred at 600 K and the high temperature part shows a flat background with two different slopes. One could argue that there is a very flat peak at around 800 K. As before, heating and cooling are well superimposed, which shows that the microstructure is stable.

Figure 3.5 a) shows the mechanical loss spectrum of a polycrystalline sample in comparison to the single crystalline sample. The peak P1 is present in both spectra since the material is the same and therefore Cu atom pairs cause a relaxation peak in both samples. The peak P2 is only present in the polycrystal and can therefore be related to the presence of grain boundaries. If it was due to dislocations, a relaxation peak should be observed in both the single crystal and the polycrystal. With respect to the polycrystal, the single crystal has a very low mechanical loss at temperatures above 700 K. Subtracting P2 from the polycrystal's spectrum is not sufficient to superpose both spectra. The polycrystal possesses a much higher background. In the past, such a background has been attributed to the motion of dislocations [Tkal09].

Figure 3.5 b) shows isothermal measurements of the high temperature background of the
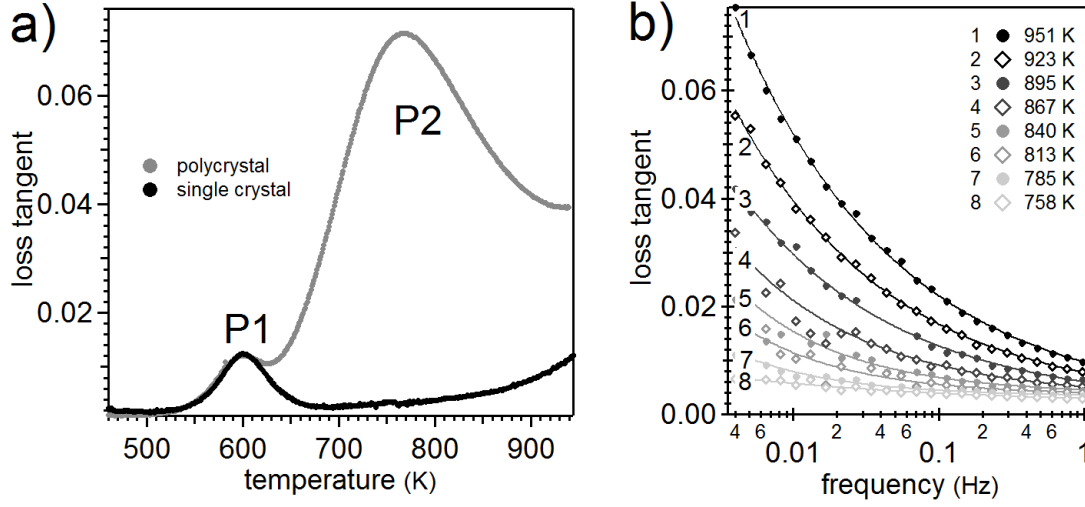
Figure 3.5 – a) Comparison of single and polycrystal of the same material. P2 is only present in the polycrystal and absent in the single crystal. The background in the single crystal is much lower than in the polycrystal. b) Isothermal measurements of the monocrystalline background. For lower temperature the background shifts to lower frequencies.

single crystal. When decreasing the temperature, the background shifts to lower frequencies as it could be expected from a thermally activated process.

The background is exponential and can be described by Equation (3.1) with $n = 0.37 \pm 0.02$. The black lines in Figure 3.5 b) are fits to the data points. The parameter n corresponds directly to the slope when tracing the mechanical loss versus the frequency on a log-log scale (Figure 3.6 a). One can rewrite Equation (3.1) as

$$\ln(\tan\phi) = \ln(K) - n\ln(2\pi) - n\left[\ln f - \frac{H_{act}}{k_B T}\right] \tag{3.2}$$

and it becomes clear that, for K and n independent of the temperature and the frequency, two isothermal spectra at temperatures T_1 and T_2 can be superimposed with a shift in the $\ln(f)$-axis. Figure 3.6a) shows the master curve that has been constructed from five isothermal scans at 951 K, 923 K, 895 K, 867 K and 840 K. The activation energy of the background can be obtained from the offset on a logarithmic frequency scale that is necessary to superimpose the different frequency scans. Figure 3.6 b) shows the offset as a function of the inverse measurement temperature for the five highest temperatures. The slope of the linear fit corresponds to E_{act}/k_B and we find $E_{act} = 1.96 \pm 0.04$ eV for the background of the single crystal.

The activation energy of the background is slightly higher than that of the Zener peak P1. Since the broadening factor $n = 0.37$ is much lower than 1, it is likely that the underlying relaxation mechanism is not a point defect relaxation but a mechanism that includes the movement of multiple atoms with varying relaxation times τ. One possibility is that the background issues from a dislocation relaxation mechanism.
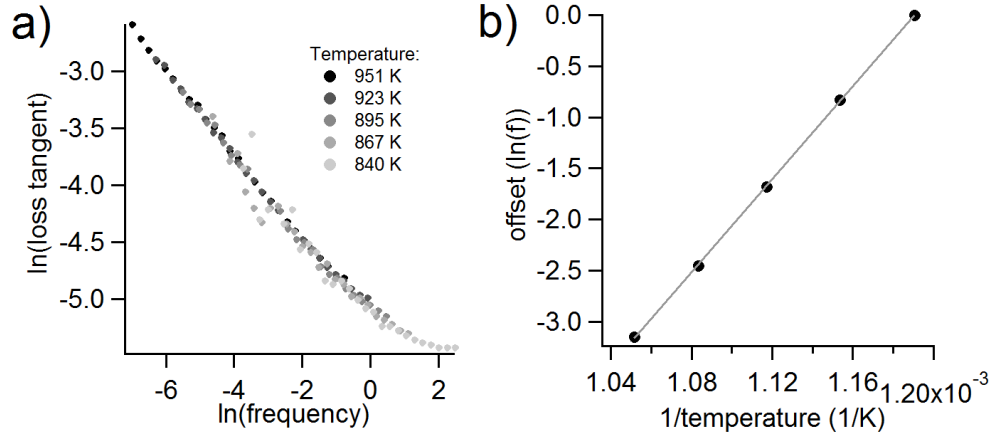
Figure 3.6 – a) Master curve from the frequency scans at high temperatures. The exponential nature of the background gives a line on a log-log scale. b) Activation energy of the background from the offset of the master curve is equal to $E_{act} = 1.96 \pm 0.04$ eV.

3.1.3 Activation Parameters
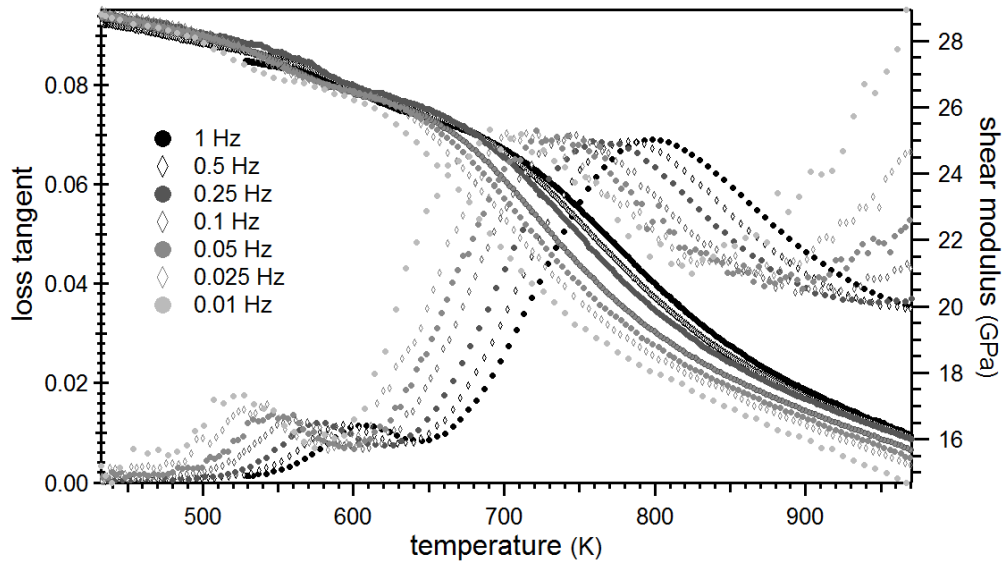
Figure 3.7 – Polycrystal spectrum as a function of temperature, measured at different frequencies from 1 Hz to 0.01 Hz. Both peaks and the background shift to lower temperatures when decreasing the frequency.

In order to characterize the peak P2, the activation parameters were measured with an Arrhenius plot. For this, the polycrystal was measured in isochronal mode as a function of temperature (Figure 3.7) and in isothermal mode as a function of frequency (Figure 3.8). Both modes show the characteristic feature of thermally activated processes over the whole measurement range. By changing either the frequency or the temperature, the peaks shift, keeping their initial shape.

One feature of the Zener peak P1 is the so called Curie-Weiss behaviour [Mort67, Henn09b] when approaching a critical ordering temperature from solid solution. The relaxation strength and thus the peak height increase when the temperature is decreased. It is observed in the temperature spectra, where P1 increases for lower frequencies and it can be seen in the frequency scans of Figure 3.8 b) that the peak increases for decreasing measurement temperatures.
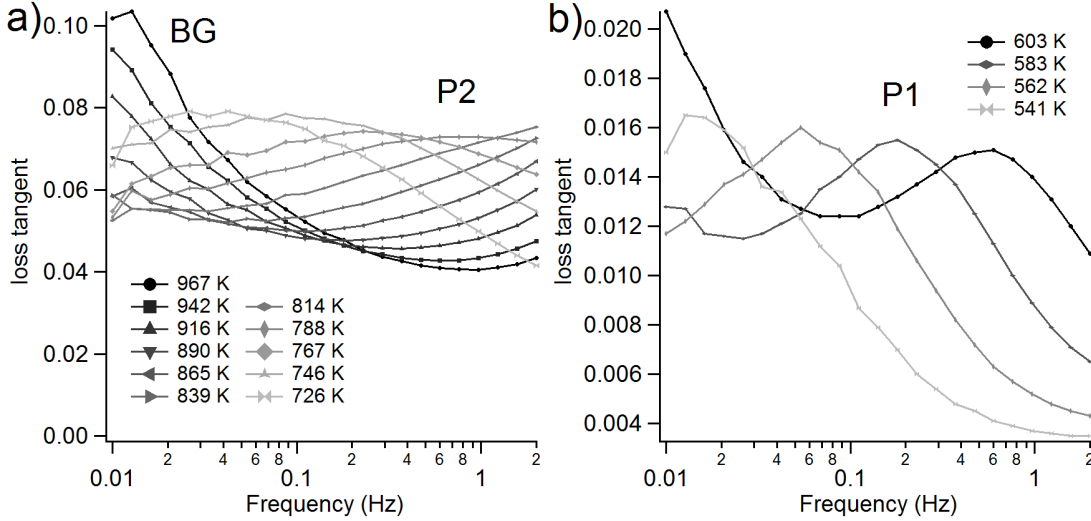
Figure 3.8 – Frequency scans at various temperatures. In a), the higher temperatures are shown where the background (left boarder) and the P2 peak are probed. b) shows lower temperatures. The peak P1 shifts to lower frequencies when decreasing the temperature.

The peak P2 does not show any change in height when the frequency or the temperature is changed. The relaxation strength is independent of T and of f. From the relative shift of the peak maximum, the activation energy can be extracted. For this purpose, the peak positions of P1 and P2 are found for every temperature scan of Figure 3.7 with the help of the fitting procedures described in the beginning of this chapter. The uncertainties of the fits contributes to the statistical errors on the temperature scale in the Arrhenius plot.

When tracing the relaxation time $\tau = 1/\omega = 1/(2\pi f)$ on a logarithmic scale as a function of the inverse peak temperature, the activation energy can be found as the slope of the linear fit multiplied by k_B. Figure 3.9 a) and b) show the Arrhenius plots for P1 and P2. The data points are taken from the isochronal measurements shown in Figure 3.7. For both peaks, the 7 data points from the temperature scans in the upper part lie on a straight line. One additional data point obtained from a measure on a free decay torsion pendulum has been included in the diagrams. The corresponding temperature spectrum is shown in Figure 3.10. For P1, the linear fit passes through all data points and therefore, the free mode has been included in the analysis for the activation parameters. For the Zener relaxation, we find $H_{act} = (1.48 \pm 0.2)$ eV and a limit relaxation time $\tau_0 = (7 \pm 2) \cdot 10^{-14}$ s. This value for τ_0 agrees very well with the estimations from the Debye frequencies of Au and Cu done in Chapter 2.

For the grain boundary peak P2, the activation energy calculated from the measurements in
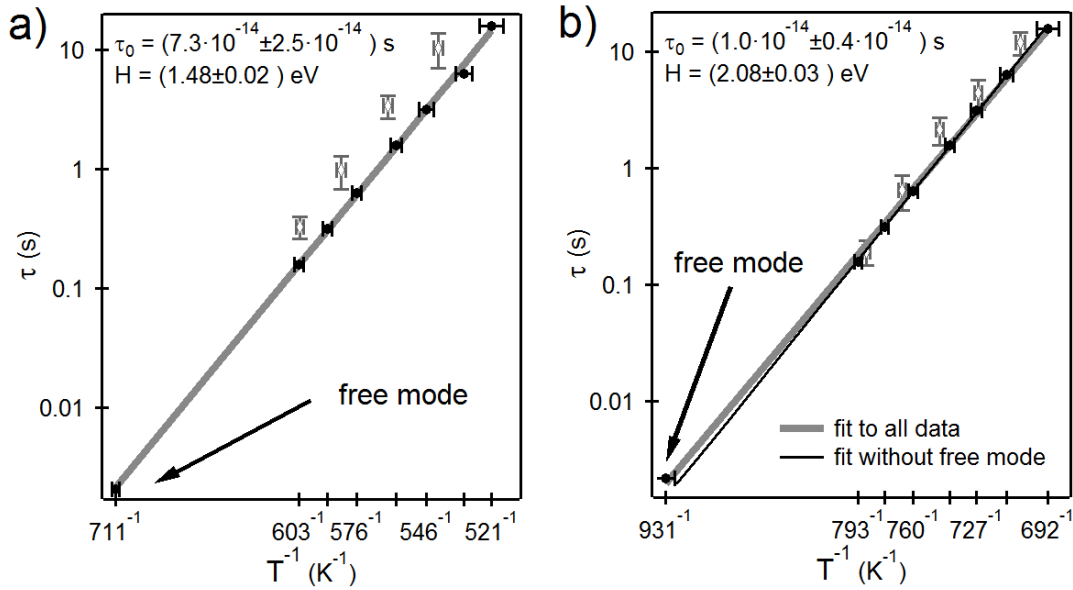
Figure 3.9 – Arrhenius plots a) for the Zener peak P1 and b) for the GB peak P2 from the isochronal measurements of Figure 3.7 (black markers). The open grey markers are from isothermal measurements of Figure 3.8 and are not included in the fit. The error bars include statistical errors from the fitting procedure and systematic errors. The black line in b) is the best fit if the data from free decay mode is excluded from the fit.
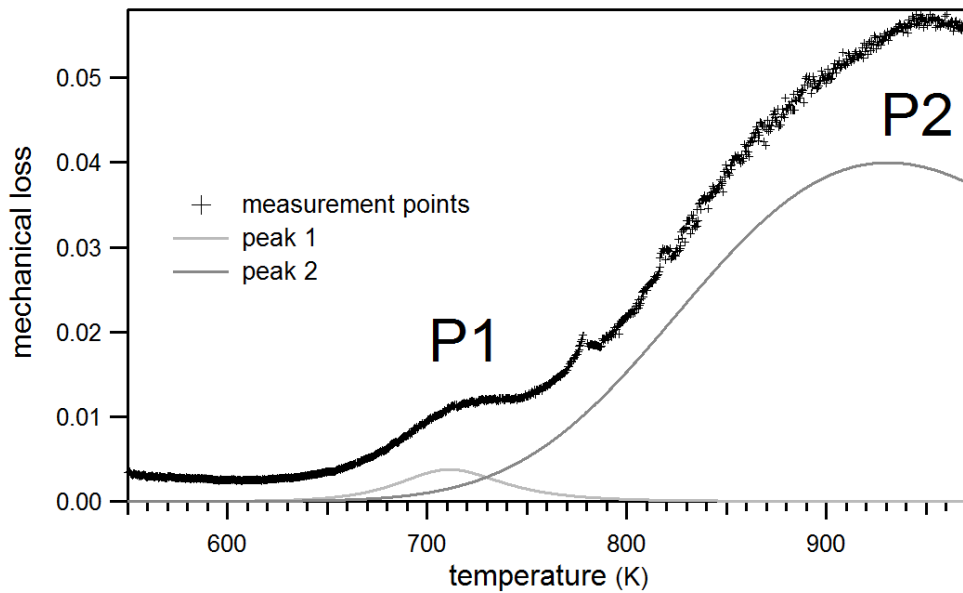
Figure 3.10 – Polycrystal spectrum measured in free decaying mode. The resonance frequency varies between 70 Hz and 80 Hz. Peaks P1 and P2 are shifted to much higher temperatures.

forced mode only gives a value of $H_{act} = (2.3 \pm 0.1)$ eV and $\tau_0 = 3 \cdot 10^{-16 \pm 1}$ s. The activation enthalpy of the GB peak is significantly higher than the one of P1 which is related to Cu diffusion. It is an apparent value since the corresponding relaxation time shows a too low value leading to an attempt frequency much higher than the Debye frequency.

In Figure 3.9 b), the thin black line fitting only the upper points does not pass through the point from free mode. This means that not all data points are compatible with the same linear fit and thus a unique and constant activation enthalpy. If the measurement in free decaying mode is included in the analysis, the Arrhenius plot yields a smaller activation enthalpy and a higher relaxation time. Since the additional point is far away from the others, the uncertainties are significantly smaller and we find $H_{act} = (2.08 \pm 0.3)$ eV and $\tau_0 = (1.0 \pm 0.4) \cdot 10^{-14}$ s. The enthalpy of the GB peak is still higher than that of the point defect peak P1 and the limit relaxation time is now of the same order of magnitude for both peaks.

Since the data points for the GB peak do not show a linear relationship, it is possible that the microscopic origin of the GB peak is related to some sort of phase transition, which leads to apparent activation parameters. It is a problem from a practical point of view, since for many experiments, only a small range of the peak temperature can be explored. One way to determine if the activation enthalpy reflects an apparent value or the real barrier height of the relaxation process is to examine τ_0. If its value leads to non-physical frequencies much below the Debye frequency, one is probably concerned with apparent activation parameters.
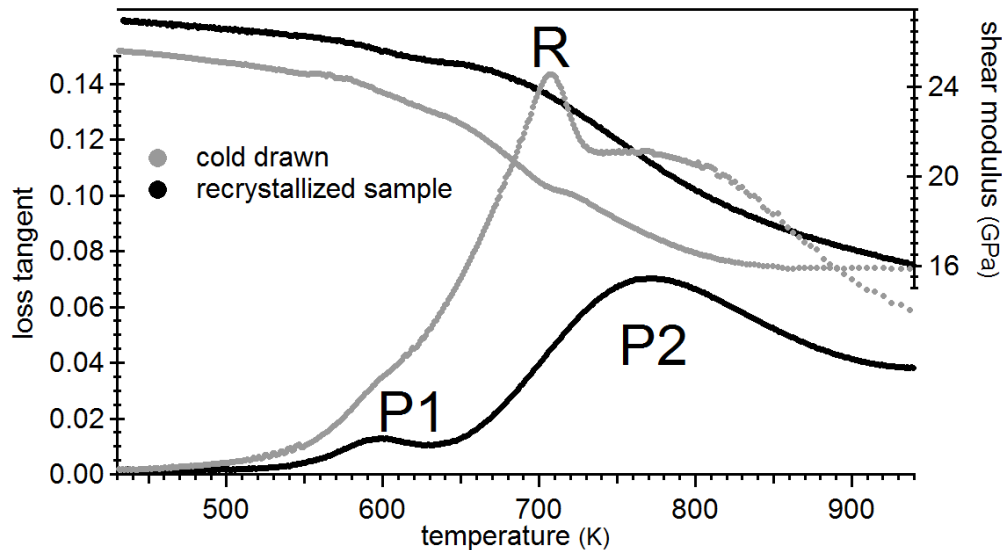
3.1.4 Recrystallization Peak

Figure 3.11 – Mechanical loss spectrum of a heavily deformed specimen. Recrystallization is marked by a maximum of the mechanical loss and an increase of the dynamic modulus.

Recrystallization of a heavily deformed solid takes place when the material is heated up and

dislocation mobility increases. During the first stage, called recovery, the dislocation density is reduced by mutual annihilation of dislocations with opposite Burgers vectors. Reordering of the remaining dislocations leads to the formation of sub-grains (low dislocation density) and sub-grain boundaries (high dislocation density) [Hump95]. The formation of well-defined grain boundaries followed by grain growth leads to the final polycrystal.

Figure 3.11 shows the first heating of a cold drawn specimen with a deformation of 70%, which undergoes recrystallization. Below 700 K, internal friction increases very steeply. The peak P1 is barely visible on top of the exponential curve. At 700 K, a maximum is reached and the mechanical loss drops sharply by approximately 20%. The recrystallization peak R is accompanied by a plateau in the modulus measurement. Above 750 K, the peak shape of P2 can be observed, but it lies at a much higher value. At high temperatures, the modulus increases. After annealing at 950 K for 3 h, the stable polycrystal spectrum is observed in cooling.

The high temperature part of the recrystallization spectrum can be seen as a P2 peak that is superimposed on a much higher background than in the polycrystal. The annealing at 950 K causes the background to further decrease and the fully recrystallized sample shows a lower background.

One indication that R is not a thermally activated relaxation peak is its narrow and asymmetric shape. Secondly, the modulus shows a plateau and not a modulus drop at the peak position. Isothermal measurements of a cold drawn specimen during the first heating (not shown here) confirm that the mechanical loss has an exponential shape at all temperatures and R is only an apparent peak because at 700 K, this background drops sharply in amplitude.

The exponential background is caused by dislocations and since the dislocation density is very high in the original sample, this effect is already visible at comparably low temperatures. The recrystallization peak R marks the temperature at which the dislocations become mobile and move over long distances. Annihilation of dislocations with opposite Burgers vectors occurs and the dislocation density is reduced at once. The reduction of dislocations also causes an increase in the dynamic modulus, not only at the recrystallization temperature, but also during the annealing of the microstructure at higher temperatures.

Just above the peak R, the shape of the grain boundary peak P2 is visible. This indicates that grain boundaries are already formed. Moreover, it means that at the peak temperature of R, the first two states of the recrystallization process are happening: recovery, which means the reduction of excess dislocations and the formation of grain boundaries. Above this temperature, grain growth and further reduction of the dislocation density occurs.

3.2 Grain Boundary Formation Stages

During the first heating of a heavily deformed specimen, different stages of recrystallization like recovery and grain boundary formation happen at the same temperature and it is therefore complicated to observe these contributions to the overall recrystallization process separately. The purpose of this section is to investigate the evolution of the microstructure during the recrystallization process and the relation to the mobility of defects such as dislocations. In a strongly deformed sample, an excess energy is stored in form of dislocations and the energy can be reduced by elimination of dislocations and by reorganisation of a part of the dislocations in form of grain boundaries. It is not clear how the nucleation of grain boundaries is realized.

A common belief is that the new grains start to grow on the fragments of old grain boundaries that existed previous to the deformation process. But what happens if there are no such pre-existing grain boundaries? This situation is encountered in a single crystal that is subjected to cold work. A simple energetic consideration shows that nucleation is not a process where dislocations in a certain volume reorganize spontaneously to create a surrounding grain boundary and a recrystallized grain. The conservation of elastic energy stored in form of dislocations ($\Delta G_V = 4/3 \cdot \pi r_c^3 W$) and released forming a grain boundary ($\Delta G_S = 4\pi r_c^2 \gamma$) leads to

$$0 = -\Delta G_V + \Delta G_S = -4/3 \cdot \pi r_c^3 \cdot 0.5 \Lambda M b^2 + 4\pi r_c^2 \gamma \tag{3.3}$$

where M is the modulus. $W = 0.5 \Lambda M b^2$ is an expression for the energy density per volume in form of dislocations and $\gamma = Mb/(4\pi(1-\nu))$ is the surface boundary energy of a tilt boundary [Hull75]. $b \approx 3 \cdot 10^{-10}$ m is the length of a typical Burgers vector and $\Lambda = 10^{11}$ cm^{-2} is the dislocation density in a cold worked sample. The nucleation radius of spontaneously formed grains is calculated to

$$r_c = \frac{6}{4\pi(1-\nu)\Lambda b} \approx 3 \cdot 10^{-6} \text{m} = 6\mu\text{m} \tag{3.4}$$

This nucleation radius is orders of magnitude too big and the converted energy would be of the order of 10^6 eV. Grain boundaries, at least high angle boundaries, cannot form by this process and nucleation must be a stepwise process.

Hu's model [Hu63] describes the nucleation of new grains first by the formation of zones with high dislocation density and zones with lower dislocation density. The zones with high dislocation density are reorganized into sub grain boundaries and the absorption of more and more dislocations lead to boundaries with higher misorientation angles. A coalescence of sub grains leads then to the formation of a nucleus with high angle grain boundaries.

Figure 3.12 shows a schematic outline of the experiments described in this section. The objective of the experiment is to observe and interpret different recrystallization stages dependent on the initial microstructure. The idea is to start with a single crystal that has a stable structure with a low dislocation density. Upon annealing, the microstructure will change locally since
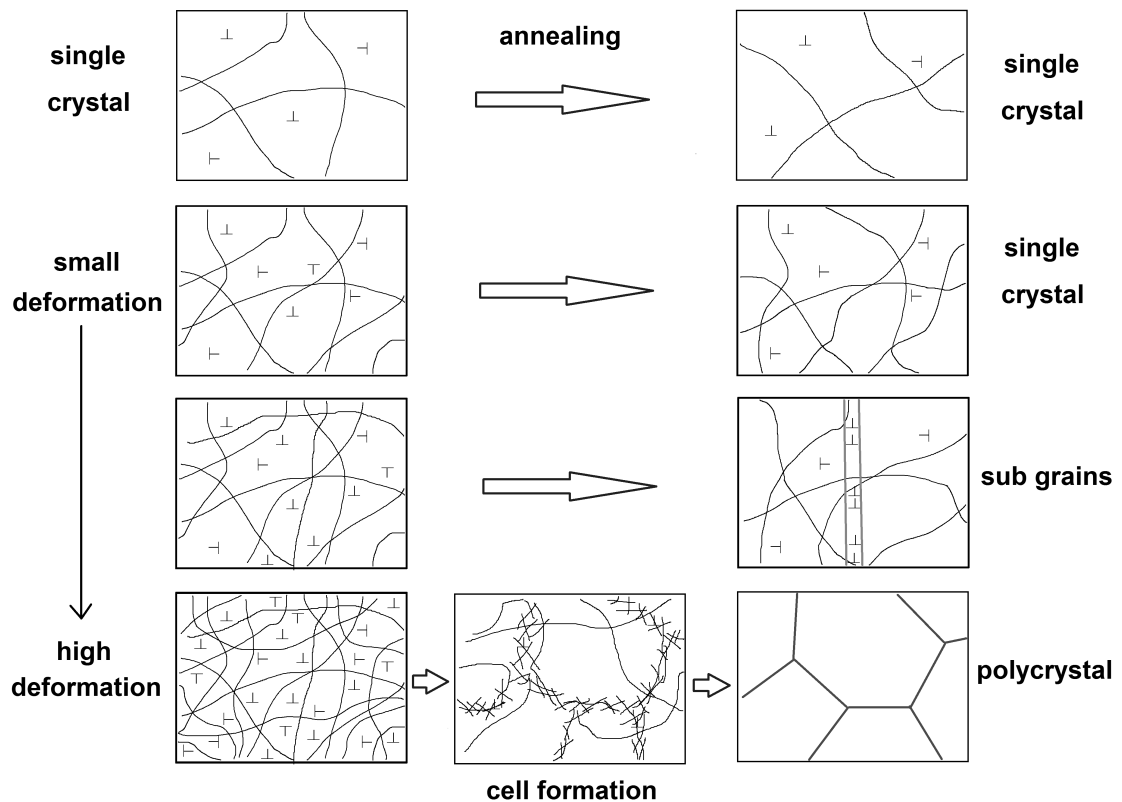
Figure 3.12 – Schematic representation of the deformation experiment. The microstructure after annealing changes according to the initial deformation and the number of dislocations in the sample.

some dislocations become mobile and will find energetically more favourable arrangements. From a global point of view, the structure of the single crystal will not change with annealing.

The dislocation density can be increased by a small amount of cold work, for example by twisting the cylindrical sample by a small angle around its symmetry axis. For a low deformation, the sample is still single crystalline and an annealing process will reduce excess dislocations from the bulk.

A higher deformation will lead to a fundamental change in the microstructure. If at some point there are dislocations of the same type but on different glide planes, it is energetically favourable that these dislocations arrange to form a sub grain boundary. Only with a very high initial dislocation density a classical recrystallization is observed upon heating together with a cell formation process.

In the following, we will show that to each of the four pictures of the right side of Figure 3.12 can be attributed a characteristic mechanical loss spectrum with either relaxation peaks or with a thermally activated background.

3.2.1 Low Deformation

Figure 3.13 – a) Deformations from 2% to 8% of the single crystal cause an increase in the background. b) Glide lines appear on a polished surface during the deformation at room temperature. The main slip system (lines from the left bottom to the right top) is probably a slip in <110> direction on {111} type planes. A secondary slip system can be distinguished in form of lines running from the left top to the right bottom.

The deformation of the single crystal, which has been analysed in Section 3.1.2, was performed stepwise from small to large deformations on the same sa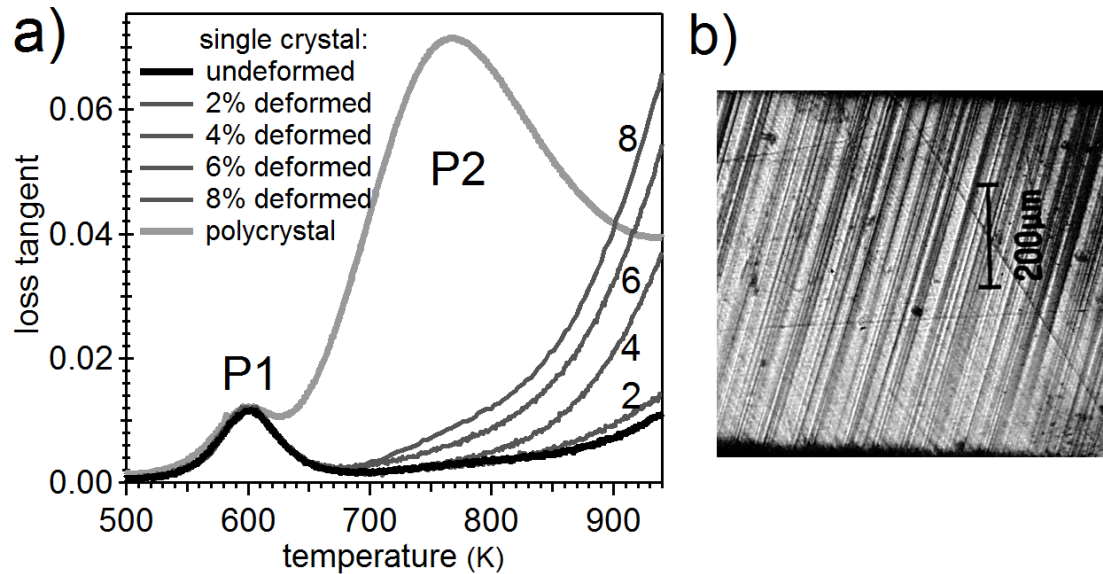mple. The single crystalline wire was clamped on both ends and it was twisted four times into each direction by an angle corresponding to 2%, 4%, 6%, 8% and 10% shear deformation at room temperature around the sample axis. After each deformation, the isothermal and isochronal measurements were performed in the torsion pendulum. After 10% deformation, the sample was polished and etched in order to observe the grain structure.

Temperature scans for deformations up to 8% are shown in Figure 3.13 together with the undeformed single crystal and a polycrystal as reference. The peak P1 is present in all measurements and not affected by deformation. The background shows a gradual increase as a function of plastic deformation. The 2% deformed sample has an internal friction slightly higher than the monocrystalline sample at temperatures above 850 K. From 4% deformation on, the increase in internal friction is much more pronounced for temperatures higher than 700 K and at high temperature the exponential background is higher than for the polycrystal. The deformed single crystal shows no peak in the temperature range of the peak P2.

Directly after the first deformation step, glide lines appeared on a polished face manifesting the presence of mobile dislocations. An optical microscope image is shown in Figure 3.13 b). The Laue pattern (not shown here) was still the same after 2% deformation showing a global

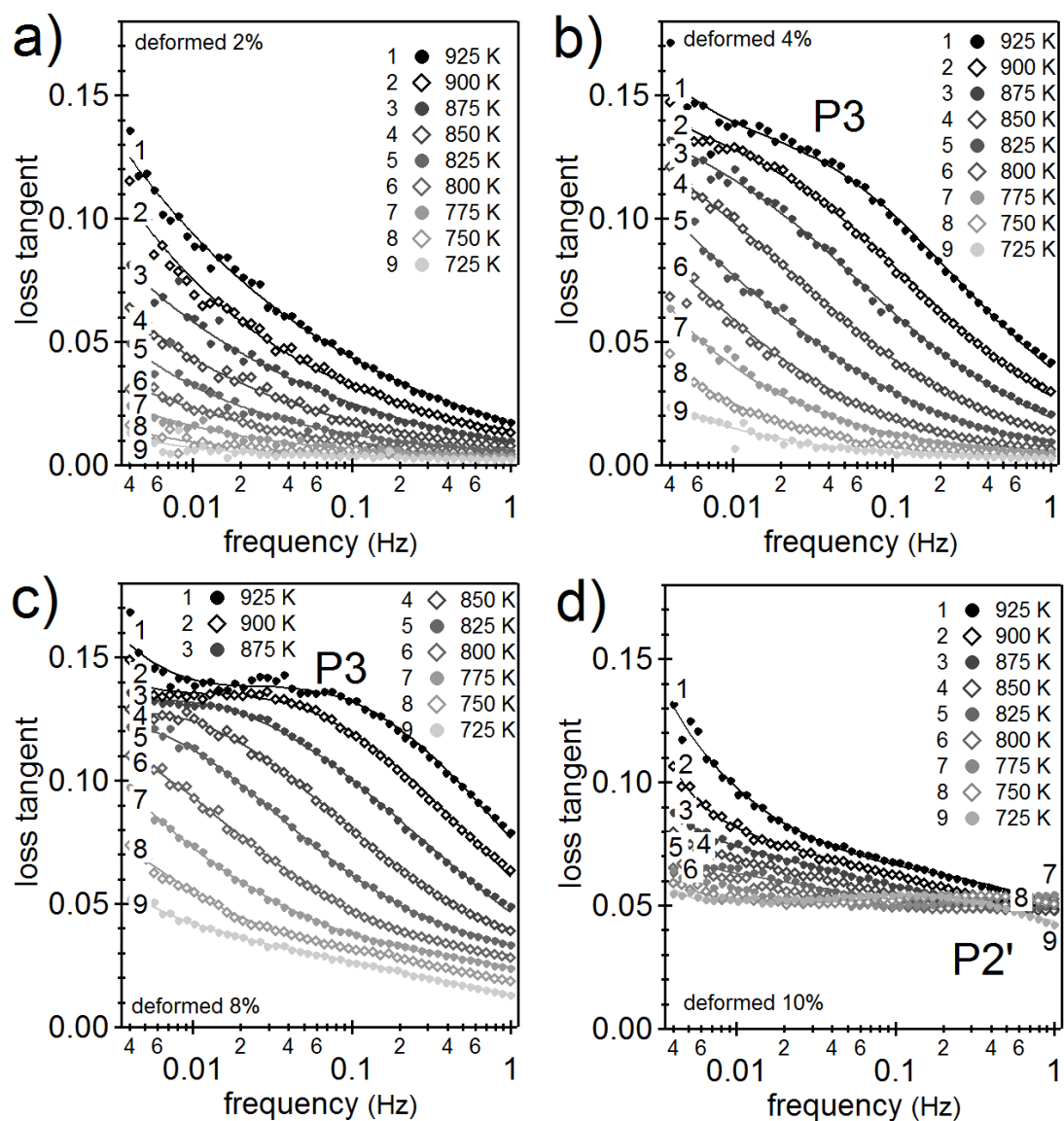Figure 3.14 – Isothermal measurements of the single crystal deformed by a) 2%,b) 4%, c) 8% and d) 10%. The solid lines represent a fit to each measurement curve: An exponential background for 2% deformation and one or two Debye peaks superimposed on a background for higher deformations. In d), several temperatures have been left out for a clearer representation and the additional frequency scan at $T = 675$ K has been added.

single crystalline status of the sample, but the spots were more diffuse with respect to the spots of the single crystal. The direction of the crystal lattice turned slightly by a few degrees over the sample length.

Isothermal measurements for a maximum deformation of 2% (Figure 3.14 a) are very similar to the ones of the original sample shown in Figure 3.5 b). The only difference is that the curves related to the deformed sample have a slightly increased exponential mechanical loss. When fitting the curves with an exponential background (3.1), the broadening factor n is slightly higher than before with a value of $n = 0.38 \pm 0.02$. The energy of the background for 2% deformation is found to be $E_{act} = (2.11 \pm 0.03)$ eV.

For a deformation of 4%, a high temperature peak P3 becomes visible in the frequency scans in Figure 3.14 b). The peak is superimposed on an exponential background and has its maximum at around 0.04 Hz at $T = 925$ K. This peak gets more pronounced for 6% (not shown) and 8% deformation (Figure 3.14 c). The high temperature peak shifts to lower frequencies when the temperature is increased, which is normal for a thermally activated relaxation process.

The attempt to construct master curves from the frequency scans for 4%, 6% and 8% deformation did not succeed since the height of the high temperature peak P3 changed for different measurement temperatures. This can be seen in Figure 3.14 c) for example. The scans for 925 K and 900 K form both a sort of plateau between the high temperature background and the peak P3 at $f = 0.04$ Hz. The $T = 925$ K curve always lies higher than the one for $T = 900$ K in this range and it is therefore impossible to superimpose these two curves with an offset in the frequency direction only. Such changes are more and more remarkable when the deformation is beyond 8%. The impossibility of making a master curve, is a strong hint of microstructure change with temperature during the series of frequency scans.

3.2.2   High Deformation

Each frequency scan in Figure 3.14 lasted about 1 hour, which means that the sample spends more than 4 hours at temperatures above 850 K. During such time interval, if the deformation is high enough, recrystallization may occur leading to a new characteristic spectrum. A comparison between the temperature spectra of the 8% deformed sample before and after a series of frequency scans in Figure 3.15 shows a remarkable difference at around 800 K: an additional peak P2' superimposed on the background is present with respect to the original measurement just after deformation.

Further deformation by 10% led to the growth of the peak P2' at intermediate temperatures and the disappearance of peak P3 at high temperatures. The alternative presence of these two peaks is confirmed by frequency scans. Internal friction of the high frequency side of P3 in Figure 3.14 b) for 4% deformation goes down to values below 0.01. This shows the absence of any relaxation mechanism at $T = 725$ K and a frequency between 0.1 and 1 Hz in the case of 4% and 6% deformation. On the contrary, the 8% deformed sample in Figure 3.14 c) does not go
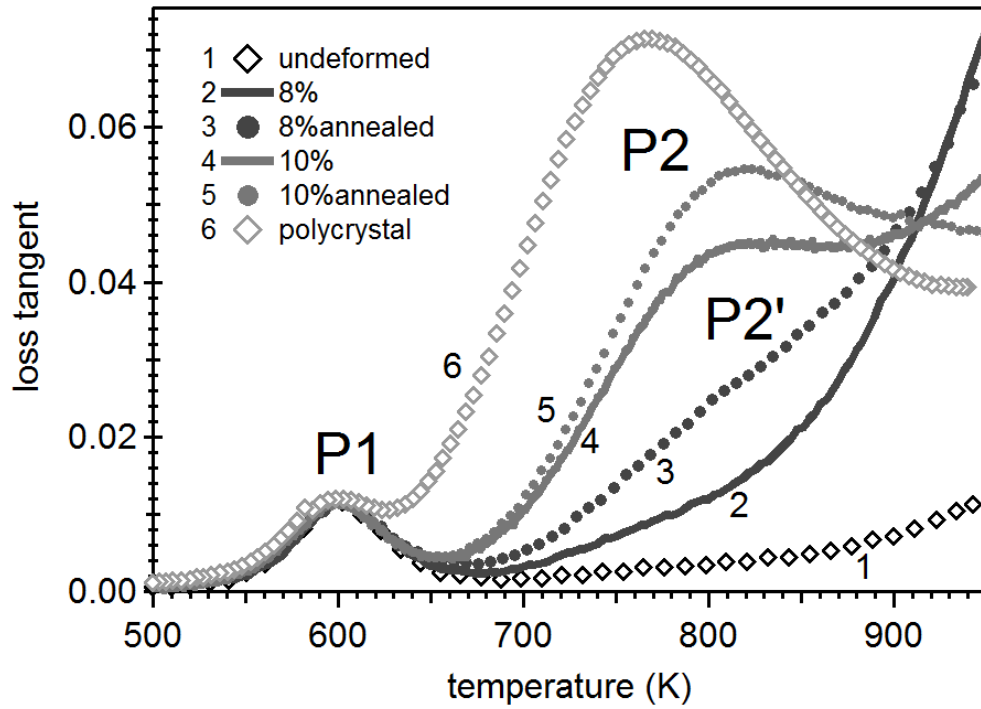
Figure 3.15 – Temperature scans of the deformed single crystal for different deformations: In the case of 8% and 10%, annealing causes an evolution of the spectrum during measurements and the peak P2' appears gradually while the background decreases. The spectrum of the polycrystal with its large peak P2 and relatively low background is shown for comparison.

down to 0 on the high frequency side of peak P3 and in the case of the 10% deformed sample in Figure 3.14 d) the situation has changed completely. The peak P3 at $T = 925$ K has disappeared and a peak at $f = 0.2$ Hz and $T = 725$ K is present in the intermediate temperature range. This peak can be identified with the peak P2' visible in temperature spectra of Figure 3.15. The newly appeared peak P2' is also a thermally activated relaxation peak as it shifts to lower frequencies with decreasing temperature.

Figure 3.15 summarizes the various temperature scans. For small deformations up to 6% the background grows. At a critical deformation of 8% the background is at its maximum and the spectrum is sensible to temperature cycle history. A peak appears at intermediate temperature at about 800 K and becomes more and more pronounced for 10% deformation. At the same time, the background decreases. The spectrum of the highly deformed sample becomes more and more similar to the spectrum of the polycrystal with its large peak at around 750 K.

The activation enthalpy and the limit relaxation time τ_0 from Equation (2.15) of the peak obtained at 10% deformation were measured with an Arrhenius plot. Values of $H_{act} = 2.37$ eV and $\tau_0 = 5.4 \cdot 10^{-16}$ s were obtained, which is very close to the values found for a polycrystal peak $H_{act} = (2.35 \pm 0.10)$ eV and $\tau_0 = 9.6 \cdot 10^{-17}$ s from Section 3.1.3. The analysis has been done on a set of temperature scans obtained in the forced torsion pendulum. The activation
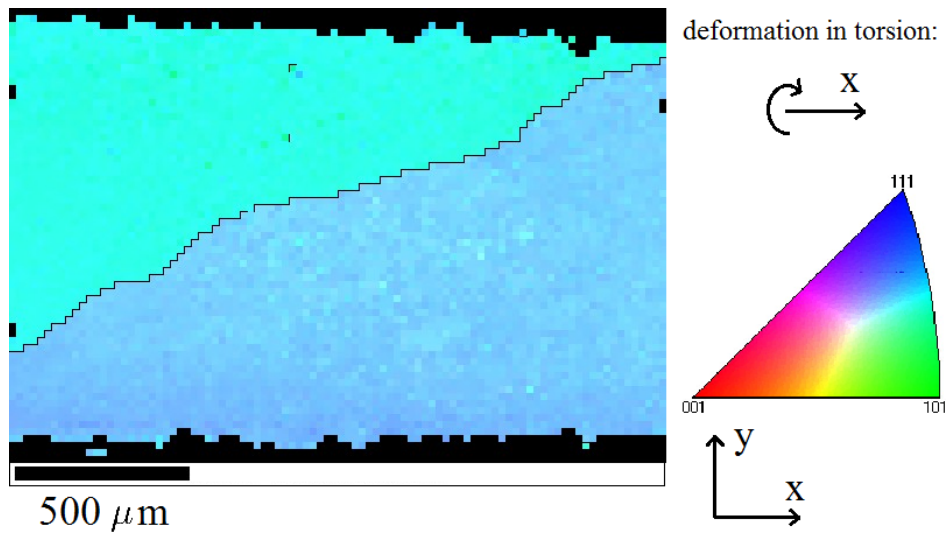
Figure 3.16 – EBSD map of one of the three boundaries in the LAGB sample. The colour map on the right are the inverse pole figures with respect to the x-axis (e.g. the deformation axis in the pendulum). The step size is 20 μm. The grain boundary is marked in black for a misorientation larger than 4°. The corresponding Laue patterns can be found in Figure 2.11 on page 30.

parameters are apparent values for both P2 and P2' since τ_0 is two orders of magnitude below the values of point defects.

Metallographic analysis of the 10% deformed sample showed that the sample was polycrystalline with a mean grain size of $d = (330 \pm 20)\mu$m. The grains showed no preferred crystal lattice orientation or elongation.

Another deformation step of 12% was performed (not shown), but the result was more or less the same as in the case of 10%. Temperature scans started with a high background that diminished during the measurement cycles and with annealing time at high temperatures. The peak P2' did not change with annealing time and the grain size stayed the same with $d = (330 \pm 20)\mu$m.

3.3   Relaxation Peak of Low Angle Grain Boundaries (LAGB)

Another sample was grown with the Bridgman technique with the same alloy composition. X-ray observations with a Laue camera and optical microscopy observations made after polishing and chemical etching showed the presence of three grains with different orientations. The misorientation angle of two adjacent grains varied between 3° and 10° and they can be considered as Low Angle Grain Boundaries (LAGB). The normal to the grain boundary planes form an angle between 30° and 70° with the symmetry axis of the cylindrical wire.

One of the grain boundaries is shown in the EBSD map in Figure 3.16. The sample axis corresponds to the x-axis and the angle between grain boundary and the x-axis is approximately
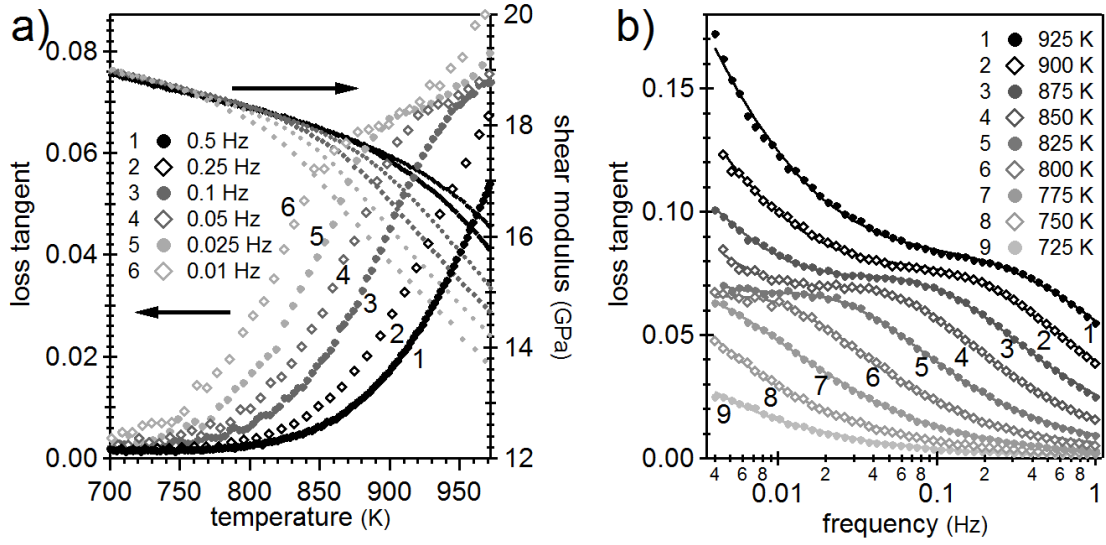
Figure 3.17 – a) Mechanical loss spectra and dynamic shear modulus of the LAGB sample as a function of temperature at different frequencies. b) Frequency scans of the same sample. A high temperature peak is superimposed on an exponential background.

30°. A black line has been drawn for a difference in the orientation of adjacent pixels for more than 4°. The misorientation between the upper and the lower grain is $(5 \pm 1)°$. The variation of orientation inside the upper grain is 1.7° and 1.2° inside the lower grain. The grain boundary goes through the whole sample, but it is not flat on the scale of millimetres. The other two grain boundaries look similar.

3.3.1 High Temperature Relaxation Peak

In Figure 3.17 a), the results of mechanical spectroscopy measurements as a function of temperature are shown. The curve for $f = 0.5$ Hz (solid black markers) corresponds to the same temperature cycle conditions as the deformed single crystal and can therefore be compared easily with the temperature scans of Figure 3.13 a) or Figure 3.15. The polycrystal peak P2 is absent at 800 K and the height of the background at 950 K corresponds to the 4% deformed single crystal. From measurements at lower frequencies (0.05 Hz to 0.01 Hz) it becomes clear that the high temperature spectrum of the LAGB sample is composed of a peak (P3') and an exponential background which are both thermally activated.

By comparing isothermal measurements of the LAGB sample shown in Figure 3.17 b) with the deformed single crystal in Figure 3.14 b) and c), one can see that the high temperature peak P3' is similar, but not exactly the same. The LAGB peak is situated at $f = 0.3$ Hz for $T = 925$ K, while P3 of the deformed single crystal is centred at lower frequencies ($f = 0.02$ Hz) for the same measurement temperature. The height and the broadening are approximately the same for both samples.

	BG		P3 / P3'			
	H_{act} in eV	n	H_{act} in eV	τ_0 in s	β	Δ
0%	1.96 ± 0.04	0.37 ± 0.02				
2%	2.11 ± 0.03	0.38 ± 0.02				
4%			2.12 ± 0.03	$(1.1 \pm 0.7) \cdot 10^{-10}$	2.3 ± 0.3	0.23 ± 0.04
6%			2.13 ± 0.04	$(5 \pm 3) \cdot 10^{-11}$	2.6 ± 0.4	0.43 ± 0.05
8%			2.10 ± 0.06	$(9 \pm 6) \cdot 10^{-11}$	2.8 ± 0.5	0.45 ± 0.05
LAGB	2.6 ± 0.5	0.35 ± 0.03	2.01 ± 0.04	$(3 \pm 1) \cdot 10^{-11}$	1.3 ± 0.4	0.09 ± 0.02

Table 3.1 – Activation parameters for the exponential background, the high temperature peak P3 of the deformed single crystal and the high temperature peak P3' of LAGB sample.

	H(P2) in eV	τ_0 in s	Δ	β	
10%	2.37 ± 0.02	$(5.4 \pm 0.8) \cdot 10^{-16}$	0.25	3.6	(P2')
polycrystal	2.35 ± 0.02	$(9.6 \pm 0.9) \cdot 10^{-16}$	0.32 ± 0.01	3.95 ± 0.05	(P2)

Table 3.2 – Activation parameters from Arrhenius plots for the peaks P2' and P2 of the 10% deformed single crystal and the polycrystal.

Figure 3.18 a) shows the transient peak P3 in different samples. The frequency scans are all taken at $T = 950$ K. In the deformed sample, P3 is present for 4% and 8% deformation and the peak is situated at about $f = 0.04$ Hz, whereas the peak of the LAGB sample P3' appears at 0.2 Hz.

3.3.2 Activation Parameters

The activation energy of the LAGB sample was obtained with the Arrhenius plot shown in Figure 3.18 b) where the temperature scans of Figure 3.17 were used. We find $H_{act} = 2.01$ eV and the limit relaxation time $\tau_0 = 3 \cdot 10^{-11}$ s. It is clear from Figure 3.18 b) that the difference in the position of P3 and P3' is due to a different τ_0.

Table 3.1 summarizes the activation parameters of the background and the peaks P3 and P3' for the deformed single crystal and the LAGB sample. The background energy and the broadening factor n for the background have been obtained from the slope and the offset when constructing a master curve. The limit relaxation time τ_0 could be calculated from the peak position after background subtraction in the case of the deformed single crystal where the broadening factor β and the relaxation strength Δ are fitting parameters. In the case of the LAGB sample, τ_0 has been obtained directly from an Arrhenius plot. The errors reported there are statistical errors, true errors including systematic errors might be larger.

The activation parameters of the intermediate temperature peaks P2 and P2' in Table 3.2 are obtained from Arrhenius plots since this method gives a higher precision. Fitting the temperature scans with broadened Debye peaks (Equation (2.18)) and an exponential background (Equation (3.1)) provides the relaxation strength Δ and the broadening factor β.
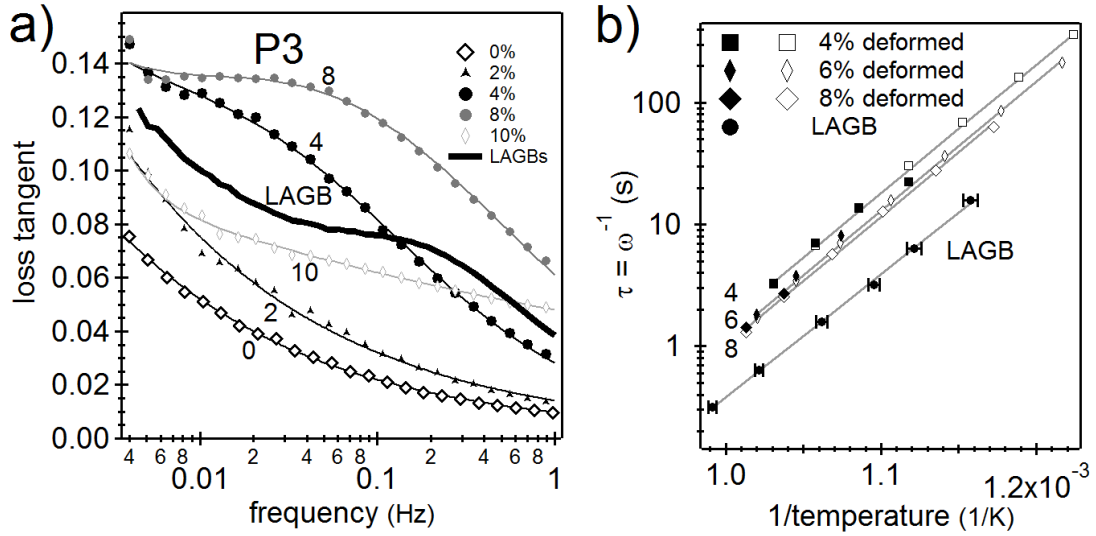
Figure 3.18 – a) High temperature peak P3 for deformations between 4% and 8% visible in frequency scans at $T = 950$ K. The LAGB sample has a similar peak P3. b) Arrhenius plot for the peaks P3 in the 4%, 6% and 8% deformed single crystal and for P3' in the LAGB sample. Black markers corresponds to data points of the relaxation time $\tau = 1/\omega$ as a function of the inverse peak temperature $1/T$ evaluated at the maximum of the peak after background subtraction. The white points are obtained from the offset value when construction a master curve. The absolute value of τ (offset in vertical direction) is unknown and has been adapted for each deformation step in order to fit the values from the peak maxima (black markers). The grey lines are linear fits which provide the activation energies. Error bars are only shown for the LAGB sample, but they are of comparable size for all data points.

From Table 3.1 and 3.2 it can be seen, that the high temperature peak P3 of the deformed single crystal and of the LAGB sample have quite similar activation parameters and it is plausible that the microscopic mechanism responsible for stress relaxation is the same. The polycrystal peak P2 and the peak P2' of the 10% deformed sample seem also to emerge from the same mechanism as activation parameters are similar and both peaks are found in fully recrystallized samples. However, the parameters of P2 and P3 differ a lot: The activation energy of the polycrystal peak and the 10% deformed single crystal show values of 2.37 and 2.35 eV (see Table 3.1) which differ significantly from the activation energy of the peak P3 with $H \approx 2.1$ eV. P3 has a lower activation energy even if the process becomes active at higher temperatures compared to the polycrystal peak P2.

The limit relaxation time of P3 is within the range between 10^{-10} - 10^{-11} s, whereas we find values between 10^{-15} and 10^{-16} s for P2. These values are too small for a physical process in a crystal and the activation energy for P2 should be considered as an apparent value. Comparing the activation energy of the background with the energy of P3, the values all lie near $H_{act} = 2.1$ eV except for the background energy of the LAGB sample with a value of 2.6 eV. Notice that in this case, the error is rather important.

The observation of different relaxation mechanisms in a plastically deformed single crystal allows a description of the microstructure evolution. The mechanical loss spectrum of a single crystal shows only a very low exponential background at high temperature and no relaxation peak. This background is due to dislocation relaxation in the bulk as in [Scho64, Rivi76] and not due to point defect migration as stated in [Kali12, Zolo95], since its amplitude grows with increasing deformations up to 6%. These freshly introduced dislocations can move freely in the crystal.

At this point, the dislocation density is not yet high enough to lead to recrystallization and only an exponential background is visible in the accessible frequencies of present experiments. The introduction of dislocations by cold work increases the total energy of the crystal and at a critical dislocation density, the dislocation network will start to reorganize itself in order to minimize the free energy of the system.

Recrystallization starts with cell formation in the bulk where zones with high and low dislocation density are formed [Hu63]. A reorganization of dislocations leads to the formation of LAGBs where dislocations of one type in the case of a symmetric tilt boundary or different types of dislocation families are stacked one over the other.

In LAGBs, an individual dislocation movement is constrained by the presence of the other grain boundary dislocations. Nó et al. [No89, No93] showed that LAGBs with more than one dislocation family can form a polygonized structure. Despite the interactions with surrounding dislocations, one can attribute a Burgers vector and a direction to an individual grain boundary dislocation. The nature of the dislocation is preserved for boundaries with misorientation angles below $10°$ since the minimum distance between dislocations in the case of a symmetric tilt boundary in an fcc metal would be $5.74b$ where b is the length of the Burgers vector of a $1/2 < 110 >$ dislocation.

The first relaxation phenomenon in the deformed crystal, that differs qualitatively from the behaviour of a single crystal, is the high temperature peak P3 that is only observed in frequency spectra. It appears at 4% deformation and it disappears for deformations above 10%. The similarities in the activation parameters for P3' obtained for LAGBs represent a strong evidence supporting the same underlying mechanism. P3 and P3' should be both dislocation peaks with a relaxation mechanism that appears within the grain.

Examples for dislocation peaks in other materials can be found in [Rivi08, Rivi09]. The particular dislocation sub-structure of the LAGBs would provide the necessary conditions for a peak to appear. The dislocations within the LAGBs could be responsible for a relaxation peak if the presence of the other grain boundary dislocations can provide the necessary restoring force that is not present in the bulk.

On the other hand, P3 in the deformed sample and the high temperature peak of the LAGB sample are not exactly the same. They are situated at different temperatures and frequencies, and P3 is broader than P3' with values of β between 2.3 and 2.8 compared to 1.3 for P3'. Δ of

P3 is 2 to 4 times larger than the corresponding value for P3'.β and Δ are fitting parameters with uncertainties up to 20%. From Table 3.1 it can be seen that Δ increases when β increases. The large differences for peak P3 and P3' when comparing the values for β and for Δ could be due in part to the fitting procedure.

A possible physical reason for the differences could be the presence of low angle grain boundaries of various different types in the deformed single crystal at 6% and 8% deformation which, contribute to a distribution of relaxation times. In the case of P3', the distribution is then logically much narrower. The amplitude difference could be justified by a larger number of sub grain boundaries in the deformed sample, which implies a larger density of GB dislocations. Comparing the 6% and the 8% deformed single crystals, we can see that an initially higher dislocation density leads to a higher sub-grain boundary density and therefore to a higher peak P3.

In Figure 3.18, a lower τ_0 in the LAGB sample is clearly observed. Since in a dislocation peak $\tau_0 \sim L^2$ and $\Delta \sim \Lambda L^2$ (L being the free length of a dislocation and Λ the dislocation density) [Scha01], a decrease of τ_0 leads to a decrease of Δ. However, in both cases the underlying microscopic mechanism for the peaks P3 and P3' should be the same.

A further element supporting the fact that P3 and P3' are due to dislocations is the similarity of their activation energy with that of the background. In this case, it is very likely that the high temperature background is due to dislocations.

The final stage of recrystallization is grain growth. The LAGBs disappear and the misorientation between adjacent grains increases. At the same time, the dislocation density in the grains decreases as grain boundaries absorb these residual dislocations. The activation energy of P2 and P2' is the same, both peaks differ slightly in height and position. In Section 3.4.3 it will be shown that the difference in the peak position is due to a difference in grain size.

The grain size of the deformed specimen is relatively large with its 330 μm. Such large grains are the result of the small level of deformation (10%). The polycrystalline samples for example were deformed by 70% and annealed at 923 K for 30 min in the last processing step and had a grain size of 56 μm before any high temperature annealing step was performed. High deformation and a resulting high density of dislocations before recrystallization leads to smaller grain sizes.

3.4 Characteristics of the Grain Boundary Peak

3.4.1 Polycrystal Peaks in different Materials (Au5N, Cu5N, AuPd, AuIn, AuPdIn)

We have found peaks that should be attributed to grain boundaries in various metals and metal alloys at around half the melting temperature T_m. Figures 3.19 through 3.21 show relaxation spectra of the two pure metals Au and Cu as well as some other gold based alloys. For each
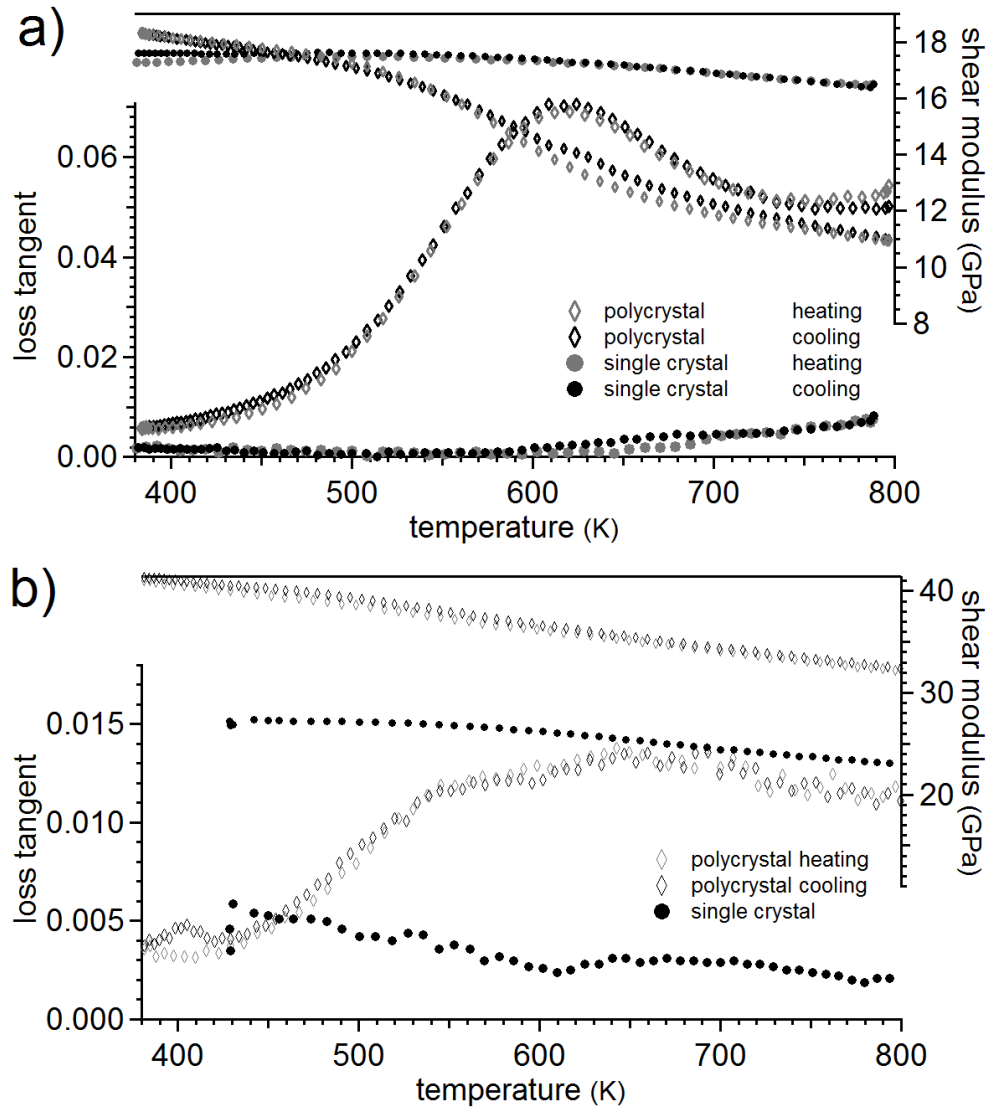
Figure 3.19 – Mechanical loss spectra of polycrystals and single crystals a) in pure Au and b) in pure Cu. The peak in Cu is much smaller than in Au.

material, the mechanical loss of polycrystal and a single crystal is shown. In all materials, the single crystal presents a low background and the polycrystal has a peak P2.

The pure metals (Figure 3.19) as well as the binary alloys AuIn and AuPd (Figure 3.20) do not show any point defect peak of Zener type as in the case of AuAgCu (Figure 3.1) since there are no isolated Cu atom pairs in a surrounding matrix. The ternary white gold alloy AuPdIn containing 34.5% Pd atoms and 2.5% In atoms, presents a spectrum very similar to that of the yellow gold alloy in Figure 3.1. A point defects peak is situated at temperatures slightly lower than the grain boundary peak P2. The absolute temperatures, at which the peaks appear, are approximately 200 K higher in the white gold.
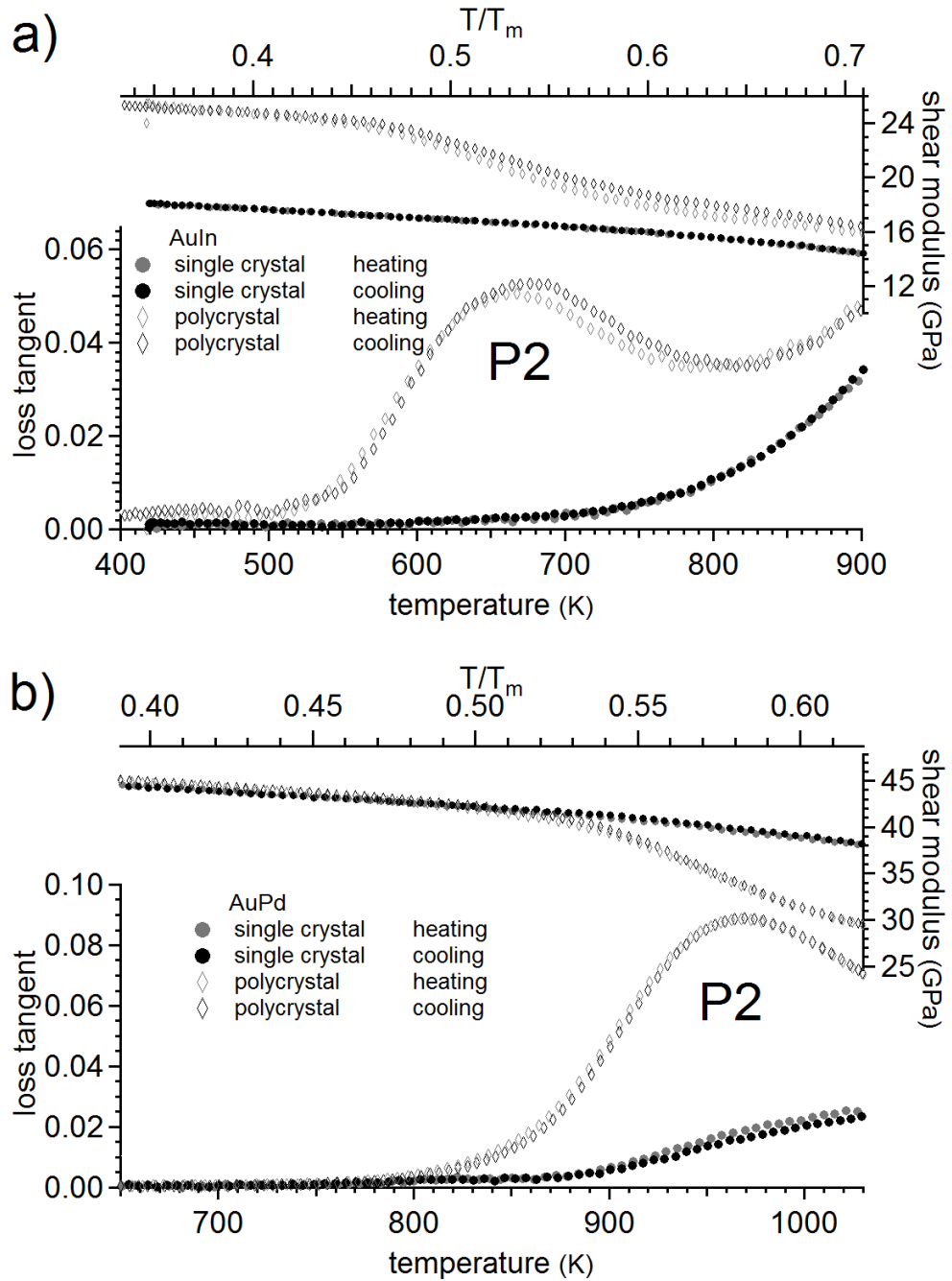
Figure 3.20 – a) Mechanical loss and dynamic shear modulus of the binary alloy AuIn containing 4.5 at.% indium as a function of temperature. The peak P2 in the polycrystal is situated slightly above $0.5 T_m$, where the melting temperature is $T_m = 1260$ K. The single crystal has no peak. b) Mechanical loss and dynamic shear modulus of AuPd containing 38.2 at.% palladium. P2 is situated at 970 K in the polycrystal, which corresponds to $0.57 T_m$, with $T_m = 1660$ K.
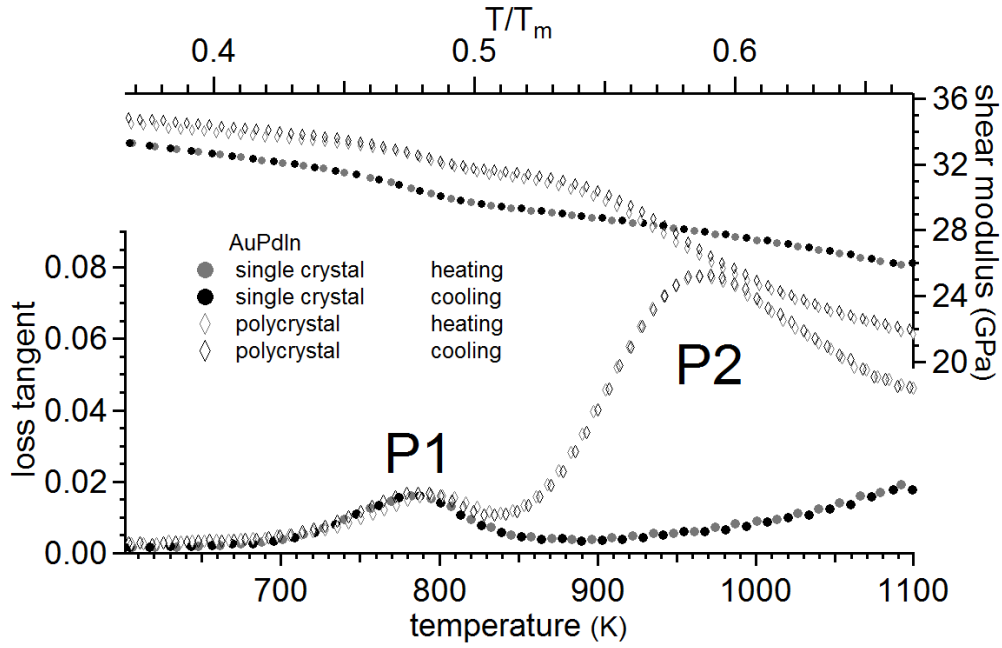
Figure 3.21 – Mechanical loss spectra at f = 0.25 Hz of polycrystals and single crystals in a ternary white gold alloy AuPdIn containing 62.1 at.% Au, 35.4 at.% Pd and 2.5 at.% In. In addition to the grain boundary peak P2 at about 1000 K, there is also a point defect peak P1' at 780 K. The top axis shows the relative temperature with respect to the melting temperature T_m = 1640K of the white gold alloy. The dynamic shear modulus in torsion is shown on the upper part of the graph.

It has been shown that the peak P1 is due to a rearrangement of In-Pd pairs in a gold matrix [Maie13]. The elastic dipole cannot be formed of one single element, In or Pd, because otherwise a peak P1 should be visible in Figure 3.20 a) or b).

For a better comparison of the peak temperature of P2, a relative temperature scale has been added in Figure 3.20. The top axis shows the ratio between the measurement temperature and the melting temperature T_m, which is 1260 K for AuIn, 1660 K for AuPd and 1640 K in the ternary alloy AuPdIn. In case of solid solutions when the crystal structure does not change, adding an element with a low melting temperature as In (T_m = 430 K) will reduce the melting temperature of the alloy and adding an element with a high T_m as palladium will increase the alloy's melting temperature. The same trend is seen for the appearance of mechanical loss peaks and it can be stated that P2 appears between $0.5 T_m$ and $0.6 T_m$.

The P2 peak in Cu differs in several points from the Au based alloys. The peak height is smaller by a factor 4 and the peak is asymmetric. It looks more like a double peak with a small dip in the middle and it is spread over more than 200 K. Figure 3.22 shows another peculiarity of P2 in copper: It is sensible to oxidation. The peak disappears after a heat treatment at 900 K under only primary vacuum. The sample was oxidized, the surface was covered by a brown layer. The oxide layer was removed by mechanical polishing and a chemical etching with a 5% solution
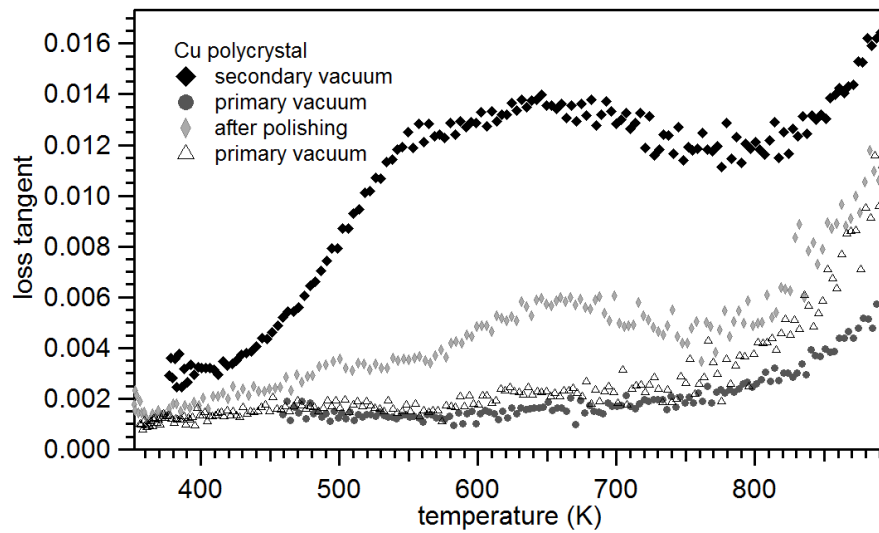
Figure 3.22 – Effect of oxidation on the Cu polycrystal: The original polycrystal (black squares) was measured under a secondary vacuum better than 10^{-4} mbar. A drop of the vacuum to 10^{-2} mbar at high temperature caused the disappearance of P2 and a decrease of the background (grey circles). A small peak reappeared after mechanical polishing and etching (light grey diamonds) and disappeared after a second increase in the pressure (open triangles).

of $(NH_4)_2S_2O_8$. The sample showed grains with a mean size of $d = 200 \pm 30$ μm. After several measurements under secondary vacuum, a small peak at 750 K was visible. After a second heating under primary vacuum, the level of mechanical loss was again very low without peak (open triangles).

These consecutive measurements show that the peak P2 can disappear, even if the grain boundaries are present in a polycrystal. The change in the mechanical loss spectrum is linked to oxidation occurring at low vacuum at $T = 900$ K. The sample is visibly oxidized at the surface, but a removal of the oxide layer does not restore the full peak. In copper, surface oxidation leads to passivation. It is nevertheless possible, that oxides diffuse along the boundaries, also because the Cu sample had a thickness of 520 μm before and 300 μm after polishing.

From the mechanical spectroscopy measurements, one can conclude that the mechanism causing a stress relaxation at the grain boundaries is blocked after the oxidation. The residual peak after the polishing is probably due to the formation of some new grains after mechanical polishing, which were formed by dislocations and distortions in the surface region.

In the other materials, which are mostly Au based alloys, the grain boundary peak never disappeared or changed in an other way due to oxidation, even if some samples were (accidentally) heat treated under primary vacuum only. Gold as a metal is largely non-reactive and it is stable in air up to very high temperatures. The same is true for gold alloys if the concentration of Au atoms is sufficiently high, which is the case in the materials presented here and no oxidation occurred that could have blocked the grain boundary peak.

3.4.2 Stress Amplitude Dependence and Activation Volume

The linear anelastic solid with a Debye peak as solution of the motion equation is an idealisation of what is observed in a real solid. It is a very good approximation for point defect relaxations as the Zener peak, where the peak is only slightly broadened. The GB peak P2 with its strong broadening is even further away from the simple description of a linear anelastic solid, but the observed spectra of polycrystals could be fitted by using a Debye peak with a broadening factor $\beta > 3$. In this section, we will show that the GB peak and the high temperature background cannot be described with a linear differential equation connecting $\epsilon, \dot{\epsilon}, \sigma$ and $\dot{\sigma}$, but an additional σ-dependence of the relaxation strength Δ and of the activation energy is necessary to explain the experimental observations.

One existing non-linear theory is the one by Granato and Lücke [Lüc56, Gran81], which calculates the mechanical loss of a dislocation line pinned by segregated point defects. At high stresses, the dislocation can break away and the oscillating loop length of the dislocation line is increased. Supposing a random distribution of point defects segregated on the dislocations, the breakaway process takes place at different stress amplitudes. A calculation in the Appendix A is presented to derive the Granato-Lücke (GL) damping expression:

$$\tan\phi = \Delta_0 \left(\frac{\sigma_{0cr}}{\sigma_0}\right)^{0.5} \cdot \exp\left(-\left(\frac{\sigma_{0cr}}{\sigma_0}\right)^{0.5}\right) \qquad (3.5)$$

where Δ_0 is the relaxation strength without a depinning process, σ_0 is the applied stress amplitude and σ_{0cr} is the critical stress for depinning to take place. The exponent 0.5 takes into account the effective stress distribution in a cylindrical sample geometry. The GL theory predicts an increase of the mechanical loss at low stresses and a decrease of the loss above the critical stress σ_{0cr}.

If the point defects are distributed on the glide plane of the dislocation, the movement of a dislocation is characterized by a sucessive pinning-depinning mechanism [Scha01]. The corresponding mechanical loss increases steeply above σ_{cr} and reaches its maximum at $2\sigma_{cr}$. In the materials studied here, the pinning-depinning behaviour is not observed, but the stress dependent part of the mechanical loss spectrum can be fitted using the GL expression (3.5). This indicates that the underlying microscopic mechanism cannot be described by a linear differential equation, probably because a new and different type of mechanism becomes active at higher stresses. In the case of depinning from segregated atoms, the loop length increases and a much longer dislocation segment vibrates instead of several small ones. The fact that a defect like a dislocation is composed of thousands of atoms surrounding the theoretical dislocation line, provides the possibility to cause a non-linear, complex relaxation mechanism.

In the following the results of stress dependent measurements are presented. This will give a hint to the underlying microscopic mechanism. Varying the stress amplitude in a temperature scan can result in two different changes of the loss spectrum. A relaxation peak can change its height or its maximum can be shifted to higher or lower temperatures. From a phenomenolog-

ical point of view, a change in height can be modelled by a stress dependence of the relaxation strength Δ and a shift of the peak position can be accommodated either by a σ-dependence of τ_0 or H_{act}. Physically, an increase of the peak height with σ indicates that a larger number of defects are activated by a higher stress or that the relaxation mechanism becomes more efficient with σ.

On the other hand, if the stress dependence is linear in the term of the activation enthalpy in a first approximation, $H_{act} = H_0 + \alpha \cdot \sigma_0$, the coefficient α has the dimension of a volume:

$$H_{act} = H_0 - V_{act}\sigma_0 \qquad (3.6)$$

V_{act} is called activation volume. If this quantity is divided by the atomic volume of the crystal, it provides the number of atoms included in a one-step process of the microscopic mechanism.

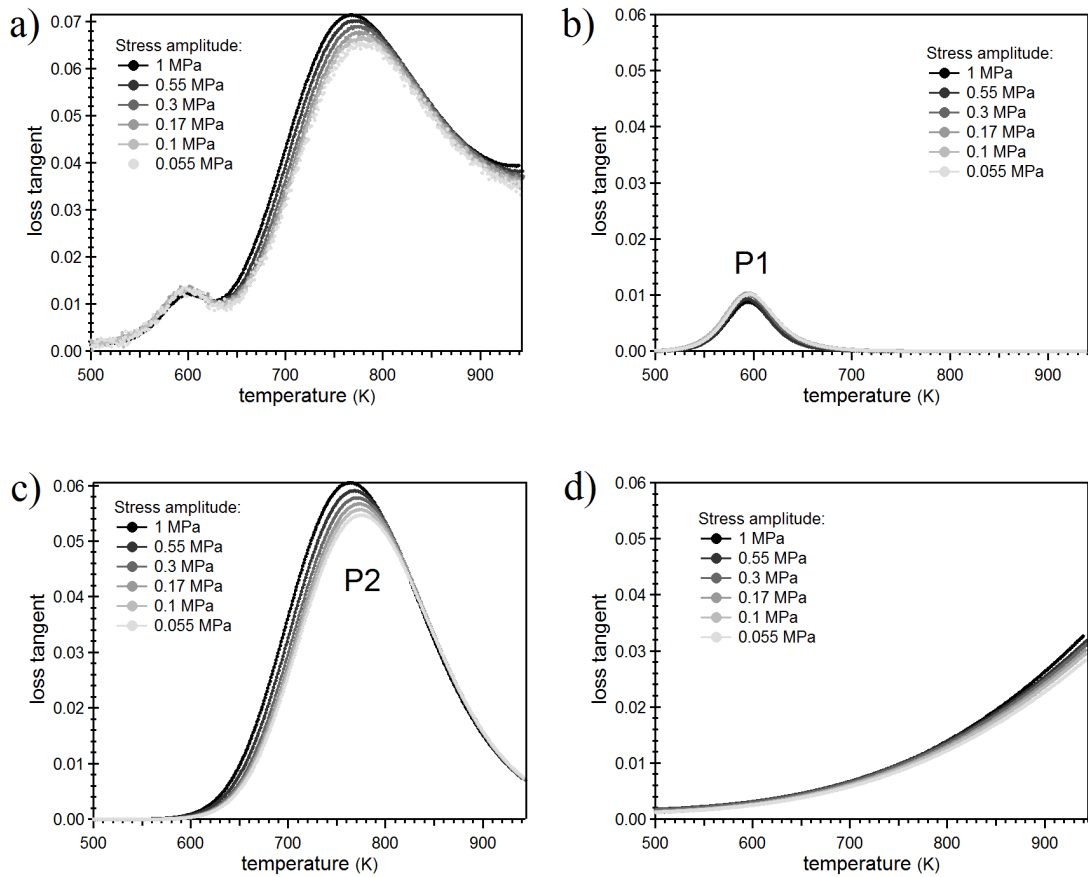Figure 3.23 – a) Dependence of the mechanical loss spectrum of the yellow gold alloy on stress amplitude. Effects of the vibration amplitude on b) the Zener peak P1, c) the GB peak P2 and d) the background, separately.

Figure 3.23 shows the temperature mechanical loss spectra as obtained at the same frequency but for different stress amplitudes from 0.055 MPa to 1 MPa. This corresponds to strains from

$2 \cdot 10^{-6}$ to $4 \cdot 10^{-5}$ at room temperature. Figure 3.23 b), c) and d) show the effects of the vibration amplitude on the Zener peak, the GB peak and the background separately.

The Zener Peak is unaffected by the vibration amplitude, but the GB peak varies in height and temperature position. When the stress is increases, the peak P2 is higher and the peak maximum is slightly shifted to lower temperatures. More precisely, the low temperature side of the peak undergoes a significant amplitude dependence whereas the high temperature side is not affected. At higher temperature one can see that the background increases also slightly with increasing the stress amplitude. It appears clearly that the largest modification of the spectrum by the variations of the applied stress originates from the grain boundary peak P2.
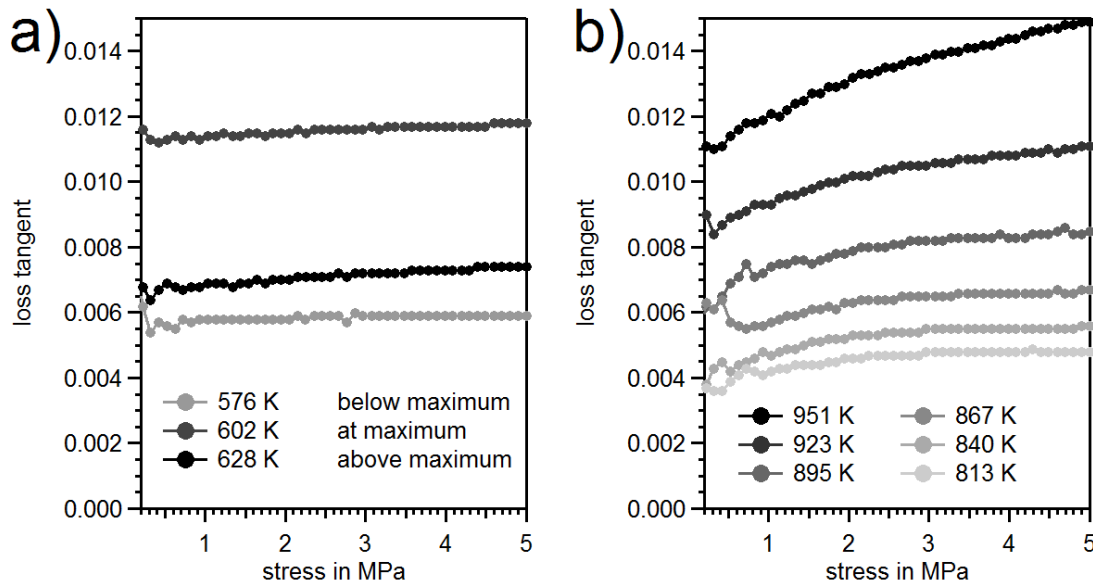

Figure 3.24 – a) Amplitude scans of the peak P1 in the single crystal presented in Section 3.1.2. The 3 different temperatures correspond to the maximum of P1 (602 K, grey markers) and of approximately half the height at lower temperatures (light grey markers) and at higher temperatures (black markers). The mechanical loss does not depend on the stress amplitude. b) Amplitude dependence of the background in the single crystal. The loss increases with increasing excitation amplitude.

In order to study the stress dependence more quantitatively, amplitude scans have been performed at a fixed frequency of 0.5 Hz and at a fixed temperature. The excitation amplitude is varied between 0.1 MPa and 5 MPa. One temperature value corresponds to one position in Figure 3.23 a). For example a measurement at 700 K probes the low temperature flank of the peak P2.

The peak P1 in Figure 3.23 b) depends very little on the stress amplitude. As shown in Figure 3.24 a) the dependence to all parameters of P1 are practically independent of the amplitude, even if the stresses were increased up to 5 MPa. In order to measure P1 without any side effects from the GB peak or the background, the measurements of Figure 3.24 were taken on a single crystal.

In Figure 3.24 b), amplitude scans of the background are shown, where the mechanical loss increases with stress for all temperatures. This behaviour might be justified with a dislocation relaxation, where at high temperatures and high stresses new dislocations can be created.
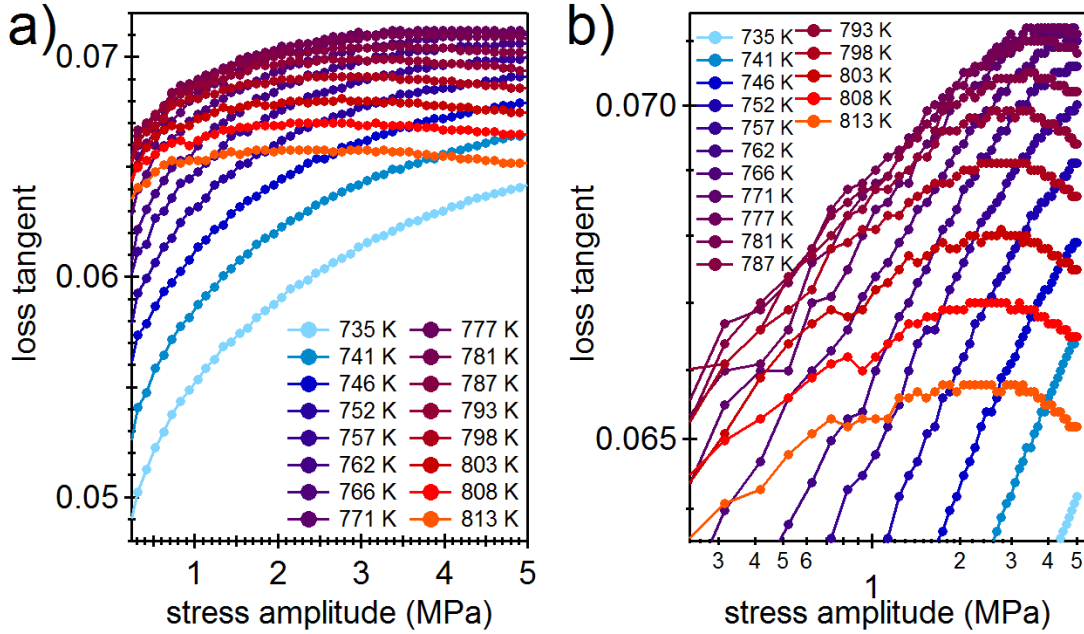

Figure 3.25 – a) Stress amplitude dependence of the GB peak: The blue curves show the variation of the mechanical loss of the low temperature flank of P2. Red and orange curves belong to the high temperature flank above the maximum. The amplitude dependence is stronger for lower temperatures. b) The same data set as in a) on a logarithmic scale. The maximum of the mechanical loss shifts to higher stresses with decreasing temperature.

The GB peak behaves much differently in terms of amplitude dependence: Figure 3.25 a) shows amplitude scans of the GB peak at different temperatures. The low temperature flank (blue) shows an increase of the mechanical loss similar to the high temperature background. In both cases, the relative increase up to 5 MPa is approximately 20%. At temperatures beyond the maximal peak temperature of 777 K, the amplitude scans show a maximum and the mechanical loss decreases for high stresses. Plotting the same data set on a logarithmic scale (Figure 3.25 b) better visualizes the maximum and it becomes clear that for increasing temperatures, the maximum shifts to lower stresses.

From the temperature scans of Figure 3.23 it could have been thought that the high temperature flank of P2 is inert to stress variations. That this is not the case becomes clear from the amplitude scans, where the loss undergoes a local maximum. The amplitude scans show quite evidently a simultaneous increase and a shift to lower temperatures when increasing the stress amplitude.

The amplitude dependent measurements of the GB peak can be fitted by using the expression for a broadened Debye peak (2.11) and (2.18) and introducing a stress amplitude dependence
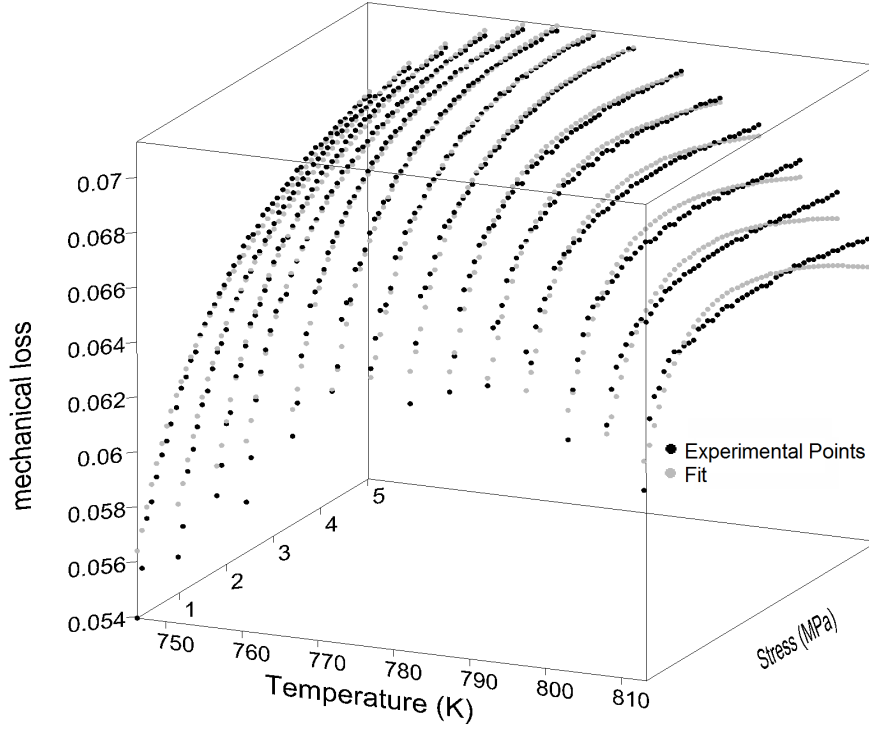
Figure 3.26 – Amplitude scans of the GB peak represented as a function of the temperature and the stress amplitude. The experimental data points are shown in black and the corresponding fit using the GL expression is marked with grey points. The presence of a high temperature background is not taken into account.

in form of an activation volume (3.6) and by changing the relaxation strength according to a GL expression:

$$\tan\phi = \Delta_0 \left[1 + \alpha \left(\frac{\sigma_{0cr}}{\sigma_0} \right)^{0.5} \cdot \exp\left(-\left(\frac{\sigma_{0cr}}{\sigma_0} \right)^{0.5} \right) \right] \frac{\omega\tau}{1 + \omega^2\tau^2} \tag{3.7}$$

where the thermally activated relaxation time is given by

$$\tau = \tau_0 \exp\left(\frac{H_0 - \sigma_0 V_{act}}{k_B T} \right) \tag{3.8}$$

Figure 3.26 shows the data points of Figure 3.25 in black in a 3D representation together with the fits (grey markers). Especially for low temperatures, the fits describe very well the experimental data. At high temperatures, the fits overstate the decrease of the mechanical loss at high stress values. The fit function did not include a contribution from the high temperature background, since the data set does not contain the high temperature data. Nevertheless, the high temperature background is not negligible at 810 K and the discrepancy between data points and fit at high temperatures and high stresses could be partially due to the disregard of

the background.

The fitting procedure provide values for the parameters α, σ_{0cr} and V_{act}. The fraction of the stress dependent relaxation strength is $\alpha = 0.367 \pm 0.004$ and the critical stress for depinning is found to $\sigma_{0cr} = (5.03 \pm 0.09)$ MPa.

A physically interesting parameter in Equation (3.8) is the activation volume V_{act}, since it can provide a footprint of the relaxation mechanism. The value obtained from the fit of Figure 3.26 is $V_{act} = (1660 \pm 30)$ Å^3. Since it is linked to the tilt of the fitting curve at high stresses, where the difference is largest between data and fit, it is probably better to use another analysis method for the activation volume.

In principle, the activation volume could be extracted from the shift of the GB peak in Figure 3.23 c). A more direct measurement of V is to measure the activation enthalpy H with an Arrhenius plot for different values of σ_0 and then analyse its variation as a function of the stress. The fitting values of the linear regression $f(x) = a + bx$ corresponding to Figure 3.27 are $a = (2.35 \pm 0.02)$ eV and $b = -(0.087 \pm 0.012)$ eV/MPa. The activation enthalpy at zero stress is $H_0 = (2.35 \pm 0.02)$ eV and the activation volume is $V_{act} = (14000 \pm 2000)$ Å^3. This corresponds to 230 ± 30 unit cells in a crystal with a lattice parameter $a = 3.93$ Å. Since a unit cell in an fcc crystal contains a total of 4 atoms, this means that the relaxation process causes the movement of ~900 atoms.
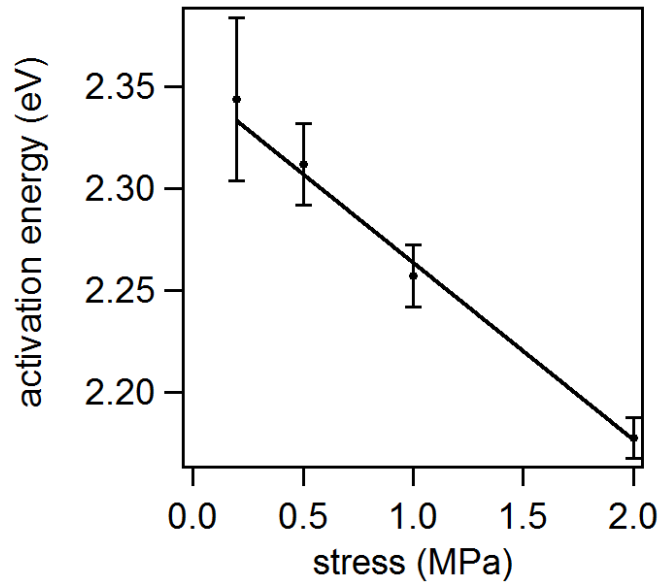
Figure 3.27 – Activation energy of the polycrystal peak P2 as a function of the stress amplitude. The data points are obtained from series of temperature scans at different frequencies similar to Figure 3.7, where each series was measured at a distinct stress amplitude. The error bars are statistical errors taken from Arrhenius plots.

Already in Section 3.1.3, the polycrystal showed a particular behaviour with respect to the activation energy. It is probably an apparent value and therefore too high in order to be

interpreted in terms of atomic movement. It is likely that the activation volume is equally too high. From the shift of P2 in Figure 3.23 c), the activation volume is of the order of 5000 Å^3 and thus less then half as big as the volume from the activation energy. Nevertheless, there are probably several hundreds of atoms involved in the microscopic mechanism associated with GB movement.

3.4.3 Influence of Grain Size

In 1941, the first model for the mechanical loss caused by GB sliding in metals was developed by Zener [Zene41] and predicted a relaxation peak in internal friction measurements. The peak amplitude should not depend on the size of the crystallites in the polycrystal while its position should show a linear dependence on the grain size d. The purpose of this section is to verify the grain size dependence of the GB peak P2 according to Zener's theory.

Grain Growth in Polycrystals

The polycrystalline specimen that was used for the grain growth experiment was cut from a wire with 2 mm in diameter. The as received wires had been cold-drawn and heat-treated in order to obtain a homogeneous and small-grained structure with an average grain diameter of 30 μm.

The experiment was performed as follows: the sample was heated up to the annealing temperature while measuring internal friction. The measurement continued during annealing and the sample was cooled down to room temperature in the pendulum. Then the microstructure was analysed after polishing and chemical etching. The annealing time was increased gradually from 30 min up to 9 hours at 923 K until the microstructure stabilized. Two additional annealing steps were performed at 950 K and 1000 K in order to get even larger grains.

The first heating and cooling cycle are shown in Figure 3.28 a). During annealing of 30 min at 923 K, the background decreases slightly and the cooling curve lies below the heating curve in the following cooling spectrum. On the other hand, the maximum of the grain boundary peak P2 slightly shifts to higher temperatures after the annealing step.

Figure 3.28 b) summarises all the cooling spectra after various annealing treatments. The first and second curves have been measured after 30 min at 923 K in the pendulum, which gives total annealing times of 60 min and 90 min, as the original sample had been treated for 30 min before. Then, for cycles 3 to 5 the annealing time has been increased up to 9 h since the effect on the mechanical loss spectrum decreased. The last two measurements have been performed at annealing temperatures of 950 K and 1000 K respectively. Annealing at higher temperature causes qualitatively the same effect as an annealing step with longer annealing time.

All measurement curves have been fitted using 2 Debye peaks and a background. The fits for the peak P2 are shown in Figure 3.29. The annealing steps cause a shift to higher temperatures.
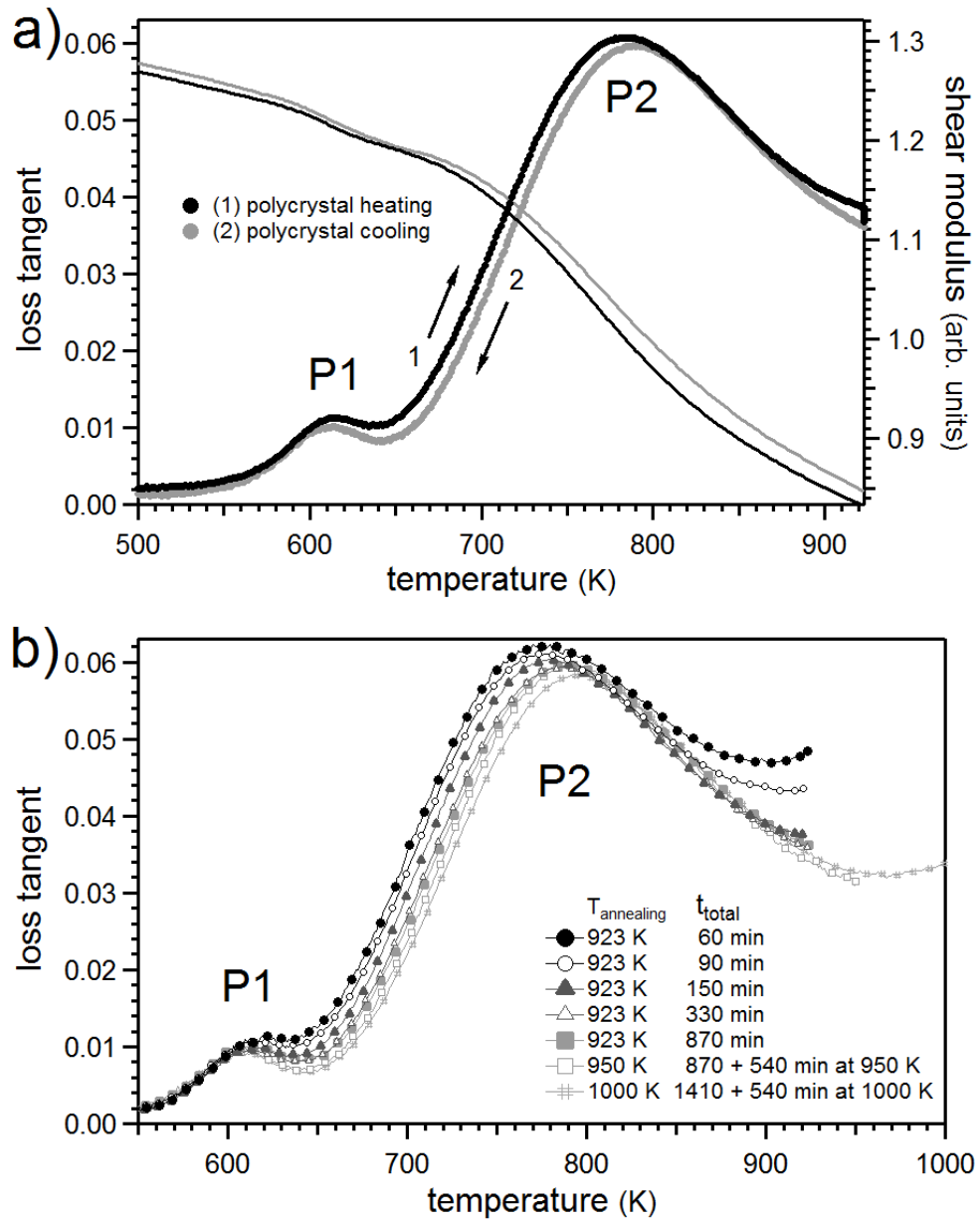
Figure 3.28 – a) Heating/cooling cycle of a polycrystalline sample with annealing for 30 min at 923 K. Internal friction decreases during high temperature annealing and the grain boundary peak P2 is slightly lower and shifted to higher temperatures after the annealing. The dynamic shear modulus shows a drop at the position of the relaxation peaks. b) Cooling curves after consecutive high temperature heat treatments. At each step the background decreases and the peak P2 shifts to higher temperatures.
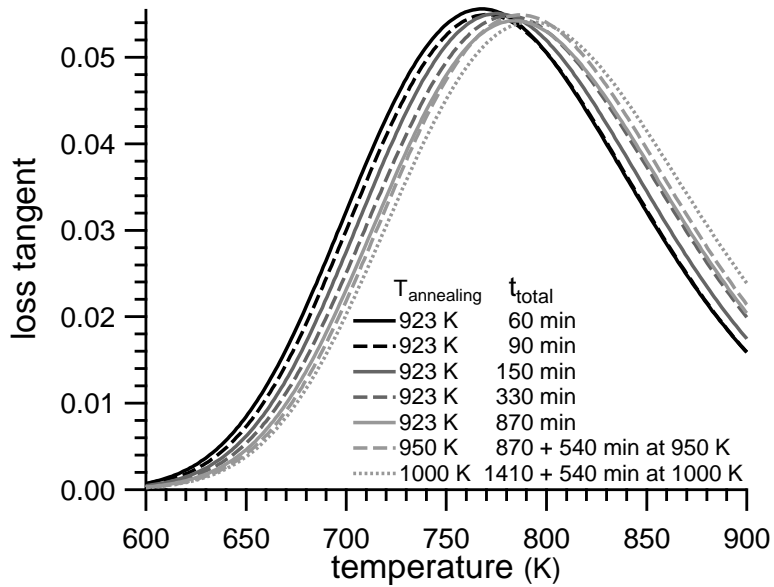
Figure 3.29 – Fits of the grain boundary peak at different annealing times: the peak position changes to higher temperatures with longer annealing time and higher annealing temperature. Height and shape remain constant.

At the same time, the peak shape does not change at all. The height and the broadening are constant for all curves and therefore, the relaxation strength Δ and the broadening factor β are not affected by the heat treatment.

The grain size obtained after subsequent annealing of the sample were monitored by optical microscopy and image analysis. Figure 3.30 a) shows the structure of the original water quenched sample before internal friction measurements. Figure 3.30 b)-f) refer to the measurement curves of Figure 3.28 b) after cooling down to room temperature. Individual grains are clearly visible. They are either separated by a dark line marking a grain boundary or grains with different orientation appear in different colours when observing the sample surface with a polarisation filter. Many grains show a twinned structure. The grain size increases after each annealing step.

In order to quantify the size, the area of a large number of grains has been measured with the image analysis software ImageJ ignoring twin boundaries. The characteristic diameter d of each grain is then the diameter of a circle with the same area. This approximation is justified by the absence of grain texture.

Mendelson et al. [Mend69] showed that the grain size value obtained from intersecting lines has to be multiplied by a constant factor depending on the statistical distribution to obtain a true value for grain size. This numerical factor of 1.56 cannot be applied here without deeper investigation because it was obtained for the transformation of a 1D measurement to a 3D polyhedral grain structure. Here, we measure 2- dimensional areas to get information on a 3D

object. In any case the correction of d should be a constant, since the size distribution does not change during the experiment. This is likely the case as all structures are grown from a much smaller grain structure.
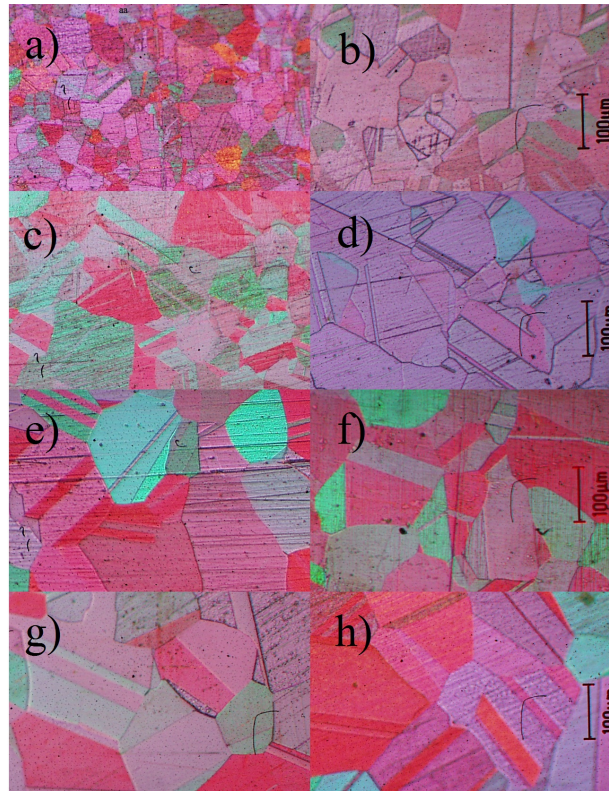
Figure 3.30 – Grain structure recorded by optical microscope: The grain size increases from top to bottom with progressive heat treatment. a) original water quenched sample b)- f) Microstructures that correspond to the measurement curves in Figure 3.28 b). Many crystallites have a twinned structure.

The peak of the deformed single crystal with 330 μm grain size shown in Figure 3.31 a) has its maximum at slightly lower temperatures than the 420 μm grain size sample originally polycrystalline. It is therefore a general property of the GB peak that it is situated at higher temperatures for a larger grain size. The way the polycrystalline microstructure was obtained does not play a role for the peak position, since the 90 μm and the 420 μm samples were obtained from a small grained sample via grain growth, whereas the 330 μm sample issues from a sample with low angle grain boundaries.

The peak of the deformed single crystal in Figure 3.31 a) is slightly smaller than the polycrystal peaks from the grain growth experiment and the difference cannot be explained by a difference in the background. The height of a relaxation peak is directly related to the relaxation strength Δ (Equation (2.11)) that changes according to the individual microstructure.

69

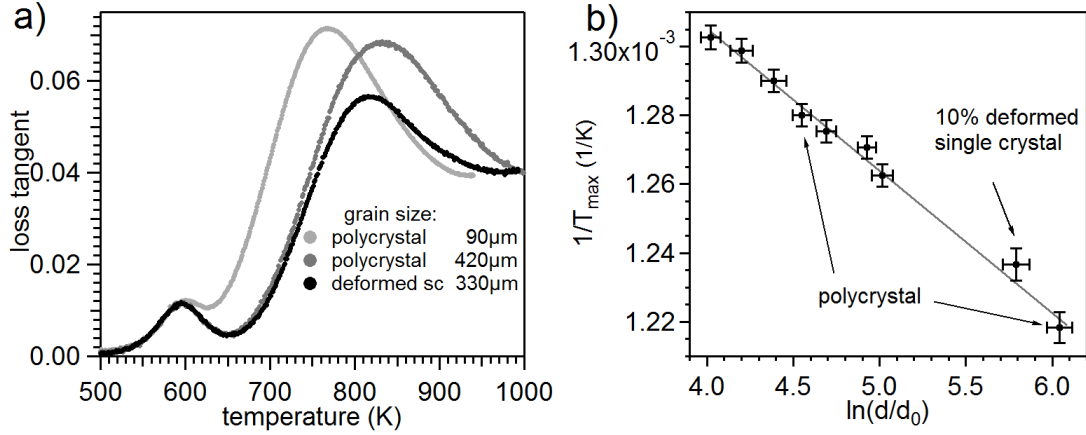Figure 3.31 – a) Comparison of the deformed single crystal of section 3.2.2 with polycrystals at different grain sizes. b) Grain size exponent: m is obtained from a linear fit of the inverse temperature of the peak maximum against the logarithmic grain size. The peak position of the deformed single crystal matches perfectly with the other polycrystals.

Grain Size Exponent

According to the Zener model [Zene41] then reworked by Nowick and Berry [Nowi72a], the relaxation time τ is given by $\eta(T) \cdot d / (bM_u)$ where η is the grain viscosity, d is the grain size, b is the grain boundary thickness and M_u is the unrelaxed shear modulus. Since the grain boundary viscosity depends on thermal activation, a proper formulation of the relaxation time given in Equation (2.15) should be

$$\tau = \tau'_0 \left(\frac{d}{d_0} \right)^m \exp \left(\frac{H_{act}}{k_B T} \right) \tag{3.9}$$

The exponent m has been introduced for sake of generality and should be one if the relaxation time strictly follows Zener's model. d_0 is a reference length scale and has been chosen as $d_0 = 1~\mu$m in the present analysis. At the peak maximum, we have $\omega\tau = 1$ and m can be obtained when plotting the inverse temperature of the peak maximum versus the grain size d (see Figure 3.31 b). Then, in Equation (3.9), a constant factor could be absorbed into d_0 without changing the results for the grain size exponent m.

According to Equation (3.9), a plot of the inverse temperature $1/T$ as a function of the grain size d on a logarithmic scale should give a line with slope $b = m \cdot H_{act} / k_B$, where $H_{act} = 2.35$ eV has been measured in Section 3.1.3. From Figure 3.31 b) one can see that the measurement points lie very well on a line and a linear fit gives the grain size exponent $m = 1.09 \pm 0.10$. The uncertainty of the temperature scale comes mostly from systematic errors of the temperature measurement.

A second error source is the statistical error of the fitting procedure of the peak. The uncertainty of the grain size d is mostly due to statistical errors coming from a limited number of grains

analysed by metallography. Only 150 to 250 grains could be analysed for each annealing step. The size of individual grains for one annealing time scatters a lot because we cut polyhedral grains at different heights. A cutting area of the same grain can thus be very large when the grain is cut in the middle or very small when only a small slice near the surface is cut. Systematic errors come from the uncertainty of the measurement scale in the microscope and have been estimated to 4 to 10 μm depending on the magnification of the microscope.

The grain size exponent obtained in Figure 3.31 b) agrees very well with Zener's prediction. In his model, Zener considered a periodic array of hexagons, which is submitted to an external stress while viscous slip controls grain boundary sliding. The deformation is anelastic since triple points pin grain boundaries so producing a restoring force. The relaxed average shear angle is given by the relative displacement of neighbouring grain centres. Without solving the equilibrium equations of elastostatics, two important consequences can be deduced. First, as the strain field is an intensive thermodynamic parameter, it remains the same under a scale transformation, i.e. $\epsilon(\alpha \vec{r}) = \epsilon(\vec{r})$. So the relaxed and the unrelaxed deformation ϵ_{an}^{∞} and ϵ_{el} are both independent of the grain size d.

Then, the relaxation strength Δ of Equation (2.4) and therefore the peak height is independent of d. Second, as the displacement field is extensive, i.e., $u(\alpha \vec{r}) = \alpha u(\vec{r})$, the overall sliding distance scales with the grain size. On the other hand, the sliding velocity $v = u/\tau$ is controlled by microscopic processes and must not depend on the grain size. Therefore, the relaxation time must be proportional to grain size: $\tau \propto d$.

However, if grain boundary sliding is controlled by grain accommodation achieved by diffusion within the grains [Naba48, Herr50] or along the grain boundaries [Cobl63] then m should take the values 2 or 3 respectively. From the measured data, a grain size exponent of 2 or 3 can be ruled out. The sliding mechanism is therefore different from processes that occur in ceramics. The precision obtained in these experiments allows to fully confirm Zener's model for the first time. The present result exclude models involving grain deformation by diffusion either in the bulk or at interfaces as a controlling mechanism for grain boundary relaxation.

3.5 Study of Isolated Boundaries: The Bi-crystal

Up to this point, the measurements have been performed on single crystals or polycrystals, which means samples with a homogeneous microstructure over the whole sample length. In polycrystals, the mechanical loss spectrum is a measure of the mean contribution caused by the polycrystal's microstructure. From the absence of P2 in a single crystal we concluded that P2 is a grain boundary peak without specifying the microscopic mechanism. In a polycrystal, there are many different grain boundary types with tilt and twist orientations, with random plane orientations and a certain distribution over the misorientation angle.

In Section 3.3, we excluded that P2 is due to the presence of LAGBs, since samples with only this type of boundaries show a high temperature relaxation peak P3 and no peak P2. But then,
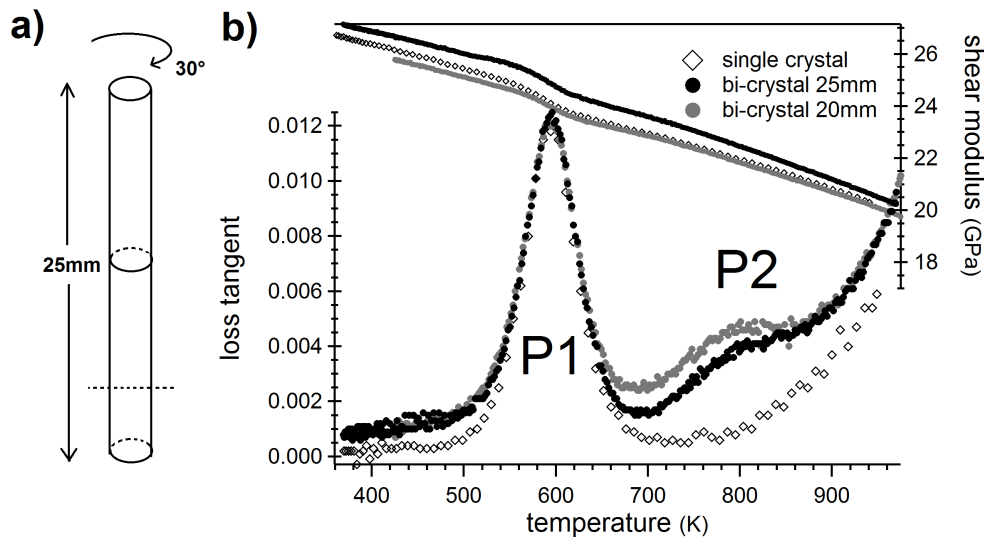
Figure 3.32 – Schematic drawing of the bi-crystal: Two halves of a single crystal are joint with a rotation of 30°. After the internal friction measurement, the lower part is cut such that the effective sample length is reduced to 20 mm. b) Mechanical loss spectrum of the diffusion bonded sample as a function of temperature at $f = 0.5$ Hz in comparison to a single crystal. At 800 K, a peak is visible in the bi-crystals. The peak of the 20 mm sample is slightly higher than that of the 25 mm sample.

the metallography images showed that yellow gold polycrystals show a high amount of twin boundaries in polycrystalline microstructures. Furthermore, it is known that the dislocation density in polycrystals is much higher than in single crystals. The analysis of the mechanical loss spectrum of an isolated high angle grain boundary should distinguish between a relaxation process due to dislocations, twin boundaries or general HAGBs.

An important advantage of bi-crystals is, that it gives access to a variety of parameters that can be changed independently. Since there is only one grain boundary, its plane orientation with respect to the sample geometry and therefore with respect to the deformation axis can be chosen. The misorientation angle and the GB density can be varied. Finally, on one sample, several geometrical parameters like the clamping length, the width or the centring of the boundary plane can be changed by removing material.

3.5.1 Diffusion Bonding

Starting from a single crystal, the cylindrically shaped sample of Figure 3.32 a) is cut perpendicular to the sample axis and joined by diffusion bonding (Section 2.1.5). The rotation angle between upper and lower crystal half is 30°. Figure 3.33 a) shows the boundary after the annealing. The width of the boundary is thinner than the optical microscope's resolution.

The diffusion bonded sample could be measured in the forced torsion pendulum, its mechan-
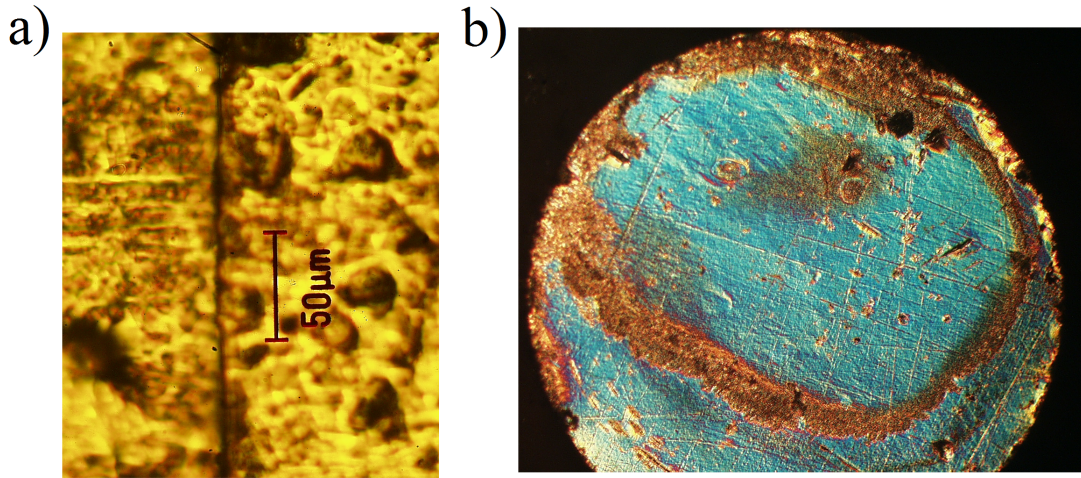
a)

b)

Figure 3.33 – a) Optical microscope image of the joint sample. The width of the boundary is below the resolution of the microscope. b) Image of the boundary section of the broken bi-crystal. Only the brown zones were in contact with the other half.

ical loss spectrum is shown in Figure 3.32 b) together with the single crystal that had been served as source material. A very small peak at 800 K is present in the bi-crystal's spectrum. This peak increases slightly, when the sample length is reduced by 20% from 25 mm to 20 mm. The dynamic modulus is unchanged by the introduction of a boundary.

After several measurement cycles, the sample broke apart at the boundary plane. Figure 3.33 b) shows one section after breaking. The image shows that only a small percentage of approximately 10% was actually joined together. It shows one of the disadvantages if the presented technique to produce a bi-crystal: It is complicated to control the quality of the boundary. The surface preparation was not precise enough to prevent cavities along the boundary. Furthermore, we do not know if the fabrication process introduces impurities or other defects at the grain boundary.

On the other hand, the mechanical loss peak in the diffusion joint bi-crystal is very similar to the polycrystal peak P2. The peak is situated at the same temperature and its amplitude increases with increasing stress amplitude (Figure 3.34). The peak amplitude is smaller by a factor 10 with respect to the polycrystal, but this is reasonable since there is only one boundary in the bi-crystal and a real boundary was only formed on a small part of the boundary surface.

The activation energy $H_{act} = 1.95 \pm 0.05$ eV of the bi-crystal differs significantly from the energy of the polycrystal's peak $H_{act} = 2.35$ eV, but we argued that the polycrystal's energy was an apparent value, since τ_0 was too small. For the bi-crystal, we find $\tau_0 = 10^{(-13\pm1)}$ s, which is more than 2 orders of magnitude higher than for the polycrystal. The attempt frequency $1/\tau_0$ being close to the Debye frequency we could affirm that the activation energy of the bi-crystal is a more reasonable value of the microscopic mechanism's activation energy.
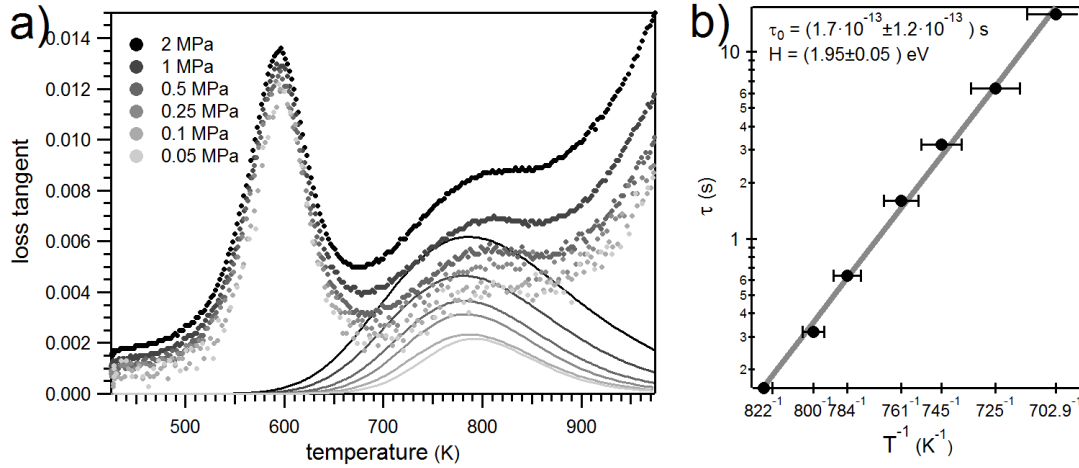
Figure 3.34 – a) Stress amplitude dependence of the bi-crystal prepared by diffusion bonding. The lines represent the contribution from the GB peak. b) Arrhenius plot of the GB peak at $\sigma = 1$ MPa.

3.5.2 Giant Peaks in Columnar Structures

The grains in the polycrystals presented in previous sections are all more or less spherically or polyhedrally shaped. No elongation along a specific axis is observed. The samples, which are presented in this section, are different, since they contain 3 columnar grains, a schematic drawing of the tri-crystals is shown in Figure 3.35 a). The GBs are all high angle GBs with misorientations higher than 20° between adjacent grains. The particularity of the columnar grain structure is, that the grain boundary surface is very high with respect to the volume of one grain, since the sample length is 28 mm and the grain width is less than 1 mm.

Two specimens have been grown vertically by the Bridgman technique producing a columnar structure with several grain orientations. The dynamic shear modulus in Figure 3.35 b) decreases drastically between 800 K and 900 K. At the same time, the corresponding mechanical loss has a huge peak, which is 2 to 3 times higher than the polycrystal's peak (open grey markers). At this scale, the bi-crystal's peak from the diffusion bonded sample is not distinguishable from zero.

The peak temperature for $f = 0.5$ Hz is higher for the tri-crystals than for the polycrystal. Taking into account a shift of the GB peak due to a dependence on d in the relaxation time τ_0 according to Equation (3.9), an equivalent grain diameter for a peak position at 870 K would be $d = 4$ mm. This should be compared to a sample diameter of 2 mm and a length of 28 mm for the columnar samples. The position of the giant peaks is therefore in agreement with the position of a general polycrystal's peak P2.

The polycrystal's peak has a constant height, even if the grain size changes. The bi-or tri-crystals show peaks, where the peak height differs by a factor 100. This difference can be understood partially by supposing a dependence of the relaxation strength $\Delta \propto A/V$, where A
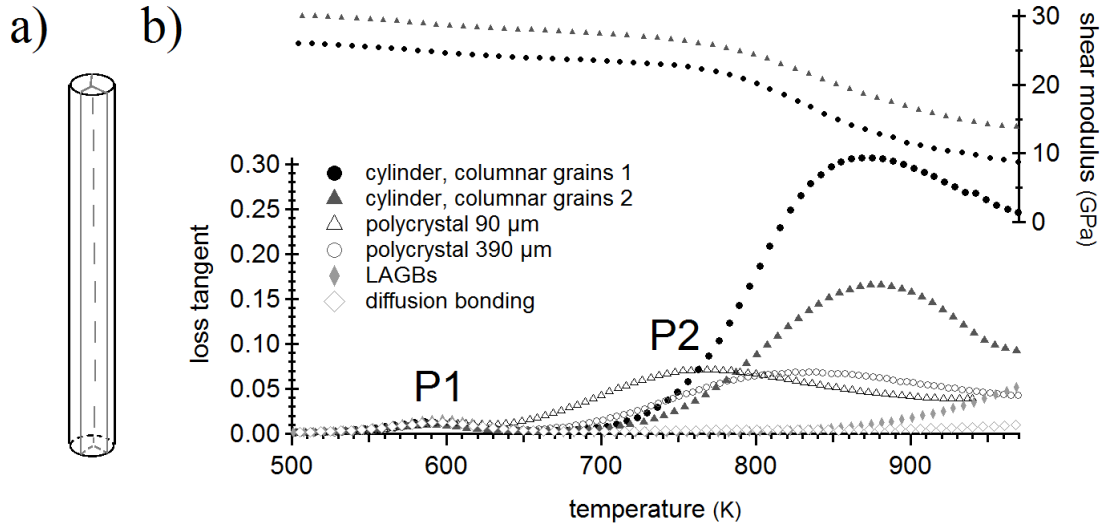
Figure 3.35 – a) Schematic drawing of the supposed grain structure of sample 1 and 2 having columnar grains over the whole sample length. b) Mechanical loss spectra of different grain structures. Huge relaxation peaks at 860 K for $f = 0.5$ Hz mark the spectrum of two cylindrically shaped samples with a vertical grain structure over the whole length. The polycrystals' peaks (open triangles and open circles) are smaller and shifted to lower temperatures. The peaks of the LAGB sample and the diffusion bonded bi-crystal are not visible on the presented scales. The dynamic shear modulus corresponding to the giant peaks is also shown in the upper part of the graph. The modulus decreases by over 40% at the peak position.

is the grain boundary surface and V the sample volume. The bi-crystal has a radius of 1 mm and $l = 20$ mm, and thus $A/V = 50$ m^{-1}. For the three columnar grains, the sample length is $l = 28$ mm and we obtain $A/V = 955$ m^{-1}. The expected factor between the relaxation strengths of the cylindrical tri-crystal and the bi-crystal obtained by diffusion bonding would be 19.1. In the experiment, we observe $\Delta_{tri}/\Delta_{bi} = 59.1$. Taking into account, that the bi-crystal formed only a partial boundary (Figure 3.33 b), the expected value should be adjusted upwards.

It turned out that the spectra of the giant peaks were not as stable and reproducible as the other spectra presented here. One heating/cooling cycle had typically a small hysteresis at the high temperature part of the spectrum and sometimes the peak shape changed slightly. This is a sign that some microstructure changes occurred during the measurements at high temperatures.

3.5.3 Observation of GB Migration

The "single crystals" produced by the Bridgman technique sometimes contain some GBs. These samples presented one or two peaks in the mechanical loss spectrum and the shape, height and position changed from one sample to another. The exact characterization of this kind of samples is difficult since the Laue camera has a spot size of several hundreds of

micrometers and for metallography and electron microscopy, a polished surface is needed. Therefore, it is easy to miss a grain boundary. The most reliable technique to identify a single crystal is mechanical spectroscopy.
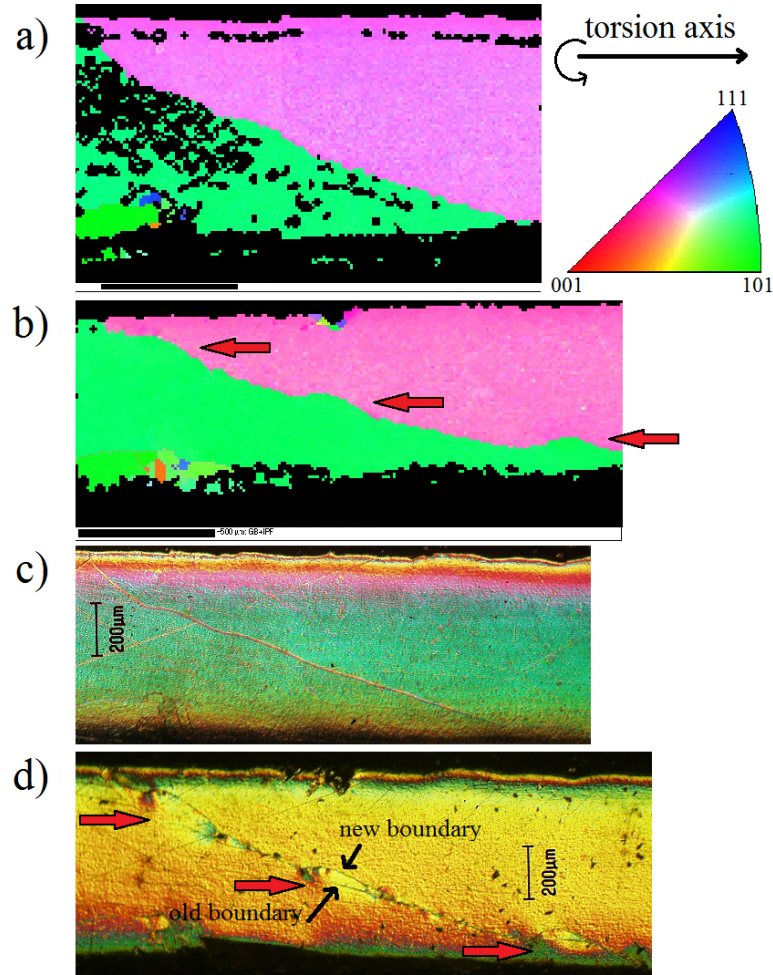
Figure 3.36 – EBSD map of a high angle GB a) before measurements in the pendulum and b) after the measurements. The same GB under the optical microscope c) before and d) after the measurements. The zones marked with a red arrow show grain boundary migration.

In this section, some observations of naturally grown grain boundaries by optical microscope and EBSD are presented. The pictures are taken on a polished surface before and after a mechanical spectroscopy experiment. The original sample in Figure 3.36 a) and c) has a grain boundary that forms an angle of 25° with the horizontal sample axis. The boundary is not completely flat, especially in the upper part of the image, the GB is curved. The optical image shows one line and the EBSD image proofs that this line corresponds to a GB with 30°±2° misorientation.

After 6 heating/cooling cycles in the torsion pendulum with maximal temperatures of 990 K, the grain boundaries were again examined. The boundary appears more wavy in Figure 3.36 b)

and the optical microscope image shows double lines, marked with red arrows in Figure 3.36 d). The surface had not been polished after the measurements. A comparison with the EBSD map shows that the upper, newly appeared line belongs to the actual boundary position, whereas the lower line is the previous boundary position. Consequently, the grain boundary migrated to the upper right in three regions.

The optical image in c) and d) have been obtained using a polarisation filter. Curved surfaces, for example the sample boarders appear in rainbow colours. Some zones at the grain boundary also appear in different colours, mainly the endpoints of the migrated areas, which indicate a height gradient. Contrarily to the very smooth surface in c), the surface near the migrated zones is not flat any more.
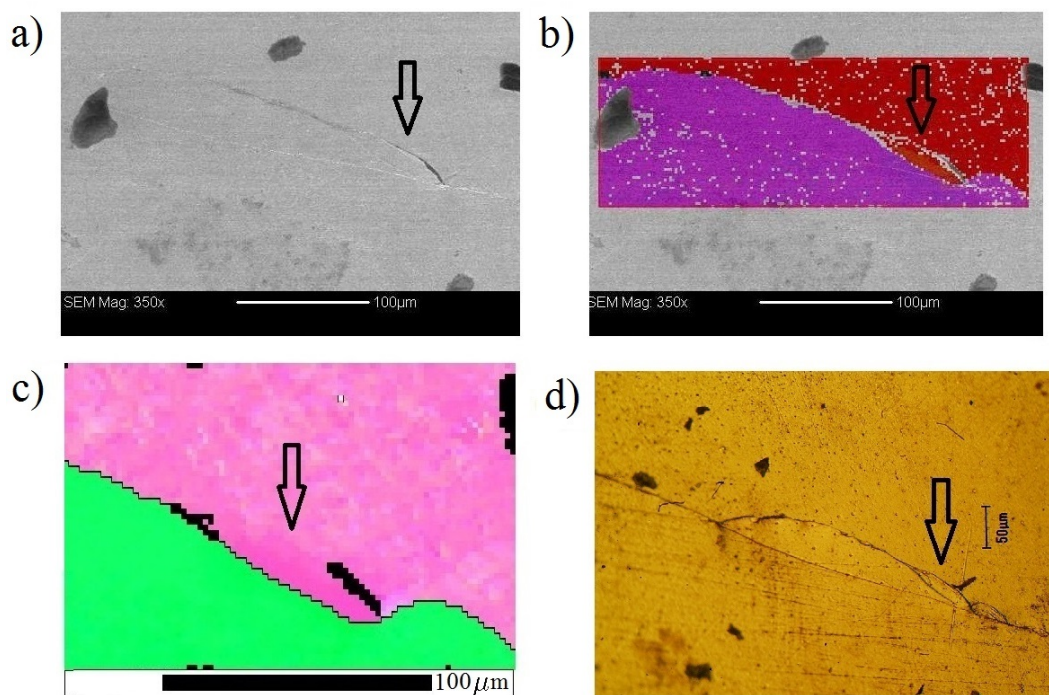
Figure 3.37 – Detailed view of Figure 3.36: a) shows the SEM image and b) the overlay of SEM and EBSD map. The lattice orientation is shown in IPF colours in c). The black arrow marks a zone with a back migration. d) Optical microscopy image showing the same GB region.

Figure 3.37 shows SEM and EBSD maps of the centred part of Figure 3.36. Due to the topology sensitivity of the SEM image, the upper and the lower line are visible. The arrow indicates a zone, where the GB first migrated upwards forming a relatively smooth GB line and in a second time moving backwards. From the shape of the GB line it seems that the GB bulges out between several pinning points. Apparently, a driving force acting on the boundary at high temperatures caused a migration. The GB surface did not advance uniformly over the whole GB, but some zones were more easily activated causing a migration between pinning points. The migration process seems to be at least partially reversible, since we observe a zone, where the grain boundary moved first forwards and then backwards.

Figure 3.38 – Optical microscope image of 4 grains a) before and b) after GB migration occurred. The red arrows indicate the migration direction. c) Crystallographic direction measured by EBSD. The map corresponds to the white square in b).

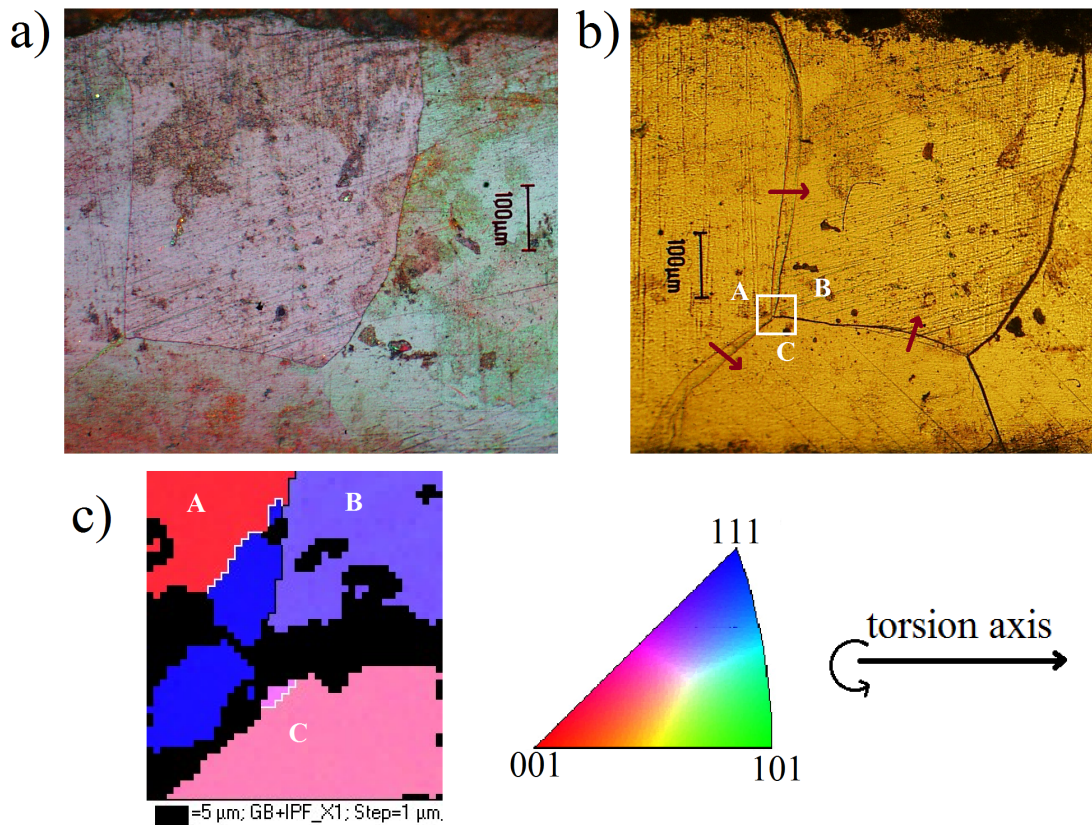The role of pinning points on GB migration can be seen in a different way in Figure 3.38, where another part of the same sample is shown. Three of the five GBs migrated in the directions indicated by the red arrows in Figure 3.38 b). The migration occurs more homogeneously over the whole GB line. The triple points, where three grains meet, act as pinning points for grain boundary migration.

The surface topology after the passage of a grain boundary appears as terrace steps. Figure 3.39 a) shows a picture of a migrated GB, where the focal point is set to the left surface. The grain on the right side lies higher and is therefore out of focus. Since we observe steps connecting the difference in height, grain boundary migration is not a complete smoothly process. Otherwise, the zone between the starting line and end line of the migration process should be a smooth surface with a resolution of an optical microscope.

Grain boundary migration could be the microscopic mechanism causing the GB peak P2, since this process becomes activated at a temperature lying between room temperature and the maximum temperature $T = 990$ K of the experiment, which was performed between the two observations with EBSD and optical microscopy. Triple lines in a grain network act as pinning
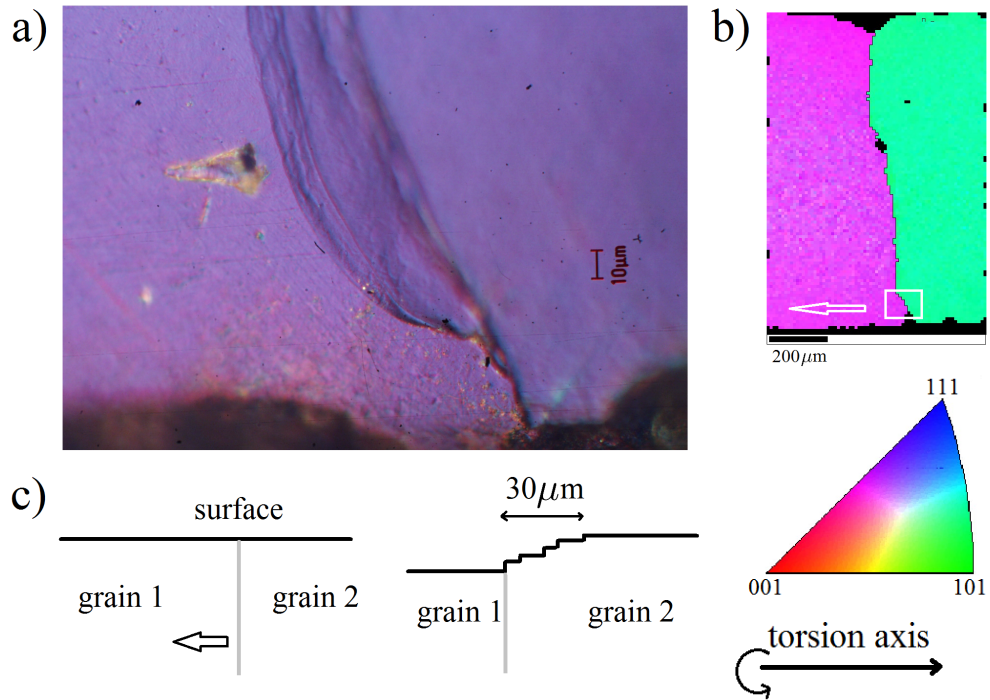
Figure 3.39 – a) Steps at the surface after GB migration. b) EBSD map in IPF colouring before GB migration occurred. The image in a) corresponds to the position of the white rectangle. c) Schematic drawing of the topology before and after GB migration.

lines that prevent the boundary to move away from its original position. The pinning lines provide a source for a restoring force, which is necessary for the appearance of a mechanical loss peak. Without a restoring force, the relaxation mechanism manifests itself as a high temperature background.

Another fundamental ingredient for a relaxation peak is a driving force, which acts on the grain boundary in our case and which is caused by an external stress. A deformation mechanism that has been observed in various metals is the so-called coupled GB motion, where a shear deformation parallel to the boundary plane is accompanied by a normal shear migration. In symmetrical low angle tilt GBs, this deformation mechanism can be easily understood as a collective glide of edge dislocations [Read50, Home13]. The shear stress acting parallel on the boundary causes a glide force on each GB dislocation which results in a migration of the boundary plane.

In GBs with higher misorientations, the dislocation model is no longer applicable, but theoretical analyses by Cahn et al. [Cahn04, Cahn06] and Caillard et al. [Cail09] predicted a coupled GB motion also in the case of high angle GBs. Coupled GB motion has been observed and studied experimentally in bi-crystals in pure Al [Winn01, Gork09, Gork11] and in Zn [Fuku81]. Activation energies depend strongly on the GB type, e.g. the misorientation angle.
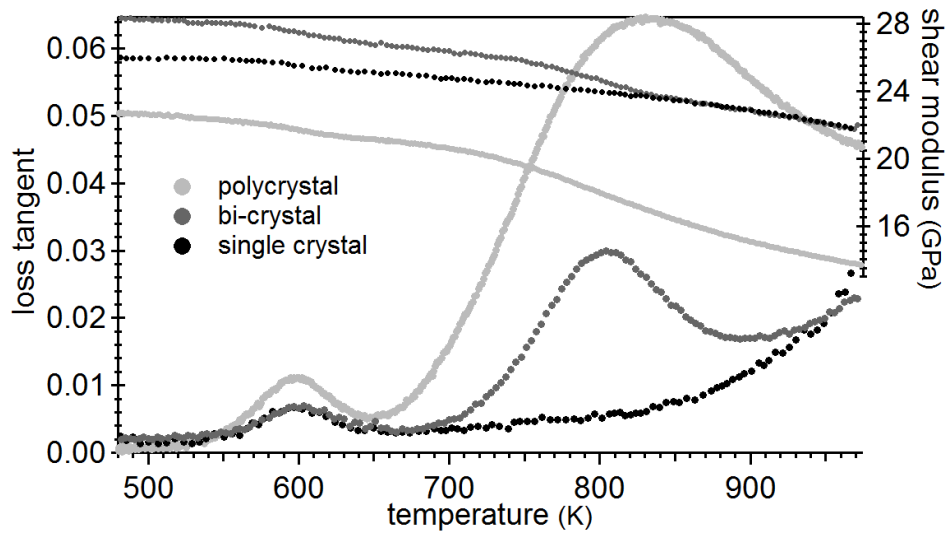
Figure 3.40 – Mechanical loss spectrum of the bi-crystal with a vertical GB. A relaxation peak accompanied by a modulus drop is observed at 800 K. The spectrum of a polycrystal and a single crystal is shown for comparison. The single crystal has been cut from one side of the bi-crystal.

Since in our samples a migration with a corresponding shear deformation at the surface was observed, it is likely that coupled shear migration is a deformation mechanism active at temperatures above room temperature.

3.5.4 Bi-crystal with a Vertical GB

Bi-crystals were produced in the Bridgman oven and the sample was cut such that the GB is vertical in the torsion pendulum and the torsion axis lies in the GB plane. The dimensions at the beginning were (12.3 x 4.3 x 0.78)mm. Length c, width d and thickness a were reduced step by step to observe in which way the loss spectrum of the bi-crystal depends on these parameters. The grain structure and the misorientation angle were controlled before and after the measurements. The misorientation angle remained stable at $\delta = (51.7 \pm 0.2)°$.

In a first cutting step, the width of the specimen was reduced parallel to the boundary plane without cutting through the GB. The residual material was single crystalline and it could be measured in the torsion pendulum. Figure 3.40 shows the spectrum as a function of temperature of the bi-crystal and the single crystal, which had been part of the bi-crystal before. Both spectra superimpose very nicely except for the peak P2. The polycrystal's spectrum is equally shown and its GB peak is about twice as high and much broader.

With this measurement, it can be ruled out that the peak P2 is due to dislocation relaxation in the bulk or to a relaxation related to twin boundaries. The contribution of the bulk material is given by the spectrum of the single crystal and thus, the difference between both spectra must

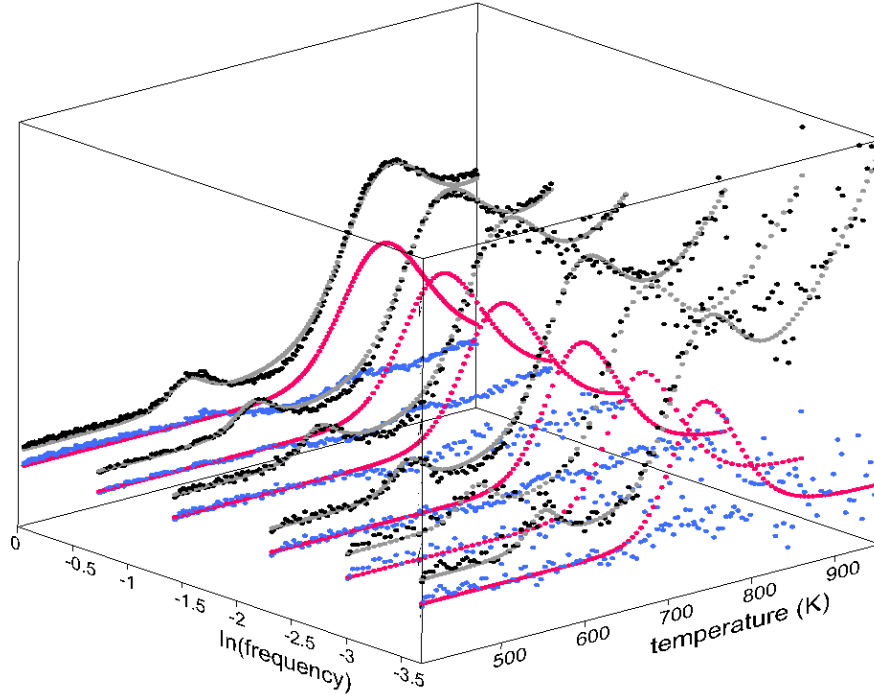be due to the grain boundary, which is the only structural defect that distinguishes single and bi-crystal.

Figure 3.41 – Temperature scans of the bi-crystal (black markers) at different frequency varying from $f = 1$ Hz to $f = 0.025$ Hz. The fitted values are marked in grey, the contribution of the GB peak is shown in red and the residues in blue. The fitting parameters are the same for all measurement points.

In order to extract the activation parameters of the bi-crystal, a different method than the Arrhenius method has been used, which gives a higher confidence level in the parameter values. For a data set of 6 temperature scans presenting a good experimental quality without measurement artefacts, all data points have been fitted at once with the same parameter set. The fitting function is the sum of 2 Debye peaks (2.18) and an exponential background (3.1) as before plus a constant offset a and an offset $b \cdot f$ accounting for experimental noise in the low frequency measurement points. Since the relaxation strength Δ of the Zener peak P1 is temperature dependent, we used the parameters for the Curie-Weiss constant C and the ordering temperature T_c instead.

All parameters are independent and the statistical errors are not artificially small because some parameters have been fixed during the fitting procedure. The fit of the bi-crystal is shown in Figure 3.41 together with the contribution of the GB peak (red). Table 3.3 summarizes the values obtained for the parameters of P1 (first column), P2 (second column), the exponential background (K, n and H_{BG}) as well as the two offset parameters a and b. The activation energy $H_2 = (1.99 \pm 0.03)$ eV is the same as in Section 3.5.1 for the bi-crystal made by diffusion bonding.

	P1			P2			BG	
	value	error		value	error		value	error
$C\,[\mathrm{K}]$	1.8	0.5	Δ_2	0.060	0.002	K	11	2
$T_c\,[\mathrm{K}]$	400	50	$\tau_{02}\,[\mathrm{s}]$	$2.0\cdot 10^{-13}$	$9\cdot 10^{-14}$	n	0.239	0.007
$\tau_{01}\,[\mathrm{s}]$	$5\cdot 10^{-17}$	$<2\cdot 10^{-16}$	$H_2\,[\mathrm{eV}]$	1.99	0.03	$H_{BG}\,[\mathrm{eV}]$	2.01	0.05
$H_1\,[\mathrm{eV}]$	1.88	0.14	β_2	1.55	0.08	a	0.0039	0.0002
β_1	0.9	0.4				b	-0.0013	0.0002

Table 3.3 – Fitting parameters of the bi-crystal. The first column belongs to P1, the second to P2 and the third to the background and offset. The errors are statistical errors (standard deviation with $1\,\sigma$ confidence). In the case of τ_{01}, the third column is the upper limit with $2\,\sigma$ confidence.

Another similarity of both bi-crystals is their behaviour as a function of stress or strain amplitude. The measurements in Figure 3.42 show that the GB peak increases with the strain amplitude while the position varies very slightly. The activation volume that can be inferred from the nearly invisible shift of the peak is therefore quite small with $V_{act} = (760 \pm 1000)\,\text{Å}^3 = (31 \pm 4)b^3$, where b is the Burgers vector of a perfect dislocation.
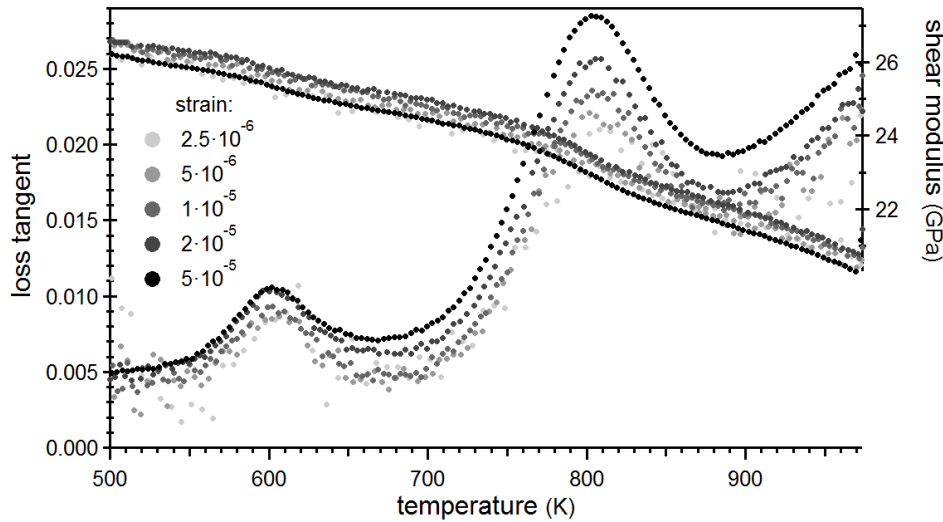
Figure 3.42 – Strain dependence of the bi-crystal's peak: The loss increases with increasing strain, but the peak position remains the same with $T = 800$ K.

3.5.5 Dependence on the Geometrical Parameters

In general, mechanical loss peaks do not depend on the sample geometry but they depend on intrinsic parameters like the impurity content or the dislocation density. If the relaxation mechanism is highly stress dependent, the geometry can play a role since the distribution of the stress in the sample can vary with the sample shape. Other geometry dependencies can be

due to the experimental set up. For example a temperature gradient along the sample length can cause a peak broadening. Using a shorter sample can reduce the gradient and the peak appears narrower.
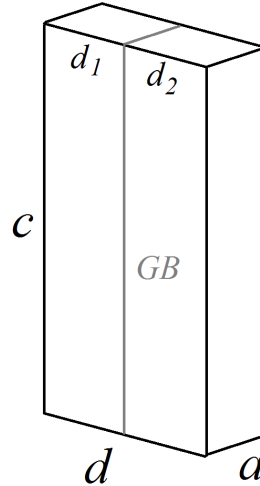
Figure 3.43 – Schematic drawing of the bi-crystal with vertical GB showing the width d, the thickness a and the length c. The deformation axis is the vertical axis along c.

The bi-crystal depicts a complete different behaviour since the relaxation strength depends intrinsically on parameters like the sample width or the thickness. The specimen geometry is shown in Figure 3.43. The names for the different sample lengths have been chosen to be in agreement with the formulas in Chapter 5 and to permit an easy comparison of the experimental results with the theory.
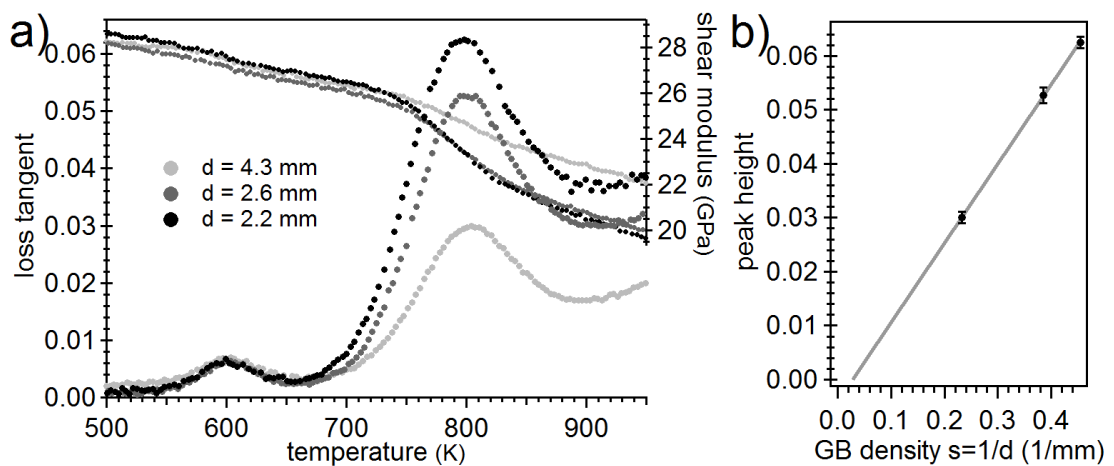
Figure 3.44 – a) Dependence of the bi-crystal's peak on the width d. The peak height increases with decreasing d. The background changes in the same way. The peak position remains unchanged. b) The peak height as a function of the inverse width $1/d$ shows a linear relationship.

Reducing the width d by cutting single crystalline material from both sides leads to a strong

increase in the peak height (Figure 3.44). In fact, it is not only the peak that increases, but the whole high temperature part of the spectrum. Figure 3.44 b) shows the peak height of the bi-crystal's peak as a function of the inverse width $1/d$. It turns out that the height and therefore the relaxation strength is directly proportional to the grain boundary density $s = A/V = ac/acd = 1/d$.

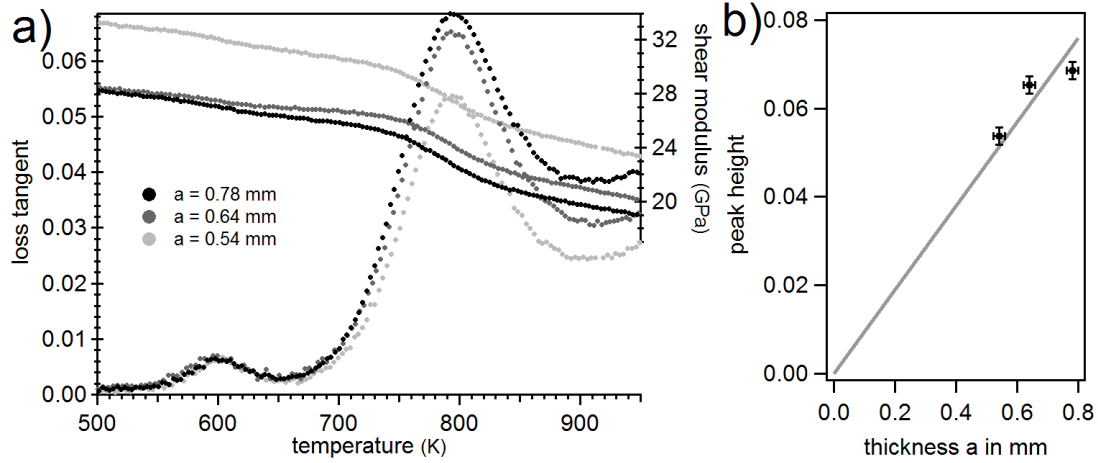Figure 3.45 – a) Mechanical loss spectrum of the bi-crystal with different thickness a. A reduction of a by polishing leads to a decrease of peak P2 and the background. b) Peak height as a function of the thickness a. The black line is only a guide for the eyes.

Figure 3.45 a) illustrates the dependence on the sample thickness a. It shows the inverse behaviour as in the case of the width: When a decreases, the peak height and the background decrease simultaneously. The first polishing reduced the thickness by 18% and the second by 16%. The background behaves accordingly since the difference between the black and the dark grey curves continues on the high temperature part of the spectrum. Figure 3.45 b) shows the peak height as a function of a together with a linear fit through the origin. We observe a trend that the peak height increases with a, even if the data points do not lie on a line.

As a third geometric parameter, the height dependence was tested on a bi-crystal having the GB in the middle. The parameter c has no influence on neither the peak height nor the position (Figure 3.46). The slight shift of the $c = 7.45$ mm curve is more likely to be a measurement artefact than a real effect.

The last geometrical parameter, on which a dependence of the GB peak height was observed, is an asymmetry factor $|d_1 - d_2|/d$, where d_1 and d_2 are the widths of the two single crystalline parts in Figure 3.43. This parameter varies between 0 and 1, where a centred GB has the value 0 and a completely off-centered GB has a value close to 1.

A dependence on the asymmetry factor has been observed only qualitatively. A sample with a curved GB illustrated in Figure 3.47 a) has been measured as a function of the length l. Since the peak of a bi-crystal with a centred GB does not depend on the length, the only parameter, which
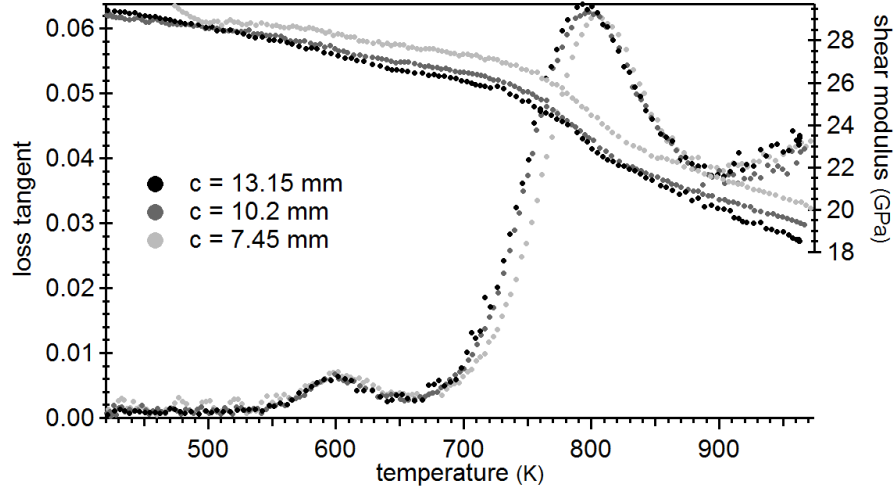
Figure 3.46 – Spectrum of the bi-crystal with varying clamping lengths. The mechanical loss does not depend on the parameter *c* in the case of a centered GB.

changes in the curved GB sample, is the mean position of the GB. Figure 3.47 b) shows, that the GB peak decreases in height when the GB is shifted to the sample border. The background remains unchanged.

In Section 3.4.3, a grain size exponent of 1 was measured, which is in full agreement with the Zener model [Zene41] and grain boundary sliding in a polycrystal. If we make the hypothesis that GB sliding on a microscopic scale has a macroscopic effect as if two elastic solids can glide along their common surface, we can perform finite element (FE) simulations to test the geometric dependencies.

The simulations were performed on two vertical bars, which are joined to form a bi-crystal with a flat sliding surface. Along the GB, the material can slide without friction. The simulations used gold as a bulk material and the geometry and forces were chosen according to the experimental set-up shown in Figure 3.43. As in the experiment, a torque is applied along the vertical axis along *c*. For different geometries changing d, a, c and the asymmetry factor $|d_1 - d_2|/d$, the relaxation strength is simulated. A more detailed description of the FE simulations can be found in the Appendix B.

Figure 3.48 shows the quantitative results of the FE simulations, where the relaxation strength has been measured for various sample geometries. The absolute relaxation strength is much higher than the one measured in a real bi-crystal, because the FE model has a completely flat boundary and the gliding is frictionless.

Observations of grain boundaries by electron microscopy in transmission in Al [Sutt95] an in Au [Pond03, Hsie89] show a crystalline GB structure with a zig-zag profile at room temperature, which becomes more flat upon heating. Even if the GB is flat on atomic scale at temperatures where GB sliding becomes active, we expect a friction due to an amorphous structure in the GB
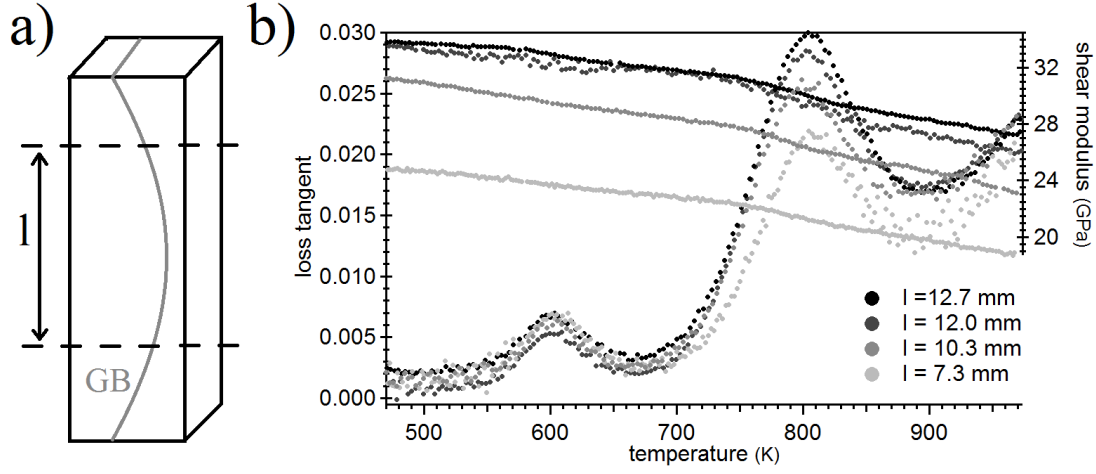
Figure 3.47 – a) Schematic drawing of a bi-crystalline sample with a shifted and curved grain boundary. A reduction of the length shifts the mean position to the right side. b) Temperature spectra of the bi-crystal at different lengths l, which is more a parameter for the shift of the GB to one side. The GB peak decreases when the mean GB position is shifted to the border of the sample.

plane. Therefore, the relaxation strength caused by a real GB is expected to be much smaller than the simulated relaxation strength.

The FE simulations are in general agreement with the experimental findings presented in the beginning of this section. Δ varies very slightly with the sample length c both for a centred GB and a GB shifted to one side so that $d_1 = 3 \cdot d_2$. In both cases, the GB plane is a perfectly flat surface. As in the experiments, the simulated relaxation strength is proportional to the thickness a (Figure 3.48 b) and inversely proportional to the width d (Figure 3.48 c). If the GB is shifted to one side of the sample, the relaxation strength decreases. These geometric dependencies can be summarized in a phenomenological formula:

$$\Delta = \Delta_0 \cdot \frac{a}{d}\left(1 - \left(\frac{|d_1 - d_2|}{d}\right)^\alpha\right). \tag{3.10}$$

Δ_0 is the relaxation strength for a centred GB in a rectangular sample with square base $a = d$. The simulated data set provides values $\Delta_0 \approx 1.1$ and $\alpha = 4.34 \pm 0.09$. A comparison to the experimental findings shows a qualitative agreement with Equation (3.10). The parameter n cannot be extracted from the experimental data, since we do not know the exact correlation between the clamping length l and the mean GB position for the curved GB.

The interpolation of Figure 3.44 b) for a sample with square base $a = d = 0.78$ mm leads to $\Delta_0 = 0.189$, which is six times smaller than the value from the FE simulations. The difference between simulation and experiment indicates that friction plays and important role, if the microscopic mechanism responsible for the GB peak is related to GB sliding.
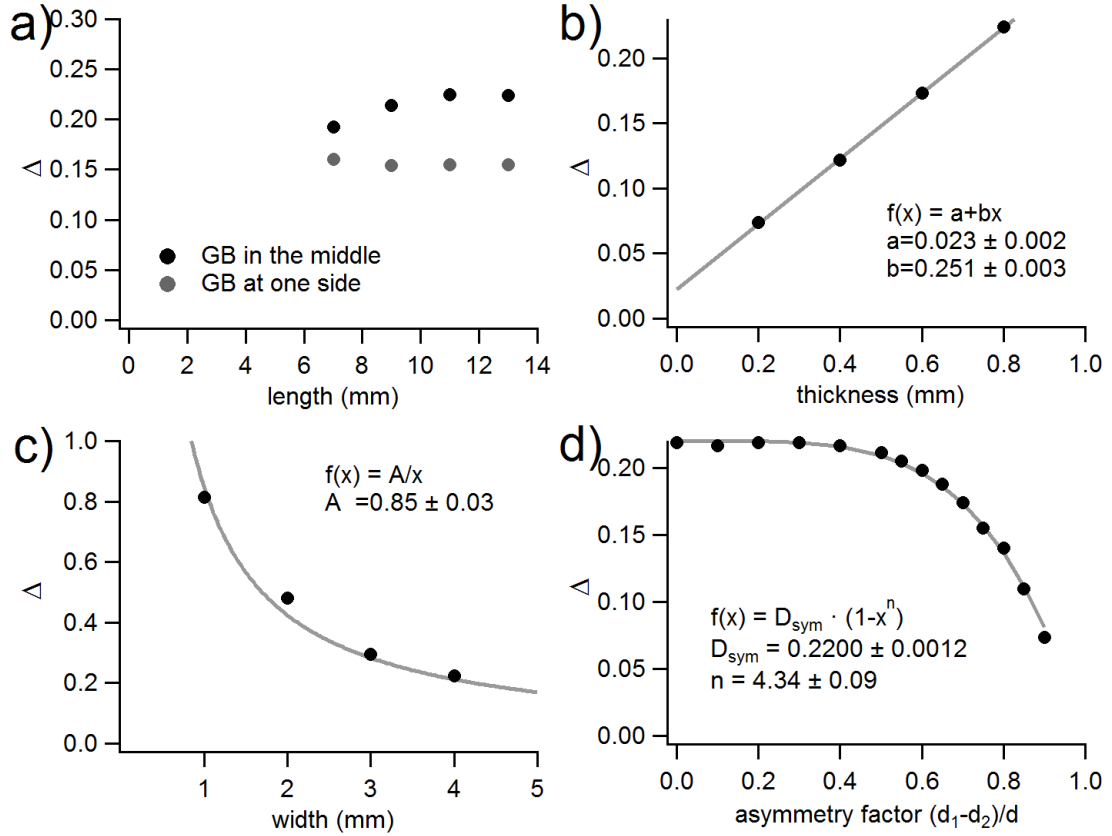
Figure 3.48 – Relaxation strength calculated from finite elements simulations. a) Length dependence for a centred GB and a GB at 1/4 of the total width. b) Dependence on the thickness a with a linear fit. The fit passes close to the origin. c) Dependence on the total width d. The relaxation strength is inversely proportional to d. d) Dependence on the asymmetry factor $|d_1 - d_2|/d$. Δ decreases for an off-centred boundary. The parameter D_{sym} is the relaxation strength of a symmetric boundary plane.

3.5.6 Bi-crystal with a Horizontal GB

Two more parameters can be tested on a bi-crystal: the misorientation angle and the GB plane orientation. The question of the misorientation angle has been answered partially in Section 3.3, where a quantitative difference between polycrystals with HAGBs and LAGBs was observed. The relaxation peak P3 in the LAGB sample is situated at much higher temperatures than the polycrystal's peak P2. The activation energy of P3 is significantly lower than for P2. Such a difference between HAGBs and LAGBs has been observed in Al bi-crystals [Shi06]. Among the HAGBs, the activation parameters scatter around a mean value, but no specific trend is observed. All the Al samples had a vertical GB.

Samples with a horizontal GB plane were cut from the same sort of bi-crystals than the samples with a vertical GB. From the beginning, the samples were rather small with (9 x 2 x 0.9) mm. In a sample with a horizontal GB, the length takes the role of the inverse GB density, and l was

87
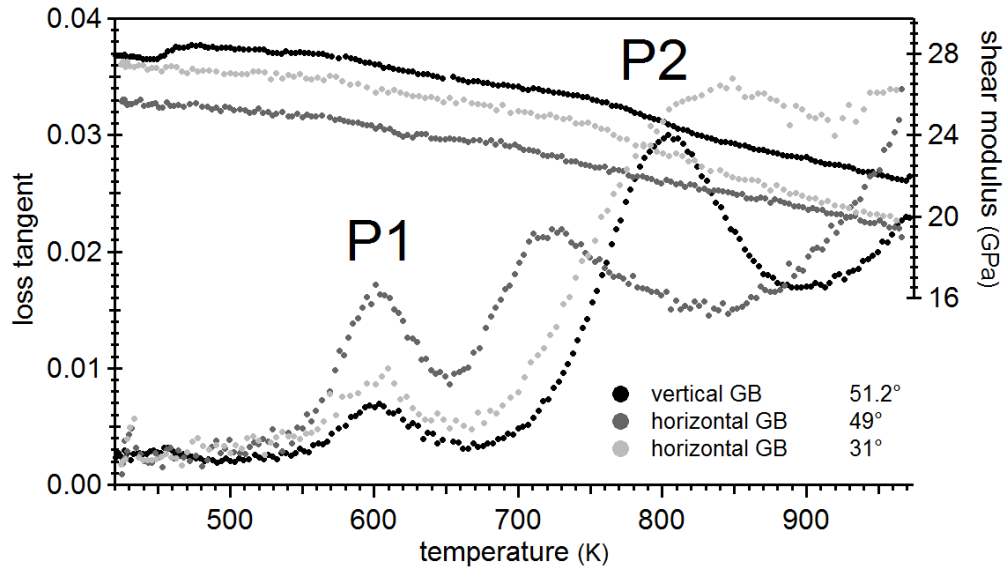
Figure 3.49 – GB peaks in bi-crystals with different misorientation angles and GB plane orientations. The position and the height of P2 changes between the samples.

chosen small from the beginning in order to observe a GB peak with reasonable height. The misorientation angle was measured with a Laue camera.

Figure 3.49 shows the loss spectrum of 2 samples with horizontal GBs, but with different misorientation angles in comparison to the sample with vertical GB from the previous section. The three GB peaks are rather different, position, height and broadening change from one specimen to the other. Even if the misorientation angle between the black and the dark grey spectrum is very close, the peaks are separated by nearly 100 K.

FE simulations could not be performed with a sample geometry containing a horizontal GB, since the two crystal halves would fall apart without fixing arbitrary boundary conditions. A much more realistic kind of simulations will be presented in the following Chapter 4.

Locally, the GB plane is subjected to a shear stress, whose direction changes over the GB plane. Therefore, we do not expect a fundamental difference between a horizontal, vertical or inclined GB plane.

4 Microscopic Stress Relaxation Mechanisms Observed in Molecular Dynamics Simulations

The mechanical spectroscopy measurements have revealed a stress relaxation peak which is closely related to grain boundaries. It shows the characteristics of a GB sliding peak predicted in the framework of the Zener model for polycrystals. On the other hand it is well known that for grain growth processes, GB become mobile and migrate in the direction of the plane normal. In our samples, this phenomenon has been observed by EBSD, but it is not clear if the migration mechanism couples to an external stress and if this mechanism can produce a relaxation peak.

In the last years, computer simulations at the atomic scale have gained more and more importance in research areas like physics, materials science, chemistry and biology. Due to an increasing calculation power and progress in parallel computing and cluster computing, many-body simulations can be run on larger samples over longer simulation times. The molecular dynamics simulations using for example the Embedded Atom Method (EAM) as a semi-classical potential without solving quantum mechanics can give a realistic picture of structure defects in a crystal.

In this chapter, the results of molecular dynamics simulations are presented. The first section gives an overview about the simulations. A comparison of the simulation of the dislocation line tension with the experimental data is presented as a quality test of the simulations using EAM potentials. The structure of GBs with different misorientation angles are presented as a function of temperature.

The second and third section present stress relaxation mechanisms on microscopic level, which are activated in a low temperature regime and a high temperature regime. At low temperature, a shear coupled migration is observed and at high temperatures, GB sliding becomes the dominant deformation mechanism at the GB. The transition is achieved by a change in the GB structure.

4.1 Molecular Dynamics Simulations

Molecular dynamics simulations are N-body computer simulations where the physical movement of each atom or molecule is monitored. The simulation gives access to the position and the speed of each particle at each simulated time step t. The trajectories of the atoms are determined by solving Newton's equation of motion at each time step. The atoms are therefore considered as classical particles which interact by means of an interaction potential due to the surrounding atoms. This is in contrast to the fact that quantum mechanics dominates at the length scales of atoms and that next to all properties of solids like crystal structures, electric and magnetic properties cannot be explained by classical theories. Ab initio simulations, during which Schrödinger's equation is solved, are used for example to calculate vacancy formation energies, but the sample size is limited to several hundreds of atoms.

For a certain class of materials, here metal alloys, it is nevertheless possible to simulate the material's structure and mechanical properties in the framework of molecular dynamics simulations, where the calculation is much faster. The choice of the interaction potential is crucial, since we seek to include quantum mechanical effects as much as possible, in order to simulate the material in a realistic way.

Semi-classical methods like EAM [Daw84] or the Finnis-Sinclair method [Finn84] use approximations of the quantum mechanical theory to include the dominant effects in the form of an effective potential. Since these potentials are short ranged potentials, the numeric evaluation can use a cut-off parameter, up to which distance the potential is considered. In order to calculate the force acting on one atom in presence of the surrounding particles, only a limited number of neighbours need to be considered. For sample sizes of the order of 10 000 or more atoms, it is important that the calculation time does not increase proportional to N^2, but much slower, preferentially proportional to N.

4.1.1 Embedded Atom Method (EAM) Potentials

The embedded atom method (EAM) is a semi-empirical potential, many-body potential, which is used to calculate the total energy of a metal. It has been developed by Daw, Baskes and Foiles [Daw83, Daw84, Daw93] and it is especially useful for large systems. It has been shown by Ackland et al. [Ackl90] that many-body potentials like EAM work particularly well in the case of noble-metal alloys and that the fine details of the electronic structure are less important in determining the atomic structure.

The total energy of the solid is viewed as the energy obtained by embedding an atom into the local electron density provided by the surrounding atoms of the system. A second term represents the electrostatic interaction between atom pairs:

$$E = \sum_i G_i \left(\sum_{j \neq i} \rho_j(R_{ij}) \right) + \frac{1}{2} \sum_{i,j(i \neq j)} U_{ij}(R_{ij}) \tag{4.1}$$

where G_i is the embedding energy of atom i evaluated for a certain value of the total electron density formed by the rest of the atoms. ρ is the spherically averaged electron density at a distance R_{ij} between atom i and j, and U is the electrostatic two-atom interaction.

G is a cohesive energy describing the interaction of one atom with the background electron gas. This term can be understood by considering the physical picture of the metallic bond, where each atom is embedded in a host electron gas created by the neighbouring atoms. Since the embedding term does not contain an angular dependence, it is directly understandable that EAM potentials do not work well for elements, where directional bonding plays an important role, for example semiconductors or transition elements with half filled d-shells. Furthermore, the EAM cannot describe materials satisfactorily, in which covalent bonds as well as effects of the Fermi-surface are important or in which charge transfer occurs. It works best for elements with a strong metallic character and no directional bonding, for example noble elements Au, Ag and Cu.

The atom-host interaction expressed by the embedding term G is intrinsically more complex than a pair-bond model and it incorporates some important many-body interactions. A pair bond model of the type Lennard-Jones cannot be fitted to the properties of any real material, whereas an EAM potential can represent the characteristics of a specific element.

Equation (4.1) has three *a priori* unknown functions that need to be established by a fitting procedure to experimental material properties like density and bulk modulus: The embedding function $G(r)$, the pair-wise interaction $U(r)$ and the electron cloud contribution function $\rho(r)$. For a binary alloy containing elements A and B, the EAM potential requires 7 functions: 2 embedding functions of type A or B, 3 pair interactions AA, BB and AB, and 2 electron density functions A and B.

For the simulations presented in the following, we used EAM potentials for Au [Groc05], AuAg [Zhou04, Ward12] and Al [Wine09, Wine10], which had been tested before by other research groups.

4.1.2 Simulation Set-up

During the simulation, the forces onto each atom are evaluated once every femtosecond. This is sufficiently often for atomistic simulations, where typical time scales of crystal vibrations are given by the Debye frequency $\nu_D \approx 10^{13}$ Hz. Therefore, the forces are evaluated $\tilde{1}00$ times during one oscillation cycle due to lattice vibrations. The simulation frequency is equally much faster than typical frequencies for diffusive processes.

After calculating the forces that act onto each atom at a time step t, the atoms are moved during the time interval Δt according to $\vec{r}^{i+1} = \vec{r}^i + \vec{v}^i \Delta t + \frac{1}{2}(\Delta t)^2 \vec{f}^i / m$. When the time moves forward $t^{i+1} = t^i + \Delta t$, the calculation process is repeated from the beginning by calculating the forces.

The simulations are performed by imposing a finite temperature to the system. Since the atom velocities determine the temperature of the particle ensemble through their kinetic energy, the speed of each particle has to be adapted in order to reach the imposed temperature. At each calculation step, a thermostat removes or adds energy to the system. Using the Berendsen thermostat [Bere84], the temperature of the system is corrected such that the deviation decays exponentially with a time constant τ_B: $\dot{T} = (T_0 - T)/\tau_B$. The updated positions and velocities are consistent with the microcanonical ensemble, since the atom number N is constant as well as the simulation volume V and the energy is controlled by the thermostat. The Berendsen thermostat is efficient for the calculation of large systems and yields thermodynamically correct results for systems with more than 1000 atoms.
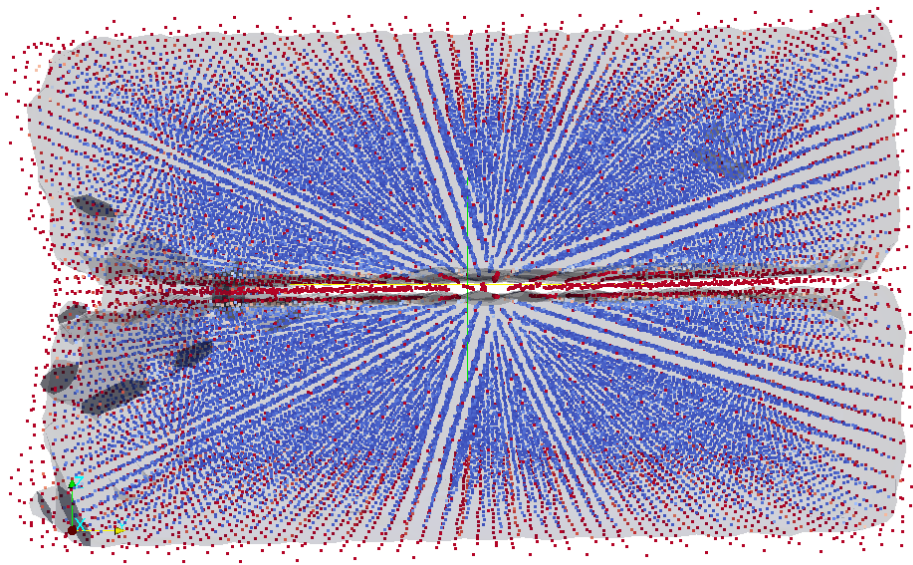

Figure 4.1 – Snapshot during a molecular dynamics simulation. Two different crystal orientations are separated by a GB (horizontal plane).

The simulations have been performed using the software package Lammps [Plim95b, Plim95a], which stands for Large Scale Atomic/Molecular Massively Parallel Simulator. It is an open-source software package written in C++, that can be parallelized easily with the Message passing Interface (MPI) on multiple processors. Further acceleration of the simulation can be achieved by calculating on a 48-cores Nvidia graphics card via the CUDA platform, which works together with Lammps.

The parallelization of the MD simulation using the graphics card is very good, since the crystal can be divided into geometrical chunks, for example horizontal slices, which can be treated on parallel cores. Since the heaviest calculation is the one of the forces and the update of particle positions, the main calculation is done between neighbouring atoms. Thus, most calculations can be performed inside one chunk and the information exchange between chunks is rather small. The speed-up from parallelization is nearly linear for a pure simulation of the atom positions, which means that doubling the number of processors approximately halves the
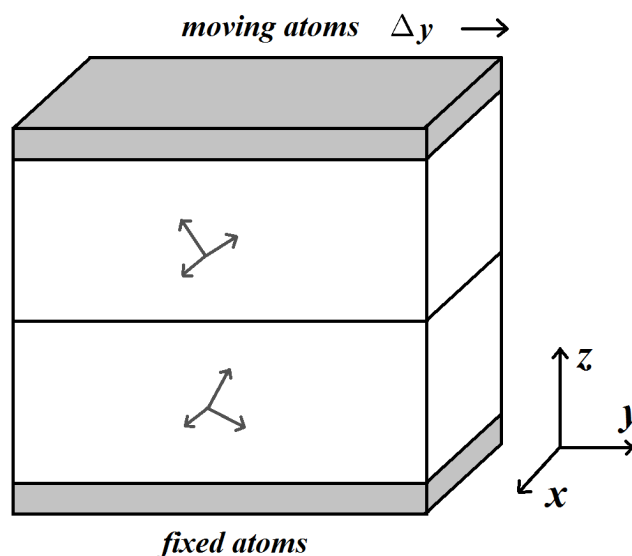
Figure 4.2 – Geometry of a typical MD simulation. The sample is composed of two blocks with different crystal orientations. An upper and a lower slice of 5 Å are hold fixed. After a thermalization step the upper atoms are moved in positive y direction with a velocity of 10 m/s.

runtime. Generating output files like the snapshot in Figure 4.1 costs comparably a lot of computing resources, since the whole simulation data has to be transferred to the CPU, which destroys the advantages from parallelization.

Lammps works with an input file, in which a first part sets up the simulation and a second part contains commands how to run the simulation and what to write as output files. The crystal structure can be created directly via the input file by defining a certain volume in space and by filling it up with atoms in form of an fcc lattice of a defined orientation. Defects like dislocations can be introduced into a perfect crystal by performing displacement operations to each atom dependent on their position from the dislocation line. GBs can be created from two adjacent volumes filled up with crystal lattices of different orientations.

Care must be taken by bringing both lattices into contact. A GB in a bi-crystal has eight degrees of freedom in total: five are macroscopic degrees of freedom (DoF) and can be chosen as three angles to bring the two crystal lattices into superposition and two DoF to define the GB plane normal vector. The remaining three DoF are microscopic that define the relative translation parallel and perpendicular to the GB plane of one crystal part with respect to the other. If the microscopic translations are chosen in a wrong way, the bi-crystal does not relax into the lowest energy state and the simulations cannot be compared with observations in real materials.

To overcome the difficulty of finding the experimentally realized GB structure, a series of simulation with different translations should be performed calculating the energy of the

final GB structure [Alex13], or the relaxed GB structure should be compared to microscopic observations of GBs. The equilibrium GB structure of a Σ5 symmetric tilt boundary has been observed by MD simulations [Trau12, Chen14] and by TEM imaging [Merk87, Wang11]. The main part of the simulations in this chapter is done with a Σ5 boundary so that we can be sure to start with a boundary observed in fcc polycrystals.

All simulated geometries have free surfaces in x, y and z direction, which differs from most MD simulations on bi-crystals, where periodic boundary conditions are applied in the xy-plane to simulate an infinite boundary. We chose another approach with a finite sample, since this geometry does not restrict the simulation to coincidence-lattice-site (CLS)-boundaries. Also, the boundary box does not need an adjustment upon a temperature change to avoid internal stresses due to the periodic boundary condition.

Due to the free surfaces, the outer sample regions will differ from the bulk, but artefacts due to free surfaces are easily identified, since their effect will be limited to a surface region. The analysis of the sample was limited to the inner part, 10-20 Å away from any surface.

Typical sample sizes are 100 x 100 x 60 Å with 20 000-40 000 atoms. A schematic drawing of a bi-crystal is shown in Figure 4.2. In order to apply a shear stress onto the GB, a surface layer of 5 Å thickness at the bottom is fixed and a constant velocity along y is imposed on the atoms situated in a top layer. The simulated times were typically between 0.1 ns and 1 ns, but sporadic long-time simulations up to 5 ns showed the same effects as measured with the shorter simulations.

After creating the geometry and introducing defects like dislocations, all atoms are thermalized using the Berendsen thermostat. The temperature is monitored until an equilibrium is reached. If there are parts of the geometry, where the atoms are fixed like the upper and the lower slice of Figure 4.2, these atoms are excluded in a second thermalization step and their position is fixed. These atoms are not fixed in the first place, because their lattice parameter would not be the same as for the free atoms. After reaching thermal equilibrium for a second time, the top layer is moved with a constant velocity of 10 m s^{-1} to apply a stress to the GB.

4.1.3 Analysis of Structural Defects

MD simulations are a powerful tool to understand the atomic structure of solids because the simulation output is either in form of per-atom data or global quantities. Per-atom variables can be the x-, y- and z-coordinates or velocity components. Global quantities like the temperature or the speed of a group of atoms are calculated from per-atom data already during the simulations.

One important per-atom quantity is the centro-symmetry parameter [Kelc98], which is a useful measure of the local lattice disorder around the atom. It can be used to characterize weather the atom is part of the perfect lattice or a local defect. The centro-symmetry parameter (CS) is
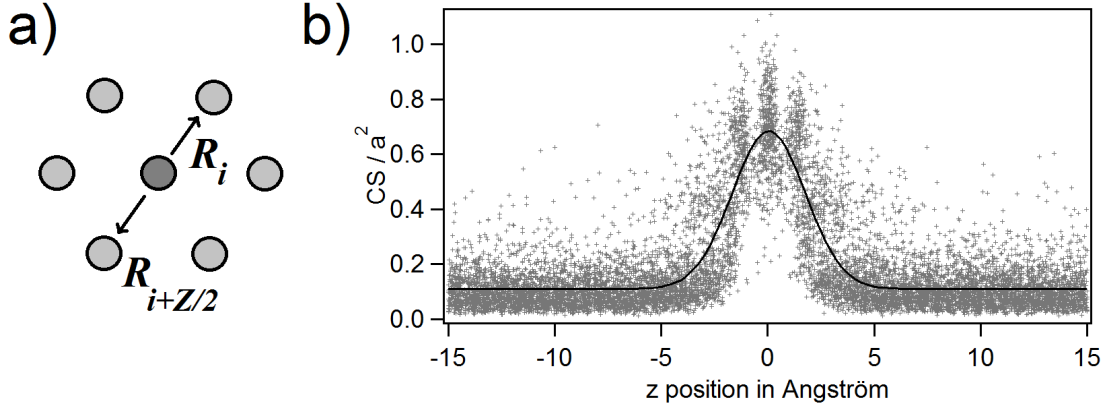
Figure 4.3 – a) Definition of the CS-parameter: The central atom is surrounded by Z nearest neighbours. Vectors to pairs of opposite neighbours are summed up. An atom in a perfect lattice has $CS = 0$. b) Centro-symmetry parameter CS in units of a^2 (lattice parameter $a = 4.1$ Å) across a GB as a function of the z coordinate in Å for $T = 700$ K and $t = 40$ ps without shear deformation. The solid line is a Gaussian fit that provides values for the grain boundary position and width.

calculated as follows:

$$CS = \sum_{i=1}^{Z/2} \left| \vec{R}_i + \vec{R}_{i+Z/2} \right|^2 \tag{4.2}$$

where $\vec{R}_i$ are the vectors between the central atom and the ith nearest neighbour, see Figure 4.3 a). The sum is calculated over pairs of opposite nearest neighbours. For an atom on a lattice site, surrounded by atoms on a perfect lattice, the CS parameter is 0. It will be near 0 for small thermal perturbations of a perfect lattice. Atoms next to point defects, dislocations or crystal surfaces, where the symmetry is broken, show a larger positive value for CS.

The atom colouring in Figure 4.1 is due to the CS parameter calculated for each atom. Red atoms are either situated on the surface or are part of the GB. Atoms coloured in blue have a low CS near to 0 and are part of the fcc crystal. If not stated differently, the same colour code is used in other pictures throughout this chapter.

The CS parameter highlights the GB plane in red and it can be further used to quantify the position of the GB. Figure 4.3 b) shows CS/a^2 of each atom as a function of the local z-coordinate. The GB position is marked by a CS/a^2 value between 0.6 and 0.8, whereas the surrounding crystal has mainly values below 0.2. Atoms at the surface have been excluded from the analysis and the outlying spots are due to thermal fluctuations. A Gaussian fit (black line) yields the exact z-position and the width of the boundary.

Other defects like dislocations and stacking faults were identified by using the dislocation extracting algorithm (DXA) [Stuk10, Stuk12], which is a post processing analysis tool for atom-position datasets. It identifies dislocations by constructing Burgers circuits from the atom
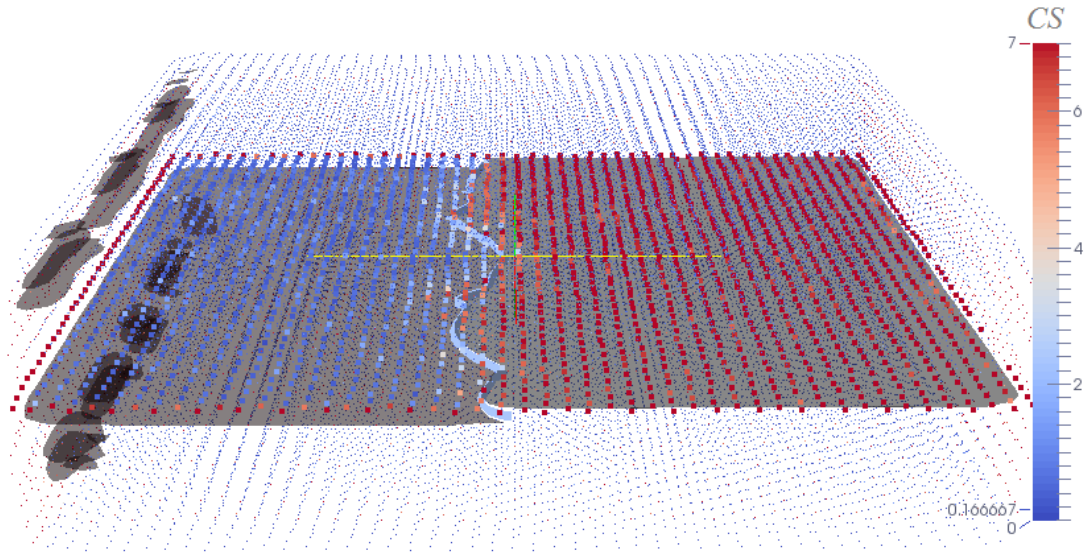
Figure 4.4 – Simulation of a stacking fault (grey plane) containing a partial dislocation (light blue line) at $T = 200$ K. The atoms on one dense plane are amplified showing right half of the stacking fault in red. The dislocation line marks the colour transition from red to blue.
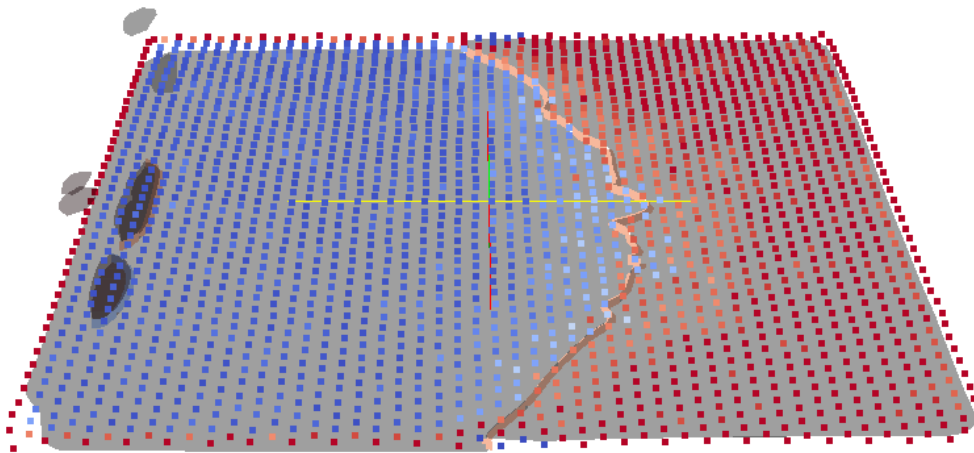
Figure 4.5 – Partial edge dislocation under a static shear stress. The dislocation is blocked at the borders. The curvature radius allows the calculation of the line tension.

positions. Partial and perfect dislocations are represented as lines and stacking faults are illustrated as planes. The defects and atom positions can be visualized simultaneously with the open source software ParaView.

Figure 4.4 shows the simulation of a stacking fault (grey layer) containing a step. One of the horizontal dense planes is highlighted by enlarging the atoms. On the right side, the atoms are red, thus having a high CS value and the stacking fault lies in this plane. On the left side, the

stacking fault is situated one dense layer below. The step is delimited by a partial dislocation (light blue line). The dislocation line is undulated, contrarily to what would be expected from a free dislocation.

One can see from the atom colouring, that the lattice is distorted around the step and that the dislocation core spreads over a few atom distances. The simulation is performed at $T = 200$ K, which is a low temperature compared to the other simulations presented here, but thermal fluctuations are still visible.

The influence of the free surfaces is apparent on the left border of Figure 4.4, where two double stacking faults have been detected. These are distortions of the lattice entering the crystal over a few atom spacings. The spontaneous creation of stacking faults near the borders has been observed frequently in Au samples, since the stacking fault energy is rather low in this material.

4.1.4 Verification of the Interaction Potential: Line Tension

In order to measure the line tension of a partial edge dislocation, the dislocation of Figure 4.4 has been pinned at the sample borders by fixing the atom positions in two small volumes. The atoms in a top layer are then moved in negative y-direction to apply a shear stress to the stacking fault and the dislocations. The dislocation line is bended with a curvature radius of $R = 93$ Å at equilibrium (Figure 4.5). The mean displacement of the dislocation is 11.8 Å for an elastic strain $\epsilon_{el} = 9.8 \cdot 10^{-2}$, which can be calculated from the geometry. The stress is $\sigma = M \cdot \epsilon_{el} = 2.6$ GPa and the line tension becomes

$$T = \sigma b R = 2.6 \, \text{GPa} \frac{1}{3\sqrt{3}} \cdot 4.04 \, \text{Å} \cdot 93 \, \text{Å} \approx 2 \, \text{nN} \tag{4.3}$$

This result can be compared to experimental values measured in Cu [Mugh01]: For near-edge dislocations, a line tension of $T_{edge} = 1$ nN is measured and for near-screw dislocations $T_{screw} = 2.5$ nN. The simulated value in the case of a partial dislocation is very close to the experimental findings, which shows a reliability of the EAM potential.

4.1.5 LAGBs Under Shear Stress

A low angle GB with a misorientation angle of $\alpha = 10,5°$ has been prepared by introducing 5 perfect edge dislocations of type 1/2[110] with a spacing of $d = 15$ Å. The edge dislocations lie in the xy-plane as shown in Figure 4.6. The Burgers vector points in the z direction and the dislocations can glide in the xz-plane.

The equilibrium structure of the LAGB at $T = 200$ K is shown in Figure 4.7 a). The previously rectangular sample bended to accommodate internal stresses due to the introduction of the dislocation array. In the boundary, the perfect dislocations do not dissociate into partial dislocations, as it would be the case for an individual perfect dislocation.
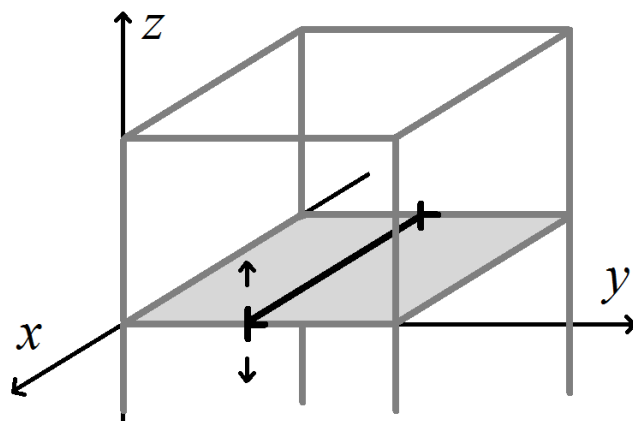
Figure 4.6 – Schematic drawing of the LAGB simulation. The edge dislocation line lies in the light grey plane parallel to the x-axis. The glide plane is the xz-plane, which is marked with small black arrows. A shear stress of type σ_{yz} is applied on the GB plane (light grey).
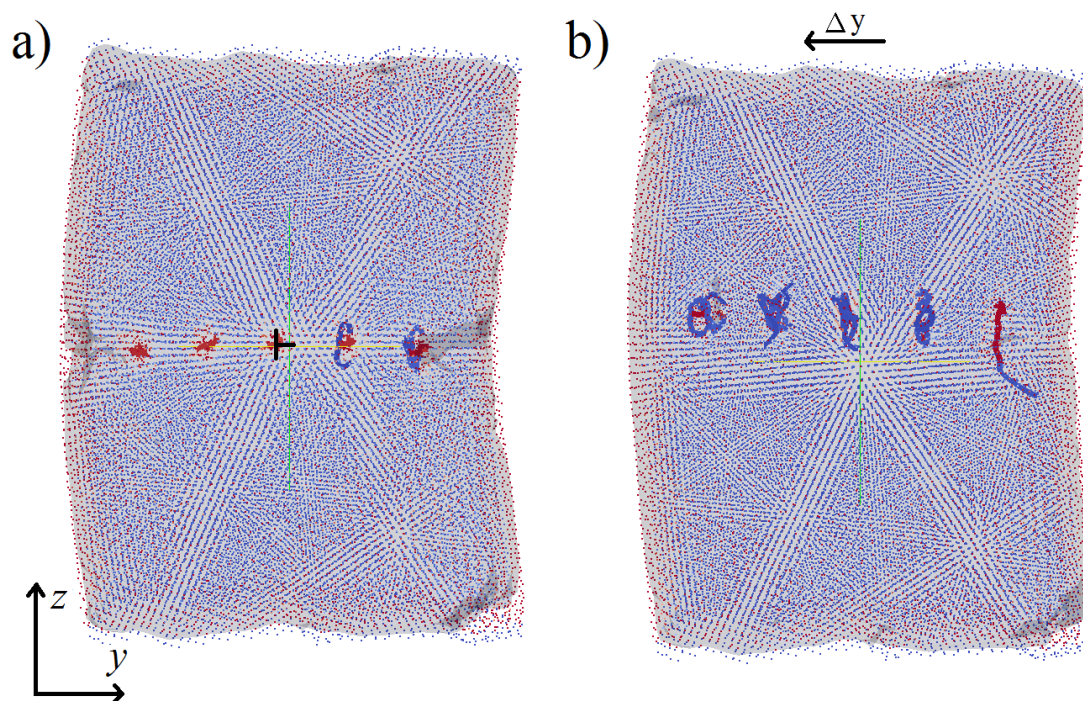
Figure 4.7 – a) Equilibrium structure of a LAGB composed of 5 perfect edge dislocations (red). The Burgers vector points along z. b) Displacing the upper atoms in negative y-directions causes a GB migration upwards.

Under a shear stress σ_{yz}, the dislocations forming the LAGB migrate in positive z direction (Figure 4.7 b). Their movement is a slip along a slip plane perpendicular to the dislocation line, which lies in the x-direction. It is not a standard dislocation movement due to a Peach-Koehler force, since the shear direction (y) is perpendicular to the Burgers vector (along z).

The stress relaxation mechanism observed in the LAGB is also called shear coupled grain boundary migration, where a shear deformation parallel to the boundary plane is accompanied by a normal boundary migration. This deformation mechanism is a collective glide of parallel edge dislocations [Read50]. The shear deformation of the region traversed by the dislocations leads to a coupled lateral translation of the grains forming the bi-crystal. Defining the coupling factor β as the shear displacement parallel to the boundary $u_{\parallel}$ with respect to the normal boundary displacement $u_{\perp}$:

$$\beta = \frac{u_{\parallel}}{u_{\perp}} \tag{4.4}$$

The dislocation model for LAGBs predicts that $\beta = \theta$, where θ is the misorientation angle of tilt boundary. Coupled GB motion has been studied experimentally in bi-crystals in pure Al [Winn01, Gork09, Gork11] and in Zn [Fuku81]. In GBs with higher misorientation angles, the dislocation model is no longer applicable, but a theoretical analysis by Cahn et al. [Cahn04, Cahn06] and Caillard et al. [Cail09] predicted a coupled GB motion to also occur in the case of HAGBs. The coupling factor for general boundaries is given by $\beta = 2\tan(\theta/2)$ [Suzu05], where θ is the misorientation angle of the tilt component.

The type of LAGB studied here is particularly mobile, since the boundary is formed of one sort of dislocations with the same glide plane. The GB can move without changing the structure and without diffusive mechanisms like dislocation climb.

If a there are no boundary conditions on the GB like in the simulation of Figure 4.7, the GB plane migrates in z direction as a whole keeping its flat shape. The free surfaces do not act as pinning points. In a polycrystal, one grain boundary is surrounded by other grains, which impose boundary conditions. In Section 3.5.3, we have observed GB migration, which was limited by the presence of triple nodes that acted as strong pinning points.

In order to simulate a GB plane that is fixed at its borders, the ends of the LAGB dislocations were immobilized. In Figure 4.8 a), the sample is turned by 90° with respect to Figure 4.7, such that the perfect dislocations are visible as horizontal red lines. Local fluctuations lead to a dissociation into partial (blue) dislocations separated by a grey stacking fault surface. A displacement of the upper atoms in positive y-direction causes a migration downwards (Figure 4.8 b), but since the sides are pinned, the GB plane bends down. The GB migration is completely reversible. If the shear direction is reversed, the GB migrates upwards. The mean GB displacement is proportional to the applied shear stress.

Stress relaxation at LAGBs manifests itself as shear coupled GB migration, where the GB plane moves in normal direction. Since LAGBs are composed of one or more equally spaced
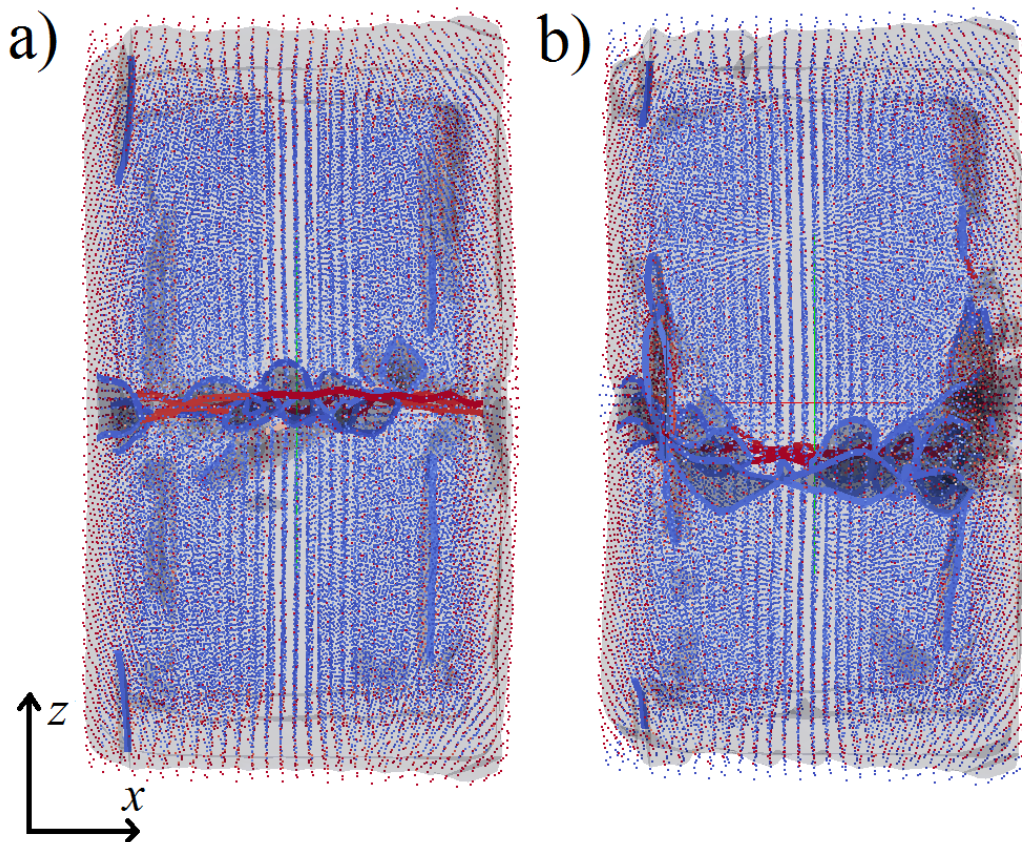
Figure 4.8 – a) LAGB seen along the y-axis: the dislocations forming the LAGB appear as perfect dislocation lines (red) or as loops of partial dislocations (blue). The dislocations are pinned at their ends. b) Pinned GB under a shear stress along the y-axis is bended downwards.

dislocation arrays, the GB movement can be interpreted as a movement of the individual dislocations.

4.2 Stress Relaxation at Low Temperatures: GB Migration

4.2.1 Σ5 GB Structure at 700 K

For the study of a high angle GB, a Σ5(310) tilt boundary has been chosen as a model boundary. It is a Coincidence Site Lattice (CLS) boundary, where 1/5 of the lattice positions of crystal 1 are situated on a lattice position of crystal 2. In the boundary plane, one out of five atoms belongs to both crystals. The (310) denotes the GB plane normal direction. The lowest Σ value is found in the twin boundary or stacking fault, where every 3rd atom in the boundary plane belongs to both crystal lattices. CLS boundaries with low Σ have a boundary energy presenting a local minimum in the energy landscape [Wolf90a, Wolf90b, Bula14]. The probability of finding a Σ5 boundary in a polycrystalline sample is therefore higher than that of finding a random GB.

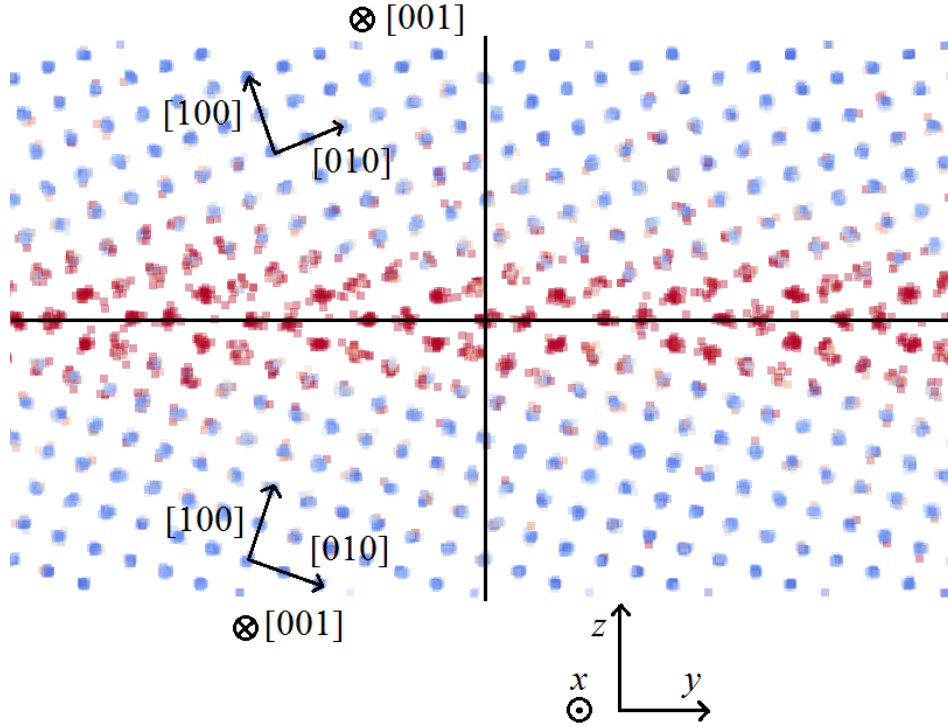Figure 4.9 – Σ5 (310) symmetric tilt boundary at T = 700 K. The atom positions are projected on the yz-plane, showing columns of atoms as spots. The colouring is due to the CS-parameter showing a low centro-symmetry in red. The black arrows indicating the crystallographic directions have a length a = 4.1 Å and connect two atoms situated on the corners of the cubic unit cell.

Figure 4.9 shows the thermalized structure of the Σ5 GB at 700 K. The atom positions are projected onto the yz-plane and therefore the spots are atom columns. The atoms of two adjacent spots normally do not belong to the same plane but they can have different x-components. The crystallographic directions are indicated in both crystal halves. The length of the black arrows correspond to the lattice parameter a = 4.1 Å. The GB is constructed by a rotation of θ = 36.9° around the x-axis, which corresponds to the [001] crystal direction. It is a symmetric tilt boundary, since the rotation axis lies in the GB plane and the GB forms a mirror plane.

The GB at 700 K has a crystalline structure, which is composed of kite-shaped units every 7 Å. The kites can bee seen as the cores of perfect 1/2[110] edge dislocation having their dislocation line along the x-axis. The dislocations lie very close to each other so that it is not possible to trace a Burgers circuit around an individual dislocation. As in the case of the LAGB of Section 4.1.5, the perfect dislocations are confined in the GB and do not dissociate into partial dislocations. The analysis of the CS parameter (Figure 4.3) yields values $z = (-0.038 \pm 0.008)$ Å for the position and a width of $w = (2.310 \pm 0.011)$ Å for the GB at T = 700 K.
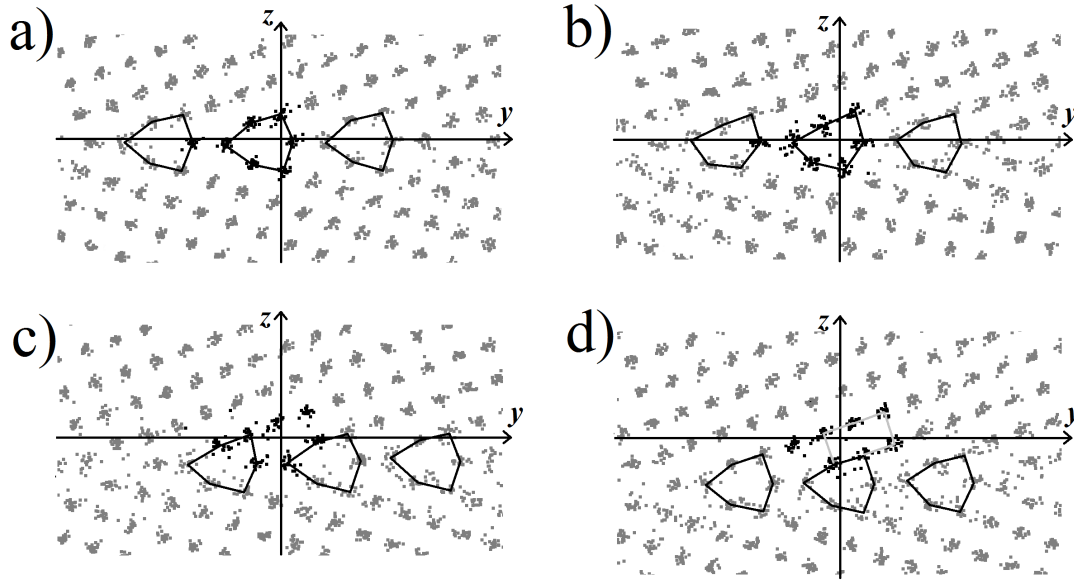
Figure 4.10 – Snapshots of the atom positions at $T = 700$ K after a) 40 ps, b) 60 ps c) 70 ps and d) 80 ps. a) shows the thermalized grain boundary structure before shear deformation. The black lines show the kite-shaped units that form the grain boundary plane. From b) to d) the units get deformed and move downwards under an external shear stress. Atoms marked in black have originally been on the seven atom positions in the middle of image a).

4.2.2 GB Migration Coupled to Shear Stress

When a shear stress is applied to the GB plane by a displacement of an upper slice of atoms in positive y-direction, a movement of the boundary plane in negative z direction occurs.

A closer look on the samples reveals that the single crystalline parts do not undergo an apparent elastic shear deformation but the structure relaxes along the grain boundary plane. Figure 4.10 a) shows the atom positions in the yz-plane before shearing. The grain boundary lies at $z = 0$ and the kite-shaped unit in the middle has its centre at a slightly negative y value.

When the crystal is sheared, the kites first deform (Figure 4.10 b), then the grain boundary moves stepwise as a whole in the negative z direction (Figure 4.10 c and d). The atoms, which previously formed the second kite, form a rectangle marked with a broken grey line in Figure 4.10 d) after the passage of the GB. The centre of the rectangle lies at a positive y value, which indicates that the upper crystal effectively moved to the right with respect to the lower crystal.

The deformation mechanism at $T = 700$ K is a stepwise process where one step of shear deformation of the upper crystal is accompanied by a normal displacement of the GB in the negative z direction. The underlying microscopic mechanism is a GB movement coupled to shear [Cahn06], which has been observed before in the LAGB simulations in Section 4.1.5.
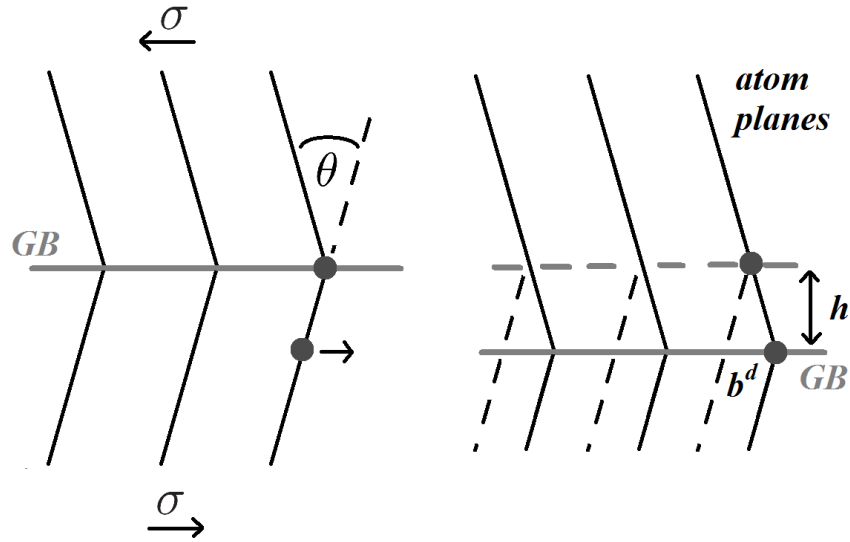
Figure 4.11 – Schematic view of the coupled GB motion of a symmetric tilt boundary with misorientation angle θ. A shear deformation parallel to the boundary of b_d leads to a migration step h.

Under an external shear stress parallel to the boundary plane, the GB dislocations perform a collective glide along (110)-type planes, which results in the coupled motion of Figure 4.10.

The schematic drawing of a GB with tilt angle θ (Figure 4.11) visualizes the coupled GB motion: if the lower part of the crystal is displaced by b_d to the right, the incoming lattice planes of the upper crystal are extended downwards. Effectively, the GB migrates by an amount h while the crystal is sheared. The notation is taken from reference [Khat12], where b_d is the Burgers vector of a "disconnection", a line defect with both dislocation and step character. One particular example of a disconnection is the partial dislocation in the presence of a stacking fault discussed in Section 4.1.4.

4.3 Stress Relaxation at High Temperatures: GB Sliding

4.3.1 Disordered GB Structure and GB Broadening

The same simulations as described in the previous section have been performed on a $\Sigma 5$ boundary at $T = 1000$ K. After a thermalization step, a shear stress is applied parallel to the boundary plane.

At high temperatures above 1000 K, the structure of the simulated high angle GB changes substantially. The atoms coloured according to their centro-symmetry (Figure 4.12) reveal a much more disordered structure. The GB zone is much less crystalline with defined atom positions than in the low-temperature case in Figure 4.9. The kite-shaped units are hardly identifiable. Thermal fluctuations become important in such a way that the GB is no longer
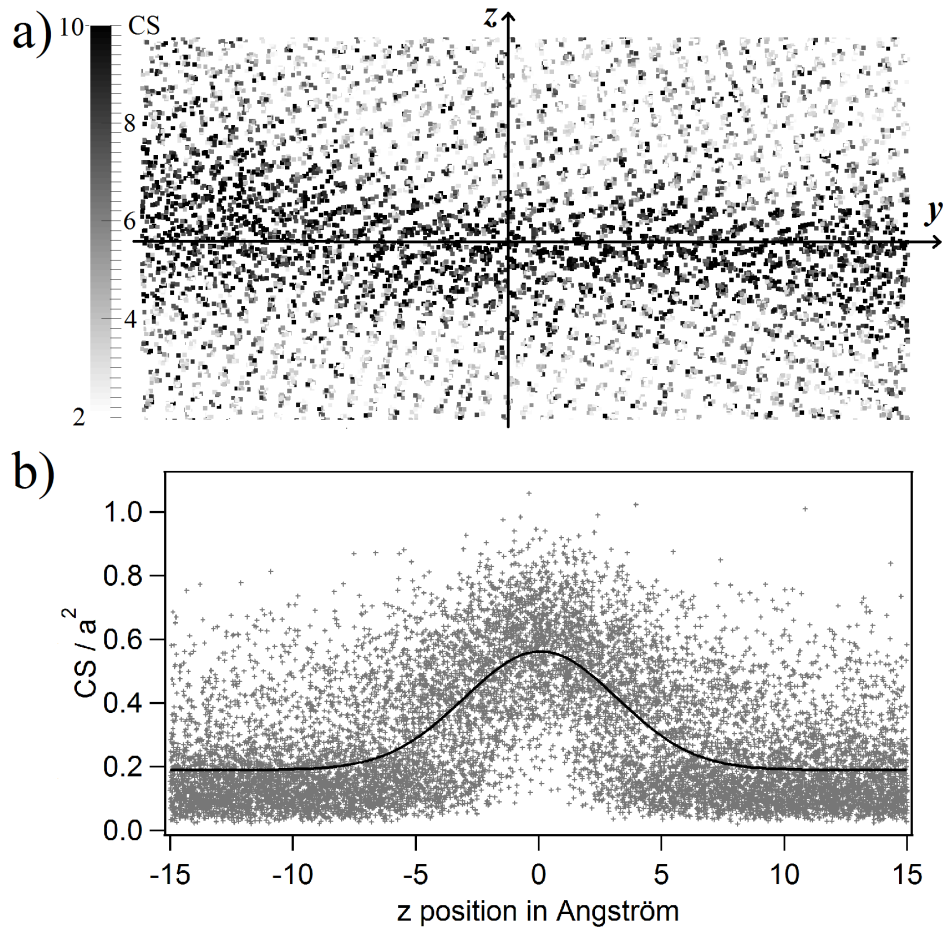
Figure 4.12 – a) Snapshot of the atom positions at $T = 1000$ K after the shear deformation at $t = 140$ ps. The colour is a measure for the centro-symmetry parameter. The grain boundary is visible as a disordered band around $z = 0$. No grain boundary migration occurred. b) Distribution of the centro-symmetry parameter CS/a^2 with $a = 4.1$ Å as a function of the z position at $T = 1000$ K. The solid line is a Gaussian fit to the data points.

a flat plane. The crystal far away from the boundary is still ordered, since the temperature is 337 K below the melting temperature of gold. As before, the analysis of CS as a function of z (Figure 4.12 b) yields the position and width of the GB. With $w = 6$ Å, the GB at 1000 K is more than twice as wide as the GB at 700 K.

Figure 4.13 shows the position of the GB during the simulation at $T = 700$ K in black and at $T = 1000$ K with grey open markers. After 50 ps, a shear deformation is applied. At the same time, the GB at 700 K starts to migrate in negative z direction. At 100 ps, a constant shear is imposed and the GB position stabilizes approximately 4 Å away from its starting position. The behaviour at 1000 K under shear is fundamentally different. The boundary fluctuates around its initial position (open markers in Figure 4.13), but no migration occurs and no correlation to the shear deformation is observed.

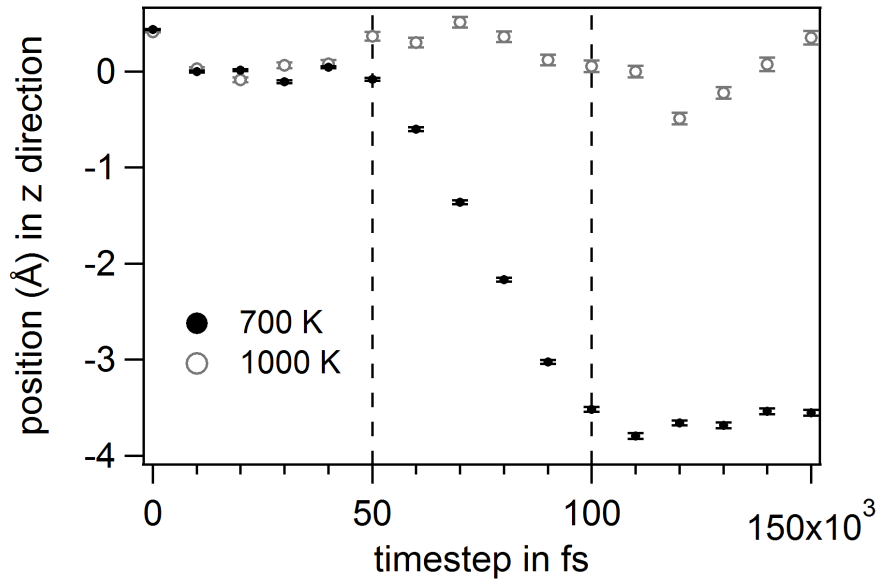Figure 4.13 – Grain boundary position as a function of the simulation time step at two different temperatures: The shear deformation starts after 50 ps and stops at $t = 100$ ps. At $T = 700$ K, the grain boundary moves in negative z direction as soon as the sample is sheared. At $T = 1000$ K, the grain boundary plane fluctuates around its original position at $z = 0$, but it does not migrate. The error bars indicate the uncertainty of the position parameter in z direction taken from a Gaussian fit.

In the good crystal parts far away from the disordered GB zone at 1000 K, the cubic lattice structure is preserved also during the shear deformation. Therefore, the elastic part of the deformation can only be very small and the main shear deformation is due to sliding of the upper crystal as a whole with respect to the lower crystal. Apart from local fluctuations, no perpendicular movement of the boundary plane is observed at 1000 K.

4.3.2   Diffusion and Premelting at the GB

Since the GB in the high temperature regime has a disordered structure, other parameters than local atomic arrangements should be considered. The analysis of the diffusion, which is directly related to the motion of atoms, can give insight into the microscopic mechanisms that trigger GB sliding.

Diffusion is observed in Figure 4.14, where the positions of a group of GB atoms is followed over time. In a), the starting positions in the yz-plane are shown, where the GB is situated along the horizontal axis. Seven atom columns are marked in large red squares. Figures 4.14 b) and c) show the thermalized structure at $T = 1000$ K after 100 ps and after 300 ps. From the original seven positions, the tagged atoms diffuse mainly in the GB region. The cloud of marked atoms is three times as wide as it is high, which indicates an anisotropic diffusion. The atom mobility in the GB plane is higher than perpendicular to the GB.
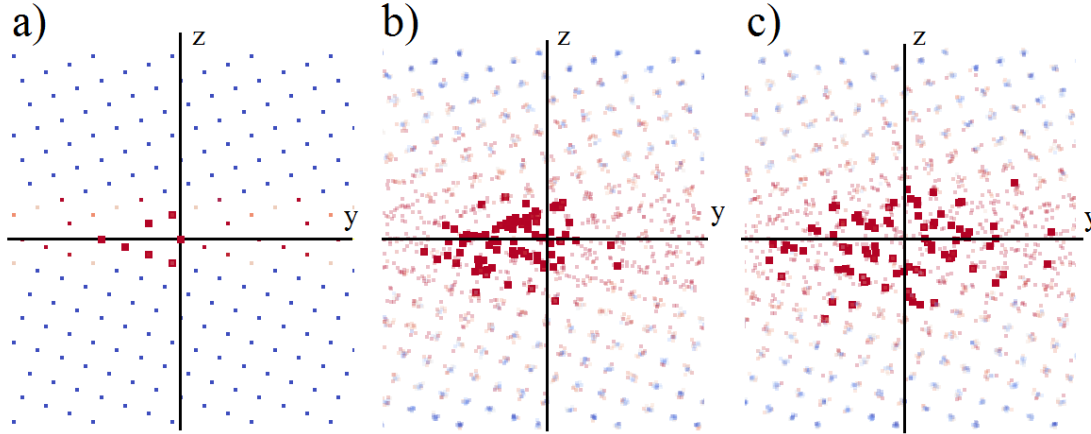
Figure 4.14 – a) Initial atom position before thermalization seen as a projection on the yz-plane. The seven atom columns are tagged in red. b) Snapshot of the atom positions after 100 ps and c) after 300 ps at 1000 K.

The ongoing debate about whether atoms at grain boundaries are premelting or not [Brou98, Alsa05, Qi07] is directly related to the atom dynamics at the GB. To evaluate the atomic motions at different positions in the simulated sample, the root-mean-square displacement (RMSD) is calculated for groups of atoms. The RMSD is the mean distance that is covered after a time T and it is calculated as follows:

$$\text{RMSD}(\mathrm{d}t) = \sqrt{\left\langle (r_i(t+\mathrm{d}t) - r_i(t))^2 \right\rangle_i} \tag{4.5}$$

This quantity depends on the time increment $\mathrm{d}t = 20$ ps. Lammps can calculate automatically the MSD without the square root, where $(r_i(t+\mathrm{d}t) - r_i(t))$ are either the squared displacements $\mathrm{d}x^2$, $\mathrm{d}y^2$ and $\mathrm{d}z^2$ in a single direction or the total squared displacement $(\mathrm{d}x^2 + \mathrm{d}y^2 + \mathrm{d}z^2)$. If the atoms in a group do not diffuse, the RMSD converges quickly as a function of $\mathrm{d}t$ after a ballistic regime of thermal movement. If there is diffusion, the RMSD will not converge until the atoms of the initial group are uniformly distributed over the whole sample and the RMSD has a value of the order of the sample size. If diffusion is isotropic, the total RMSD in 3 dimensions is larger by a factor $\sqrt{3}$ than the 1-dimensional quantity RMSD(dx).

In the present study, the RMSD is measured as a function of the vertical z position. For this, the bi-crystal is divided into 19 slices of thickness 2 Å along z illustrated in Figure 4.15 a), where each slice contains approximately 720 atoms. Figure 4.15 b) shows the RMSD as a function of z for two different temperatures containing a $\Sigma 5$ GB at $z = 0$. The GB position is marked by an increase of the RMDS value up to $0.45 a_0$ for $T = 750$ K and $0.83 a_0$ for 1000 K, a_0 being the distance to the nearest neighbour. The atoms near the GB experience the largest mismatches with their neighbours, which indicates that these atoms are more mobile than the atoms in the bulk. This leads to a higher displacement for atoms near the GB.

In the region of the ordered crystals, the RMSD is flat and decreases slightly to the sample
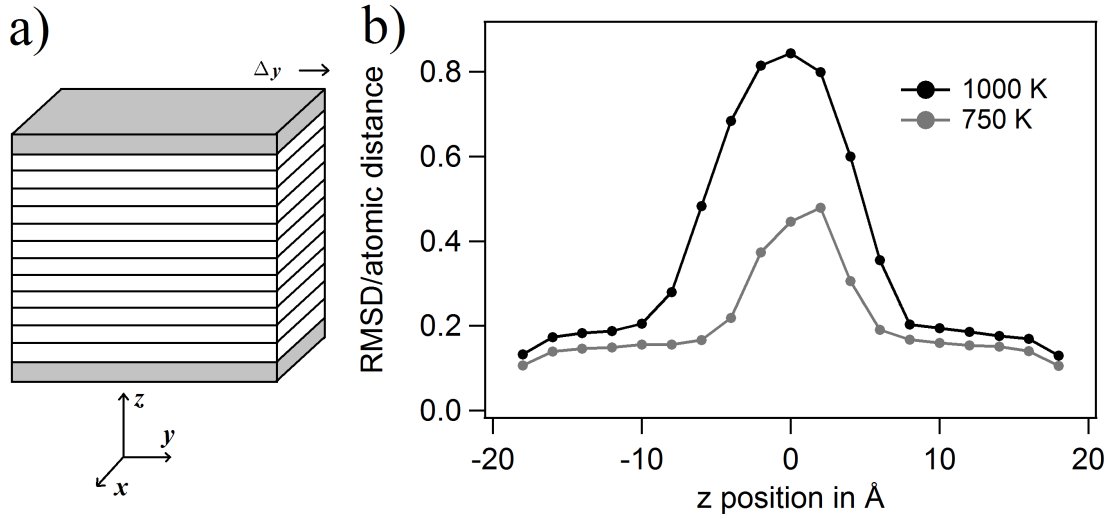
Figure 4.15 – a) Sketch of the atom groups for the RMSD parameter calculation. The sample is divided into slices along the z axis. The grey slices represent fixed atoms which are excluded from the analysis. The specimen is sheared in positive x-direction. b) Average atomic RMSD as a function of the slice position z. The peak marking the GB is twice as high at 1000 K than the peak at 750 K.

borders, where the top and bottom atoms are artificially hold in place. The main difference of the atom dynamics at low and high temperature lies in the GB region, where the atoms are nearly twice as mobile at 1000 K.

Also, the GB zone, which shows an increased mobility with respect to the "good" crystal, is much wider at 1000 K. At 750 K, the width obtained from a Gaussian fit is $w = (4.4 \pm 0.4)$ Å and at 1000 K, the GB is $w = (6.5 \pm 0.2)$ Å wide. Both values are larger than the width obtained from the CS-parameter (2.3 Å and 6 Å for 700 K and 1000 K respectively).

From Figure 4.14 it was found that diffusion is enhanced in the directions of the GB plane. In order to quantify the anisotropy of the atom mobility, the RMSD parameter has been separated into its x, y and z components. Figure 4.16 shows the atom displacement along single directions at 750 K and at 1000 K during the bi-crystal's shearing along the y-direction. In the lower crystal part, the RMSD is constant and the atom mobility is isotropic.

At the GB, the RMSD(dx) and RMSD(dy) lie above the RMSD(dz) curve and the difference is shown as a blue hatched area in Figure 4.16 marking the anisotropy of diffusion. The atom displacement in the GB plane is approximately 30% higher than perpendicular to the plane at $T = 1000$ K.

In the upper crystal part for $z > 10$, the RMSD(dy) is significantly higher than the (dx) and (dz) components during shear deformation of the bi-crystal. The difference (red hatched area) is due to the displacement of the upper crystal with respect to the lower part, since the atom motion is a sum of the thermal displacement and the global motion of the crystal.
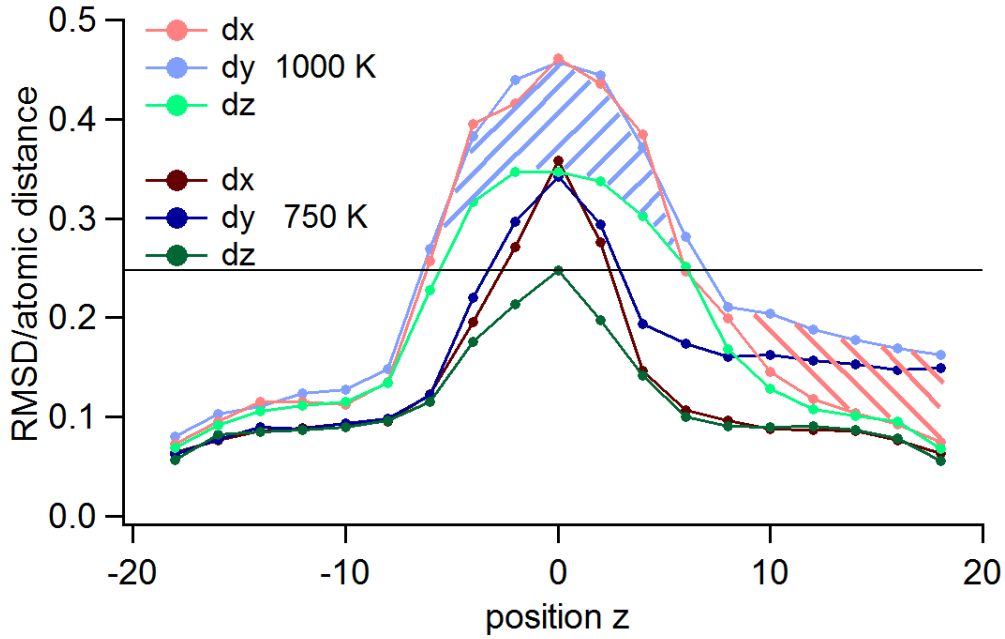
107

Figure 4.16 – RMSD as a function the z position separated into contributions along the x, y and z directions during a shear deformation experiment. The difference between the dx and the dy curves at positive z (red hatched area) is due to the superimposed shear deformation of the upper crystal. The horizontal line indicates the Lindemann melting criterion of $0.25a_0$.

The difference between the (dy) and the (dz) curve in Figure 4.16 disappears abruptly when approaching the GB zone from high z values for both temperatures. This means that the bi-crystal mainly deforms at the GB. If the deformation were purely elastic, the difference between RMSD(dy) and RMSD(dz) would decrease gradually over the whole sample height. Therefore, GB sliding manifests itself in a high temperature regime in form of an anelastic deformation, where one crystallite moves as a whole with respect to the other.

The Lindemann criterion [Lind10] relates the origin of melting to the atomic mobility. It states that melting occurs when the RMSD of the atoms in a crystal reaches a critical fraction of the equilibrium inter-atomic distance a_0. The Lindemann criterion for bulk materials is typically 7.1% for fcc metals like Au, Ag and Cu [Shap70].

MD simulations on Ni nanoclusters [Qi01] have shown that a Lindemann criterion of $0.25a_0$ is more adapted for surface atoms. This means that atoms moving more than 0.71 Å in 20 ps are likely to diffuse into another lattice position and they might be considered to be premelted. It is important to state the time scale, at which we ask the question if a material is solid or liquid. If there is diffusion in a sample region, it is sufficient to increase the integration time in order to obtain a RMSD value superior to the Lindemann criterion.

In Figure 4.16, the melting criterion is marked with a horizontal black line. It cuts the peak marking the GB position, such that a GB zone of 10 Å width can be considered as being melted
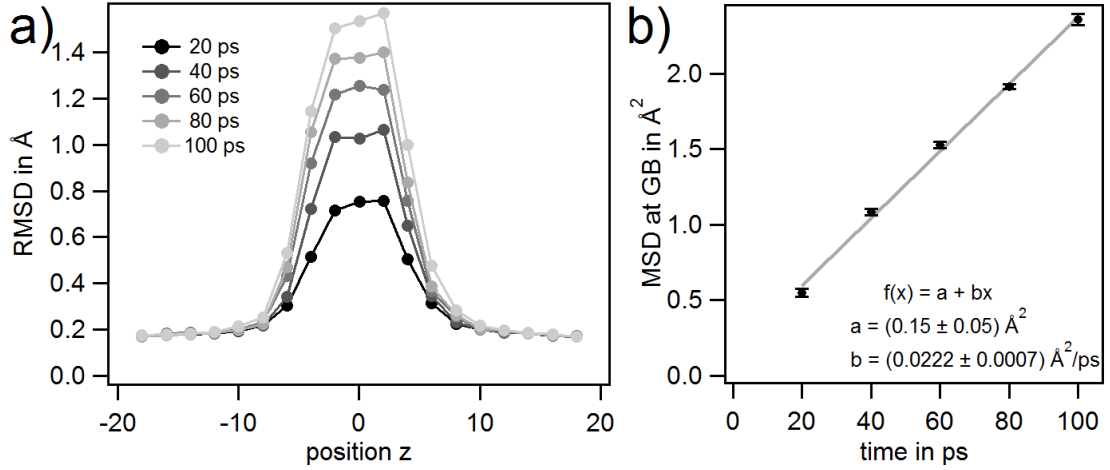
Figure 4.17 – a) RMSD for different integration times dt at 1000 K. Diffusion occurs in the GB zone, where the peak increases with increasing dt. Mean square displacement of the GB zone as a function of dt. The atom groups at -2, 0 and 2 Å contributed to the MSD. The slope of the linear regression yields the double of the diffusion coefficient D.

at 1000 K. The melting applies for atom movements in x, y and z directions. At 750 K, only the x and y curves are cut by the melting line and the width of the melted zone is 4 Å wide, which corresponds to 1 cell parameter $a = 4.08$ Å. The RMSD(dz) curve lies below $0.25a_0$, which means that the in-plane diffusion is enhanced, but the GB cannot be regarded as being melted in a layer of finite thickness.

In order to quantify the diffusion, the RMSD can be calculated with different time increments dt. If diffusion occurs on a certain time scale, the atoms can change their lattice position and the mean displacement increases with increasing time interval. Figure 4.17 a) shows, that over a time span of 100 ps, relevant diffusion occurs exclusively in the GB region. The crystalline parts above and below the GB are unaffected by the increase of the time increment dt.

According to Einstein's theory of Brownian motion [Eins56], the mean square displacement (MSD) of particles performing a random walk can be related to the elapsed time and the diffusion coefficient D:

$$\langle x^2 \rangle = 2D \cdot t \tag{4.6}$$

Thus, if the squared value of the RMSD at the GB is plotted as a function of the time increment dt, the slope yields the double of the diffusion coefficient D. A linear fit to the MSD data points in Figure 4.17 b) yields a slope of $b = (2.22 \pm 0.07) \cdot 10^{-6}$ cm^2/s. The diffusion coefficient in the GB region at $T = 1000$ K is $D = (1.11 \pm 0.04) \cdot 10^{-6}$ cm^2/s.

At $T = 750$ K, the diffusion coefficient is $D = (1.09 \pm 0.03) \cdot 10^{-7}$ cm^2/s, which is one order of magnitude lower than at 1000 K. This difference is compatible with an Arrhenius behaviour, where the diffusion coefficient is thermally activated: $D = D_0 \exp(-H_{GB}/k_B T)$. A rough estimate

from these two temperatures gives a GB diffusion energy of $H_{GB} = 0.6$ eV and a temperature independent diffusion coefficient $D_0 = 1.2 \cdot 10^{-3}$ cm^2/s. These results can be compared with the literature, where the self diffusion coefficient in pure Au has been measured in polycrystals and single crystals [Duhl63, Neum08]. The diffusion coefficient at 1000 K is $D = 8 \cdot 10^{-11}$ cm^2/s and the activation energy for self diffusion in the bulk is measured between 1.7 and 1.8 eV. The GB diffusion coefficient has been measured in Au-Ni thin films [Abdu03] and the activation energy for GB diffusion was measured to 0.94 eV. The GB diffusion coefficient from our simulations at 1000 K is therefore 3 orders of magnitude higher than in the Au bulk material and the activation energy (0.6 eV) is not so far away from the values measured in Au-Ni films. With respect to the activation energy measured for the relaxation peak P2 (2.08 eV), the value from the diffusion coefficient seems to be very low, but the simulations have been made on pure Au, whereas we measured the AuAgCu alloy in the experiments.

The simulations on an alloy containing 60% Au atoms and 40% Ag atoms did not reveal a fundamental difference with respect to the simulations using only Au atoms. At low temperature, coupled GB migration occurs and a transition to GB sliding is observed under stress at high temperatures. The atomic structure is similar and the only difference is observed by analysing the atom mobility. The RMSD at the GB is reduced by 25% indicating that the GB diffusion is lower in the alloy.

At high temperatures, the deformation mechanism under a shear stress is GB sliding, since the position of the GB remains the same and the upper crystal moves as a whole parallel to the boundary plane. The sample is not sheared elastically, but the shearing occurs at the GB zone as demonstrated in Figure 4.16, where the difference between the RMSD(dy) and (dx) curves (marked as a red hatched area) disappears abruptly when approaching the GB zone from high z values. The GB at high temperatures is marked by a high local disorder and a strong increase in GB diffusion. The diffusion is anisotropic, so that the in-plane diffusion is increased with respect to the diffusion perpendicular to the GB plane.

The simulations suggest that the appearance of GB sliding is accompanied with a microstructure change in the grain boundary layer. The thickness of the grain boundary zone increases by a factor 2 when changing between migration and sliding regime. The former kite shaped grain boundary units are not distinguishable any more at high temperatures where sliding is active. The notion of grain boundary dislocations forming the boundary disappears completely. It seems that it is more appropriate to describe the grain boundary zone as a amorphous layer confined between two solids.

The application of the Lindemann criterion to the simulations showed, that the GB in the high temperature regime can be considered as being melted, whereas at 750 K, the GB zone is too thin and the atom mobility is too low in order to speak about a melted layer. At 1000 K, the GB is mobile and the sliding behaviour is similar to the shearing of a liquid. The simulation reveals that the GB sliding behaviour is directly related to the thickness of the melted layer at the GB.

In conclusion, the molecular dynamics simulations reveal two different microscopic stress relaxation mechanism at the GB, which are active in different temperature ranges.

- A low temperature mechanism below 750 K, where the GB migrates perpendicular to GB plane under a shear stress. This deformation mechanism is called coupled shear migration and can be observed for high as well as for low misorientations.
- A high temperature mechanism active above 1000 K, where one grain slides with respect to the adjacent grain.

The transition between the mechanism is marked by an increase of the diffusion on the GB region and by a widening of the boundary layer. The GB can be seen as being melted, but the liquid layer does only exist in the presence of the adjacent crystalline structure with a sufficiently high misorientation angle between the grains.

5 Modelling of Grain Boundary Relaxation

The molecular dynamics simulations presented in the previous chapter suggest two possible microscopic mechanisms that could be responsible for the mechanical loss peak observed in gold and in many other metals and metallic alloys. Consequently, in this chapter two models are developed to describe the mechanical loss spectrum due to stress relaxation at GBs.

The first model (membrane model) is inspired by a coupling mechanism causing the grain boundary to migrate in normal direction under an applied shear stress.

The second model (sliding model) supposes that grain boundary sliding is the relaxation mechanism where the boundary plane remains at its original position during a shear deformation. The explicit expressions of the mechanical loss peak contain parameters such as the grain size d, the viscosity η and the misorientation angle θ of adjacent grains that can be directly derived from the experimental results. Comparing the experimental results from mechanical spectroscopy with the mechanisms found in the simulations will allow us to give a clear interpretation of the GB peak.

5.1 Membrane Model

In this first model, application of a shear stress on the GB plane gives rise to a displacement of the GB in the normal direction. The smallest unit to consider are two crystallites separated by a grain boundary, which has a favourable orientation with respect to the external stress. In the presence of the surrounding crystallites no long range deformation can occur and one can assume that triple lines are fixed.

For GB migration coupled to shear, the external stress is applied in a direction parallel to the GB plane and the GB migration is allowed in the normal direction. In tilt boundaries as shown in the sketch of Figure 4.11 on page 103, the GB migrates by one step h, when the crystal is sheared parallel to the boundary plane by one unit of b_d.

The migration step h and the shear displacement b_d can be related to the misorientation angle
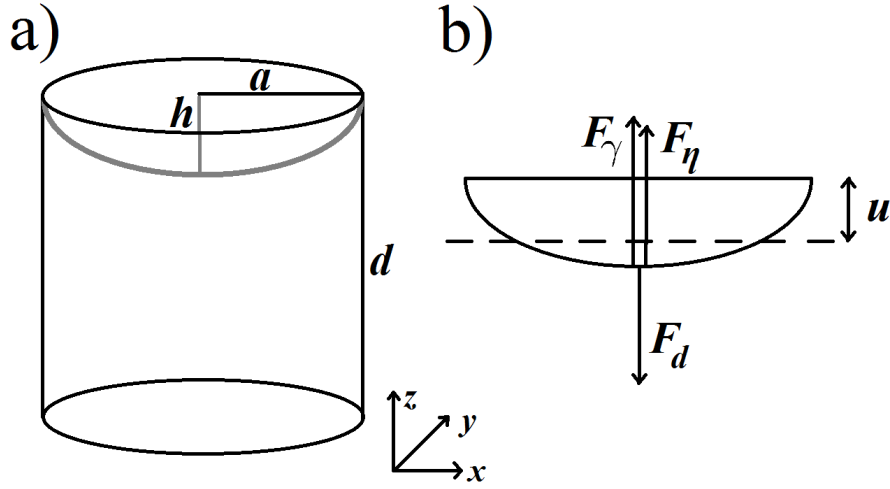
Figure 5.1 – a) Smallest unit in a polycrystal considering a model with a normal displacement of the GB plane. A shear stress leads to a bending of the surface and the formation of a spherical cap. b) Forces acting on the advancing surface: driving force F_d, restoring force due to a finite surface energy F_γ and friction force F_η. u is the average displacement of the surface.

θ and the nearest neighbour distance a_0:

$$b_d = 2a_0 \sin \frac{\theta}{2} \quad \text{and} \quad h = a_0 \cos \frac{\theta}{2} \tag{5.1}$$

which leads to

$$\frac{b_d}{h} = 2 \tan \frac{\theta}{2}. \tag{5.2}$$

If the misorientation angle θ is small, Equation (5.2) can be simplified to $b_d/h = \theta$.

5.1.1 Moving Surface: Spherical Cap Model

The smallest unit to consider is one grain with one grain boundary. The bulk of the grain provides the elastic deformation, while the grain boundary movement provides the anelastic one. A simple geometry for this problem shown in Figure 5.1 a) is a cylindrical grain with height d and base area πa^2. The grain boundary plane is fixed on the circular border. An external stress causes a normal displacement of the boundary plane, which will bend forming a spherical cap.

The GB can be seen as a membrane that moves under a shear stress. Three forces can be defined that act on the GB plane (Figure 5.1 b):

F_d : a driving force due to the applied stress,

F_γ : a restoring force due to the surface energy,

F_η : a friction force proportional to the speed of the advancing surface.

The volume of the spherical cap V_c with height h and the corresponding surface A_c are:

$$V_c = \frac{\pi h^3}{6} + \frac{\pi h a^2}{2} \quad \text{and} \quad A_c = \pi(a^2 + h^2) \tag{5.3}$$

The surface energy $E_\gamma = \gamma A_c$ and its infinitesimal change due to a change of the height are:

$$E_\gamma = \gamma \pi (a^2 + h^2) \quad \rightarrow \quad \mathrm{d}E_\gamma = 2\gamma\pi h \, \mathrm{d}h = F_\gamma \, \mathrm{d}h \tag{5.4}$$

which gives the restoring force $F_\gamma = 2\gamma\pi h$, where γ has the unit J/m^2. The friction force is proportional to the change in volume when the membrane moves:

$$\mathrm{d}V_c = \frac{\pi}{2} h^2 \, \mathrm{d}h + \frac{\pi}{2} a^2 \, \mathrm{d}h \approx \frac{\pi}{2} a^2 \, \mathrm{d}h \qquad (h \ll a) \tag{5.5}$$

The friction force per unit area can therefore be written as

$$F_\eta = -\eta \frac{\mathrm{d}V_c}{\mathrm{d}t} \frac{1}{\pi a^2} = -\frac{\eta}{2} \frac{\mathrm{d}h}{\mathrm{d}t} = -\frac{k_B T}{2D_0} \exp\left(\frac{H}{k_B T}\right) \frac{\mathrm{d}h}{\mathrm{d}t} \tag{5.6}$$

where η is the viscosity of the grain boundary and D_0 is the diffusion coefficient. When a shear stress is applied to the upper grain, the total deformation has an elastic and an anelastic component (2.3):

$$\epsilon_{tot} = J_u \sigma + \frac{\mathrm{d}x}{d} = J_u \sigma + \frac{u}{d} \frac{b_d}{h} = J_u \sigma + \frac{u}{d} \theta \tag{5.7}$$

where $\mathrm{d}x$ is the displacement in shear direction due to the movement of the grain boundary plane. u is the mean displacement of the boundary in the normal direction and can be expressed as the volume of the spherical cap divided by the cylinder base:

$$u = \frac{V_c}{\pi a^2} = \left(\frac{\pi h^3}{6} + \frac{\pi h a^2}{2}\right) \frac{1}{\pi a^2} \approx \frac{h}{2}. \tag{5.8}$$

Therefore, the anelastic part of the strain becomes

$$\epsilon_{an} = \frac{h\theta}{2d}. \tag{5.9}$$

The anelastic strain energy for the cylindrical grain is

$$E_{an} = \frac{1}{2} \sigma \epsilon_{an} \cdot V = \sigma \frac{h\theta}{4d} \pi a^2 d = \sigma \frac{\theta}{4} \pi a^2 h. \tag{5.10}$$

The corresponding force (from $E_{an} = F \, \mathrm{d}h$) that acts perpendicular to the GB plane and that corresponds to the driving force F_d of the grain boundary movement, is

$$F_d = \sigma \frac{\theta}{4} \pi a^2. \tag{5.11}$$

5.1.2 Anelastic Relaxation due to GB Migration

From Newton's equation in vertical direction in the case of a steady state movement (Figure 5.1 b)

$$-F_d + F_\gamma + F_\eta = -\sigma \frac{\theta}{4} \pi a^2 + 2\gamma \pi h + \frac{\eta}{2} \frac{dh}{dt} = m \frac{d^2 h}{dt^2} \approx 0 \tag{5.12}$$

one can find an expression for the speed of the advancing surface

$$\frac{dh}{dt} = \frac{\pi}{\eta} \left(\frac{1}{2} \sigma \theta a^2 - 4\gamma h \right). \tag{5.13}$$

Since the anelastic strain (5.9) is proportional to h, one can express ϵ_{an} as follows:

$$\dot{\epsilon}_{an} = \frac{\theta}{2d} \frac{dh}{dt} = \frac{\theta\pi}{2d\eta} \left(\frac{1}{2} \sigma \theta a^2 - 4\gamma h \right) = \frac{\theta\pi}{2d\eta} \left[\frac{1}{2} \sigma \theta a^2 - 8\gamma \frac{d}{\theta} (\epsilon_{tot} - J_u \sigma) \right] = \dot{\epsilon}_{tot} - J_u \dot{\sigma} \tag{5.14}$$

where the definition of the total strain ϵ_{tot} (2.3) has been used twice. A reorganisation of Equation (5.14) leads to the differential equation of the standard anelastic solid (2.5):

$$\tau \dot{\epsilon}_{tot} + \epsilon_{tot} = \tau J_u \dot{\sigma} + \underbrace{\left(\frac{\theta^2 a^2}{16\gamma d} + J_u \right)}_{J_r} \sigma \tag{5.15}$$

where the relaxation time τ is given by

$$\tau = \frac{\eta}{4\pi\gamma}. \tag{5.16}$$

If the viscosity η of the moving surface is thermally activated, one can express the relaxation time in terms of the diffusion coefficient D_0 and the activation energy H:

$$\tau = \frac{k_B T}{4\pi\gamma D_0} \exp \left(\frac{H}{k_B T} \right) \tag{5.17}$$

The differential equation (5.15) can be solved for a harmonic excitation of the form $\sigma = \sigma_0 \exp(i\omega t)$ as shown in Section 2.2.1. The mechanical loss shows a relaxation peak of the form (2.11):

$$\tan \phi = \Delta \cdot \frac{\omega\tau}{1 + \omega^2 \tau^2} \tag{5.18}$$

where the relaxation strength is given by

$$\Delta_{\text{migration}} = \frac{\delta J}{J_u} = \frac{J_r - J_u}{J_u} = \frac{\theta^2 a^2}{16\gamma d J_u} \tag{5.19}$$

using Equation (5.15).

In order to calculate the relaxation strength of a polycrystal composed of many crystallites separated by GBs, one needs to calculate the density of GB, in analogy to the dislocation density Λ for dislocation relaxations. If the number of dislocations is doubled, the relaxation strength Δ will double, since the anelastic deformation increases, whereas the elastic deformation remains the same. We will see in the following, that this GB density is essentially equal to 1 since it is the number of GBs per crystallites, provided the relaxation strength is calculated for one crystallite (intensive parameters) and not for the complete sample (extensive parameters).

Application to a Bamboo Structure

If the GB density is increased, for example by introducing a second GB in a bi-crystal parallel to the first GB, the resulting geometry is a bamboo-sample with two boundaries. Since the anelastic deformation due to gliding on both GBs is twice as high, the resulting relaxation strength doubles. More generally, the relaxation strength scales with the number of bamboo-boundaries.

Equation (5.19) contains the geometrical lengths a and d, which, for a bi-crystal with a single boundary corresponds to the radius and the length of the sample. On the other hand, we could think of a bamboo-structure as being composed of N identical bi-crystals with a length of L/N, L being the total sample length. The relaxation strength can be written as

$$\Delta_{\text{bamboo}} = N \cdot \frac{\theta^2 a^2}{16\gamma L J_u} = \frac{\theta^2 a^2}{16\gamma (L/N) J_u} \tag{5.20}$$

where the first expression of (5.20) can be seen as that of a bi-crystal of radius a and length L, where $N-1$ additional boundaries have been introduced, and the second expression decomposes the bamboo-structure into identical bi-crystals of length $l = L/N$, using Equation (5.19) with the geometric parameters of the individual crystallites.

Since both expressions in Equation (5.20) are equal, it is possible to consider only the smallest unit (one grain with one GB) and derive Δ and τ without using extensive parameters like the total sample length L. If the sample is divided into equal units containing one GB each, Equation (5.19) can be used directly for a polycrystal or a bamboo-structure, provided the geometric parameters a and $d = l$ of the crystallites are used. This approach is especially useful for the application to polycrystals, because the total number of grains is an unknown parameter, whereas height and width of a typical grain is a much more accessible information to an experimentalist.

In conclusion, the relaxation strength of a bamboo structure scales with the number of boundaries N and it is proportional to a^2/L, where L is the total sample length.

Application to a polycrystal

In a polycrystal, the grains are polyhedrally shaped entities. If we want to apply the membrane model to such a structure, the easiest choice would be to model cylindrically shaped grains with a height d and a radius $a = d/2$. For a simple shear deformation, only grain boundaries perpendicular to the z axis contribute in a first approximation and thus, every crystallite of volume $\pi a^2 d$ contributes with one GB with a surface πa^2 to the anelasticity of the polycrystal.

The same arguments as in the case of the bamboo structure can be used to convince oneself that the total relaxation strength of the polycrystal is the same as the relaxation strength for one typical grain with one adjacent GB. The relaxation strength of a crystallite with height d and base surface πa^2 and therefore Δ of a polycrystal is:

$$\Delta_{\text{migration,poly}} = \frac{\theta^2 d}{64 \gamma J_u} \quad \propto d \tag{5.21}$$

and the relaxation time $\tau = (\eta/4\pi\gamma)$ is independent of the grain size d.

In Section 3.4.3 it has been shown that the polycrystal's peak P2 has a relaxation strength independent of the grain size, whereas τ is proportional to d. This leads to the immediate conclusion that the migration model that describes the GB as a moving membrane under an applied stress cannot explain correctly the grain size dependence of the relaxation peak observed in polycrystals.

5.2 Sliding Model

At high temperatures, the simulations performed in Section 4.3 show that grain boundaries should glide without migration. The increased temperature promoted the formation of a disordered layer, on which the mobility and therefore the diffusion of atoms is greatly increased. The analysis of the RMSD parameter showed that the GB at 1000 K possesses the statistical characteristics of a melted interface layer.

5.2.1 Viscous Sliding Blocked by Triple Lines

GB sliding can be modelled assuming a viscosity η on a film of thickness δ. Figure 5.2 a) shows the sample geometry of two crystallites separated by a GB. The friction force due to the sliding of the grain boundary surface is given by

$$F_\eta = \frac{\eta a c}{\delta} \frac{\mathrm{d}\bar{u}}{\mathrm{d}t}. \tag{5.22}$$

We assume the presence of a restoring force F_k, which limits the mean displacement $\bar{u}$ of one crystal part with respect to the other. This restoring force represents the blocking of triple lines in a polycrystal (dark grey lines in Figure 5.2). As it acts along the whole depth in y direction,
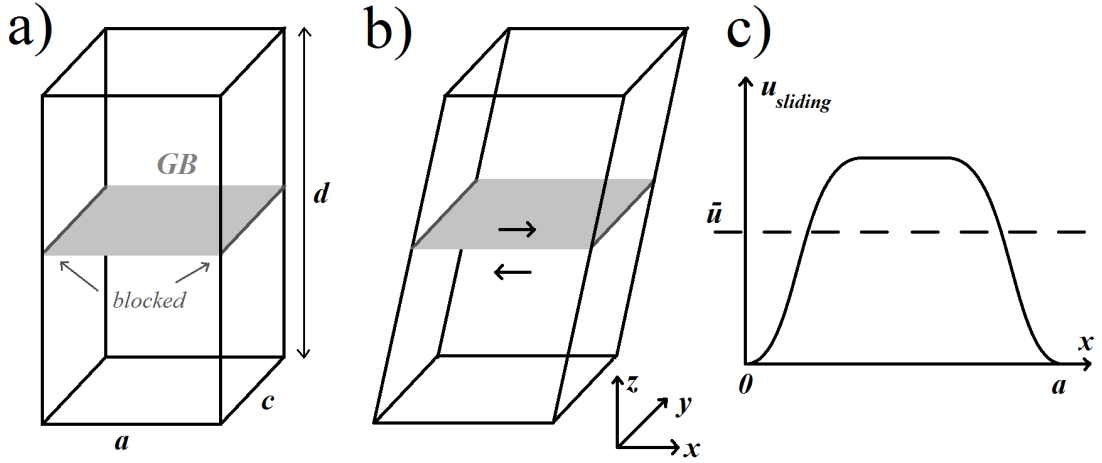
Figure 5.2 – a) and b): Geometry for the GB sliding model. Triple lines (dark grey) are fixed such that no long-range sliding occurs under an external shear stress in the x-direction. c) Relative displacement $u_{sliding}$ of the upper grain with respect to the lower grain as a function of the horizontal position x. The mean displacement $\bar{u}$ is also shown.

the restoring force should scale with the depth c of the sample: $F_k = kc\bar{u}$. The constant k is independent of the length scales a, c and d. The total deformation (2.3) is:

$$\epsilon_{tot} = J_u \sigma + \frac{\bar{u}}{d} \tag{5.23}$$

where the elastic part comes from the grains and the anelastic part is due to sliding at the GB. Since the GB is blocked at the borders, not every part of the upper crystal can slide with respect to the lower part. The sliding is highest in the centre region of the GB plane and it goes to 0 at the borders as shown in Figure 5.2 c). Without knowing the exact form of $u_{sliding}(x)$, we can define the mean displacement $\bar{u}$, which characterizes the anelastic behaviour of the GB plane. The energy due to the anelastic deformation can be expressed as

$$E_{an} = \frac{1}{2}\sigma\epsilon_{an}V = \frac{1}{2}\sigma\frac{\bar{u}}{d}\cdot acd = F_d \cdot \bar{u} \tag{5.24}$$

with the driving force $F_d = \sigma ac/2$. Newton's equation analogous to equation (5.12) gives an expression for the mean velocity:

$$\frac{d\bar{u}}{dt} = \frac{\delta}{\eta a}\left(\frac{1}{2}\sigma a - k\bar{u}\right) \tag{5.25}$$

and one finds expressions for the relaxation strength and for the relaxation time for GB sliding:

$$\tau = \frac{\eta a}{\delta k} = \frac{k_B T a}{\delta k D_0}\exp\left(\frac{H}{k_B T}\right) \tag{5.26}$$

$$\Delta_{sliding} = \frac{\delta J}{J_u} = \frac{a}{2dkJ_u} \tag{5.27}$$

119

5.2.2 Application to Polycrystals, Columnar Grains and Bi-crystals

The calculations in the previous section have been made on one GB that represents a small unit in a polycrystalline sample. In the case of a polycrystal where no preferred orientation occurs, one can assume that the grains have a more or less cubic shape. In an array of cubic grains, only two sides of the cubes will be in good sliding condition, that means parallel to the applied shear stress. Since one grain boundary is shared by two cubic grains, there will be one boundary for each grain in sliding condition. In the sliding model, one can set $a = d$ to approximate uniformly shaped grains with grain size d.

In order to calculate the relaxation strength Δ of a polycrystal, one can use the same arguments as for the example of the bamboo structure in Section 5.1.2. Instead of calculating Δ for a polycrystals of N grains, the result is given by considering one typical grains with one GB parallel to the applied stress using Equation (5.27) directly with $a = d$. Thus, for a polycrystal with grain size d, one finds the following expressions:

$$\Delta_{\text{sliding,poly}} = \frac{1}{2kJ_u} \qquad \text{and} \qquad \tau = \frac{k_B T d}{\delta k D_0} \exp\left(\frac{H}{k_B T}\right) \tag{5.28}$$

The main difference between the migration model and the sliding model is the different dependence on d. The sliding model predicts a relaxation strength and therefore a peak height independent of the d whereas the migration model predicts a linear dependence. For the limit relaxation time, the behaviour is exchanged: the sliding model shows $\tau \propto d$ whereas the migration model has a relaxation time τ independent of d.

In 1941, Zener [Zene41] first calculated the relaxation strength for grain boundary sliding in an array of spherical grains. He found that the relaxation strength is a constant that depends only on the Poisson's ratio of the material. Elastic accommodation of grain boundary sliding leads to a relaxation time $\tau \propto d$. In Section 3.4.3 it was demonstrated that the Zener model describes correctly the grain size dependence $\tau \propto d$ of the peak P2. Furthermore, the relaxation strength does not depend on the grain size d.

Therefore, the Zener model is qualitatively in agreement with our mechanical spectroscopy results, but it predicts a sample independent relaxation strength, where the only parameter is the Poisson's ratio v. As for the yellow gold alloy's Poisson's ration, $v = 0.41$ should be a good estimate, given the room-temperature Poisson's ratios of gold (0.44), silver (0.37) and copper (0.34). The relaxation strengths predicted by the continuum models of Zener/Kê [Zene41, Ke47a], Ray and Ashby [Raj71] and Ghahremani/Fotiu [Ghah80, Foti95] are 0.49, 0.31 and 0.19 respectively. The relaxation strength in the polycrystal was measured to 0.32 (Table 3.2), which is closest to the prediction of the Raj/Ashby model.

The sliding model as well as the migration model do not make a prediction on the absolute value of Δ. On the other hand, the measurement of the relaxation strength Δ allows us to obtain a value for the free parameter k, the restoring force due to the triple lines in Equation (5.28). In the case of the yellow gold polycrystal, $\Delta = 0.32$ and $M_u \approx 24$ GPa at the peak temperature,

the parameter k becomes:

$$k = \frac{1}{2\Delta J_u} = \frac{M_u}{2\Delta} \approx 37.5\,\text{GPa} \tag{5.29}$$

The free parameter in the migration model is the surface tension γ.

Comparing our models to the mechanical spectroscopy measurements, the experiments clearly favour the sliding model with respect to the migration model considering the dependence on d in a polycrystal. The sliding model presented here has the advantage over previous continuum models, that it provides explicit expressions for Δ and τ. Expressions (5.19) and (5.27) can be applied to a homogeneous polycrystal, but also to other structures like bi-crystals, bamboo-samples or polycrystals with textures, where grain length and thickness can differ considerably.

The application of the sliding model to the samples with columnar grains (Section 3.5.2) is not completely straightforward, since the deformation is in torsion and the geometry of one crystallite is more like a pie slice of a very high cylinder than a rectangular solid. It is therefore not obvious, which length should be used for a and d in Equation (5.27). In a simple bi-crystal as in Figure 5.2 a), the GB density A/V is equal to d^{-1}, whereas the a corresponds to the length of the GB plane, in which direction the sliding occurs.

In Section 3.5.2, it was observed, that the relaxation strength should be proportional to the GB density A/V from the observation of Δ in the columnar tri-crystals. From the comparison of the columnar samples with the diffusion bonded bi-crystal it seemed that the latter had relaxation strength smaller than expected. It was argued that the partially joined surface could be responsible for that. If we take into account the additional dependence $\Delta \propto a$, the small amplitude of the diffusion bonded GB peak becomes more understandable. The sliding length a in this sample is much smaller than the diameter or the radius of the sample (Figure 3.33 on page 73), and therefore the relaxation strength is reduced.

The sliding model is easily applied to the bi-crystal with a vertical GB, since the nomenclature of the geometric parameters in Section 3.5.4 has been chosen such that d is perpendicular to the GB plane and thus being the inverse GB density A/V. The thickness a takes the role of the sliding length. The phenomenological formula (3.10) obtained from FE simulations is very similar to Δ_{sliding}, namely by its dependence on a/d. The FE simulations as well as the experiments on the bi-crystal showed an additional dependence on the asymmetry factor $|d_1 - d_2|/d$, which is not included in the model calculations. Actually, the asymmetry factor has its origin in the torsional deformation of a rectangular sample geometry. If a simple shear is applied on a bi-crystal, the position of the GB within the sample does not play a role.

From Equation (5.26) it becomes clear that the limit relaxation strength τ_0 is proportional to a and therefore the relaxation peak in the bi-crystal should shift when changing the thickness a. Such a behaviour is not observed in Figure 3.45 on page 84. The peak decreases in height but a shift to lower temperatures is not visible. Probably the effect is too small to be detected, since

the parameter a was only reduced by 30%. In contrast, during the grain growth experiment presented in Section 3.4.3, the grain size d was changed by a factor 14 from 30 μm to 420 μm. In consequence, a shift of the GB peak in the grain growth experiment could be observed rather easily.

5.3 Stress Dependence Model

The relaxation strength Δ of the sliding model does not depend on the stress amplitude σ_0 and therefore, the model cannot explain the increase of the relaxation peak with stress amplitude in polycrystalline samples (Figure 3.23) and in bi-crystals (Figures 3.34 and 3.42). An ideal sliding process requires a flat GB with a sufficiently high viscosity η on a liquid-like layer of thickness δ. These conditions are achieved in the simulations at high T in Section 4.3.

On the other hand, from the optical microscope observations it becomes clear that a GB is not flat on macroscopic scales like the sample diameter. The wavy profile of Figure 3.36 is formed by GB zones of different orientations on microscopic scales. Instead of being flat, the GB contains steps and ledges, which hinder GB sliding. These steps can have a dislocation character with a Burgers vector b and are then called "disconnections" [Hirt06, Hirt07, Khat12]. More general, a linear defect can be considered at the limit between the part of the GB, which has slid, and the one, which has not slid. This line can be considered as a dislocation line [King80] and it can be pinned by irregularities of the GB plane.

The Burgers vector of a disconnection is not necessarily a vector connecting two atom positions in the crystal lattice, but it depends on the GB parameters, notably on the tilt angle. b can be larger or smaller than the nearest neighbour distance, but it is a conserved quantity along the dislocation line. Thus, the dislocation string model can be used to calculate the mechanical loss due to the motion of the disconnections.

The Granato-Lücke expression due to the depinning of a dislocation line from segregated point defects is given by (Appendix, A.15):

$$\tan\phi_{GL} = \frac{\Lambda b^2 \bar{L}^2}{12\pi\gamma J_u} \frac{\sigma_{0cr}}{\sigma_0} \exp\left(-\frac{\sigma_{0cr}}{\sigma_0}\right) \tag{5.30}$$

If Equation (5.30) is applied to a cylindrical sample deformed in torsion, one needs to account for the inhomogeneously distributed effective stress in the sample. This can be done by adding an exponent $\xi = 0.5$ [Pere65, Bati72] to the stress σ, wherever it appears in (5.30).

Equation (5.30) does not contain a temperature dependence, but it could be introduced in principle through the critical depinning stress σ_{0cr}. On the other hand, we have seen in Section 3.4.2, that an activation volume can describe well the shift of the relaxation peak P2 with stress. Even at very low stresses, the peak P2 has nearly its full height and the stress dependent part is only $\approx 10\%$, which means that the major part of the relaxation strength Δ is stress independent and can be described by the expression (5.27) of the sliding model. The

stress dependent part can be seen as a corrective term of the relaxation strength Δ:

$$\tan\phi = \Delta_0 \left[1 + \alpha \left(\frac{\sigma_{0cr}}{\sigma_0} \right)^\xi \exp\left(-\left(\frac{\sigma_{0cr}}{\sigma_0} \right)^\xi \right) \right] \frac{\omega\tau}{1 + \omega^2 \tau^2} \tag{5.31}$$

with a thermally activated relaxation τ time including an activation volume V:

$$\tau = \tau_0 \exp\left(\frac{H_{act} - \sigma_0 V}{k_B T} \right) \tag{5.32}$$

A peak broadening can also be introduced according to Equations (2.17) and (2.18). Since the depinning term is introduced as a correction of the relaxation strength due to GB sliding, the mechanical loss will show a stress dependence exclusively on the relaxation peak. Only if the GBs are mobile and contribute to the mechanical loss, the disconnections or generalized GB dislocations can cause a stress relaxation.

6 Discussion

6.1   Grain Boundary Sliding as Stress Relaxation Mechanism

The mechanical loss spectrum of yellow gold alloy polycrystals exhibit a relaxation peak, which is in excellent agreement with the GB sliding model (presented in Section 5.2). We can therefore conclude, that GBs do effectively slide under an applied stress giving rise to a relaxation peak at $T = 780$ K (P2). The measurement of the grain size exponent showed, that the relaxation time scales linearly with the grain size d in agreement with the model calculations. This means, that grain boundary sliding along the interfaces is accommodated elastically by a deformation of the grains.

In ceramics, GB sliding is recognized as being the main deformation mechanism at high temperatures. An amorphous inter-granular phase resulting from sintering aids allows the grains to slide against each other [Lakk95]. Even in ceramics with crystalline boundaries at room temperature, the formation of a disordered GB phase at high temperature has been observed [Test02, Dara07]. In most ceramics, GB sliding together with diffusion is the only way to obtain plastic deformation since dislocation mobility is low, and it is then responsible for creep above a certain temperature. Metals are much more ductile already at low temperatures, since plastic deformation is achieved by dislocation movement in the bulk material.

In yellow gold, a dislocation mechanism in the bulk cannot be responsible for the peak P2, since no peak is observed in the spectrum of a single crystal, even if this single crystal contains a certain amount of dislocations. If fresh dislocations are introduced in a single crystal, a dislocation effect is observed, but only in form of an increase of the high temperature background (Section 3.2.1).

An even stronger evidence that the peak P2 is related to a mechanism acting in the GB is the mechanical loss spectrum of bi-crystals. Having a single GB in the sample, the bi-crystals show a relaxation peak approximately at the same temperature as the polycrystal's peak (Figures 3.40 and 3.49). The bi-crystal peaks are generally less broad than the peaks in the polycrystal accounting for the presence of a single type of GB. When cutting a part of a bi-

crystal, which does not contain the boundary and measuring that part, the GB peak is absent, while the rest of the mechanical loss spectrum remains identical.

In a polycrystal, the relaxation strength is unchanged when varying the sample geometry and even if the microstructure is changed by high temperature treatments that reduce the dislocation density and increase the grain size (Figure 3.29). In samples with only one GB however, the relaxation strength depends strongly on the sample geometry. This shows the close relationship between the boundary type and the height of the bi-crystal's peak. Without making any assumption about the microscopic mechanism acting at the boundary, the FE simulations (Section 3.5.4 and Appendix B) can exactly reproduce the relaxation strength dependencies on geometrical parameters like thickness, length and width. Therefore, the relaxation mechanism responsible for the P2 is directly related to the presence of the GB plane.

From the model calculations of Section 5.2 it becomes clear, why the polycrystal's peak has a constant relaxation strength, whereas the bi-crystal's peak depends intrinsically on geometrical length scales. The relaxation strength of one boundary depends on the ratio a/d (5.27) (a and d being the sliding length and the height of the crystallites respectively), whereas for cubic shaped grains, a and d cancel out each other (5.28).

Since the grains in the bi-crystal are limited by the sample borders, the parameters a and d correspond to sample dimensions and therefore the peak height is influenced by variations of the external sample geometry. In the case of a polycrystal, the grains are principally limited by neighbouring grains and therefore, a and d are internal parameters. A change of the relaxation strength could probably be observed in polycrystals with elongated grains, when a and d do no longer cancel out in Equation (5.27).

6.2   Microscopic Mechanism Acting at GBs

MD simulations on a high angle GB (Sections 4.2 and 4.3) have shown that GB migration is active at low temperatures and sliding occurs only above a certain temperature. A systematic study on Cu [Cahn06] has shown that this transition temperature between migration and sliding depends on the misorientation angle of symmetric tilt boundaries. If the stress is high enough to make the boundary migrate at least by one step, coupled grain boundary motion should be observable at all temperatures down to 0 K.

From the simulations presented in this work, the transition temperature of Au from migration to sliding lies between 750 K and 1000 K for a $\Sigma5$ boundary. The transition does not occur at a precise temperature, but there exists a transitory temperature range, where GB migration is interrupted by occasional sliding events. This shows that sliding is a thermally activated mechanism. The transition temperature range also depends on the deformation speed and on the GB type.

A thermally activated relaxation peak in a mechanical loss spectrum marks the temperature at

which a relaxation mechanism becomes active. At temperatures below the peak temperature, the mechanism is blocked. In our case, the peak temperature would correspond to the temperature where grain boundary migration or sliding becomes possible on time scales imposed by the experimental conditions, e.g. the measurement frequency f.

In the simulations, the migration mechanism is a collective glide of dislocation, since a special symmetric tilt boundary has been used as an example boundary. This GB contains a single type of dislocations, so that all dislocations have the same glide plane. It is well known that the glide of edge dislocations leads to the appearance of relaxation peaks below room temperature (Bordoni relaxations [Fant82]). Thus, it is unlikely that the GB migration in form of a collective glide of edge dislocations in a symmetric tilt boundary should be responsible for the relaxation peak P2 at 780 K.

It has been shown by Trautt et al. [Trau12], that also more general GBs containing different types of dislocations, can perform a GB migration coupled to shear. The phase field crystal simulation method that can also take into account diffusive processes has shown that GB migration of general boundaries is assisted by dislocation climb. The boundary cannot migrate in a uniform way, since not all dislocations have the same glide plane. The controlling mechanism for migration of a general boundary would therefore be dislocation climb.

The temperature, at which sliding is observed in the simulations, does not correspond exactly to the peak temperature of the GB peak in pure Au (T = 620 K). According to the simulations, the peak should be observed at higher temperatures than what is actually measured by mechanical spectroscopy. However, the measurement frequency in the experiment was f = 0.5 Hz which results in a deformation velocity of $\dot{\epsilon}_{max} = \epsilon_{max} \cdot \omega = 3.1 \cdot 10^{-5}$ s^{-1}, whereas the observation times in the simulations are of the order of nanoseconds and therefore the deformation velocity of $\dot{\epsilon} = v/h = 10^{9}$ s^{-1} (v = 10 m/s being the speed of the upper atoms in the simulations and h being the sample height) is orders of magnitude higher. Measuring at higher frequencies shifts a thermally activated relaxation peak to higher temperatures. Thus, it is possible that the sliding gives rise to the GB peak observed in metals.

Given only the results from the MD simulations the GB peak P2 could be attributed to GB migration or to sliding. The proof, that GB sliding gives rise to the relaxation peak in mechanical spectroscopy measurements, is given by the analysis of the models in Sections 5.1 and 5.2. According to the migration model, the relaxation strength Δ in a polycrystal should be proportional to the grain size d and the relaxation time τ should be independent of d. This is not observed in the experiment (Figure 3.29 on page 68), whereas the sliding model can reproduce correctly the dependencies of Δ and τ in a polycrystal of different grain sizes. Furthermore, the relaxation strength Δ of the bi-crystal in Section 3.5.4 is proportional to a/d, in agreement with the sliding model.

Taking into account the results from the models, the GB peak should be a thermally activated peak due to GB sliding and not migration. The transition temperature, at which the deformation mechanism in the simulations occurs, marks the activation of the sliding mechanism. It is

important to notice that the sliding mechanism is associated with a change in the structure of the GB at high temperatures that becomes disordered over tens of nanometers and resembles a liquid or amorphous phase. The diffusion in this new GB phase is significantly higher than in the bulk.

From the simulations carried out by Cahn et al. [Cahn06] it can be foreseen that the transition of the relaxation mechanism would depend strongly on the misorientation angle θ. If θ is small, the GB dislocations are far away from each other and the crystalline structure of the GB plane should be preserved up to higher temperatures. This would mean that samples having exclusively low angle GBs should show a relaxation peak at much higher temperatures. Such a relaxation peak has been observed in the low angle GB sample discussed in Section 3.3.

From Equation (5.26) one can infer that a distribution of relaxation times and therefore a peak broadening stems from a varying viscosity η. Since η does not appear in the relaxation strength (5.28), the peak height remains unchanged. A similar result has been found in [Lee10] from a numerical analysis of a periodic interface where the periodicity reflects different grains in a polycrystal. The authors find that the relaxation peak broadens when introducing different viscosities η_1 and η_2 for different grain boundaries. Choosing different grain sizes in one sample leads to a decrease of the peak height without changing the peak shape.

6.2.1 Pinning Points on the GB Plane

From optical microscopy and EBSD observations on single boundaries in Section 3.5.3 it was shown that GBs are not flat over macroscopic distances. The GB plane is wavy and the observed GB migration occurs on localized parts of the GB. From Figure 3.38 on page 78 it can be seen that triple junctions act as strong pinning points but also an isolated boundary (Figure 3.36) may contain pinning points, which block certain parts of the boundary.

In a bi-crystal, the restoring force for sliding, which is necessary to produce a relaxation peak in the mechanical loss spectrum, can have two origins: Either it comes from the global wavy profile of the boundary plane as it is modelled in the Ashby model [Ashb72], or it is due to microscopic pinning points. In a pure metal, microscopic pinning points can be steps in the boundary plane as well as sessile GB dislocations or disconnections [Pond03]. It is also possible that the microscopic GB structure leads to a distribution of intrinsic pinning points, where some zones of the GB are in "good coincidence" and form pinning points, whereas the rest of the boundary can slide easily.

Due to the pinning points, the GB surface cannot slide as a whole block, but the sliding distance varies in the GB plane. Between the pinning points, a linear defect can be considered at the limit between the part of the GB, which has slid and the one, which has not slid. This line bends between pinning points under an external stress and can be considered as a mobile dislocation line. Hence the elementary GB slip can be described by the sliding model presented in Section 5.2.2 together with a dislocation model. At a certain stress, the pinning force of

the coincidence sites can be overcome and GB sliding occurs over longer distances. In a polycrystal, the maximum length of the GB dislocation is of the order of the grain size d.

The depinning process of the GB dislocations has been modelled with a Granato-Lücke expression (Section 5.3 and Appendix A), which turns out to be in good agreement with the stress amplitude measurements of Section 3.4.2. The joint model of GB sliding with a depinning of GB dislocations can reproduce a relaxation peak, which shows an increase in height as well as a decrease of the peak temperature when the stress amplitude is increased.

The model predicts a critical stress, at which the relaxation peak has its maximum relaxation strength. This stress value corresponds to the situation, for which the majority of the GB dislocations oscillates at their maximum length between strong pinning points. The analysis of the stress dependent mechanical loss measurements (Figure 3.26 on page 64) show, that the critical stress should be at around 5 MPa. This means, that a temperature scan measured at stresses above 5 MPa should show a smaller relaxation strength Δ than at 5 MPa, since at this stress, the weaker pinning points are not efficient any more. Strong pinning points, which define the maximum oscillation length, are probably the borders of the GB, at least for small grain sizes.

When comparing the temperature scans at different amplitudes of the polycrystal (Figure 3.23 on page 61) with the one of the bi-crystal (Figure 3.42 on page 82), one can see that the peak height variation with stress amplitude in the case of the bi-crystal is larger (approximately 40%) than the peak height variation in the polycrystal (only 15%). Considering Equation (5.31) on page 123, which contains both the sliding and the depinning contribution, we can see that the depinning part weighted by the parameter α must be more important in the case of the bi-crystal. Since $\alpha = \Lambda b^2 \bar{L}^2 / (12\pi\gamma J_u) \propto \bar{L}^2$ with $\bar{L}$ the length of depinned dislocations (Equation (5.30)), the isolated GB in the bi-crystal contains longer dislocation segments, whereas the total length $\bar{L}$ is limited by the grain size d in the polycrystal.

6.2.2 Viscous Sliding at the GB

In a polycrystal, the parameter $\alpha = 0.37$ has been measured, which means that only 37% of the GB relaxation is due to depinning, whereas the main contribution to the GB peak comes from a viscous sliding process in the GB plane. This also means that the activation parameters H_{act} and τ_0 as well as the broadening of the peak should be interpreted in terms of the sliding behaviour of the GBs. The relaxation time $\tau \propto \eta/\delta$ in the expression of the sliding model (5.26), where η is the GB viscosity and δ is the thickness of the viscous boundary layer. The GB viscosity η is thermally activated, thus the experimental values of H_{act} measured throughout Chapter 3 should reflect activation energies for GB diffusion.

The experimental values of activation energies of the GB peaks vary between 2.0 eV and 2.3 eV for polycrystals (Section 3.1.3) and bi-crystals (Section 3.5.4). These values are much higher than the activation energy for GB diffusion estimated from the MD simulations with 0.6 eV

for pure Au. But it was also shown that the activation energies of the GB peak are generally apparent values and the real value should be smaller. In the MD simulations in Section 4.3.1, the analysis of the GB thickness showed that δ is nearly twice as large at 1000 K than at 750 K. Apparently, the GB thickness δ is not temperature independent in the expression (5.26) of τ in the sliding model.

A strong temperature dependence of the GB thickness would lead to a smaller shift of the GB peak on the temperature scale when changing the measurement frequency as it would have been with a constant thickness. On an Arrhenius diagram, a linear fit would be steeper and therefore the value of the activation energy appears larger. The same effect can also be seen as a sort of local phase transition appearing in the GB layer, where the structure changes from a crystalline phase to a liquid layer. The MD simulations and the analysis of the mobility of atoms in the GB layer (Section 4.3.2) support the hypothesis of a phase transformation at the GB giving rise to a change from coupled GB migration to sliding. When sliding becomes active, the mechanical loss spectrum shows a relaxation peak in metals.

6.3   High Temperature Relaxations: LAGBs and Dislocations

6.3.1   Dislocation Mechanisms in LAGBs

An entirely different relaxation peak than the GB peak observed in polycrystals and bi-crystals is the high temperature peak observed in LAGBs. It is a mechanical loss peak, where dislocations give rise to a relaxation mechanism.

The LAGB peak appears at much higher temperatures than the polycrystal's peak and the activation parameters differ (Tables 3.1 and 3.2). LAGBs can be seen as dislocation walls composed of one or more parallel dislocation families. The MD simulations on LAGBs (Section 4.1.5) have shown that in fcc metals, the perfect dislocations forming a LAGB do not dissociate into partial dislocations. Under a shear stress, the dislocations glide together such that the GB performs a migration movement.

In the MD simulations, this LAGB migration is observed even at very low temperatures, since the dislocations glide on their glide plane. The simulation was done on a very special boundary, a symmetric tilt boundary composed of only one dislocation type. More general LAGBs contain several different dislocation types such that the boundary can be visualized as a net of intersecting dislocations. Two factors can hinder such a dislocation net from migrating uniformly: dislocation intersections act as pinning points and the glide plane is not the same for all dislocation types. A stress relaxation on form of a migration of the LAGB is only possible if dislocation climb is involved as well [Lakk98]. This necessitates the formation of jogs and the migration of these jogs along the dislocation line. Then, climb and not glide is the rate-controlling process and it is reasonable that a relaxation peak should be observable at high temperatures with respect to the melting point, where diffusive mechanisms are active.

6.3.2 High Temperature Background

The mechanical loss spectrum of single crystals shows no peak in the medium and high temperature range. The mechanical loss is low and only increases continuously towards the high temperatures in an exponential manner. This exponential background in single crystals is due to dislocations in the bulk material, since an increase of this background is observed when dislocations are introduced by cold working (Figure 3.13 on page 46). The background increases with increasing the stress amplitude, which can also be understood in terms of dislocation relaxation. The vibration length of a dislocation segment can increase under a higher stress amplitude due to unpinning from point defects, which leads to a higher mechanical loss.

The spectrum of a polycrystal or a bi-crystal also show a high temperature background in the loss spectrum. In the polycrystal, the background decreases slightly when the sample is annealed at high temperatures, which is in agreement with a reduction of the dislocation density in the sample.

On the other hand, an inspection of the spectra of polycrystals in different materials (Section 3.4.1) shows, that independently of the absolute value of the mechanical loss, the high temperature background always starts from approximately half the peak height and increases towards the high temperatures. The same behaviour is observed in the bi-crystal (Section 3.5.4). If the background were exclusively due to dislocations in the grains, one would expect the same background level in a very well annealed polycrystal as in the single crystal. That the background of single and polycrystals is not the same can be seen from Figure 3.28 on page 67, where the last spectrum was measured after 9 h annealing at 1000 K. The mechanical loss at 1000 K in the annealed polycrystal is still higher by a factor 2.5 than the corresponding value in a single crystal.

The correlation between the GB peak and the high temperature background is even more visible in the bi-crystal spectra. For example in Figure 3.44 on page 83 the background increases in the same manner as the GB peak, when the width d is reduced. If the background were only due to dislocations in the crystalline parts, than it would be difficult to understand, why the background should increase when a part of the single crystalline material is removed. It seems that at least part of the background in polycrystals and bi-crystals is closely related to the relaxation mechanism causing the GB peak.

Morris and Jackson [Morr09] presented an analysis of the Raj/Ashby model of GB sliding, where energy dissipation is caused by two mechanisms: boundary sliding and GB diffusion. If the characteristic time scales for both mechanisms are sufficiently separated from each other, the mechanical loss spectrum presents a low frequency (high temperature) background as well as a mechanical loss peak. The peak is due to a viscous sliding along the GBs, whereas the background is due to GB diffusion. Taking only the diffusional term into consideration, the model predicts a steady state creep for low frequencies (high temperature).

From the mechanical loss spectrum in polycrystals, the diffusional mechanism producing a local creep at the GB can be understood in the following way. The polycrystal's spectrum shows a relaxation peak due to GB sliding. The restoring force due to the presence of adjacent grains is supposed to be temperature independent and at high temperatures or low frequencies, a perfect relaxation peak should tend to 0. If on the other hand the pinning points responsible for the restoring force start to weaken at high temperatures, the restoring force decreases and one should observe the onset of local creep. In the mechanical loss spectrum, the relaxation peak transforms into a high temperature background instead of decreasing to 0.

Therefore, the high temperature background is probably caused by two different mechanisms, dislocations in the bulk and local creep at GBs. The dislocation relaxation is observed individually in single crystals and the background is stress amplitude dependent. In samples that contain GBs, a part of the background is due to GB diffusion, superimposed on the background caused by dislocations in the bulk. An annealing can reduce the background due to dislocations, but not the diffusional part, which is why polycrystals and bi-crystals maintain a relatively high background.

Conclusion

The mechanical loss spectrum of yellow gold alloy polycrystals is mainly composed of two relaxation peaks and a high temperature exponential background. The first peak (P1), which is observed at about 600 K for a 1 Hz frequency, is due to a Zener type anelastic relaxation. The second stable peak (P2), which appears in polycrystals and not in single crystals, is due to a relaxation associated with the GBs. The peak P2 changes position as a function of the grain size, whereas the height of the peak is independent of d. The relaxation time τ changes linearly with d, which confirms Zener's model of GB sliding. The relaxation is due to a GB mechanism elastically accommodated by the grains.

Introducing dislocations into a single crystal by cold work gives rise to a continuous evolution of the mechanical loss spectrum. For low deformation, the high temperature exponential background, which is due to dislocation damping, grows continuously with the deformation rate. When the dislocation density is increased above a certain level, polygonization with sub grain formation is expected. This phenomenon gives rise to a new relaxation peak (P3) accounting for a dislocation damping mechanism in sub grains with low misorientation angles. The transition from sub grain to a new grain structure is accompanied by the appearance of the GB peak P2.

The production of bi-crystals with different misorientations and different plane orientation allowed a study of individual GBs. The mechanical loss spectrum shows a relaxation peak with activation parameters similar to the parameters measured in the polycrystals. The peak is narrower than in a polycrystal and its height depends on external geometrical parameters like the sample thickness and the width. Since the sample is deformed in torsion, local shear stresses act on GB planes independent of their plane orientation. Therefore, GB peaks are observed in bi-crystals with horizontal, vertical and inclined GB planes.

In order to understand the microscopic fundamental mechanism at the origin of such grain boundary movement, molecular dynamics simulations on bi-crystals containing one flat GB were performed. A shear deformation parallel to the boundary plane has been applied to the bi-crystal. Depending on the simulated temperature, a different microscopic stress relaxation mechanism has been observed: below 700 K, the grain boundary performed a migration perpendicular to the GB plane coupled to shear, whereas above 1000 K, GB sliding occurred.

Conclusion

For both mechanisms, a simple mechanical model of a bi-crystal was developed, where the relaxation strength Δ and the relaxation time τ have been calculated. The two models depend differently on the geometric parameters like height and width of the sheared crystal containing one boundary plane. The application to a polycrystal with uniform grains predicted a grain size independent peak height for the sliding model and a peak height proportional to d in the case of the migration model. Mechanical spectroscopy measurements are only compatible with the predictions of the sliding model, whereas the migration model cannot describe the features of the polycrystal's relaxation peak. The simulations predict that grain boundary sliding is related to the formation of a disordered layer at high temperature.

Since GBs are not perfectly flat objects, GB sliding does not occur uniformly over macroscopic distances. The stress amplitude dependence of the GB peak indicated a depinning mechanism, which was modelled with a Granato-Lücke expression. As a consequence, the GB peak is interpreted as due to GB dislocations which mark the zones, where a grain has slid and parts, where sliding has not occurred yet. Obstacles like steps in the GB plane or coincidence sites can act as pinning points for these GB dislocations.

The high temperature background in single crystals is due to the motion of dislocations in the bulk, since an increase of the background was observed when introducing fresh dislocations by cold deformation. In polycrystals and bi-crystals, the background has two different origins: dislocation motion in the grains and extensive GB sliding resulting in a creep behaviour at temperatures close to the melting point.

Therefore, we can conclude that a relaxation peak due to GB sliding is expected in most polycrystalline metals at intermediate temperatures. The observation of the GB peak by mechanical spectroscopy provides a tool to selectively study the mobility of GBs and their impact on mechanical properties of the material.

A Calculation to Derive the Granato-Lücke Expression
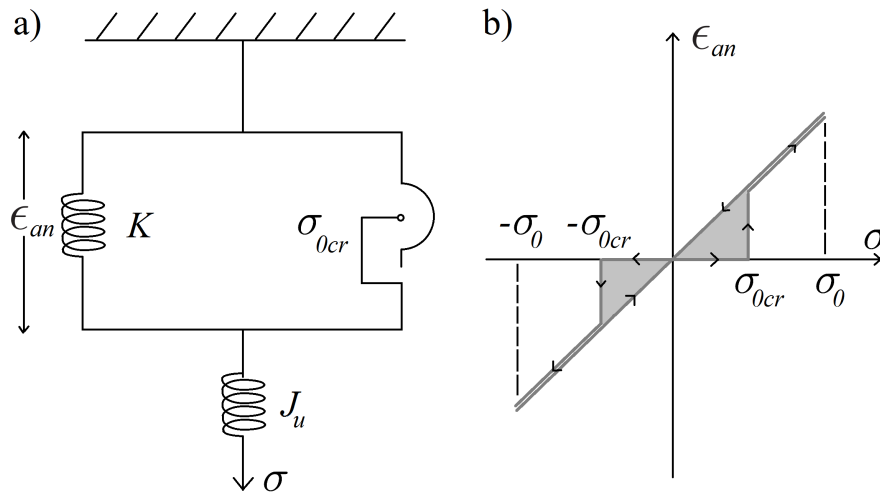
Figure A.1 – a) Rheological model and b) stress-strain curve of the Granato-Lücke model

One example of an amplitude dependent relaxation is the Granato-Lücke mechanism [Gran56], where a dislocation is pinned by a number n of immobile segregated point defects and it breaks away if the applied stress exceeds a critical stress amplitude σ_{0cr}. The average total length $\bar{L} = \bar{l}\bar{n}$ of the dislocation can be taken as the depth c of the GB plane in Figure 5.2, where $\bar{l}$ is the length between segregated point defects. The breakaway mechanism takes place, when the amplitude σ_0 becomes higher than the critical stress σ_{0cr}, which is related to the depinning force amplitude f_{0cr} by

$$\sigma_{0cr} = \frac{f_{0cr}}{bl} \tag{A.1}$$

necessary to obtain a depinning of the dislocation from one pinning point. The rheological model for the breakaway mechanism is represented in Figure A.1 a), where a lock with critical stress σ_{0cr} replaces the dash pot of the anelastic solid. The anelastic response in Figure A.1 presents a hysteresis curve with a sudden jump at the critical stress value σ_{0cr}. If the applied

stress σ_0 is smaller than the critical stress, the dislocation is pinned and no hysteresis is observed. Since the dissipated energy ΔW during one loading cycle corresponds to the area below the stress-strain curve, and the mechanical loss is given by

$$\tan\phi = \frac{1}{2\pi}\frac{\Delta W}{W_{max}} \tag{A.2}$$

the mechanical loss is 0 for the pinned dislocation. In the depinned situation for $\sigma_0 > \sigma_{0cr}$, the anelastic strain is controlled by the line tension restoring force of the dislocation segment of length $\bar{L}$. For one dislocation, the strain is given by [Scha01]

$$\epsilon_{an} = b\bar{u} = \frac{b^2\sigma}{K} = \frac{b^2\bar{L}^2}{12\gamma}\sigma \tag{A.3}$$

where γ is the line tension of the dislocation. From the definition of the mechanical loss (A.2) and ΔW being equal to the grey area in Figure A.1 b), the mechanical loss is given by

$$\tan\phi = \frac{1}{2\pi}\frac{\sigma_{0cr}\epsilon_{an}(\sigma_{0cr})}{\sigma_0\epsilon_0/2} = \frac{b^2\bar{L}^2}{12\pi\gamma J_u}\frac{\sigma_{0cr}^2}{\sigma_0^2} = \Delta_0(\bar{L})\frac{\sigma_{0cr}^2}{\sigma_0^2}. \tag{A.4}$$

In the second step of (A.4), Equation (A.3) was evaluated at $\sigma = \sigma_{0cr}$. The relaxation strength of one dislocation with length $\bar{L}$ between strong pinning points upon depinning is given by

$$\Delta_0(\bar{L}) = \frac{b^2\bar{L}^2}{12\pi\gamma J_u} \tag{A.5}$$

and for an arbitrary positive value of σ_0, we can write in a more compact form

$$\Delta(\bar{L}) = \Delta_0(\bar{L})\left(\frac{\sigma_{0cr}}{\sigma_0}\right)^2\Theta(\sigma_{0cr} - \sigma_0) \tag{A.6}$$

where $\Theta(x) = 1$ for $x > 0$ and $\Theta(x) = 0$ for $x < 0$ is the Heaviside step function. In this calculation, it was omitted that the point defects segregated on the dislocation follow a statistical distribution $\rho(n)$. The distribution function for a purely random segregation has been developed by Koehler [Koeh52]. The number of segments $N(l)$ with a distance l between the point defects follows an exponential distribution of the form

$$N(l)dl = \frac{\Lambda}{\bar{l}^2}\exp\left(-\frac{l}{\bar{l}}\right)dl \tag{A.7}$$

where Λ is the dislocation density and $\bar{l}$ is the average distance between segregated point defects. $N(l)\,\mathrm{d}l$ is the number of dislocation loops, which have lengths between l and $l + \mathrm{d}l$. The mechanical loss resulting from this distribution is given by Granato and Lücke [Gran56]:

$$\tan\phi = \int_0^{\bar{L}} l\Delta(\bar{L})N(l)\,\mathrm{d}l \tag{A.8}$$

The integration has to be taken over contributions of the relaxation strength $\Delta(\bar{L})$, since the only contribution to the loss comes from an oscillating depinned dislocation of length $\bar{L}$. Using Equation (A.6) and the definition of σ_{0cr} (A.1), we can express (A.8) as follows:

$$
\begin{aligned}
\tan\phi &= \int_0^{\bar{L}} l\Delta_0(\bar{L})\left(\frac{f_{0cr}}{bl\sigma_0}\right)^2 \Theta\left(\frac{f_{0cr}}{bl} - \sigma_0\right) \cdot \frac{\Lambda}{\bar{l}^2}\exp\left(-\frac{l}{\bar{l}}\right)\mathrm{d}l \\
&= \int_{f_{0cr}/b\sigma_{0cr}}^{\bar{L}} l\Delta_0(\bar{L})\left(\frac{f_{0cr}}{bl\sigma_0}\right)^2 \cdot \frac{\Lambda}{\bar{l}^2}\exp\left(-\frac{l}{\bar{l}}\right)\mathrm{d}l
\end{aligned}
\tag{A.9}
$$

A change of variables expressing the lengths between segregated point defects by the number of defects $l = \bar{L}/n$ and $\bar{l} = \bar{L}/\bar{n}$ in Equation (A.9), leads to:

$$
\tan\phi = \Delta_0(\bar{L})\Lambda\left(\frac{\bar{n}}{n_{max}}\right)^2 \int_1^{n_{max}} \frac{1}{n}\exp\left(-\frac{\bar{n}}{n}\right)\mathrm{d}n
\tag{A.10}
$$

where

$$
n_{max} = \frac{\bar{L}b\sigma_0}{f_{0cr}}
\tag{A.11}
$$

is the maximum number of point defects on a dislocation of length $\bar{L}$, for which depinning occurs. Also, in order to depin the dislocation, a minimum number of 1 point defect is necessary in the lower limit of the integral. Another change of variables $x = \bar{n}/n$ leads to the integral

$$
\tan\phi = \Delta_0(\bar{L})\Lambda\left(\frac{\bar{n}}{n_{max}}\right)^2 \int_{\bar{n}/n_{max}}^{\bar{n}} \frac{1}{x}e^{-x}\mathrm{d}x
\tag{A.12}
$$

for which the solution is called Exponential Integral $Ei(-x)$ and which can be developed in form of a series:

$$
Ei(-x) = e^{-x}\cdot\left(-\frac{1}{x} + \frac{1}{x^2} - \frac{2}{x^3} + \frac{6}{x^4} + O\left(\frac{1}{x^5}\right)\right)
\tag{A.13}
$$

if $x > 1$. Equation (A.12) becomes

$$
\tan\phi = \Delta_0(\bar{L})\Lambda\left(\frac{\bar{n}}{n_{max}}\right)^2 \left[e^{-\bar{n}}\left(-\frac{1}{\bar{n}} + \frac{1}{\bar{n}^2}\right) - e^{-\bar{n}/n_{max}}\left(-\frac{n_{max}}{\bar{n}} + \frac{n_{max}^2}{\bar{n}^2}\right)\right]
\tag{A.14}
$$

If $\bar{n}$ is sufficiently large, in particular $\bar{n} > n_{max}$, we can neglect the quadratic terms, i.e. the second and the fourth term in the squared brackets of (A.14). If n_{max} is also sufficiently larger

than 1, the third term is dominant and we can write in a first approximation

$$
\begin{aligned}
\tan\phi &= \Delta_0(\bar{L})\Lambda\left(\frac{\bar{n}}{n_{max}}\right)e^{-\bar{n}/n_{max}} \\
&= \frac{\Lambda b^2 \bar{L}^2}{12\pi\gamma J_u}\frac{\sigma_{0cr}}{\sigma_0}\exp\left(-\frac{\sigma_{0cr}}{\sigma_0}\right)
\end{aligned}
\tag{A.15}
$$

This expression corresponds to the well-known damping expression of Granato and Lücke.

B Finite Elements Simulations on a Bi-crystal

Finite Elements (FE) simulations were performed on a bi-crystalline sample geometry in order to check, if the geometry dependencies observed in the experiment are linked to the GB type or to the stress distribution in the sample. In the FE simulations, the GB is represented in the most simple way as a free surface, where one part of the solid can slide along the adjacent material. The GB is infinitely thin and we do not take into account that the misorientation or the plane direction with respect to the crystal lattice could influence the GB structure. The only parameter that is probed in these simulations is the relaxation of local stresses in the vicinity of the GB.

Figure B.1 a) shows the model, where the two vertical bars have a free surface, along which the material can slide without friction. The bars are fixed on the bottom and the thin top layer holds the bars together. A static torque is applied to the top surface. The simulations used gold as a bulk material and the geometry and forces were chosen according to the experimental set-up described in Section 3.5.4.

In the experiment, the relaxation strength Δ is given by the peak height (2.11), but in principle it could also be measured in a static deformation experiment (Figure 2.5). The relaxation strength is given by $\Delta = \epsilon_{an}/\epsilon_{el}$ and in the FE simulation, it can be calculated from the deformation of a sample without GB and with GB. At a constant force, ϵ_{el} is given by the maximum deformation of a continuous sample without GB. ϵ_{an} can be extracted from the difference $\epsilon_{tot} - \epsilon_{el}$, where ϵ_{tot} is the maximum deformation of the sample with a GB.

For each sample geometry, the force on the top surface was adapted, such that the total strain ϵ_{tot} reached 10^{-5}, since the experiments were also performed in constant strain mode. Figure B.1 b) shows a simulation of a continuous sample without GB. The black lines show the sample position without deformation and the surface colour illustrates the displacement in z-direction. Mainly the vertical edges show a displacement upwards (red) or downwards (blue). At the GB line, no displacement in z-direction occurs. A cylindrical sample sheared in torsion around its symmetry axis would not show any z-displacement, but a rectangular bar does.
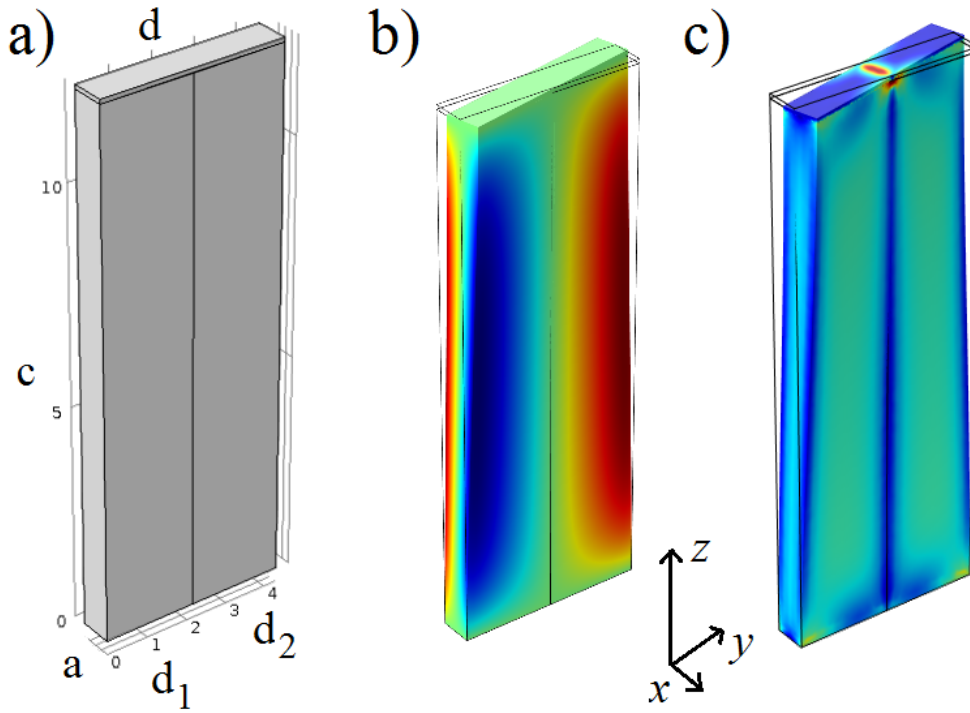
Figure B.1 – a) Sample geometry of the bi-crystal and definition of the parameters a, c, d, d_1 and d_2. b) Finite elements simulation of a continuous rectangular bar without GB. The deformation is enhanced by a factor 3200. The colours on the surface indicate the displacement in z-direction, where red zones have moved upwards and blue zones downwards. c) Von-Mises-stresses on a sample with GB. Very low stresses (blue) are observed in the GB region.

The introduction of a vertical GB leads to a stress relaxation along the GB. Figure B.1 c) illustrates the Von-Mises-stresses on the surface of the strained sample. The Von-Mises-stress can be expressed in terms of stress tensor components [Ford63] as

$$\sigma_v = \sqrt{\frac{1}{2}\left((\sigma_{11} - \sigma_{22})^2 + (\sigma_{22} - \sigma_{33})^2 + (\sigma_{33} - \sigma_{11})^2 + 6 \cdot (\sigma_{12}^2 + \sigma_{13}^2 + \sigma_{23}^2)\right)} \tag{B.1}$$

and it is used to predict the yielding of an elastic material by expressing the local internal stresses in a scalar field. At the vertical corners as well as along the GB, no internal stresses are observed (blue colour). The highest stresses occur at the pinning line of the GB. Figure B.2 a) and b) visualizes 2 different sliding modes that occur at the GB. Figure B.2 a) shows the z-displacement in presence of a GB, and this time the colouring is discontinuous at the boundary. The right side slides upwards with respect to the left side. A shear component ϵ_{zy} is observed at the GB plane, where the first index corresponds to the direction of the shear displacement and the second index is the normal direction of the shear plane. The small diagram left of the coloured bi-crystal depicts that the sliding amount is highest in the middle of the GB.

The grain boundary also slides along the perpendicular x-axis, as can be seen from Figure B.2 b). The sample is viewed from above with the green surface being the bi-crystal's top
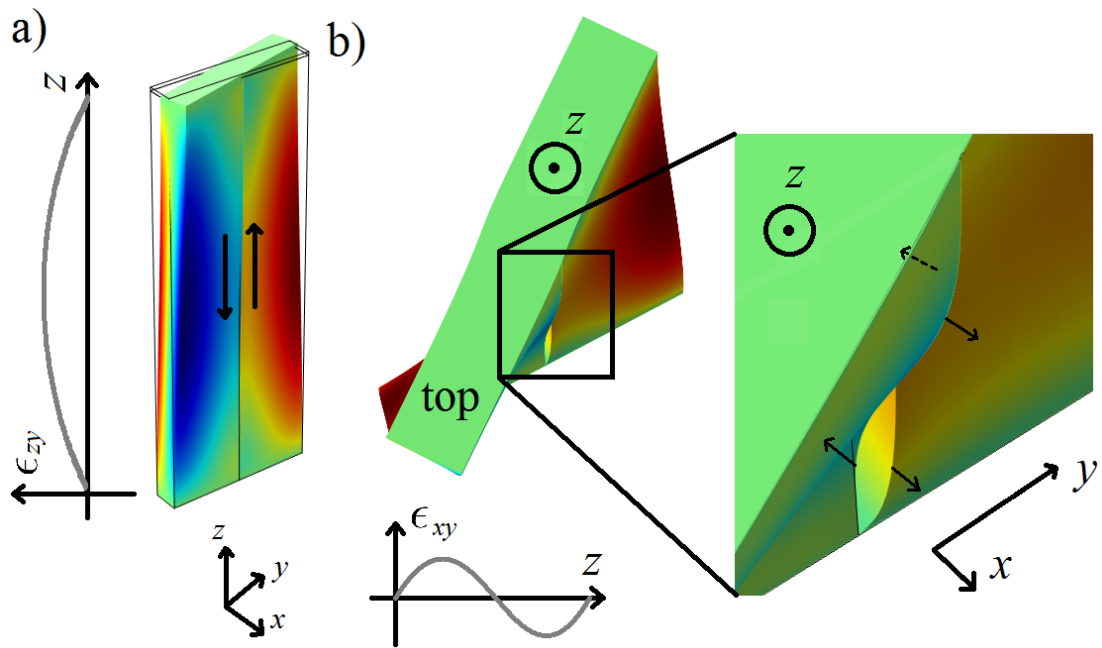
Figure B.2 – a) z-displacement of a sample with GB. The colour is discontinuous along the boundary plane indicating a glide. The effect is most pronounced in the middle of the sample and tends to 0 on to and on the bottom. b) Top view of the same sample: The green surface is the top surface and the curved line belongs to the GB. A sliding along the x-axis occurred with different directions in the bottom half and the top half. No sliding in x-direction is observed in the centre of the sample. The displacement is enhanced by a factor 8000.

surface. The grain boundary is seen as a curved line, where a relative displacement of both sample parts occurred. The sliding in the top half is opposite to the sliding in the bottom half. A diagram below the figure shows qualitatively the shear component ϵ_{xy}.

The shear along x and z together can be seen as a rotational shear around the y-axis. The right part of the sample coloured in red turns in negative y-direction, whereas the left part turns in positive y-direction. On a local scale, the shear stress varies along the GB plane and has different directions in form of a simple shear component.

C Copper Bi-crystals and Twin Boundaries

The copper bi-crystals were fabricated with the crucible with two seed crystals described in Section 2.1.4. The sample had the dimensions of 30mm x 10mm x 1mm after a first cutting. Observations with a Laue camera showed a misorientation angle of $\delta = (18.0 \pm 0.3)°$. Two smaller samples with a tilted GB were cut as sketched in Figure C.1 a). The GB plane forms a 45° angle with the deformation axis in mechanical spectroscopy measurements.

a)

b)
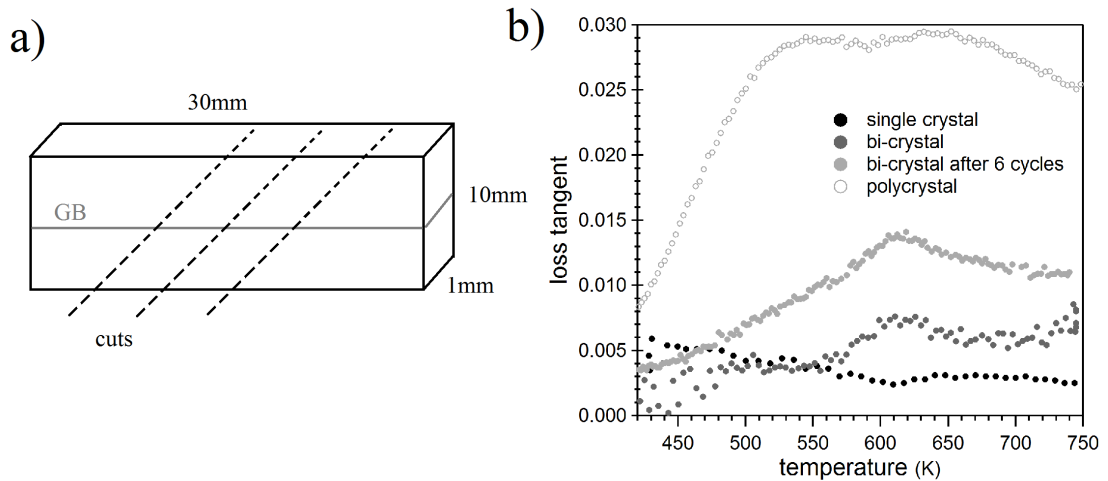
Figure C.1 – a) Sample geometry of the Cu bi-crystal. The broken lines indicate the cutting direction to make sample with dimensions of 9.1mm x 2mm x 1mm and a GB with 45° to the sample axis. b) Mechanical loss spectrum of the Cu bi-crystal in comparison to the single crystal and the polycrystal of the same material. After 6 measurement cycles, the level of mechanical loss in the bi-crystal's spectrum increased.

The bi-crystal shows a small mechanical loss peak at 600 K superimposed on a background (Figure C.1 b). With respect to the polycrystal's peak that stretches between 450 K and 750 K, the bi-crystal's peak is much narrower and has a 5th of the height. The bi-crystal has only one maximum and the peak shape is close to a Debye peak. Heating and cooling curves (not shown) do not superimpose well. The cooling curve lies slightly above the heating. After

143

6 measurement cycles, the loss spectrum has changed significantly (light grey markers in Figure C.1) so that the mechanical loss curve lies well above the original spectrum and the peak is broadened.

The evolution of the mechanical loss can be understood by looking at the metallography image shown in Figure C.2. The original boundary is still visible, forming a 45° with the borders of the Cu sample. Additionally to this GB, many other grains are present in the surroundings of the initial GB. In approximately 2 mm distance of the boundary, the sample is single crystalline. The newly formed grains near the original boundary show a highly twinned structure with many stacking faults. There are many parallel lines indicating the progression of partial dislocations and leaving a stacking fault behind them. The twinning process is incomplete since many twin lines stop in the middle of a grain. The grain in the lower right part of the photography possesses two twin systems forming a 90° angle with each other.

Since the recrystallized grain structure is only observed in the vicinity of the original GB, we can conclude that the HAGB acts as a starting point or source for recrystallization. In contrast to cold worked samples, which recrystallize upon heating, the initial dislocation density in the bi-crystal is low and cannot trigger recrystallization, since the sample far away from the boundary remains single crystalline.

What is observed in the Cu bi-crystal is also called military transformation [Pond03] and has been observed in other pure metals like Zn or Au. Partial dislocations of the same type but on subsequent glide planes move all in the same direction. Only the first partial dislocation creates a stacking fault. The dislocation on the next gliding plane propagates along the existing stacking fault and displaces it by one step when shearing the crystal.

The dislocations in pure Cu are very mobile, at least at the maximum measurement temperatures of 750 K. Also, the stacking fault energy in pure copper is very low 40 mJm^{-2} compared to Aluminium with 135 mJm^{-2} [Smal99] for example. Both of these factors are necessary to form a microstructure as observed in Figure C.2. But it is still difficult to understand, why a microstructure with a single grain boundary should tend to form a recrystallized zone with many grain boundaries. Even if the twin boundaries are very low in energy, the original boundary has not completely disappeared. It is possible that the change of crystal orientation due to twinning in the adjacent grains has changed the nature of the initial boundary and so lowered its energy.

Another possible explanation is that due to the deformation during the experiment, stresses are accumulated at the GB. These stresses can be released by the formation of dislocations. Since in a single crystalline material, they can propagate over long distances, the GB acts effectively as a source of dislocations, which can then reorganize in form of grain boundaries.

As stated in Section 3.2.1, the increase of the mechanical loss in the high temperature part of the spectrum is due to an increase of the dislocation density. In order to measure the activation parameters of the small GB peak in Figure C.1 b), we cannot use temperature scans since the
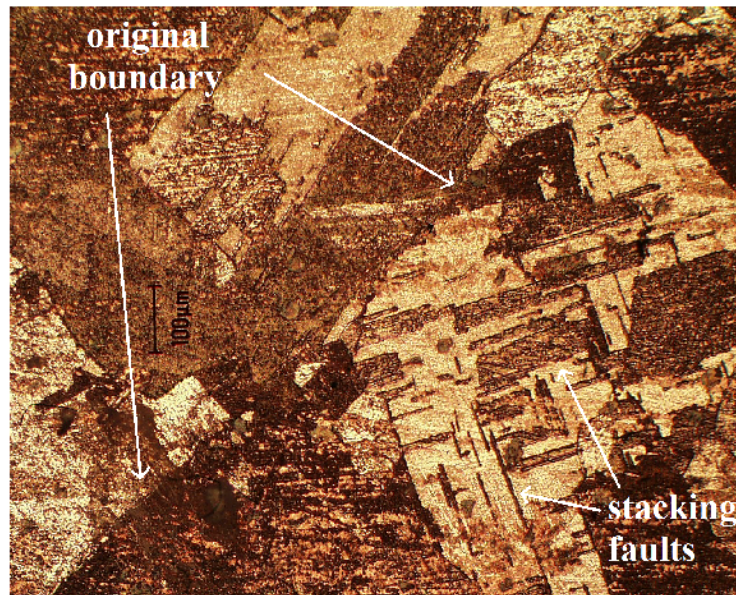
Figure C.2 – Grain structure under the optical microscope after the measurements: the original boundary inclined by approximately 45° is surrounded by new grains, which contain many stacking faults.
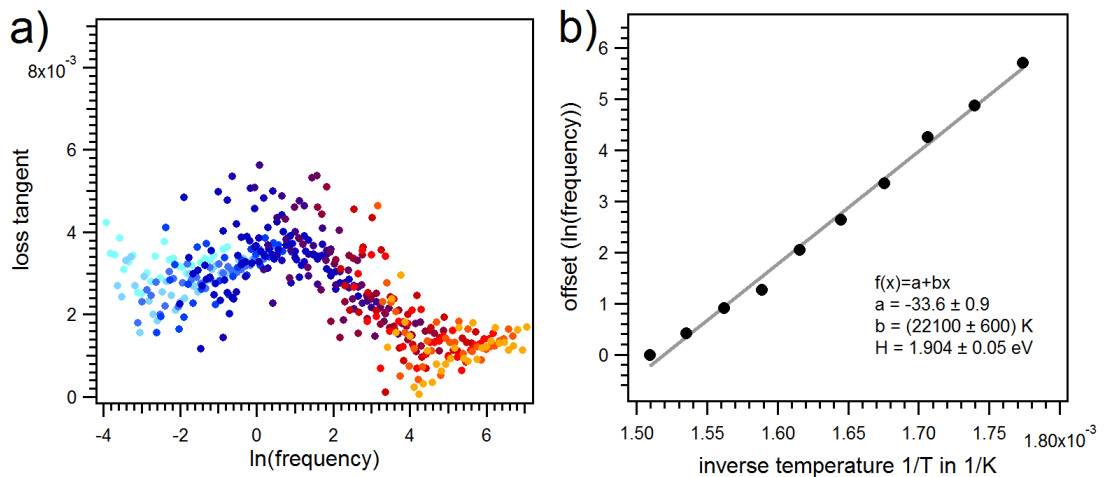

Figure C.3 – a) Master curve from frequency scans during the first heating on a new copper bi-crystal. A peak is visible. b) Shift on the frequency axis to construct the master curve as a function of the inverse temperature. The slope multiplied by k_B yields the activation energy of the peak.

microstructure changes and the resulting sample is no bi-crystal any more. To overcome these difficulties, frequency scans at low stress amplitude $\epsilon = 5 \cdot 10^{-6}$ were recorded during the first heating on a new sample.

The master curve from the superposition of the frequency scans is shown in Figure C.3 a). Different colours belong to different temperatures. The emerged peak is superimposed on a very low background suggesting that the original GB is measured and not the recrystallized microstructure. The activation energy $H_{act} = (1.90 \pm 0.05)$ eV is extracted from the shift to construct the master-curve. A fit to one of the frequency scans provides the limit relaxation time $\tau_0 = (1.6 \pm 0.2) \cdot 10^{-16}$s and the broadening factor $\beta = 2.0 \pm 0.2$.

Bibliography

[Abdu03]   A. M. Abdul-Lettif, "Grain boundary diffusion coefficients in gold–nickel thin films," *Surface and Interface Analysis*, vol. 35, no. 5, pp. 429–431, 2003. –>

[Ackl90]   G. J. Ackland and V. Vitek, "Many-body potentials and atomic-scale relaxations in noble-metal alloys," *Phys. Rev. B*, vol. 41, pp. 10 324–10 333, May 1990. –>

[Alex13]   K. C. Alexander and C. A. Schuh, "Exploring grain boundary energy landscapes with the activation-relaxation technique," *Scripta Materialia*, vol. 68, no. 12, pp. 937 – 940, 2013. –>

[Alsa05]   A. Alsayed, M. Islam, J. Zhang, P. Collings, and A. Yodh, "Chemistry: Premelting at defects within bulk colloidal crystals," *Science*, vol. 309, no. 5738, pp. 1207–1210, 2005. –>

[Ashb72]   M. F. Ashby, "Boundary defects and atomistic aspects of boundary sliding and diffusional creep," *Surface Science*, vol. 31, pp. 498–542, 1972. –>

[Ashc81a]   N. W. Ashcroft and D. N. Mermin, *Determination of Crystal Structures by X-Ray Diffraction*, international ed., ch. 6, p. 95, in [Ashc81b].

[Ashc81b]   N. W. Ashcroft and D. N. Mermin, *Solid State Physics*, international ed., D. G. Crane, Ed.   Saunders College, 1981.

[Ashc81c]   N. W. Ashcroft and D. N. Mermin, *The Reciprocal Lattice*, international ed., ch. 5, p. 85, in [Ashc81b].

[Bati72]   R. D. Batist, *Internal Friction Of Structural Defects In Crystalline Solids.*   North-Holland Pub. Co, 1972, p. 350.

[Beno01a]   W. Benoit, *Grain Boundary: description and dynamics*, ch. 4.1, p. 291, in [Scha01]. –>

[Beno01b]   W. Benoit, *Grain Boundary relaxation in metals*, ch. 4.2, p. 306, in [Scha01]. –>

[Beno04]   W. Benoit, "High-temperature relaxations," *Materials Science and Engineering A*, vol. 370, no. 1-2, pp. 12 – 20, 2004. –>

[Bere84]   H. J. C. Berendsen, J. P. M. Postma, W. F. van Gunsteren, A. DiNola, and J. R. Haak, "Molecular dynamics with coupling to an external bath," *The Journal of Chemical Physics*, vol. 81, no. 8, pp. 3684–3690, 1984. –>

[Boll70]   W. Bollmann, *Crystal Defects and Crystalline Interfaces.*   Springer Berlin Heidelberg, 1970. –>

Bibliography

[Bone83]   E. Bonetti, A. Cavallini, E. Evangelista, and P. Gondi, "Internal friction peaks connected with grain boundary sliding in Al," *Journal de physique. Colloque*, vol. 44, no. NC-9, pp. 759–764, 1983.

[Brou98]   J. Broughton and G. Gilmer, "Grain-boundary shearing as a test for interface melting," *Modelling and Simulation in Materials Science and Engineering*, vol. 6, no. 1, pp. 87–97, 1998. –>

[Bula14]   V. V. Bulatov, B. W. Reed, and M. Kumar, "Grain boundary energy function for fcc metals," *Acta Materialia*, vol. 65, no. 0, pp. 161 – 175, 2014. –>

[Busi67]   W. R. Busing and H. A. Levy, "Angle calculations for 3- and 4-circle X-ray and neutron diffractometers," *Acta Crystallogr.*, vol. 22, no. 4, pp. 457–464, 1967. –>

[Cahn04]   J. W. Cahn and J. E. Taylor, "A unified approach to motion of grain boundaries, relative tangential translation along grain boundaries, and grain rotation," *Acta Materialia*, vol. 52, no. 16, pp. 4887 – 4898, 2004. –>

[Cahn06]   J. W. Cahn, Y. Mishin, and A. Suzuki, "Coupling grain boundary motion to shear deformation," *Acta Mater.*, vol. 54, no. 19, pp. 4953 – 4975, 2006. –>

[Cail09]   D. Caillard, F. Mompiou, and M. Legros, "Grain-boundary shear-migration coupling. II. Geometrical model for general boundaries," *Acta Mater.*, vol. 57, no. 8, pp. 2390 – 2402, 2009. –>

[Cao94]   B. Cao, R. Schaller, W. Benoit, and F. Cosandey, "Internal friction associated with grain boundaries in Ni–Cr alloys," *Journal of Alloys and Compounds*, vol. 211-212, pp. 118 – 123, sep 1994. –>

[Chen14]   K. Cheng, K. Tieu, C. Lu, X. Zheng, and H. Zhu, "Molecular dynamics simulation of the grain boundary sliding behaviour for Al Σ5 (210)," *Computational Materials Science*, vol. 81, no. 0, pp. 52 – 57, 2014. –>

[Cobl63]   R. L. Coble, "A Model for Boundary Diffusion Controlled Creep in Polycrystalline Materials," *J. Appl. Phys.*, vol. 34, no. 6, pp. 1679–1682, 1963. –>

[Dara07]   M. Daraktchiev, R. Schaller, L. Gremillard, T. Epicier, J. Chevalier, and G. Fantozzi, "How do the grains slide in fine-grained zirconia polycrystals at high temperature?" *Applied Physics Letters*, vol. 91, no. 12, 2007. –>

[Dari03]   B. M. Darinskii, Y. E. Kalinin, S. V. Mushtenko, and D. S. Sajko, "Structure of grain boundaries of a general type and mechanisms of the grain boundary internal friction peak," *Solid State Phenomena*, vol. 89, pp. 203–232, 2003. –>

[Daw83]   M. S. Daw and M. I. Baskes, "Semiempirical, quantum mechanical calculation of hydrogen embrittlement in metals," *Phys. Rev. Lett.*, vol. 50, pp. 1285–1288, Apr 1983. –>

[Daw84]   M. S. Daw and M. I. Baskes, "Embedded-atom method: Derivation and application to impurities, surfaces, and other defects in metals," *Phys. Rev. B*, vol. 29, pp. 6443–6453, Jun 1984. –>

148

[Daw93]   M. S. Daw, S. M. Foiles, and M. I. Baskes, "The embedded-atom method: a review of theory and applications," *Materials Science Reports*, vol. 9, no. 7–8, pp. 251 – 310, 1993. –>

[Duhl63]   D. Duhl, K.-I. Hirano, and M. Cohen, "Diffusion of iron, cobalt and nickel in gold," *Acta Metallurgica*, vol. 11, no. 1, pp. 1 – 6, 1963. –>

[Eins56]   A. Einstein, *Investigations on the Theory of the Brownian Movement*, R. Fürth, Ed. Dover Publications, Inc., 1956. –>

[Else09]   A. Elsener, O. Politano, P. Derlet, and H. V. Swygenhoven, "Variable-charge method applied to study coupled grain boundary migration in the presence of oxygen," *Acta Materialia*, vol. 57, no. 6, pp. 1988 – 2001, 2009. –>

[Fant82]   G. Fantozzi, C. Esnouf, W. Benoit, and I. Ritchie, "Internal friction and microdeformation due to the intrinsic properties of dislocations: The bordoni relaxation," *Progress in Materials Science*, vol. 27, no. 3–4, pp. 311 – 451, 1982. –>

[Fens10]   S. J. Fensin, D. Olmsted, D. Buta, M. Asta, A. Karma, and J. J. Hoyt, "Structural disjoining potential for grain-boundary premelting and grain coalescence from molecular-dynamics simulations," *Phys. Rev. E*, vol. 81, p. 031601, Mar 2010. –>

[Finn84]   M. W. Finnis and J. E. Sinclair, "A simple empirical N-body potential for transition metals," *Philosophical Magazine A*, vol. 50, no. 1, pp. 45–55, 1984. –>

[Ford63]   H. Ford and J. M. Alexander, *Advanced mechanics of materials.*   Longmans, London, 1963.

[Foti95]   P. A. Fotiu, R. Heuer, and F. Ziegler, "BEM analysis of grain boundary sliding in polycrystals," *Engineering Analysis with Boundary Elements*, vol. 15, no. 4, pp. 349 – 358, 1995. –>

[Fuku81]   H. Fukutomi and R. Horiuchi, "Stress induced migration of symmetric tilt boundaries in aluminum," *Transactions of the Japan Institute of Metals*, vol. 22, no. 9, pp. 633–642, 1981.

[Fuos41]   R. M. Fuoss and J. G. Kirkwood, "Electrical Properties of Solids. VIII. Dipole Moments in Polyvinyl Chloride-Diphenyl Systems," *J. Am. Chem. Soc.*, vol. 63, no. 2, pp. 385–394, 1941.

[Ghah80]   F. Ghahremani, "Effect of grain boundary sliding on anelasticity of polycrystals," *International Journal of Solids and Structures*, vol. 16, no. 9, pp. 825 – 845, 1980. –>

[Golo12]   I. S. Golovin, P. Pal-Val, L. Pal-Val, E. Vatazhuk, and Y. Estrin, "The Effect of Annealing on the Internal Friction in ECAP-Modified Ultrafine Grained Copper," *Solid State Phenomena*, vol. 184, pp. 289–294, 2012. –>

[Gork09]   T. Gorkaya, D. A. Molodov, and G. Gottstein, "Stress-driven migration of symmetrical <100> tilt grain boundaries in al bicrystals," *Acta Materialia*, vol. 57, no. 18, pp. 5396 – 5405, 2009.

[Gork11]   T. Gorkaya, K. D. Molodov, D. A. Molodov, and G. Gottstein, "Concurrent grain boundary motion and grain rotation under an applied stress," *Acta Mater.*, vol. 59, no. 14, pp. 5674 – 5680, 2011.

Bibliography

[Gran56]   A. Granato and K. Lücke, "Theory of mechanical damping due to dislocations," *Journal of Applied Physics*, vol. 27, no. 6, pp. 583–593, 1956. –>

[Gran81]   A. V. Granato and K. Lücke, "Temperature dependence of amplitude-dependent dislocation damping," *Journal of Applied Physics*, vol. 52, no. 12, pp. 7136–7142, 1981. –>

[Groc05]   G. Grochola, S. P. Russo, and I. K. Snook, "On fitting a gold embedded atom method potential using the force matching method," *J. Chem. Phys*, vol. 123, no. 20, p. 204719, 2005. –>

[Hans11]   L. N. Hansen, M. E. Zimmerman, and D. L. Kohlstedt, "Grain boundary sliding in san carlos olivine: Flow law parameters and crystallographic-preferred orientation," *Journal of Geophysical Research: Solid Earth*, vol. 116, no. B8, 2011. –>

[Henn09a]   J. Hennig, D. Mari, and R. Schaller, "Order-disorder phase transition and stress-induced diffusion in AuCu," *Phys. Rev. B*, vol. 79, p. 144116, Apr 2009. –>

[Henn09b]   J. Hennig, D. Mari, and R. Schaller, "Stress-induced and atomic ordering in 18-carat Au-Cu-Ag alloys," *Mater. Sci. Eng. A*, vol. 521-522, pp. 47–51, 2009.

[Henn10]   J. Hennig, "Phase transformations in 18-carat gold alloys studied by mechanical spectroscopy," Ph.D. dissertation, EPF, Lausanne, 2010.

[Herr50]   C. Herring, "Diffusional viscosity of a polycrystalline solid," *J. Appl. Phys.*, vol. 21, no. 5, pp. 437–445, 1950.

[Hirt96]   J. Hirth and R. Pond, "Steps, dislocations and disconnections as interface defects relating to structure and phase transformations," *Acta Materialia*, vol. 44, no. 12, pp. 4749 – 4763, 1996. –>

[Hirt06]   J. Hirth, R. Pond, and J. Lothe, "Disconnections in tilt walls," *Acta Materialia*, vol. 54, no. 16, pp. 4237 – 4245, 2006. –>

[Hirt07]   J. Hirth, R. Pond, and J. Lothe, "Spacing defects and disconnections in grain boundaries," *Acta Materialia*, vol. 55, no. 16, pp. 5428 – 5437, 2007. –>

[Home13]   E. R. Homer, S. M. Foiles, E. A. Holm, and D. L. Olmsted, "Phenomenology of shear-coupled grain boundary motion in symmetric tilt and general grain boundaries," *Acta Mater.*, vol. 61, no. 4, pp. 1048 – 1060, 2013.

[Hoyt09]   J. J. Hoyt, D. Olmsted, S. Jindal, M. Asta, and A. Karma, "Method for computing short-range forces between solid-liquid interfaces driving grain boundary premelting," *Phys. Rev. E*, vol. 79, p. 020601, Feb 2009. –>

[Hsie89]   T. E. Hsieh and R. W. Balluffi, "Observations of roughening/de-faceting phase transitions in grain boundaries," *Acta Metall.*, vol. 37, no. 8, pp. 2133–2139, 1989.

[Hu63]   H. Hu, *Recovery and Recrystallization of Metals*, pp. 311–378.

[Hull75]   D. Hull, *Introduction to Dislocations*, 2nd ed.   Pergamon Press Ltd., 1975.

[Hump95]   F. Humphreys and M. Hatherly, *Recrystallization and Related Annealing Phenomena*, ser. Pergamon Materials Series.   Elsevier, 1995.

[Ivan08]   V. Ivanov and Y. Mishin, "Dynamics of grain boundary motion coupled to shear deformation: An analytical model and its verification by molecular dynamics," *Phys. Rev. B*, vol. 78, pp. 1–12, Aug 2008.

[Jian05]   W. B. Jiang, P. Cui, Q. P. Kong, Y. Shi, and M. Winning, "Internal friction peak in pure al bicrystals with 100 tilt boundaries," *Phys. Rev. B*, vol. 72, p. 174118, Nov 2005. –>

[Jime98]   M. Jiménez-Melendo, A. Domínguez-Rodríguez, and A. Bravo-León, "Superplastic flow of fine-grained yttria-stabilized zirconia polycrystals: Constitutive equation and deformation mechanisms," *Journal of the American Ceramic Society*, vol. 81, no. 11, pp. 2761–2776, 1998. –>

[Kali12]   Y. E. Kalinin and B. M. Darinskii, "High.temperature backgroud of internal friction in alloys," *Material Science and Heat Treatment*, vol. 54, no. 5 - 6, pp. 221 – 224, September 2012.

[Ke47a]   T.-S. Ke, "Experimental evidence of the viscous behavior of grain boundaries in metals," *Phys. Rev.*, vol. 71, pp. 533–546, Apr 1947.

[Ke47b]   T.-S. Ke, "Stress relaxation across grain boundaries in metals," *Phys. Rev.*, vol. 72, pp. 41–46, Jul 1947.

[Kelc98]   C. L. Kelchner, S. J. Plimpton, and J. C. Hamilton, "Dislocation nucleation and defect structure during surface indentation," *Phys. Rev. B*, vol. 58, pp. 11 085–11 088, Nov 1998. –>

[Khat12]   H. Khater, A. Serra, R. Pond, and J. Hirth, "The disconnection mechanism of coupled migration and shear at grain boundaries," *Acta Materialia*, vol. 60, no. 5, pp. 2007 – 2020, 2012. –>

[King80]   A. H. King and D. A. Smith, "The effects on grain-boundary processes of the steps in the boundary plane associated with the cores of grain-boundary dislocations," *Acta Crystallographica Section A*, vol. 36, no. 3, pp. 335–343, May 1980. –>

[Kitt05a]   C. Kittel, *Introduction to solid state physics*, 8th ed.   Hoboken, NJ: John Wiley & Sons, 2005.

[Kitt05b]   C. Kittel, *Phonons II. Thermal properties*, 8th ed., ch. 5, pp. 115–140, in [Kitt05a].

[Koeh52]   J. Koehler, *Imperfections in Nearly Perfect Crystals*.   J. Wiley, New York, 1952.

[Kong09]   Q. Kong, W. Jiang, Y. Shi, P. Cui, Q. Fang, and M. Winning, "Grain boundary internal friction in bicrystals with different misorientations," *Materials Science and Engineering: A*, vol. 521–522, no. 0, pp. 128 – 133, 2009. –>

[Lakk95]   A. Lakki, R. Schaller, G. Bernard-Granger, and R. Duclos, "High temperature anelastic behaviour of silicon nitride studied by mechanical spectroscopy," *Acta Metallurgica et Materialia*, vol. 43, no. 2, pp. 419 – 426, 1995. –>

[Lakk98]   A. Lakki, R. Schaller, C. Carry, and W. Benoit, "High temperature anelastic and viscoplastic deformation of fine-grained MgO-doped Al_2O_3," *Acta Materialia*, vol. 46, no. 2, pp. 689 – 700, 1998. –>

Bibliography

[Lanc10]   F. Lançon, J. Ye, D. Caliste, T. Radetic, A. M. Minor, and U. Dahmen, "Superglide at an internal incommensurate boundary," *Nano Lett.*, vol. 10, no. 2, pp. 695–700, 2010, pMID: 20143874.

[Lee10]   L. C. Lee and S. J. S. Morris, "Anelasticity and grain boundary sliding," *Proc. R. Soc. A,* vol. 466, pp. 2651–2671, September 2010.

[Lee11]   L. C. Lee, S. J. S. Morris, and J. Wilkening, "Stress concentrations, diffusionally accommodated grain boundary sliding and the viscoelasticity of polycrystals," *Proceedings of the Royal Society A: Mathematical, Physical and Engineering Science*, vol. 467, no. 2130, pp. 1624–1644, 2011. –>

[Lind10]   F. A. Lindemann, "The calculation of molecular vibration frequencies," *Z. Phys.*, vol. 11, pp. 609–612, 1910.

[Lüc56]   K. Lücke and A. V. Granato, "Internal friction phenomena due to dislocations," *Dislocations and Mechanical Properties of Crystals*, pp. 425–455, 1956.

[Maie13]   A.-K. Maier, I. Tkalcec, D. Mari, and R. Schaller, "New In-Pd mechanical loss peak in ternary gold alloys," *Acta Mater.*, vol. 61, no. 16, pp. 6107 – 6113, 2013. –>

[Mend69]   M. I. Mendelson, "Average grain size in polycrystalline ceramics," *J. Am. Ceram. Soc.*, vol. 52, pp. 443–446, 1969.

[Merk87]   K. L. Merkle and D. J. Smith, "Atomic Structure of Symmetric Tilt Grain Boundaries in NiO," *Phys. Rev. Lett.*, vol. 59, pp. 2887–2890, Dec 1987. –>

[Molo13]   D. A. Molodov, "Grain boundary dynamics under an applied stress," *Materials Science Forum*, vol. 753, pp. 101–106, 2013. –>

[Molt97]   C. Molteni, N. Marzari, M. C. Payne, and V. Heine, "Sliding mechanisms in aluminum grain boundaries," *Phys. Rev. Lett.*, vol. 79, pp. 869–872, Aug 1997. –>

[Monz93]   R. Monzen, M. Futakuchi, K. Kitagawa, and T. Mori, "Measurement of grain boundary sliding of [011] twist boundaries in copper by electron microscopy," *Acta Metallurgica et Materialia*, vol. 41, no. 6, pp. 1643 – 1646, 1993. –>

[Morr09]   S. Morris and I. Jackson, "Diffusionally assisted grain-boundary sliding and viscoelasticity of polycrystals," *J. Mech. Phys. Solids*, vol. 57, no. 4, pp. 744 – 761, 2009. –>

[Mort66]   M. de Morton and G. Leak, "High temperature relaxation peaks in copper and gold," *Acta Metallurgica*, vol. 14, no. 9, pp. 1140 – 1142, 1966. –>

[Mort67]   M. E. Morton and G. M. Leak, "Zener relaxations in the copper-gold system," *Metal Science*, vol. 1, no. 1, pp. 182–186, 1967. –>

[Mosh74]   D. R. Mosher and R. Raj, "Use of the internal friction technique to measure rates of grain boundary sliding," *Acta Metallurgica*, vol. 22, no. 12, pp. 1469 – 1474, 1974. –>

[Mugh01]   H. Mughrabi, "Self-consistent experimental determination of the dislocation line tension and long-range internal stresses in deformed copper crystals by analysis of dislocation curvatures," *Materials Science and Engineering: A,* vol. 309-310, no. 0, pp. 237 – 245, 2001. –>

[Naba48]   F. R. N. Nabarro, "Report of a conference on the strength of solids," *Proc. Phys. Soc.*, vol. 1, pp. 1–19, 1948.

[Neum08]   G. Neumann and C. Tuijn, "Chapter 1 self-diffusion and impurity diffusion in group I metals," in *Self-Diffusion and Impurity Diffusion in Pure Metals: Handbook of Experimental Data*, ser. Pergamon Materials Series, G. Neumann and C. Tuijn, Eds.   Pergamon, 2008, vol. 14, pp. 37 – 97. –>

[Ngai79]   K. Ngai, A. Jonscher, and C. White, "On the origin of the universal dielectric response in condensed matter," *Nature*, vol. 277, no. 5693, pp. 185–189, 1979. –>

[No89]   M. Nó, J. S. Juan, and C. Esnouf, "Transition between tangled and polygonized dislocation microstructures in high-purity aluminium studied by internal friction and electron microscopy," *Mater. Sci. Eng. A*, vol. 113, no. 0, pp. 281–285, 1989.

[No93]   M. Nó and J. S. Juan, "Structure and mobility of polygonized dislocation walls in high purity aluminium," *Mater. Sci. Eng. A*, vol. 164, no. 1-2, pp. 153–158, 1993.

[Nowi72a]   A. S. Nowick and B. S. Berry, *Anelastic Relaxation in Crystalline Solids*, A. M. Alper, J. L. Margrave, and A. S. Nowick, Eds.   Academic Press, 1972.

[Nowi72b]   A. S. Nowick and B. S. Berry, *Boundary Relaxation Processes and Internal Friction at High Temperatures*, ch. 15, pp. 435–462, in [Nowi72a].

[Nowi72c]   A. S. Nowick and B. S. Berry, *Mechanical Models and Discrete Spectra*, ch. 3, pp. 41–76, in [Nowi72a].

[Okud94]   S. Okuda, F. Tang, H. Tanimoto, and Y. Iwamoto, "Anelasticity of ultrafine-grained polycrystalline gold," *Journal of Alloys and Compounds*, vol. 211–212, pp. 494 – 497, 1994, 10th International Conference on Internal Friction and Ultrasonic Attenuation in Solids. –>

[Pere65]   J. Perez, P. Peguin, and P. Gobin, "Calculation of the amplitude dependence of internal friction from measurements of torsional damping," *Brit. J. Appl. Phys.*, vol. 16, pp. 1347–1351, 1965.

[Pete64]   D. T. Peters, J. C. Bisseliches, and J. W. Spretnak, "Some Observations of Grain Boundary Relaxation in Copper and Copper–2% Cobalt," *Transactions of The Metallurgical Society of AIME*, vol. 230, pp. 530–540, 1964.

[Plim95a]   S. Plimpton, "Sandia national laboratories: http://lammps.sandia.gov, official lammps website," 1995. –>

[Plim95b]   S. Plimpton, "Fast parallel algorithms for short-range molecular dynamics," *J. Comput. Phys.*, vol. 117, no. 1, pp. 1 – 19, 1995. –>

[Poir85]   J.-P. Poirier, *Creep of Crystals: High-Temperature Deformation Processes in Metals, Ceramics and Minerals (Cambridge Earth Science Series)*.   Cambridge University Press, 1985. –>

[Pond79]   R. C. Pond and W. Bollmann, "The symmetry and interfacial structure of bicrystals," *Philosophical Transactions of the Royal Society of London. Series A, Mathematical and Physical Sciences*, vol. 292, no. 1395, pp. 449–472, 1979. –>

[Pond03]   R. C. Pond and S. Celotto, "Special interfaces: military transformation," *International Materials Reviews*, vol. 48, no. 4, pp. 225–245, 2003.

[Powe13]   T. Power, "Structural disjoining potential of grain boundary premelting in aluminum-magnesium via monte carlo simulations," Master's thesis, McMaster University, Hamilton, Ontario, Canada, 2013.

[Prie13]   L. Priester, *Grain Boundaries: From Theory to Engineering*, ser. Springer Series in Materials Science.   Springer-Verlag, 2013, vol. 172.

[Qi01]   Y. Qi, T. Çağin, W. L. Johnson, and W. A. Goddard, "Melting and crystallization in Ni nanoclusters: The mesoscale regime," *The Journal of Chemical Physics*, vol. 115, no. 1, pp. 385–394, 2001. –>

[Qi07]   Y. Qi and P. E. Krajewski, "Molecular dynamics simulations of grain boundary sliding: The effect of stress and boundary misorientation ," *Acta Materialia*, vol. 55, no. 5, pp. 1555 – 1563, 2007. –>

[Raj71]   R. Raj and M. F. Ashby, "On Grain Boundary Sliding and Diffusional Creep," *Metallurgical and Materials Transactions B*, vol. 2, no. 4, pp. 1113–1127, April 1971. –>

[Rand93]   V. Randle, *The Measurement of Grain Boundary Geometry*, ser. Electron Microscopy In Materials Science Series, B. Cantor and M. J. Goringe, Eds.   Institute of Physics Publishing Bristol and Philadelphia, 1993.

[Read50]   W. T. Read and W. Shockley, "Dislocation models of crystal grain boundaries," *Phys. Rev.*, vol. 78, pp. 275–289, May 1950. –>

[Rivi76]   A. Riviere, J. Amirault, and J. Woirgard, "Influence de l'amplitude de vibration sur les pics de frottement interne de haute témperature de l'argent polycristallin de haute pureté," *Il Nuovo Cimento B Series 11*, vol. 33, no. 1, pp. 398–407, 1976. –>

[Rivi81]   A. Rivière, J. P. Amirault, and J. Woirgard, "High temperature internal friction and dislocation motion in poly and single crystals of f.c.c. metals," *Journal de Physique: Colloques*, vol. 42, no. C5, pp. 439–444, oct 1981. –>

[Rivi93]   A. Rivière and J. Woirgard, "High temperature relaxation in aluminium studied by low frequency mechanical spectroscopy," *Materials Science Forum*, vol. 119, pp. 125–132, 1993. –>

[Rivi08]   A. Rivière, M. Gerland, and V. Pelosin, "High-temperature mechanical relaxation due to dislocation motion inside dislocation networks," *Solid State Phenomena*, vol. 137, pp. 21–28, 2008.

[Rivi09]   A. Rivière, M. Gerland, and V. Pelosin, "Influence of dislocation networks on the relaxation peaks at intermediate temperature in pure metals and metallic alloys," *Mater. Sci. Eng. A*, vol. 521-522, pp. 94 – 97, 2009.

[Scha01]   R. Schaller, G. Fantozzi, and G. Gremaud, Eds., *Mechanical Spectroscopy Q^{-1} 2001*, ser. Materials Science Forum.   Trans Tech Publications, Switzerland, 2001, vol. 366–368. –>

[Scha12]   J. Schäfer and K. Albe, "Competing deformation mechanisms in nanocrystalline metals and alloys: Coupled motion versus grain boundary sliding," *Acta Materialia*, vol. 60, no. 17, pp. 6076 – 6085, 2012. –>

[Scho64]   G. Schoeck, E. Bisogni, and J. Shyne, "The activation energy of high temperature internal friction," *Acta Metallurgica*, vol. 12, no. 12, pp. 1466–1468, December 1964. –>

[Seeg56]   A. Seeger, "On the theory of the low-temperature internal friction peak observed in metals," *Philosophical Magazine*, vol. 1, pp. 651–662, 1956.

[Shap70]   J. N. Shapiro, "Lindemann law and lattice dynamics," *Physical Review B*, vol. 1, no. 10, pp. 3982–3989, 1970.

[Shei95]   A. Sheikh-Ali, "On the influence of intragranular slip on grain boundary sliding in bicrystals," *Scripta Metallurgica et Materialia*, vol. 33, no. 5, pp. 795 – 801, 1995. –>

[Shi05]   Y. Shi, P. Cui, Q. P. Kong, W. B. Jiang, and M. Winning, "Internal friction peak in bicrystals with different misorientations," *Physical Review B*, vol. 71, no. 6, p. 060101(R), feb 2005. –>

[Shi06]   Y. Shi, W. B. Jiang, Q. P. Kong, P. Cui, Q. F. Fang, and M. Winning, "Basic mechanism of grain-boundary internal friction revealed by a coupling model," *Physical Review B*, vol. 73, no. 17, p. 174101, 2006. –>

[Sim14]   G.-D. Sim and J. J. Vlassak, "High-temperature tensile behavior of freestanding Au thin films ," *Scr. Mater.*, vol. 75, no. 0, pp. 34 – 37, 2014. –>

[Skro13]   W. Skrotzki, A. Eschke, B. Jóni, T. Ungár, L. Tóth, Y. Ivanisenko, and L. Kurmanaeva, "New experimental insight into the mechanisms of nanoplasticity," *Acta Mater.*, vol. 61, no. 19, pp. 7271 – 7284, 2013. –>

[Smal99]   R. Smallman and R. Bishop, *Modern Physical Metallurgy and Materials Engineering: Science, Process, Applications*, ser. Referex Engineering.   Butterworth-Heinemann, 1999.

[Snoe41]   J. L. Snoek, "Effect of small quantities of carbon and nitrogen on the elastic and plastic properties of iron," *Physica*, vol. 8, pp. 711–733, 1941.

[Stra14]   B. Straumal, X. Sauvage, B. Baretzky, A. Mazilkin, and R. Valiev, "Grain boundary films in Al–Zn alloys after high pressure torsion ," *Scripta Materialia*, vol. 70, no. 0, pp. 59 – 62, 2014. –>

[Stuk10]   A. Stukowski and K. Albe, "Extracting dislocations and non-dislocation crystal defects from atomistic simulation data," *Modelling and Simulation in Materials Science and Engineering*, vol. 18, no. 8, p. 085001, 2010. –>

[Stuk12]   A. Stukowski, V. V. Bulatov, and A. Arsenlis, "Automated identification and indexing of dislocations in crystal interfaces," *Modelling and Simulation in Materials Science and Engineering*, vol. 20, no. 8, p. 085007, 2012. –>

[Sutt87]   A. P. Sutton and R. W. Ballu, "Overview no. 61: On geometric criteria for low interfacial energy," *Acta Metallurgica*, vol. 35, no. 9, pp. 2177–2201, 1987.

Bibliography

[Sutt95]   A. Sutton and R. Balluffi, *Interfaces in Crystalline Materials*, ser. Monographs on the Physics And Chemistry of Materials.   OUP Oxford, 1995. –>

[Suzu05]   A. Suzuki and Y. Mishin, "Atomic mechanisms of grain boundary motion," *Materials Science Forum*, vol. 502, pp. 157–162, 2005.

[Take14]   Y. Takei, F. Karasawa, and H. Yamauchi, "Temperature, grain size, and chemical controls on polycrystal anelasticity over a broad frequency range extending into the seismic range," *Journal of Geophysical Research: Solid Earth*, vol. 119, no. 7, pp. 5414–5443, 2014. –>

[Test02]   S. Testu, R. Schaller, J. Besson, T. Rouxel, and G. Bernard-Granger, "Mechanical spectroscopy connected to creep and stress relaxation in a high resistant silicon nitride," *Journal of the European Ceramic Society*, vol. 22, no. 14–15, pp. 2511 – 2516, 2002. –>

[Tkal09]   I. Tkalcec, J. Hennig, D. Mari, and R. Schaller, "Mechanical spectroscopy of 18-carat AuCuPd white gold alloys," *Materials Science & Engineering A*, vol. 521-522, pp. 52–54, sep 2009. –>

[Trau12]   Z. Trautt, A. Adland, A. Karma, and Y. Mishin, "Coupled motion of asymmetrical tilt grain boundaries: Molecular dynamics and phase field crystal simulations," *Acta Materialia*, vol. 60, no. 19, pp. 6528 – 6546, 2012. –>

[Vela11]   M. Velasco, H. V. Swygenhoven, and C. Brandl, "Coupled grain boundary motion in a nanocrystalline grain boundary network," *Scr. Mater.*, vol. 65, no. 2, pp. 151 – 154, 2011. –>

[Waka86]   F. Wakai, S. Sakaguchi, and Y. Matsuno, "Superplasticity of yttria-stabilised tetragonal ZrO2 polycrystals," *Adv. Ceram. Mater.*, vol. 1, pp. 259–263, 1986.

[Wang11]   Z. Wang, M. Saito, K. P. McKenna, L. Gu, S. Tsukimoto, A. L. Shluger, and Y. Ikuhara, "Atom-resolved imaging of ordered defect superstructures at individual grain boundaries," *Nature*, vol. 479, p. 380–383, 2011.

[Ward12]   L. Ward, A. Agrawal, K. M. Flores, and W. Windl, "Rapid Production of Accurate Embedded-Atom Method Potentials for Metal Alloys," *ArXiv e-prints*, Sep. 2012.

[Wata84]   T. Watanabe, S.-I. Kimura, and S. Karashima, "The effect of a grain boundary structural transformation on sliding in<1010>-tilt zinc bicrystals," *Philosophical magazine. A*, vol. 49, no. 6, pp. 845–864, 1984.

[Whee13]   J. Wheeler, V. Maier, K. Durst, M. Göken, and J. Michler, "Activation parameters for deformation of ultrafine-grained aluminium as determined by indentation strain rate jumps at elevated temperature," *Mater. Sci. Eng. A*, vol. 585, no. 0, pp. 108 – 113, 2013. –>

[Wine09]   J. M. Winey, A. Kubota, and Y. M. Gupta, "A thermodynamic approach to determine accurate potentials for molecular dynamics simulations: thermoelastic response of aluminum," *Modelling and Simulation in Materials Science and Engineering*, vol. 17, no. 5, p. 055004, 2009. –>

[Wine10] J. M. Winey, A. Kubota, and Y. M. Gupta, "Thermodynamic approach to determine accurate potentials for molecular dynamics simulations: thermoelastic response of aluminum," *Modelling and Simulation in Materials Science and Engineering*, vol. 18, no. 2, p. 029801, 2010. –>

[Winn01] M. Winning, G. Gottstein, and L. Shvindlerman, "Migration of grain boundaries under the influence of an external shear stress," *Mater. Sci. Eng. A*, vol. 317, no. 1-2, pp. 17 – 20, 2001. –>

[Winn03] M. Winning, "Motion of 100-tilt grain boundaries," *Acta Materialia*, vol. 51, no. 20, pp. 6465 – 6475, 2003. –>

[Winn05] M. Winning and A. D. Rollett, "Transition between low and high angle grain boundaries," *Acta Materialia*, vol. 53, no. 10, pp. 2901 – 2907, 2005. –>

[Woir81] J. Woirgard, A. Riviere, and J. De Fouquet, "Experimental and Theoretical Aspect of the High Temperature Damping of Pure Metals," *Journal de Physique: Colloques*, vol. 42, no. C5, pp. 407–419, oct 1981. –>

[Wolf90a] D. Wolf, "Structure-energy correlation for grain boundaries in F.C.C. metals—III. Symmetrical tilt boundaries ," *Acta Metallurgica et Materialia*, vol. 38, no. 5, pp. 781 – 790, 1990. –>

[Wolf90b] D. Wolf, "Structure-energy correlation for grain boundaries in f.c.c. metals—IV. Asymmetrical twist (general) boundaries," *Acta Metallurgica et Materialia*, vol. 38, no. 5, pp. 791 – 798, 1990. –>

[Yang14] K. Yang, H.-J. Fecht, and Y. Ivanisenko, "First direct in situ observation of grain boundary sliding in ultrafine grained noble metal," *Advanced Engineering Materials*, vol. 16, no. 5, pp. 517–521, 2014. –>

[Zene41] C. Zener, "Theory of the Elasticity of Polycrystals with Viscous Grain Boundaries," *Physical Review*, vol. 60, no. 12, pp. 906–908, Dec 1941. –>

[Zene47] C. Zener, "Stress Induced Preferential Orientation of Pairs of Solute Atoms in Metallic Solid Solution," *Physical Review*, vol. 71, no. 1, pp. 34–38, Jan 1947. –>

[Zhou04] X. W. Zhou, R. A. Johnson, and H. N. G. Wadley, "Misfit-energy-increasing dislocations in vapor-deposited cofe/nife multilayers," *Phys. Rev. B*, vol. 69, p. 144113, Apr 2004. –>

[Zolo95] I. V. Zolotukhin and Y. E. Kalinin, "High-temperature internal-friction background in crystalline and amorphous solids," *Physics of the Solid State*, vol. 37, no. 2, p. 290, 1995.

The electronic version of this document (a PDF file) includes hyperlinks (–>) to electronic resources for those references available on the Internet at print time.

List of Figures

Ann-Kathrin Audren ann-kathrin.audren@gmx.de
Avenue de Préfaully, 25C 19.07.1985
1022 Chavannes (Switzerland) married
German

Education

Doctoral thesis in experimental physics	2010–2014
École Polytechnique Fédérale de Lausanne (EPFL)	
Subject: Grain boundary relaxation in 18-carat gold alloys	
- laboratory work, data analysis, simulations	
Master in physics	2008–2010
École Normale Superieur (ENS) de Lyon (France)	
Vordiplom in physics	2005–2008
Universität Karlsruhe (Germany), equivalent to a Bachelor degree	
Abitur at Rotteck-Gymnasium Freiburg (Germany)	2005

Teaching Assignments and Academic Projects

Teaching assistant for general physics classes (Bachelor level)	2010–2014
Exercise classes for engineers in materials science (Master level)	
Teaching assistant for analytical mechanics (theoretical physics)	
Master thesis in Paris, France	04.2010–07.2010
- Fundamental particle physics	
- Title: Higgs sector in a model with Dirac gauginos (40 pages)	
Research internship in Oxford, England	05.2009–07.2009
- Solid state physics, modelling	
- Title: Magnetization plateau phase in a triangular antiferro-	
magnet (30 pages)	

Professional Experience

Micronas Freiburg, Operator in the semi-conductor factory	2006
- shift work in the clean room during the summer	
Internship in the group of process engineers	2005
- steps of the fabrication of integrated circuits	

Informatics

Windows, Linux, MS Office, LaTex, Mathematica, Matlab, C++, Python,
IgorPro, LabView, Lammps (molecular dynamics), Comsol

Parallel Activities

Member the ICMP institute board at l'EPFL	since 2012
- Representative of PhD students and post-docs (~ 100 people)	
University choir (classical music)	since 2011

Conference Participations

- Poster presentation **SPS 2011** and **ICIFMS16 (2011)**, Lausanne: Grain Boundary Relaxation in 18-carat Yellow Gold
- Poster presentation **ReX&GG 2013**, Sydney: Recrystallization and Grain Boundary Formation Stages in an 18-carat gold alloy studied by mechanical spectroscopy
- Oral presentation at **Deutsche Physikerinnen Tagung 2013**, Heidelberg, Germany: Molecular Dynamics Simulations of Grain Boundary Movement
- Oral presentation at **Colloque Plasticité 2014** in Lyon, France: Relaxations anélastiques des joints de grains: de la dynamique moléculaire à la modélisation
- Oral presentation at **ICIFMS17 2014** in China: GB Relaxation in Bi-crystals

Publications

[1] Benakli, K., Goodsell, M. D., Maier, A.-K., Generating μ and B_μ in models with Dirac Gauginos, Nucl. Phys. B851, (2011), p. 445-461 →

[2] Maier, A-K., Tkalcec, I., Mari, D., Schaller, R., Grain Boundary Relaxation in 18-carat Yellow Gold, Solid State Phenomena, Conference Proceedings ICIFMS16 (2011) →

[3] Maier, A-K., Tkalcec, I., Mari, D., Schaller, R., Grain Boundary Relaxation and Grain Growth in 18-carat Yellow Gold Alloy, Scripta Materialia 66, (2012) 374-377→

[4] Maier, A-K., Tkalcec, I., Mari, D., Schaller, R., Grain Boundary Formation Stages in a yellow gold single crystal studied by mechanical spectroscopy, Materials Science & Engineering A 560 (2013) 466-472 →

[5] Maier, A-K., Tkalcec, I., Mari, D., Schaller, R., Recrystallization and Grain Boundary Formation Stages in an 18-carat gold alloy studied by mechanical spectroscopy, Materials Science Forum Vol. 753 (2013) p 17-20, Proceedings ReX&GG2013 →

[6] Maier, A-K., Tkalcec, I., Mari, D., Schaller, R., New In-Pd mechanical loss peak in ternary gold alloys, Acta Materialia 61 (2013) 6107-6113 →

[7] Maier, A-K., Tkalcec, I., Mari, D., Schaller, R., Theoretical modelling of grain boundary anelastic relaxation, Acta Materialia 74 (2014) 132-140 →

[8] Maier, A-K., Tkalcec, I., Mari, D., Schaller, R., Grain Boundary Relaxation in Bi-crystals: Mechanical Spectroscopy and Molecular Dynamics Simulations, Solid State Phenomena, Conference Proceedings ICIFMS17 (2014), to be published

[9] Maier, A-K., Mari, D., Tkalcec, I., Schaller, R., Grain Boundary Relaxation in Yellow Gold Bi-Crystals, Materials Science & Engineering A, to be published